6-20-2018

# Madden-Julian Oscillation Relationships with Cool Season Cyclogenesis, Daily Precipitation, and Cool Season Severe Weather Frequencies in the Gulf of Mexico Region

Stephen Paul Caparotta
*Louisiana State University and Agricultural and Mechanical College*, scaparotta@gmail.com

# MADDEN-JULIAN OSCILLATION RELATIONSHIPS WITH COOL SEASON CYCLOGENESIS, DAILY PRECIPITATION, AND COOL SEASON SEVERE WEATHER FREQUENCIES IN THE GULF OF MEXICO REGION

A Dissertation

Submitted to the Graduate Faculty of the
Louisiana State University and
Agricultural and Mechanical College
in partial fulfillment of the
requirements for the degree of
Doctor of Philosophy

in

The Department of Geography and Anthropology

by
Stephen Paul Caparotta
B.S., University of South Alabama, 1998
M.S., Louisiana State University, 2008
August 2018

I dedicate this to my wife, Christy, whose unwavering love and support made the 6-year journey to the completion of this research possible. I can never thank you enough for the sacrifices made for both me and our two daughters along the way. I love you more than everything.

I also dedicate this to my two beautiful daughters, Eliana and Clara, who were both born after my return to LSU in 2012. When times were tough and it seemed as though I would never reach the finish line, your smiles, laughter, and hugs carried me through. What a blessing both of you have been and I am beyond lucky to be your Dad.

# ACKNOWLEDGMENTS

I owe a deep debt of gratitude to Dr. Robert Rohli for his guidance, support, patience, and expertise provided throughout my graduate studies. Bob was one of the first people I met at LSU when I first began my master's program in 2004 and served as my advisor both then and in my more recent effort to earn a Ph.D. He has always been available for feedback, even when out of town, and his rapid responses to my endless emails and requests for edits are a huge reason that I was able to complete this project. I am proud to consider Bob not only my advisor but a good friend.

I would also like to thank my committee members, Dr. Jill Trepanier and Dr. Nan Walker. When I needed help understanding Monte Carlo simulations and attempted to run them in R, Dr. Trepanier was willing and available to help. Dr. Walker taught me an incredible amount about oceanography both through courses and countless personal communications through the years. I am also appreciative of Dr. Todd Gibson for serving as the Dean's representative on my committee.

The graphics and Monte Carlo simulations interspersed throughout my dissertation were largely created and run in Python and would not have been possible without the help of a few people. To my cousin, Andrew Dupont, and his girlfriend, Barbara Shaurette, a sincere thank you for helping this novice learn the basics of Python and for annotated explanations of scripts that served as the foundation for much of the work within this project. I would also like to thank Eric Rohli who helped me iron out issues with a Python script that was

key to this research and for his subsequent willingness to respond to a number of follow-up questions.

Finally, a special thank you to Dr. Eric Oliver and Dr. Phil Klotzbach. Dr. Oliver provided the Python script that served as the basis for the Monte Carlo simulations run in this project. Dr. Klotzbach provided feedback along the way, particularly as it related to understanding Monte Carlo techniques.

# TABLE OF CONTENTS

# ABSTRACT

Tropical cyclone variability in the Gulf of Mexico (GoM) has been the focus of a considerable amount of research. Variability on both interannual scales, related to the El Niño-Southern Oscillation (ENSO), and on subseasonal scales, related to the Madden-Julian Oscillation (MJO), is well documented. By contrast, very little research exists on the relationships between the MJO and cool season, non-tropical cyclones in the GoM.

The MJO influence on cool season (October-March) cyclogenesis in the GoM variability is explored here. Additionally, daily precipitation variability and cool season severe weather variability is examined for areas near and just inland of the GoM. Monte Carlo simulations are used to identify statistically significant relationships between specific phases of the MJO and cyclogenesis, precipitation, and severe weather variability around the GoM region.

The Monte Carlo simulation results indicate a preference for increased storminess in the GoM region during MJO Phases 7, 8, and 1, with a preference for a more tranquil pattern during Phases 4, 5, and 6. The significant associations found here between the MJO and cyclogenesis, daily precipitation, and daily severe weather frequencies are likely linked to modification of the synoptic scale Rossby wave train by the convective clusters associated with the MJO. In particular, anomaly plots of NCEP/NCAR Reanalysis data show that measures of atmospheric pressure, moisture, and instability favor (oppose) the development of convection in the GoM region during Phases 7, 8, and 1 (4, 5, and 6).

# CHAPTER 1. INTRODUCTION

## 1.1 Overview

The formation of an enclosed area of low atmospheric pressure – cyclogenesis – generally signifies the beginning of a storm, whether it be tropical, or extratropical in origin. Cyclogenesis can have significant weather impacts on both terrestrial and marine areas in and around the Gulf of Mexico (GoM). Those impacts can extend to the GoM's Outer Continental Shelf (OCS) which is among the world's most developed and busiest petroleum regions (Kaiser and Pulsipher 2007), producing approximately 1.4 million barrels of oil per day and 3.5 million cubic feet of natural gas per day (Energy Information Administration 2015). In addition to being a major hydrocarbon producer, the GoM region houses roughly 45% of U.S. oil refining capacity and roughly 50% of natural gas processing capacity (Energy Information Administration 2015). The record-setting 2005 hurricane season produced record-setting damages for the GoM energy industry, with insured losses estimated to range anywhere from $35 to $60 billion (Lyle 2005; Paganie and Buschee 2005), largely driven by two major hurricanes, Katrina and Rita. The GoM energy sector has a clear vulnerability to tropical weather.

Tropical cyclones can also have significant impacts on the coastal geomorphology of the U.S. Gulf Coast. The combination of astronomical tides, waves, and storm surge often results in significant coastal erosion along the Gulf Coast, even for areas that may not see a direct landfall from a tropical cyclone. A model used by Stockdon et al. (2012) produced water level rises of

170% along the immediate coast for a minimal hurricane (Category 1 on the Saffir-Simpson scale). An example of extreme land loss can be seen in the Chandeleur Islands off the coast of Louisiana, where it is estimated that 85% of the barrier island chain's surface area disappeared in the wake of Hurricane Katrina (Doran et al. 2010).

Considerable literature exists on tropical cyclogenesis in the GoM, including links to El Niño-Southern Oscillation (ENSO; e.g., Gray 1984; Bove et al. 1998; Tang and Neelin 2004; Patricola et al. 2014) and the Madden-Julian Oscillation (MJO; e.g., Maloney and Hartmann 2000; Aiyyer and Molinari 2008; Klotzbach 2014). However, less research has focused on GoM cyclogenesis in the cool season (fall/winter). This is unfortunate, because cool season, or extratropical (ET) cyclones, can have impacts similar to those of tropical cyclones in the GoM region.

ET cyclones in the GoM have been shown to influence coastal and inland flooding (Johnson et al. 1984), beach erosion and the morphodynamics of barrier islands (Hsu 1993; Stone et al. 2004), the GoM energy sector (Hsu 1993), coastal marsh stability (Goodbred and Hine 1995), temperature and precipitation patterns (Ropelewski and Halpert 1986), and severe weather frequencies (Cook and Schaefer 2008). The so-called "1993 Superstorm" provides an example of an ET cyclone that resulted in extreme impacts throughout the GoM region. The storm produced everything from snowfall to hurricane-force wind gusts to coastal erosion to widespread power outages and record low temperatures along parts of the Gulf Coast. The 1993 Superstorm

also resulted in more than 200 fatalities in the United States, with approximately 60 of those occurring in states bordering the GoM (Lott 1993). While ET cyclone impacts on the GoM region are not nearly as well-documented as those of tropical cyclones, it seems fair to assume that well-developed, mature ET cyclones in the GoM may produce similar impacts.

Exploring ET cyclone impacts in the GoM will also require an understanding of what drives their frequency and variability. One of the primary candidates is the MJO, because it is the dominant mode of intraseasonal variability in the tropics (Madden and Julian 1994). More than three decades ago, Anderson and Rosen (1983) were among the first to show that some effects of the oscillation can be seen propagating to the midlatitudes. In the decades that followed, numerous linkages between the MJO have been made to weather and climate phenomena in the subtropics and midlatitudes, including: precipitation patterns in North America (Mo and Higgins 1998; Mo 1999, 2000; Jones 2000), extreme precipitation events in North America (Jones et al. 2011), the south Asian monsoon (Lawrence and Webster 2001), the North Atlantic Oscillation (NAO; Lin et al. 2009), and the Pacific/North American teleconnection pattern (PNA; Schreck III and Margolin 2012).

Given the established linkages between teleconnection patterns (e.g., ENSO) and GoM cyclogenesis, and established linkages between the MJO and several North American weather variables, it seems plausible that not just a statistically significant correlation but also a causative link may exist between the MJO and cool season GoM cyclogenesis. This research aims to further

investigate this possible link by examining more than three decades of GoM synoptic weather and MJO data.

## 1.2 Study Area

The study area is a rectangular region bounded by 19°N, 33°N, 100°W, and 80°W (Figure 1). The western bound (100°W) corresponds to the one used in a prior study of winter cyclogenesis events in the northwestern GoM (Hardy and Hsu (1997). It also captures an area known to favor cyclogenesis near and just inland of the Texas coastline (Saucier 1949).

The chosen study area includes the vast majority of the GoM but also extends northward to the 33rd parallel to capture ET cyclones that form near or just inland of the northern Gulf Coast. A review of daily weather maps available

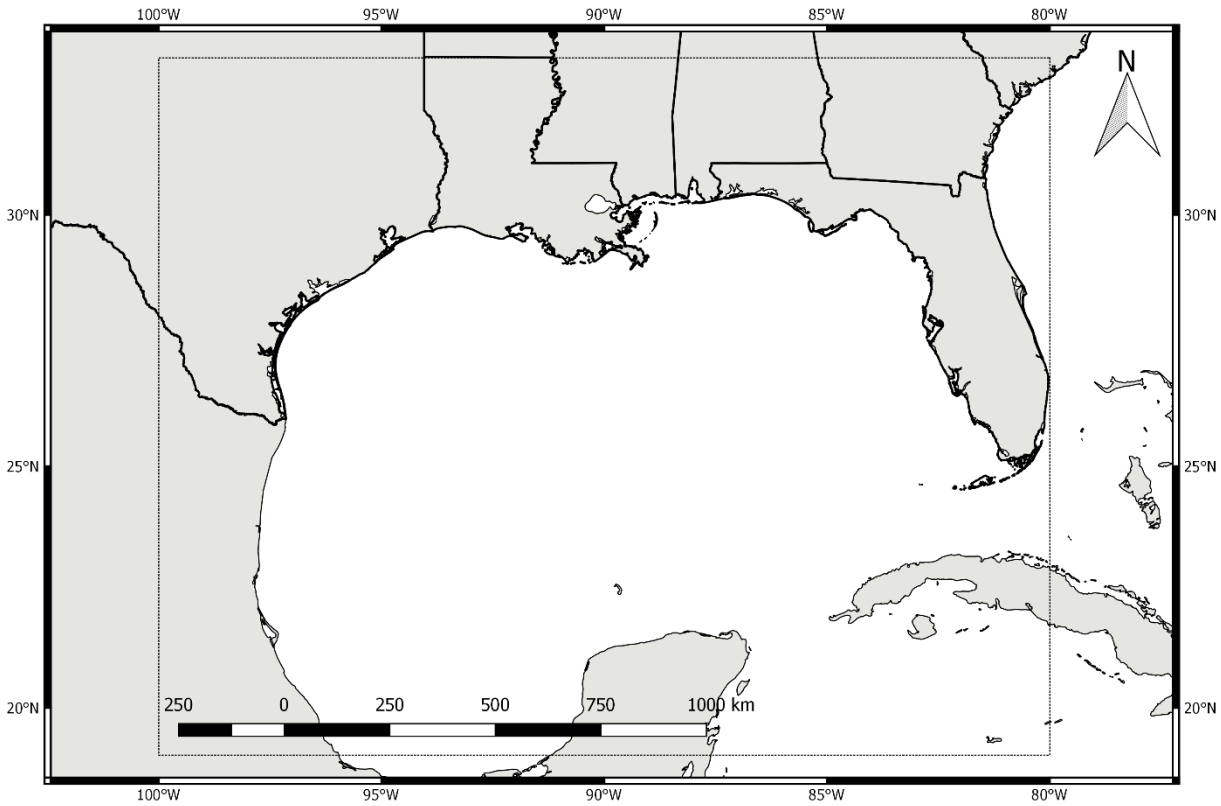


**Figure 1.1** Bounding box show the extent of the study area.

from the (U.S.) National Weather Service (NWS) Weather Prediction Center (WPC), a branch of the National Oceanic and Atmospheric Administration (NOAA), shows that it is common for ET cyclones to form in this region.

It is also possible, if not likely, that the land-sea interface is a preferred region for many ET cyclone formation events. Because of the frequent and intense land-sea thermal contrasts, coastal areas are often the site of baroclinic zones – places where warm, humid air is pushed over colder, denser air – which is a good recipe for cyclogenesis. Coastal cyclogenesis is especially favored because abundant humidity is available for releasing latent energy in the phase changes of water from vapor to liquid (condensation), liquid to solid (freezing), or vapor directly to solid (deposition). The release of such latent energy takes the form of kinetic energy, and the collective effect of billions of such molecular transformations ultimately provides the "fuel" in the form of winds that intensify and are intensified by the sharp pressure gradient, as they comprise the thunderstorms in the cyclone.

The precipitation and severe weather studies that are a part of this larger project will rely solely on data from (U.S.) sources even though the study area includes parts of Mexico. These two studies will focus on U.S. sources since there are reliable extended records of both precipitation and severe weather events that would be difficult to keep consistent across an international border.

### 1.3 Research Questions

The primary goal of this project is to fill a gap in our understanding of what influences ET cyclone formation, intensity, and frequency in the GoM.

Specifically, research will focus on the following three hypotheses:

1) *Cyclogenesis is more/less likely in the GoM during the various phases of the MJO.*
2) *Portions of the U.S. Gulf Coast are more likely to see anomalously high or low precipitation amounts during certain phases of the MJO.*
3) *Portions of the U.S. Gulf Coast are more likely to experience severe convective storms with damaging winds, hail and/or tornadoes during certain phases of the MJO.*

In Study 1, cyclogenesis events identified in the region of interest during the period 1979-2014 will be examined for potential links to the MJO. Specifically, Monte Carlo simulations will help determine whether low pressure is more or less likely to develop during any specific phase(s) of the MJO. In general terms, increased cyclogenesis frequencies during any particular phase might help forecasters identify times when instances of more impactful weather can be expected for areas in and around the Gulf of Mexico. The opposite would be assumed to be true if and when cyclogenesis frequencies are diminished in this region.

In Study 2, Monte Carlo simulations will again be used but this time to test for significant associations between MJO phase and daily rainfall for selected locations near the U.S. Gulf Coast. Additional testing will be conducted to explore potential relationships between MJO phase and daily rain events exceeding a 2.5 cm and 5.0 cm threshold. Since the MJO has a measure of predictability, any associations found could help increase forecaster lead

time in predicting times of increased or decreased precipitation for a given location or region. This in turn could prove to be valuable information for many, including those with agricultural interests who are so dependent on timing, frequency, and amounts of precipitation.

Study 3 will focus on potential associations between the MJO and severe weather frequencies for areas near and just inland of the U.S. Gulf Coast. Severe weather for the purposes of this study will be defined as those instances in which strong/severe winds, hail, and/or tornadoes were reported and documented by the NWS and NOAA's Storm Prediction Center (SPC). As in Studies 1 and 2, Monte Carlo simulations will be the statistical testing method for potential associations. In a broad sense, it is hoped that any associations identified between the MJO and severe weather frequencies would help increase the forecast lead time for potential instances of active weather in this region. In turn, the improved forecasts could enhance the protection of lives and property in the vulnerable, low-lying coastal zone and adjacent offshore waters which are utilized heavily for economic (oil and gas, fisheries) and recreational interests.

The next chapter provides a literature review that forms the foundation of the first three studies. Chapters 3, 4, and 5 contain self-contained research manuscripts that address the three research questions, one per chapter. Chapter 6 summarizes the major findings of the three studies.

## 1.4 References


Aiyyer, A., and J. Molinari, 2008: MJO and tropical cyclogenesis in the Gulf of Mexico and eastern Pacific: Case study and idealized numerical modeling. Journal of the Atmospheric Sciences, 65(8), 2691–2704.

Anderson, J.R., and R.D. Rosen, 1983: The latitude-height structure of 40-50 day variations in atmospheric angular-momentum. Journal of the Atmospheric Sciences, 40(6), 1584–1591.

Bove, M.C., J.B. Elsner, C.W. Landsea, X.F. Niu, and J.J. O'Brien, 1998: Effect of El Niño on US landfalling hurricanes, revisited. Bulletin of the American Meteorological Society, 79(11), 2477–2482.

Cook, A.R., and J. Schaefer, 2008: The relation of El Niño-Southern Oscillation (ENSO) to winter tornado outbreaks. Monthly Weather Review, 136(8), 3121–3137.

Doran, K.J., A.H. Sallenger, B.J. Reynolds, and C. Wright, 2010: Accuracy of EAARL lidar ground elevations using a bare-earth algorithm in marsh and beach grasses on the Chandeleur Islands, Louisiana. U.S Geological Survey Open File Report, 4, 1–13.

Energy Information Administration, 2015: Gulf of Mexico fact sheet. Available online at http://www.eia.gov/special/gulf_of_mexico/data.cfm. Last accessed: 5/19/2018.

Goodbred, S.L., and A.C. Hine, 1995: Coastal storm deposition: salt-marsh response to a severe extratropical storm, March 1993, west-central Florida. Geology, 23(8), 679–682.

Gray, W.M., 1984: Atlantic seasonal hurricane frequency. 1. El-Niño and 30-mb quasi-biennial oscillation influences. Monthly Weather Review, 112(9), 1649–1668.

Hardy, J.W., and S.A. Hsu, 1997: Climatology of winter cyclogenesis intensity in the northwest Gulf of Mexico. National Weather Digest, 22(1), 3–7.

Hsu, S.A., 1993: The Gulf of Mexico – A breeding ground for winter storms. Mariners Weather Log, 37(2), 4–11.

Johnson, G.A., E.A. Meindl, E.B. Mortimer, and J.S. Lynch, 1984: Features associated with repeated strong cyclogenesis in the western Gulf of Mexico during the winter of 1982–83. Postprints: Third Conference on Meteorology of the Coastal Zone, 9–13 January 1984, Miami, Florida, American Meteorological Society, 110–117.

Jones, C., 2000: Occurrence of extreme precipitation events in California and relationships with the Madden-Julian oscillation. Journal of Climate, 13(20), 3576–3587.

Jones, C., J. Gottschalck, L.M. Carvalho, and W. Higgins, 2011: Influence of the Madden-Julian oscillation on forecasts of extreme precipitation in the contiguous United States. Monthly Weather Review, 139(2), 332–350.

Kaiser, M.J., and A.G. Pulsipher, 2007: The impact of weather and ocean forecasting on hydrocarbon production and pollution management in the Gulf of Mexico. Energy Policy, 35(2), 966–983.

Klotzbach, P.J., 2014: The Madden-Julian Oscillation's impacts on worldwide tropical cyclone activity. Journal of Climate, 27(6), 2317–2330.

Lawrence, D.M., and P.J. Webster, 2001: Interannual variations of the intraseasonal oscillation in the South Asian summer monsoon region. Journal of Climate, 14(13), 2910–2922.

Lin, H., G. Brunet, and J. Derome, 2009: An observed connection between the North Atlantic Oscillation and the Madden-Julian oscillation. Journal of Climate, 22(2), 364–380.

Lott, N., 1993: The Big One!: A review of the March 12–14, 1993, "Storm of the Century." National Climatic Data Center, Research Customer Service Group.

Lyle, D., 2005: Experience blunts Katrina's wrath. Exploration & Production, 78(10), 17–19.

Madden, R.A., and P.R. Julian, 1994: Observations of the 40-50-day tropical oscillation-A review. Monthly Weather Review, 122(5), 814–837.

Maloney, E.D., and D.L. Hartmann, 2000: Modulation of hurricane activity in the Gulf of Mexico by the Madden-Julian oscillation. Science, 287(5460), 2002–2004.

Mo, K.C., 1999: Alternating wet and dry episodes over California and intraseasonal oscillations. Monthly Weather Review, 127(12), 2759–2776.

——, 2000: Intraseasonal modulation of summer precipitation over North America. Monthly Weather Review, 128(5), 1490–1505.

Mo, K.C., and R. Higgins, 1998: Tropical convection and precipitation regimes in the western United States. Journal of Climate, 11(9), 2404–2423.

Paganie, D., and P. Buschee, 2005: Operators begin cleanup, repair from Katrina, Rita. Offshore, 65(10), 24–35.

Patricola, C.M., R. Saravanan, and P. Chang, 2014: The impact of the El Niño–Southern Oscillation and Atlantic Meridional Mode on seasonal Atlantic tropical cyclone activity. Journal of Climate, 27(14), 5311–5328.

Ropelewski, C.F., and M.S. Halpert, 1986: North American precipitation and temperature patterns associated with the El Niño/Southern Oscillation (ENSO). Monthly Weather Review, 114(12), 2352–2362.

Saucier, W.J., 1949: Texas-West Gulf Cyclones. Monthly Weather Review, 77(8), 219-231.

Schreck, C., and D. Margolin, 2012: An MJO index for the Western Hemisphere. AGU Fall Meeting Abstracts, 0220.

Stockdon, K.S., K.J. Doran, D.M. Thompson, K.L. Sopkin, N.G. Plant, and A.H. Sallenger, 2012: National Assessment of Hurricane-induced Coastal Erosion Hazards: Gulf of Mexico. Open-file Report 2012–1084, U.S. Geological Survey, U.S. Department of the Interior, 51 pp.

Stone, G.W., B. Liu, D.A. Pepper, and P. Wang, 2004: The importance of extratropical and tropical cyclones on the short-term evolution of barrier islands along the northern Gulf of Mexico, USA. Marine Geology, 210(1–4), 63–78.

Tang, B.H., and J.D. Neelin, 2004: ENSO Influence on Atlantic hurricanes via tropospheric warming. Geophysical Research Letters, 31(24), Art. No. L24204.

# CHAPTER 2. LITERATURE REVIEW

## 2.1 Madden-Julian Oscillation (MJO)

The Madden-Julian Oscillation (MJO) is an intraseasonal cycle of atmospheric turbulence and associated convective precipitation with phases that correspond to the geographical locations of eastward-propagating pulses of intense convection. Roland Madden and Paul Julian – the namesakes of the MJO – stumbled upon the oscillation in 1971 when analyzing zonal wind anomalies in the tropical Pacific. The researchers were examining daily rawinsonde data at Canton Island (3°S, 172°W) when they noticed an oscillation in several atmospheric variables, including zonal winds at 850-hPa and in the upper troposphere, and station pressures (Madden and Julian 1971).

The MJO is the dominant mode of intraseasonal variability in the tropics and has periods of 30-60 days (Madden and Julian 1994). Because of its varying periodicities, it is also sometimes referred to as the 30-50 day (Krishnamurti and Subrahmanyam 1982), 30-60 day (Weickmann *et al.* 1985), or 40-50 day (Madden and Julian 1971) oscillation. A study that simulated the MJO using a series of 37 general circulation models known as the Coupled Model Intercomparison Project phase 5 (CMIP5) models found a mean periodicity around 40 days (Ahn et al. 2017).

At least some of the MJO periodicity variability has been attributed to the state of the El Niño/Southern Oscillation (ENSO) phenomenon. ENSO includes a quasi-periodic (3-7-year) breakdown of the northeast and

southeast trade winds in the "El Niño" phase, which causes the West Pacific Warm Pool near Indonesia to slosh back eastward across the tropical equatorial Pacific Ocean. The opposite phase involves an intensification of the trade winds, which concentrates and intensifies the zone of convection near Indonesia, which central and eastern equatorial Pacific waters remain relatively cool – the La Niña phase. While there are many other implications of this phenomenon, the relationship to the MJO is that the zone of the most intense convection is affected, with a general trend toward a shorter MJO when El Niño is present and a longer-period MJO when La Niña is ongoing (Pohl and Matthews 2007).

The MJO involves fluctuations in wind, SST, rainfall, and cloudiness, but Gruber (1974) provided evidence of eastward-moving cloud clusters associated with the oscillation. Madden and Julian (1971) provided the following observation of their new discovery,

> Summarizing the most fundamental characteristics of the oscillation evident from an analysis of Canton's record, we conclude that it can best be described as [a] large circulation cell oriented in zonal planes rather than as a propagating wave.

Building on Gruber's (1974) discovery, the use of outgoing longwave radiation (OLR) data has been the most often used proxy for tracking the MJO's progress (Knutson *et al.* 1986; Nakazawa 1988). Because tropical rainfall is generally convective and convective cloud tops are cold, use of satellite observations makes it rather simple to track the progress of these temperature-derived OLR anomalies and the MJO. Other researchers and indices have made use of 200-hPa velocity potential as a means of tracking the MJO (Lorenc 1984;

Ventrice et al. 2013). Upper-atmospheric velocity potential is representative of the amount of divergence present, meaning much like OLR, it can also be used as a proxy for convection since upper-tropospheric divergence is generally maximized in areas of building clouds and thunderstorms.

The mechanisms leading to the initiation of convective clusters and MJO events are still poorly understood. It is clear that the MJO is linked to both atmospheric and oceanic processes, but the fluxes that lead to its development remain difficult to simulate (DeMott et al. 2015). The ocean-atmosphere MJO connection is verified by the fact that the climate models that are best at simulating the MJO are those that are coupled. One such model, the ECHAM5-SIT, found that the MJO would increase in amplitude by about 30% by the end of the 21$^{st}$ century under a high emissions warming scenario. It also found that MJO-related precipitation would increase by 17% (Chang et al. 2015). These predicted MJO increases, combined with the knowledge that excess warmth is stored in the oceans in a warming world, would seem to verify the importance of the atmospheric-oceanic connection in the MJO.

For the past decade or so, two indices have commonly been used for tracking the MJO: the Real-time Multivariate (RMM) MJO index (Wheeler and Hendon 2004) and the index developed by NOAA's Climate Prediction Center (CPC; Xue et al. 2002). The Wheeler and Hendon (2004) RMM index is obtained through empirical orthogonal function (EOF) analysis of OLR, and 850- and 200-hPa zonal winds. The RMM index categorizes the MJO into one of eight distinct phases based on the location of the eastward-propagating convective

clusters that are generally found near the equator. The RMM index has been shown to be susceptible to high frequency "noise" (Roundy et al. 2009).

The CPC index uses extended EOF (EEOF) analysis of 200-hPa velocity potential for 15 ENSO-neutral and weak ENSO years during 1979-2000 (Xue et al. 2002). Baxter et al. (2014) found that the CPC index is better at capturing the MJO variability over the U.S., largely because it handles both interannual and subseasonal variability, whereas the Wheeler and Hendon RMM index (2004) is constructed explicitly to remove interannual variability.

Ventrice et al. (2013) created a new variant (VP200) of the Wheeler and Hendon RMM index by replacing OLR with 200-hPa velocity potential. Their research finds that VP200 is better at detecting the MJO signal during boreal summer and also performs better when relating MJO phases to Atlantic tropical cyclone activity. Much of the improved skill of VP200 in these situations is attributed to the fact that 200-hPa velocity potential provides more of a global perspective on upper-atmospheric divergence whereas OLR is better at depicting a regional signal. Conversely, Ventrice et al. (2013) found that their VP200 index is inferior to the RMM index during boreal winter. Additionally, while their index is found to better depict convective patterns in the Western Hemisphere, this comes at the expense of how it depicts those in the Eastern Hemisphere.

Wang and Rui (1990) were the first to show that the main formation region for the convective clusters identified by Gruber (1974) was the west-central equatorial Indian Ocean. Once these convective clusters or circulation

cells form, they propagate eastward across the Pacific and often into the Atlantic. The mechanisms behind this eastward movement are still not well-understood. It is also noteworthy that the OLR anomalies typically become more difficult to track once the oscillation moves into the Atlantic (Madden and Julian 1994).

While one might expect the impacts of the MJO to be confined to the tropics, Anderson and Rosen (1983) showed that some effects of the oscillation can be seen propagating to the midlatitudes. For example, Yasunari (1979) related the MJO to the Indian monsoon. In more recent years, Lawrence and Webster (2001) have also related the oscillation to the south Asian monsoon, while several others have investigated the MJO's connections to precipitation patterns in North America (Mo and Higgins 1998; Mo 1999, 2000; Jones 2000), extreme precipitation events in North America (Jones et al. 2011), U.S. tornado outbreaks (Thompson and Roundy 2013), the North Atlantic Oscillation (NAO; Lin et al. 2009), and the Pacific/North American teleconnection pattern (PNA; Schreck III and Margolin 2012).

## 2.2 The MJO and Tropical Cyclogenesis

Maloney and Hartmann (2000) were among the first to establish a correlation between tropical cyclogenesis in the Gulf of Mexico (GoM) and the MJO. They showed that when the enhanced convection phase of the MJO reaches the eastern Pacific, GoM tropical cyclogenesis becomes four times more likely. This increase in development was largely attributed to low-level westerly wind anomalies propagating into the GoM and producing an increase in

cyclonic vorticity. Gao et al. (2017) recently affirmed these findings using the High Resolution Atmospheric Model (HiRAM) from the Geophysical Fluids Dynamic Laboratory (GFDL). The model simulations not only reproduced the low-level wind anomalies, but they also depicted increases in mid-tropospheric moisture and reductions in low-level wind shear. All of these factors combined are known to be favorable for tropical cyclone (TC) development.

Several other studies have continued to build on the original work of Maloney and Hartmann (2000). TC activity is shown to peak in the Atlantic in conjunction with and immediately following the convectively-active phase of the MJO (Klotzbach 2014; Klotzbach and Oliver 2015; Lim et al. 2016). Minor differences arise in the literature with Lim et al. (2016) finding that TC genesis is more likely during RMM index phases 8 and 1, while Klotzbach (2014) and Klotzbach and Oliver (2015) found correlations with RMM phases 1, 2 and 3. Those same studies have better agreement on the opposite side of the spectrum, consistently finding that tropical genesis is reduced during RMM phases 6 and 7. It was also found that rapid intensification (RI) is more likely during phases 1 and 2 (Klotzbach 2014; Klotzbach and Oliver 2015). Additionally, the convectively-active phase of the MJO was shown to produce not only more favorable atmospheric conditions (increased convergence, increased cyclonic vorticity, decreased wind shear) for tropical cyclogenesis, but also influences steering winds such that more tropical easterly waves propagate into the GoM than straight into the eastern Pacific (Aiyyer and Molinari 2008).

## 2.3 MJO/ENSO Connections

While largely showing a positive correlation with tropical cyclogenesis in its convectively-active phase, the MJO signal can be overwhelmed by interannual and decadal modes of climate variability such as ENSO and the Atlantic Multidecadal Oscillation (AMO), respectively (Klotzbach and Oliver 2015). ENSO's oceanic components – El Niño and La Niña – are characterized by SST anomalies in the central and eastern equatorial Pacific. The warm [cool] phase, El Niño [La Niña], occurs when positive [negative] SST anomalies are present in these regions (Rasmusson and Carpenter 1982; Philander 1990). The AMO is characterized by sea surface temperature (SST) patterns in the Atlantic, with a positive AMO representing positive SST anomalies in much of the tropical and north Atlantic, whereas anomalies of the opposite sign are found in these regions during a negative AMO (Goldenberg et al. 2001). In general, if either El Niño or a negative AMO is present, the MJO alone does not appear capable of generating statistically significant increases in TC activity. In contrast, when La Niña or a positive AMO are present, the MJO influence on tropical cyclogenesis may be enhanced (Klotzbach and Oliver 2015).

Gray (1984) is credited with discovering the link between El Niño and tropical cyclone (TC) frequencies in the Atlantic; specifically, he showed that Atlantic TC frequencies decrease during El Niño events. Numerous studies in subsequent decades (e.g., Bove et al. 1998; Tang and Neelin 2004; Patricola et al. 2014) have supported and expanded on that discovery. Gray (1984)

attributed much of the El Niño negative feedback to increased vertical wind shear, but Tang and Neelin (2004) demonstrated that tropospheric temperature variability related to ENSO may also influence Atlantic TC frequencies. Their work showed that tropospheric column-averaged warm air advected eastward may decrease atmospheric instability in the Atlantic during El Niño events. This ENSO influence is important to note because it is possible that some of the atmospheric variability associated with cyclogenesis may be attributable to both ENSO and the MJO, making it difficult to discern at times which teleconnection pattern is exerting the most influence. For instance, Gray (1984) showed that vertical wind shear related to ENSO influences TC frequencies, but subsequent research has also linked the MJO to TC genesis through modification of vertical wind shear (Klotzbach 2014; Klotzbach and Oliver 2015).

ENSO alone may not be enough to explain interannual TC variability in the Atlantic. The Atlantic meridional mode (AMM) represents the north-south gradient of sea surface temperatures in the Atlantic Ocean and has been shown to also be an important modulator of TC frequencies. A positive [negative] AMM occurs when warm SST anomalies are present in the north [south] Atlantic (Chiang and Vimont 2004). The AMM could easily be confused with the Atlantic Mutidecadal Oscillation (AMO), but the AMM has been shown to influence TC activity on both interannual and decadal scales, while the AMO is limited to decadal influences (Vimont and Kossin 2007). The most active Atlantic hurricane seasons in terms of accumulated cyclone energy (ACE) have

been shown to occur when La Niña and a positive AMM are present concurrently (Patricola et al. 2014). The opposite is not necessarily true when El Niño and a negative AMM are concurrent (Patricola et al. 2014). These are leading modes of variability on interannual and decadal scales, but there are obviously many other influences, including those of the MJO on intra-annual scales.

Not only does ENSO influence Atlantic TC frequencies, the likelihood of U.S. hurricane landfalls is also modulated by its different phases (Bove et al. 1998). Specifically, landfall frequencies increase when La Niña is present and decrease when El Niño is ongoing. However, Kim et al. (2009) identified an El Niño variant that they called 'Modoki' that could actually increase Atlantic TC frequencies. During these 'Modoki' events, SST warming is more focused in the central Pacific rather than the eastern Pacific and increasing TC frequencies and landfalls are noted in the GoM and Central America (Kim et al. 2009). The TC track and frequency variability between traditional El Niño events and 'Modoki' events appears to be largely tied to changes in vertical wind shear across portions of the Atlantic basin. During traditional El Niño events, wind shear is anomalously high over much of the tropical Atlantic, but during 'Modoki' events, wind shear is found to be near-normal in the Atlantic (Kim et al. 2009).

Similar to ENSO, changes in TC landfall frequency have been linked to the MJO. Vitart (2009) noted that the most significant variability in landfall accumulated cyclone energy (ACE) – a measure of landfall risk – was found

around Australia and North America. While North American landfall frequencies as a whole show statistically significant links to certain MJO phases, isolating the data to tropical cyclones forming in the GoM fails to produce the same results (Vitart 2009). Barrett and Leslie (2009) also found links between the MJO and TC landfall, noting that both hurricane and major hurricane landfalls were four times as likely in the north Atlantic basin when the active phase of the MJO was located in the eastern Pacific. Collectively, the research shows that teleconnections such as ENSO and the MJO are not only important factors in cyclogenesis variability but they also exert some influence on cyclone tracks.

### 2.4 ENSO/MJO Links to Winter Cyclogenesis in the GoM

There is a well-established connection between El Niño and winter cyclogenesis in the GoM. In very general terms, El Niño events result in increased frequency of cyclogenesis in the GoM and therefore increased winter precipitation along portions of the U.S. Gulf Coast (Johnson et al. 1984; Hardy and Hsu 1997; Eichler and Higgins 2006; Schubert et al. 2008; Munroe et al. 2014). Seasonal precipitation amounts are shown to increase, but the likelihood of extreme precipitation events is enhanced as ET cyclones become more frequent during El Niño events (Eichler and Higgins 2006). Schubert et al. (2008) obtain similar results using empirical orthogonal function (EOF) analysis, noting that both extratropical (ET) storm intensity and extreme precipitation events are enhanced and more frequent during El Niño events. Munroe et al. (2014) show statistically significant correlations between El

Niño/La Niña and spatial and temporal variability of daily precipitation in and around the GoM. Spatial analysis by Hardy and Hsu (1997) finds that strong ET cyclones are more common in the northwestern GoM during El Niño events.

Little existing research specifically relates the MJO to GoM cyclogenesis, but Guo et al. (2017) examined ET cyclone track variability on a broader scale for the Northern Hemisphere. Their study does not specifically discuss ET cyclone trends in the GoM, but the results do indicate some preference for an increase in cyclonic activity in MJO phases 7, 8 and 1, and possibly lingering into phase 2. In general terms, Guo et al. (2017) attribute much of the Northern Hemispheric ET cyclone variability to the anomalous convective clusters associated with the MJO and a tendency for those clusters to alter the mean atmospheric flow from the tropics into the midlatitudes.

## 2.5 MJO Links to North American Weather and Climate

The convectively-active phase of the MJO has been linked to increased precipitation in the U.S., including an increased threat of extreme precipitation events. Jones et al. (2011) found that when the MJO is active in the Western Hemisphere, Africa and/or the Indian Ocean, extreme precipitation events are more likely. Times when the MJO is active in those specific regions correlate to MJO phases 7, 8 and 1 when using the Wheeler-Hendon RMM index. Their hope is that recognition of certain phases of the MJO will lead to increased predictability and longer lead times for forecasts of potential extreme precipitation events. Curtis (2017) studied the potential for the MJO to drive seasonal precipitation outlooks on a regional scale. While the MJO showed

some predictive skill, it trailed that of ENSO. One challenge that the MJO presents as a regional precipitation forecast tool is that a lag is often noted between the active MJO phases and the downstream impacts. In general, the convective bursts trigger a series of teleconnection chain reactions involving an altering of the Rossby wave pattern and that chain reaction can be difficult to time (Curtis 2017). Zhou et al. (2012) examined region-specific impacts in the U.S. and noted that both temperature and precipitation correlations to the MJO in the U.S. were strongest in the winter months. However, they note that an MJO signature is still evident in precipitation variability during hurricane season.

As noted by Zhou et al. (2012), the consensus among researchers is that MJO impacts in North America are most pronounced in the winter months. A number of studies have focused on region-specific impacts tied to different phases of the MJO (Jones et al. 2004; Lin et al. 2009; Becker et al. 2011; Schreck III and Margolin 2012; Rodney et al. 2013). Much like has been noted with other types of MJO variability, the strongest associations to regional weather and climate are found during its active phases. Specifically, the convectively-active phases are correlated with: cold season daily precipitation in the U.S. (Becker et al. 2011), wintertime surface air temperatures (Rodney et al. 2013), “atmospheric rivers” impacting the U.S. West Coast (Baggett et al. 2017), predictability of key atmospheric variables such as 500-hPa heights (Jones et al. 2004), North Atlantic Oscillation (NAO) amplitude (Lin et al. 2009), and the Pacific/North American (PNA) teleconnection (Schreck III and Margolin

2012). Schreck and Margolin (2012) went so far as to construct a new index, the Multivariate PNA (MVP), to help identify which MJO events will impact North American temperatures through interactions with the PNA teleconnection.

Moon et al. (2012) showed some success in using a case-study methodology, demonstrating a correlation between MJO variability and snowstorms in the eastern U.S. during the winter of 2009-10. They found that when the convectively-active phase of the MJO reached the central Pacific, enhancement in snowfall totals and extreme events over eastern parts of the U.S were more likely. Additionally, they note that an ongoing El Niño event likely aided in providing moisture to the eastern U.S. and enhanced the observed snowfall amounts.

One area garnering more attention in recent years is the apparent link between the MJO and the quasi-biennial oscillation (QBO). The QBO is a stratospheric oscillation of winds alternating between easterly and westerly phases with a period generally a little over two years (Naujokat 1986). Marshall et al. (2017) found that MJO activity is generally stronger during easterly phases of the QBO and that 42% of northern hemisphere winter MJO amplitude variability is explained by the QBO. Baggett et al. (2017) also noted this MJO enhancement by the QBO which in turn can enhance atmospheric rivers along the west coast of North America.

Collectively, the existing literature generally supports the notion of MJO influence on weather and climate not only in the tropics, but well into the

midlatitudes. Previous research has shown correlations between the MJO and GoM TC activity (Maloney and Hartmann 2000) and MJO influences extending even farther north into North America related to variables such as winter temperatures and precipitation (i.e., Becker et al. 2011; Rodney et al. 2013). But convincing evidence that the MJO influences cyclogenesis in the GoM during the cool season appears to be missing in the literature.

Strong ET cyclones in the GoM during the cool season can produce impacts similar to those of TCs, including large monetary losses for the energy industry and significant coastal erosion. Given the dearth of information on intraseasonal influences on ET cyclone development and frequency in this region, it is imperative to investigate possible links to the MJO. Therefore, this study will attempt to bridge this gap by examining potential relationships between specific phases of the MJO and ET development, frequency, and other sensible weather in and around the GoM.

## 2.6 Use of Monte Carlo simulations in Meteorology

Monte Carlo simulation takes on major importance in addressing the research questions listed in Section 1.3. Monte Carlo techniques involve modeling a system affected by randomness (Brandimarte 2014) through the use of repeated random sampling (Gubernatis et al. 2016). The simulations referenced in the following chapters provide pathways to test for statistically significant associations between the MJO and meteorological/climatological variability in the GoM region. There are many variants of Monte Carlo methods in published literature, but the techniques used here mirror those first

established in a study relating the MJO to Australian rainfall and circulation (Wheeler et al. 2009).

The Monte Carlo methods developed by Wheeler et al. (2009) involve establishing two vectors of equal length – the MJO (x) and a response variable (y; e.g., mean daily precipitation). Real-world responses are then calculated for each MJO phase (e.g., y(x)). A simulated random climate can then be generated by shifting the original MJO vector (x) some random amount in time while keeping the response vector (y) untouched. The new shifted MJO vector (x') is created by shifting some random quantity from the bottom of x' to the top and moving the remainder of the vector down to replace what has been shifted. Wheeler et al. (2009) repeated this shift 400 times in their research, but in the chapters that follow, 1,000 shifts (simulations) are performed for each research question. Once the simulations are completed, new response vectors (e.g., y(x')) are calculated and ranked for each MJO phase. The rankings allow for the establishment of a confidence interval, with the $2.5^{th}$ and $97.5^{th}$ percentiles representing the bounds of a 95% confidence interval. If any of the original responses (e.g., y(x)) fall outside of the $2.5^{th}$ and $97.5^{th}$ percentiles in the simulated results (e.g., y(x')), a statistically significant association exists at the 95% level. Figure 2.1 provides a schematic demonstrating the execution of the technique.

Monte Carlo simulation was introduced into scholarly research in the 1940s (Metropolis and Ulam 1949). It has been used in the social sciences (e.g.,

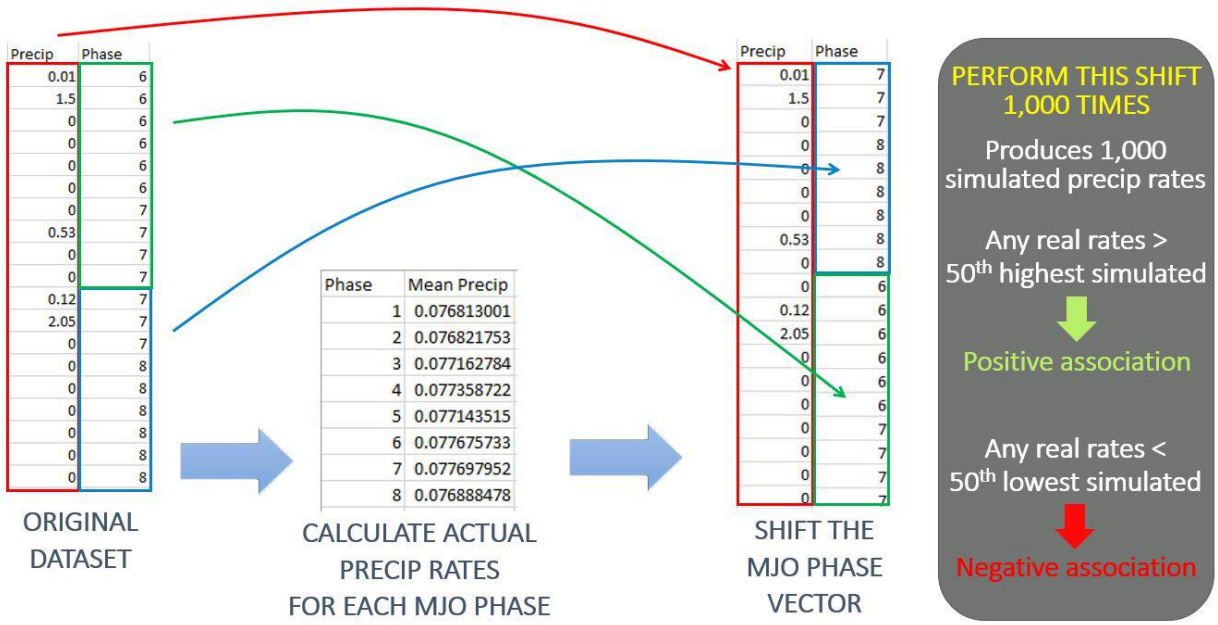


**Figure 2.1.** Schematic demonstrating the Monte Carlo methods developed by Wheeler et al. (2009) that are used in the following chapters.

Hey and Nielsen 2007; Brandimarte 2014) and in the natural sciences (e.g., Wei et al. 2015; Landau and Binder 2014). It has also been used in the atmospheric sciences, such as in circulation type classification (e.g., Philipp et al. 2016), risk of drought occurrence under a changing climate (e.g., Cook et al. 2015), ensemble forecasting (Anderson and Anderson 1999), simulation of snowflake formation (Maruyama and Fujiyoshi 2005), simulation of explosive cyclogenesis (Mullen and Baumhefner 1994), and for estimating tornado impacts (Strader et al. 2016).

The common thread in the studies that utilize Monte Carlo simulation is a need for a technique that uses randomness to estimate some deterministic quantity or outcome. The Monte Carlo simulation techniques described here provide key advantages within the context of studying the MJO, including preserving its autocorrelation structure, avoiding assumptions about

normality, and automatically accounting for the differing number of days in each MJO phase (Wheeler et al. 2009). Some have pointed out limitations or cautions in the use of Monte Carlo simulations. These include the simulations being data intensive (Ferson 2008), the potential for using an improper model of uncertainty (Brandimarte 2014), output estimates being unreliable if sample size is insufficient (Brandimarte 2014), and the simulations only producing probabilistic error bounds (Niederreiter 1992). Despite the disadvantages, the advantages of Monte Carlo simulation for understanding the relationship of the MJO to cyclogenesis, precipitation, and severe weather events make it ideal in this research.

## 2.7 References


Ahn, M.S., D. Kim, K.R. Sperber, I.S. Kang, E. Maloney, D. Waliser, and H. Hendon, 2017: MJO simulation in CMIP5 climate models: MJO skill metrics and process-oriented diagnosis. Climate Dynamics, 49(11–12), 4023–4045.

Aiyyer, A., and J. Molinari, 2008: MJO and tropical cyclogenesis in the Gulf of Mexico and eastern Pacific: Case study and idealized numerical modeling. Journal of the Atmospheric Sciences, 65(8), 2691–2704.

Anderson, J.L., and S.L. Anderson, 1999: A Monte Carlo implementation of the nonlinear filtering problem to produce ensemble assimilations and forecasts. Monthly Weather Review, 127(12), 2741–2758.

Anderson, J.R., and R.D. Rosen, 1983: The latitude-height structure of 40–50 day variations in atmospheric angular-momentum. Journal of the Atmospheric Sciences, 40(6), 1584–1591.

Baggett, C.F., E.A. Barnes, E.D. Maloney, and B.D. Mundhenk, 2017: Advancing atmospheric river forecasts into subseasonal-to-seasonal timescales. Geophysical Research Letters, 44(14), 7528–7536.

Barrett, B.S., and L.M. Leslie, 2009: Links between tropical cyclone activity and Madden–Julian oscillation phase in the North Atlantic and northeast Pacific basins. Monthly Weather Review, 137(2), 727–744.

Baxter, S., S. Weaver, J. Gottschalck, and Y. Xue, 2014: Pentad evolution of wintertime impacts of the Madden-Julian Oscillation over the contiguous United States. Journal of Climate, 27(19), 7356–7367.

Becker, E.J., E.H. Berbery, and R.W. Higgins, 2011: Modulation of cold-season US daily precipitation by the Madden-Julian Oscillation. Journal of Climate, 24(19), 5157–5166.

Bove, M.C., J.B. Elsner, C.W. Landsea, X.F. Niu, and J.J. O'Brien, 1998: Effect of El Niño on US landfalling hurricanes, revisited. Bulletin of the American Meteorological Society, 79(11), 2477–2482.

Brandimarte, P., 2014: Handbook in Monte Carlo Simulation: Applications in Financial Engineering, Risk Management, and Economics. John Wiley & Sons.

Chang, C.W.J., W.L. Tseng, H.H. Hsu, N. Keenlyside, and B.J. Tsuang, 2015: The Madden-Julian Oscillation in a warmer world. Geophysical Research Letters, 42(14), 6034–6042.

Chiang, J.C., and D.J. Vimont, 2004: Analogous Pacific and Atlantic Meridional Modes of tropical atmosphere-ocean variability. Journal of Climate, 17(21), 4143–4158.

Cook, B.I., T.R. Ault, and J.E. Smerdon, 2015: Unprecedented 21st century drought risk in the American Southwest and Central Plains. Science Advances, 1(1), e1400082.

Curtis, S., 2017: The Madden-Julian Oscillation: A tool for regional seasonal precipitation outlooks? Atmosphere, 8(9), 180.

DeMott, C.A., N.P. Klingaman, and S.J. Woolnough, 2015: Atmosphere-ocean coupled processes in the Madden-Julian oscillation. Reviews of Geophysics, 53(4), 1099–1154.

Eichler, T., and W. Higgins, 2006: Climatology and ENSO-related variability of North American extratropical cyclone activity. Journal of Climate, 19(10), 2076–2093.

Ferson, S., 2008: What Monte Carlo methods cannot do. Human and Ecological Risk Assessment: An International Journal, 2(4), 990–1007.

Gao, K., J.H. Chen, L.M. Harris, S.J. Lin, B. Xiang, and M. Zhao, 2017: Impact of Intraseasonal Oscillations on the tropical cyclone activity over the Gulf of Mexico and western Caribbean Sea in GFDL HiRAM. Journal of Geophysical Research: Atmospheres, 122(24), 13125–13137.

Goldenberg, S.B., C.W. Landsea, A.M. Mestas-Nuñez, and W.M. Gray, 2001: The recent increase in Atlantic hurricane activity: Causes and implications. Science, 293(5529), 474–479.

Gray, W.M., 1984: Atlantic seasonal hurricane frequency. 1. El-Niño and 30-mb quasi-biennial oscillation influences. Monthly Weather Review, 112(9), 1649–1668.

Gruber, A., 1974: The wavenumber-frequency spectra of satellite-measured brightness in the tropics. Journal of the Atmospheric Sciences, 31(6), 1675–1680.

Gubernatis, J., N. Kawashima, and P. Werner, 2016: Quantum Monte Carlo Methods: Algorithms for Lattice Models. Cambridge: Cambridge University Press.

Guo, Y., T. Shinoda, J. Lin, and E.K. Chang, 2017: Variations of northern hemisphere storm track and extratropical cyclone activity associated with the Madden–Julian Oscillation. Journal of Climate, 30(13), 4799–4818.

Hardy, J.W., and S.A. Hsu, 1997: Climatology of winter cyclogenesis intensity in the northwest Gulf of Mexico. National Weather Digest, 22(1), 3–7.

Hey, J., and R. Nielsen, 2007: Integration within the Felsenstein equation for improved Markov chain Monte Carlo methods in population genetics. Proceedings of the National Academy of Sciences, 104(8), 2785–2790.

Johnson, G.A., E.A. Meindl, E.B. Mortimer, and J.S. Lynch, 1984: Features associated with repeated strong cyclogenesis in the western Gulf of Mexico during the winter of 1982–83. Postprints: Third Conference on Meteorology of the Coastal Zone, 9–13 January 1984, Miami, Florida, American Meteorological Society, 110–117.

Jones, C., 2000: Occurrence of extreme precipitation events in California and relationships with the Madden-Julian oscillation. Journal of Climate, 13(20), 3576–3587.

Jones, C., D.E. Waliser, K.M. Lau, and W. Stern, 2004: The Madden-Julian oscillation and its impact on Northern Hemisphere weather predictability. Monthly Weather Review, 132(6), 1462–1471.

Jones, C., J. Gottschalck, L. M. Carvalho, and W. Higgins, 2011: Influence of the Madden-Julian oscillation on forecasts of extreme precipitation in the contiguous United States. Monthly Weather Review, 139(2), 332–350.

Kim, H.-M., P.J. Webster, and J.A. Curry, 2009: Impact of shifting patterns of Pacific Ocean warming on North Atlantic tropical cyclones. Science, 325(5936), 77–80.

Klotzbach, P.J., 2014: The Madden-Julian Oscillation's impacts on worldwide tropical cyclone activity. Journal of Climate, 27(6), 2317–2330.

Klotzbach, P.J., and E.C. Oliver, 2015: Modulation of Atlantic basin tropical cyclone activity by the Madden–Julian Oscillation (MJO) from 1905 to 2011. Journal of Climate, 28(1), 204–217.

Knutson, T.R., K.M. Weickmann, and J.E. Kutzbach, 1986: Global-scale intraseasonal oscillations of outgoing longwave radiation and 250 mb zonal wind during Northern Hemisphere summer. Monthly Weather Review, 114(3), 605–623.

Krishnamurti, T.N., and D. Subrahmanyam, 1982: The 30-50 day mode at 850 mb during MONEX. Journal of the Atmospheric Sciences, 39(9), 2088–2095.

Landau, D.P., and K. Binder, K. 2014: A guide to Monte Carlo simulations in statistical physics. Cambridge University Press.

Lawrence, D.M., and P.J. Webster, 2001: Interannual variations of the intraseasonal oscillation in the South Asian summer monsoon region. Journal of Climate, 14(13), 2910–2922.

Lim, Y.K., S.D. Schubert, O. Reale, A.M. Molod, M.J. Suarez, and B.M. Auer, 2016: Large-scale controls on Atlantic tropical cyclone activity on seasonal time scales. Journal of Climate, 29(18), 6727–6749.

Lin, H., G. Brunet, and J. Derome, 2009: An observed connection between the North Atlantic Oscillation and the Madden-Julian oscillation. Journal of Climate, 22(2), 364–380.

Lorenc, A.C., 1984: The evolution of planetary-scale 200 mb divergent flow during the FGGE year. Quarterly Journal of the Royal Meteorological Society, 110(464), 427–441.

Madden, R.A., and P.R. Julian, 1971: Detection of a 40-50 day oscillation in the zonal wind in the tropical Pacific. Journal of the Atmospheric Sciences, 28(5), 702–708.

——, 1994: Observations of the 40–50-day tropical oscillation-A review. Monthly Weather Review, 122(5), 814–837.

Maloney, E.D., and D.L. Hartmann, 2000: Modulation of hurricane activity in the Gulf of Mexico by the Madden-Julian oscillation. Science, 287(5460), 2002–2004.

Marshall, A.G., H.H. Hendon, S.W. Son, and Y. Lim, 2017: Impact of the quasi-biennial oscillation on predictability of the Madden–Julian oscillation. Climate Dynamics, 49(4), 1365–1377.

Maruyama, K.I., and Y. Fujiyoshi, 2005: Monte Carlo simulation of the formation of snowflakes. Journal of the Atmospheric Sciences, 62(5), 1529–1544.

Metropolis, N., and S. Ulam, 1949: The Monte Carlo method. Journal of the American Statistical Association, 44(247), 335–341.

Mo, K.C., 1999: Alternating wet and dry episodes over California and intraseasonal oscillations. Monthly Weather Review, 127(12), 2759–2776.

——, 2000: Intraseasonal modulation of summer precipitation over North America. Monthly Weather Review, 128(5), 1490–1505.

Moon, J.-Y., B. Wang, and K.-J. Ha, 2012: MJO modulation on 2009/10 winter snowstorms in the United States. Journal of Climate, 25(3), 978–991.

Mo, K.C., and R. Higgins, 1998: Tropical convection and precipitation regimes in the western United States. Journal of Climate, 11(9), 2404–2423.

Mullen, S.L., and D.P. Baumhefner, 1994: Monte Carlo simulations of explosive cyclogenesis. Monthly Weather Review, 122(7), 1548–1567.

Munroe, R., T. Crawford, and S. Curtis, 2014: Geospatial analysis of space-time patterning of ENSO forced daily precipitation distributions in the Gulf of Mexico. Professional Geographer, 66(1), 91–101.

Nakazawa, T., 1988: Tropical super clusters within intraseasonal variations over the western Pacific. Journal of the Meteorological Society of Japan, 66(6), 823–839.

Naujokat, B., 1986: An update of the observed quasi-biennial oscillation of the stratospheric winds over the tropics. Journal of the Atmospheric Sciences, 43(17), 1873–1877.

Niederreiter, H., 1992: Random number generation and quasi-Monte Carlo methods (Vol. 63). Siam.

Patricola, C.M., R. Saravanan, and P. Chang, 2014: The impact of the El Niño–Southern Oscillation and Atlantic Meridional Mode on seasonal Atlantic tropical cyclone activity. Journal of Climate, 27(14), 5311–5328.

Philander, S.G.H., 1990: El Niño, La Niña, and the Southern Oscillation. International Geophysics Series, Academic Press, San Diego

Philipp, A., C. Beck, R. Huth, and J. Jacobeit, 2016: Development and comparison of circulation type classifications using the COST 733 dataset and software. International Journal of Climatology, 36(7), 2673-2691.

Pohl, B., and A.J. Matthews, 2007: Observed changes in the lifetime and amplitude of the Madden–Julian oscillation associated with interannual ENSO sea surface temperature anomalies. Journal of Climate, 20(11), 2659–2674.

Rasmusson, E.M., and T.H. Carpenter, 1982: Variations in tropical sea surface temperature and surface wind fields associated with the Southern Oscillation/El Niño. Monthly Weather Review, 110(5), 354–384.

Rodney, M., H. Lin, and J. Derome, 2013: Subseasonal prediction of wintertime North American surface air temperature during strong MJO events. Monthly Weather Review, 141(8), 2897–2909.

Roundy, P.E., C.J. Schreck III, and M.A. Janiga, 2009: Contributions of convectively coupled equatorial Rossby waves and Kelvin waves to the real-time multivariate MJO indices. Monthly Weather Review, 137(1), 469–478.

Schreck, C., and D. Margolin, 2012: An MJO index for the Western Hemisphere. AGU Fall Meeting Abstracts, 0220.

Schubert, S.D., Y. Chang, M.J. Suarez, and P.J. Pegion, 2008: ENSO and wintertime extreme precipitation events over the contiguous United States. Journal of Climate, 21(1), 22–39.

Strader, S.M., T.J. Pingel, and W.S. Ashley, 2016: A Monte Carlo model for estimating tornado impacts. Meteorological Applications, 23(2), 269–281.

Tang, B.H., and J.D. Neelin, 2004: ENSO Influence on Atlantic hurricanes via tropospheric warming. Geophysical Research Letters, 31(24), Art. No. L24204.

Thompson, D.B., and P.E. Roundy, 2013: The relationship between the Madden-Julian oscillation and US violent tornado outbreaks in the spring. Monthly Weather Review, 141(6), 2087–2095.

Ventrice, M.J., M.C. Wheeler, H.H. Hendon, C.J. Schreck III, C.D. Thorncroft, and G.N. Kiladis, 2013: A modified multivariate Madden–Julian oscillation index using velocity potential. Monthly Weather Review, 141(12), 4197–4210.

Vimont, D. J., and J.P. Kossin, 2007: The Atlantic meridional mode and hurricane activity. Geophysical Research Letters, 34(7), Art. No. L07709.

Vitart, F., 2009: Impact of the Madden Julian Oscillation on tropical storms and risk of landfall in the ECMWF forecast system. Geophysical Research Letters, 36(15), Art. No. L15802.

Wang, B., and H. Rui, 1990: Synoptic climatology of transient tropical intraseasonal convection anomalies: 1975–1985. Meteorology and Atmospheric Physics, 44(1–4), 43–61.

Wei, Z., Z. Yao, C. Lan, J. Chen, Y. Yan, Y. Shi, and J. Wang, 2015: Monte Carlo simulation of fission yields, kinetic energy, fission neutron spectrum and decay γ-ray spectrum for 232Th (n, f) reaction induced by 3H (d, n) 4He neutron source. Journal of Radioanalytical and Nuclear Chemistry, 305(2), 455-462.

Weickmann, K.M., G.R. Lussky, and J.E. Kutzbach, 1985: Intraseasonal (30-60 day) fluctuations of outgoing longwave radiation and 250 mb streamfunction during northern winter. Monthly Weather Review, 113(6), 941–961.

Wheeler, M.C., and H.H. Hendon, 2004: An all-season real-time multivariate MJO index: Development of an index for monitoring and prediction. Monthly Weather Review, 132(8), 1917–1932.

Wheeler, M.C., H.H. Hendon, S. Cleland, H. Meinke, and A. Donald, 2009: Impacts of the Madden–Julian oscillation on Australian rainfall and circulation. Journal of Climate, 22(6), 1482–1498.

Xue, Y., W. Higgins, and V. Kousky, 2002: Influences of the Madden Julian Oscillations on temperature and precipitation in North America during ENSO-neutral and weak ENSO winters. Proc. Workshop on Prospects for Improved Forecasts of Weather and Short-Term Climate Variability on Subseasonal (2 Week to 2 Month) Time Scales.

Yasunari, T., 1979: Cloudiness fluctuations associated with the Northern Hemisphere summer monsoon. Journal of the Meteorological Society of Japan, 57(3), 227–242.

Zhou, S.T., M. L'Heureux, S. Weaver, and A. Kumar, 2012: A composite study of the MJO influence on the surface air temperature and precipitation over the Continental United States. Climate Dynamics, 38(7–8), 1459–1471.

# CHAPTER 3. COOL SEASON CYCLOGENESIS IN THE GULF OF MEXICO AND THE MADDEN-JULIAN OSCILLATION

## 3.1 Introduction

Tropical and extratropical cyclogenesis can have significant impacts on both terrestrial and marine areas in and around the Gulf of Mexico (GoM). The resultant cyclones can produce damaging winds, destructive waves, storm surge, flooding rainfall, and meteotsunami (Pattiaratchi and Wijeratne 2015). The northern GoM presents a particularly high financial exposure and risk, serving as one of the world's busiest petroleum production and refining regions (Kaiser and Pulsipher 2007). The region's vulnerability was exposed during the summer of 2005 when the energy industry sustained an estimated $35 to $60 billion in losses largely driven by Hurricanes Katrina and Rita (Lyle 2005; Paganie and Buschee 2005). The financial hit was in turn passed on to consumers throughout the U.S., with the average price of a gallon of gasoline soaring about 60 cents during the week of Hurricane Katrina (Lewis 2009). Disruptions in oil production caused by Katrina were only exacerbated when Rita impacted the same region about a month later. Roughly half of the refining capacity and two-thirds of the oil production capacity in the GoM region were shut down for more than a month in the wake of Rita (Lewis 2009), keeping gasoline prices high well after the pair of hurricanes had impacted the heart of the U.S. energy industry.

Considerable literature exists on tropical cyclogenesis in the GoM. Particular emphasis has been placed on its links to the El Niño-Southern

Oscillation (ENSO; i.e., Gray 1984; Bove et al. 1998; Tang and Neelin 2004; Patricola et al. 2014) phenomenon and the Madden-Julian Oscillation (MJO; i.e., Maloney and Hartmann 2000; Aiyyer and Molinari 2008; Klotzbach 2014). However, less research has focused on GoM cyclogenesis in the cool season (fall/winter).

Strong cool season extratropical cyclones can have impacts rivaling those that are tropical in nature. The so-called "1993 Superstorm" provides an example of an extratropical cyclone that resulted in extreme impacts throughout and beyond the GoM region. The storm produced snowfall, other forms of winter precipitation, and hurricane-force wind gusts, resulting in record low temperatures, widespread power outages, and accelerated coastal erosion along the fragile coastal zone (Schumann et al. 1995) with wider impacts along and beyond the Gulf Coast. The 1993 Superstorm also resulted in more than 200 fatalities in the U.S., with approximately 60 of those occurring in states bordering the GoM (Lott 1993). While extratropical cyclone impacts on the GoM region are not nearly as well-documented as those of tropical cyclones, it seems fair to assume that well-developed, mature extratropical cyclones in the GoM may produce similar impacts. It also seems prudent to explore the possible causes of cool season extratropical cyclone variability knowing that they can have far-reaching impacts extending well beyond the GoM region.

The ongoing focus on climate change and its potential future impacts also calls for a need to understand the mechanisms producing extratropical

cyclone variability. While there is a significant effort to model future climate and possible changes, those efforts might prove futile if current processes are poorly understood. One review of current literature found that the model consensus actually points toward an overall reduction in extratropical cyclone frequency along the East Coast of the U.S., but that the frequency of the more intense cyclones and heavy precipitation might actually increase (Colle et al. 2015). While the focus of Colle et al.'s (2015) review is on East Coast cyclones, their results show that one of three preferred scenarios for East Coast impacts is from cyclogenesis events occurring in the GoM. Collectively, the ongoing uncertainty about what drives cool season extratropical cyclone frequency variability around the GoM along with the interest in predicting future variability support further exploring possible associations with synoptic-scale modes of atmospheric variability.

One possible cause of the destructive cool season extratropical cyclones is convective variability associated with the MJO. The MJO is characterized by convective clusters that track eastward near the equator. One frequently used method for tracking those clusters is analysis of outgoing longwave radiation (OLR) anomalies. Negative (positive) anomalies represent areas of enhanced (suppressed) convection. Using the RMM index, the clusters propagate from the Western Hemisphere and Africa in Phase 1, to the Indian Ocean in Phases 2 and 3, to near the Maritime Continent in Phases 4 and 5, through the western and central Pacific in Phases 6 and 7, and into the eastern Pacific and Atlantic in Phase 8 (Figure 3.1). The magnitude of the anomalies is often greatest in the

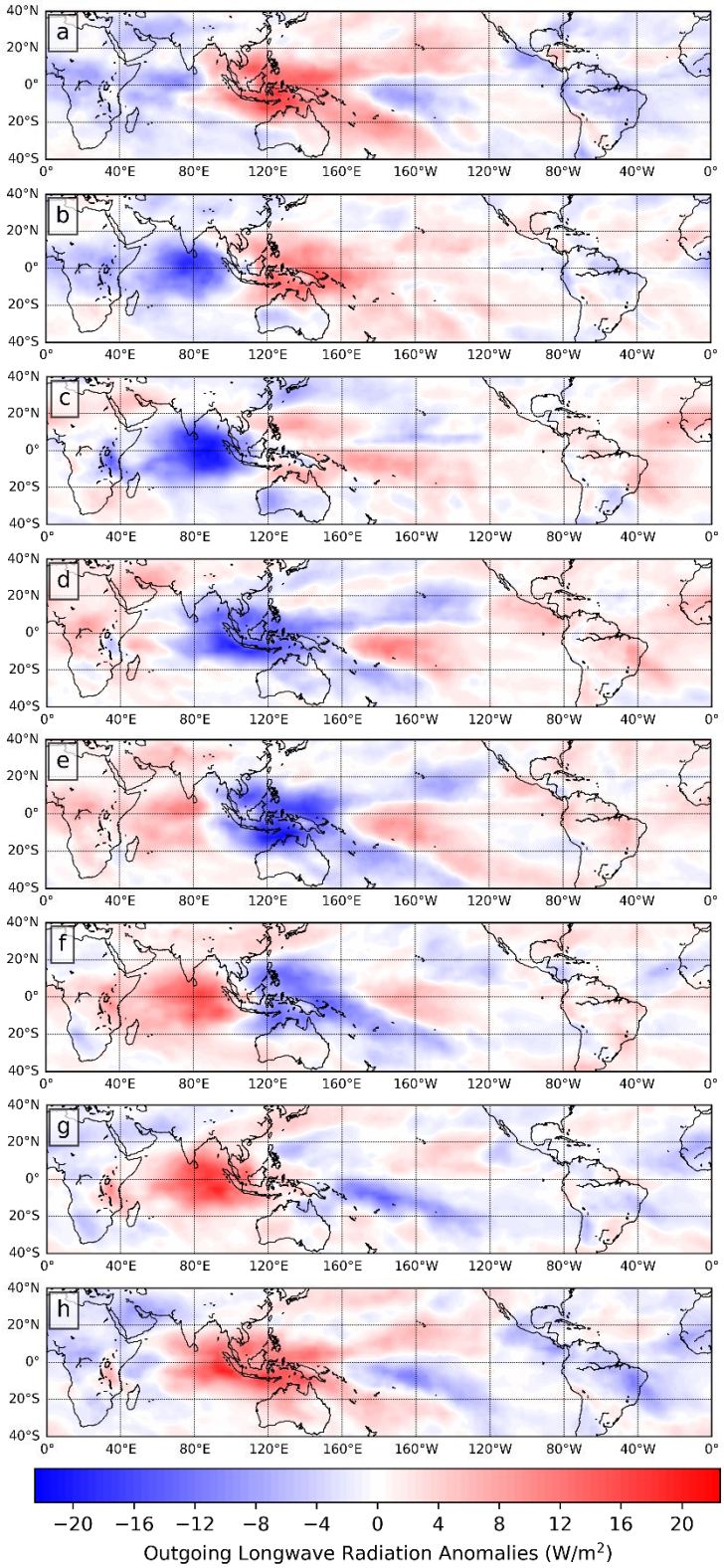


**Figure 3.1** Outgoing longwave radiation anomalies (OLR) for each MJO Phases 1-8 (a-h) from 1979-2014. Anomalies are based on the NCEP/NCAR Reanalysis 1981–2010 mean.

vicinity of the Indian Ocean and Maritime Continent (Phases 3-5), while the MJO can sometimes become difficult to track in the eastern Pacific or Atlantic basins.

The MJO has long been accepted as the dominant mode of intraseasonal variability in the tropics (Madden and Julian 1994). Since that initial discovery, impacts of the MJO have been shown to extend well beyond the tropics. For instance, even though the MJO amplitude is often weaker in the eastern Pacific and Atlantic, it has been linked to variability in North American precipitation (Mo and Higgins 1998; Mo 1999, 2000; Jones 2000; Jones et al. 2011), the North Atlantic Oscillation (NAO; Lin et al. 2009), and the Pacific/North American teleconnection pattern (PNA; Schreck and Margolin 2012). Given these established linkages, any attempt to understand GoM cool season cyclone variability must give some consideration to the MJO.

### 3.2 Data and Methods

This study analyzes extratropical cyclogenesis in the GoM during the cool season to examine possible links to the MJO. The period of analysis is 1 October through 31 March beginning on 1 October 1979–and ending on 31 March 2014, coinciding with an available dataset of Northern Hemisphere surface cyclones produced by researchers at the National Snow and Ice Data Center (NSIDC; Crawford and Serreze 2016). Cyclogenesis days in the GoM are categorized by MJO phase and intensity and then analyzed for statistical correlations, represented by increased or decreased frequencies, to the MJO phase for that date as indicated by the Real-time Multivariate (RMM) index

developed by Wheeler and Hendon (2004). Rather than use simple Pearson or Spearman product-moment correlation analysis in this study statistical testing is done through the use of Monte Carlo simulations. Wheeler et al. (2009) note several advantages to Monte Carlo simulations including maintaining the autocorrelation structure of the MJO, it makes no assumptions about normality, and it automatically accounts for the differing number of days in each MJO phase.

An online archive of the index is available from 1974 to present via the Centre for Australian Weather and Climate Research (CAWCR 2018). The RMM MJO index was derived through empirical orthogonal function (EOF; Wheeler and Hendon 2004) techniques based on the analysis of 850-hPa zonal (east-west) winds, 200-hPa zonal winds, and outgoing longwave radiation (OLR) data (Wheeler and Hendon 2004). Using phase space diagrams, Wheeler and Hendon (2004) defined eight separate phases of the MJO as it typically propagates eastward around the globe (Figure 3.2). The online archive provides not only absolute values of the daily RMM MJO index, but also the corresponding phase number.

The surface cyclone dataset is obtained directly from researchers at NSIDC. Cyclones for this dataset are identified using the Modern-Era Retrospective Analysis for Research and Applications (MERRA) developed and maintained by the National Aeronautics and Space Administration (NASA). Cyclogenesis events are identified in the NSIDC dataset using 3-hourly sea-level pressure data available from MERRA (Crawford and Serreze 2016), but for

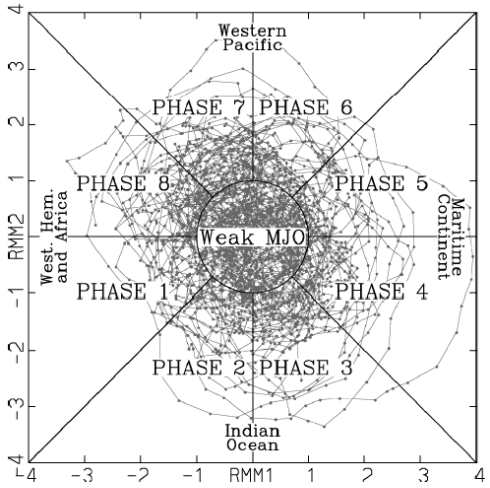


FIG. 7. (RMM1, RMM2) phase space points for all available days in DJF season from 1974 to 2003. Eight defined regions of the phase space are labeled, as is the region considered to signify weak MJO activity. Also labeled are the approximate locations of the enhanced convective signal of the MJO for that location of the phase space, e.g., the "Indian Ocean" for phases 2 and 3.

**Figure 3.2** Figure 7 from Wheeler and Hendon (2004).


the purposes of this study, it is only necessary to know the formation dates of cyclones in and around the GoM. This study uses a subset of the NSIDC cyclone dataset bounded by 19.0°N – 33.0°N, and 80°W – 100°W, to focus on the area of interest around the GoM. The original subset contained 273 cyclones within that region, but a cross-check against annual tropical cyclone events removes 12 cyclones, leaving only cool season, extratropical cyclones. Additional filtering is performed because the original dataset captured cyclones *passing through* the bounding box whereas this study focuses simply on the location at cyclogenesis for extratropical cyclones. That additional level of filtering then reduces the extratropical cyclone frequency to 136, or approximately 3.9 per season. Genesis locations are distributed throughout the GoM region, but, not surprisingly, with greater frequencies in the northern half of the study area (Figure 3.3).

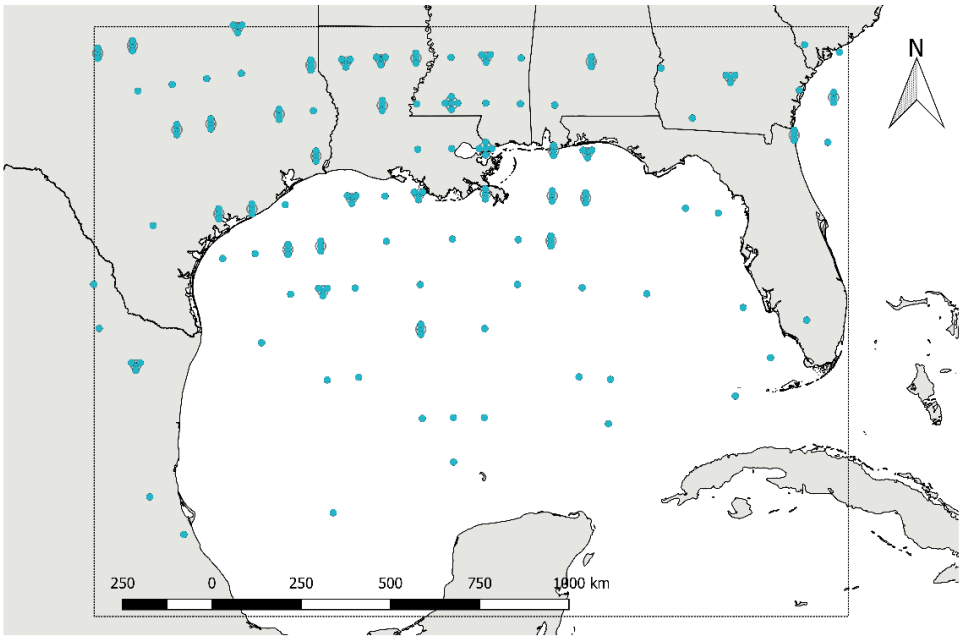


**Figure 3.3** Genesis locations for extratropical cyclones (Oct–Mar) for the period 1979–2014 for all MJO amplitudes.

A final level of filtering is performed to remove cyclogenesis events occurring on days when the Wheeler-Hendon MJO index is less than 1. The MJO is generally considered to be weak when the amplitude is less than 1 and many prior studies have excluded these "weak" MJO days from analysis (i.e., Wheeler et al. 2009; Thompson and Roundy 2013; Klotzbach and Oliver 2015). This final reduction of the original dataset leaves 82 cyclogenesis events in the study area during the 1979–2014 study period. These events are concentrated in the northwestern GoM region, but with representation across most of the area (Figure 3.4).

Both subsets of extratropical cyclones identified through the NSIDC dataset – those forming during any MJO amplitude and those forming only

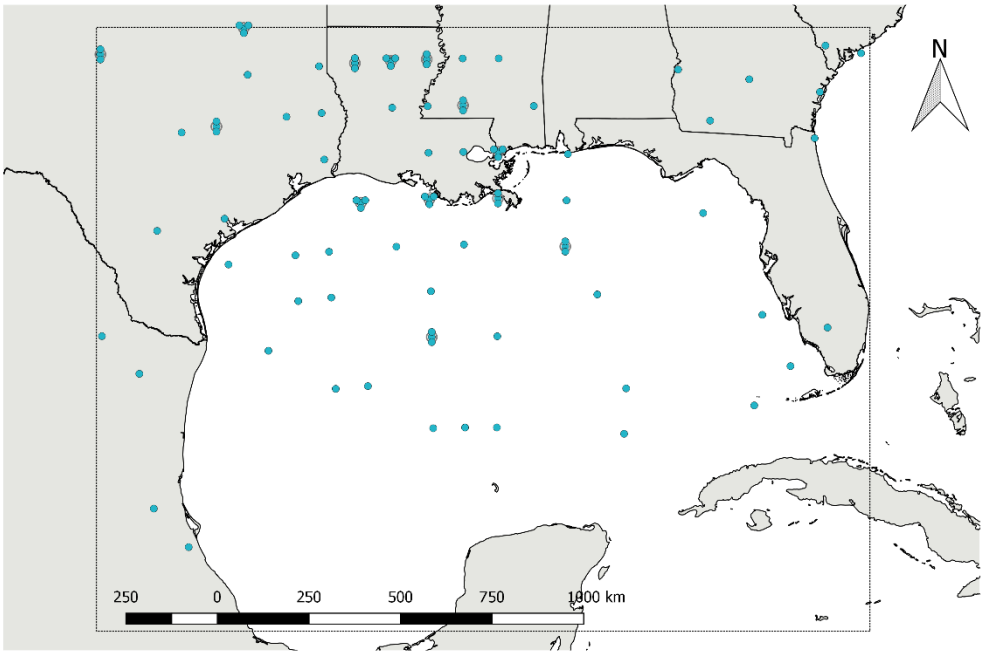


**Figure 3.4** Formation locations for extratropical cyclones (Oct–Mar) for the period 1979–2014 for MJO amplitudes ≥1.

when the MJO index ≥1 -- are then each assigned a value of 1–8 corresponding to the MJO phase on cyclogenesis date as shown by the RMM index.

Monte Carlo simulations (Mooney 1997) are then conducted to test for randomness. More specifically, the null hypothesis is that there is no association between RMM MJO phase and cyclogenesis. To run the Monte Carlo simulations, extratropical cyclogenesis rates had to be calculated for each MJO phase. Three columns of data were constructed – a series of dates from 1 Jan 1979 through 30 Dec 2014, the corresponding MJO phase for each date, and a column with a series of zeros and ones whereby a zero represents no cyclogenesis on that date and one indicates a cyclogenesis event. Cyclone formation rates are then calculated by simply dividing the number of days in a particular MJO phase that had cyclogenesis by the total number of days in that

MJO phase during the study period. Table 3.1 shows that in the "all amplitudes" analysis, all phases have cyclogenesis rates below 3.1 percent, with Phases 8 and 4 as the most and least frequent phases for extratropical cyclogenesis, respectively. Similarly, for the "≥1" analysis, Phases 7 and 4 are the most and least frequent phases for extratropical cyclogenesis, respectively, with Phase 8 following closely behind Phase 7 (see again Table 3.1). Note that the values increase in some phases for the "≥1" analysis because the frequencies are divided by the number of days with RMM MJO ≥1.

**Table 3.1** Cyclogenesis rates by MJO phase for all MJO amplitudes and for MJO amplitudes ≥1.

| All MJO Amplitudes (136 cyclones) | | | | | MJO Amplitude ≥1 (82 cyclones) | | | |
|---|---|---|---|---|---|---|---|---|
| Phase | # days | # cyclones | Rate | | Phase | # days | # cyclones | Rate |
| 1 | 719 | 15 | 0.021 | | 1 | 450 | 5 | 0.011 |
| 2 | 803 | 21 | 0.026 | | 2 | 508 | 14 | 0.028 |
| 3 | 845 | 24 | 0.028 | | 3 | 568 | 17 | 0.030 |
| 4 | 824 | 8 | 0.010 | | 4 | 492 | 4 | 0.008 |
| 5 | 848 | 11 | 0.013 | | 5 | 504 | 2 | 0.004 |
| 6 | 860 | 9 | 0.010 | | 6 | 564 | 6 | 0.011 |
| 7 | 913 | 25 | 0.027 | | 7 | 573 | 19 | 0.033 |
| 8 | 749 | 23 | 0.031 | | 8 | 479 | 15 | 0.031 |

After actual formation rates are calculated, 1,000 simulations were constructed. The 1,000 simulation columns are obtained by using a combination of the "INDIRECT" and "RANDBETWEEN" functions in Excel. Those functions randomly choose a value (0 or 1) from the column created toshow cyclogenesis on a given date, with the percentage of "1" values

corresponding to the simulated percentage frequency. Next, a unique series of randomly chosen zeroes and ones are applied to each simulation column. These values are then used to calculate a simulated cyclogenesis rate based on the dataset provided. Those simulations allow for the establishment of confidence intervals constructed from the results. Because 1,000 simulations are used, the 950$^{th}$ highest and 50$^{th}$ highest simulated values are used to represent a 90% confidence interval. The 975$^{th}$ highest and 25$^{th}$ highest are used to represent a 95% confidence interval.

The actual formation rates are then compared to the confidence intervals generated by the Monte Carlo simulations to test for statistical significance. Using the simulated 95% confidence interval as an example, any real-world cyclogenesis rates exceeding the 975$^{th}$ highest simulated value would represent a significant positive association between MJO phase and cyclogenesis at 95% confidence. Any real-world cyclogenesis rates below the 25$^{th}$ lowest simulated value would represent a significant negative association between MJO phase and cyclogenesis at the 95% level.

The Monte Carlo simulations are constructed separately for extratropical cyclogenesis events in the GoM regardless of MJO amplitude and only for those days when the MJO amplitude exceeds 1.0. Additionally, results are reported for both 90% and 95% confidence intervals in each scenario. The use of 90% confidence intervals is included in this analysis for two primary reasons: 1) the sample size for cyclogenesis events is relatively small and, 2) MJO phases as identified by the RMM index are discrete but it is assumed that there is the

potential in some occasions for a lag between a particular phase and a cyclogenesis event. It is recognized that there is an increased chance for spurious results when using a 90% confidence interval since Type I error increases to 0.10.

### 3.3 Results

A summary of the final results for both the 90% and 95% confidence intervals is shown in Table 3.2 below. When testing all events regardless of MJO amplitude, cool season cyclones are found to be less frequent during MJO Phases 4 and 6 at both the 90% and 95% confidence levels. Cyclogenesis is found to be more frequent during MJO Phase 8 at the 90% confidence level.

**Table 3.2** Monte Carlo simulation results for cyclogenesis events during any MJO amplitude. Green (red) shading indicates a significant positive (negative) association at the 90% level (*) or 95% level (**) between cyclogenesis frequency and that particular MJO phase.

| Phase | Cyclogenesis Rates |
|---|---|
| 1 | 0.020862 |
| 2 | 0.026152 |
| 3 | 0.028402 |
| 4 | 0.009709** |
| 5 | 0.012972 |
| 6 | 0.010465** |
| 7 | 0.027382 |
| 8 | 0.030708* |

Narrowing the sample size down to those days when the MJO amplitude was ≥1 produces some similar results but also shows some different associations. As in the case of all MJO days, a negative association appears for MJO Phase 4 and a positive association for Phase 8. However, the results also show a negative association for Phase 5 and a positive association for Phase 7. When narrowing it down to a 95% confidence interval, the only association that retains statistical significance is that of Phase 5 (Table 3.3).

**Table 3.3** Monte Carlo simulation results for cyclogenesis events when MJO amplitude ≥1. Green (red) shading indicates a significant positive (negative) association at the 90% level (*) or 95% level (**) between cyclogenesis frequency and that particular MJO phase.

| Phase | Cyclogenesis Rates |
|---|---|
| 1 | 0.011111 |
| 2 | 0.027559 |
| 3 | 0.02993 |
| 4 | 0.00813* |
| 5 | 0.003968** |
| 6 | 0.010638 |
| 7 | 0.033159* |
| 8 | 0.031315* |

The results obtained here corroborate other studies that have examined links between the MJO and North American/Northern Hemispheric weather and climate variability. In simplest terms, GoM cyclogenesis is most frequent during MJO Phases 7, 8, 1, 2, and 3 with a notable decrease during Phases 4, 5, and 6 (Figure 3.5). More specifically, Guo et al. (2017) examined

extratropical cyclone variability at a broader scale, looking at the entire Northern Hemisphere for the same period, 1979–2014. Figure 5 from their paper shows similar frequency variability by MJO phase as that shown in Figure 3.5 here. Additionally, Jones et al. (2011) found that extreme precipitation events are more likely in the U.S. during MJO Phases 7, 8, and 1 which again fits the general pattern shown here of increased storminess poleward of the tropics during those particular phases of the MJO.

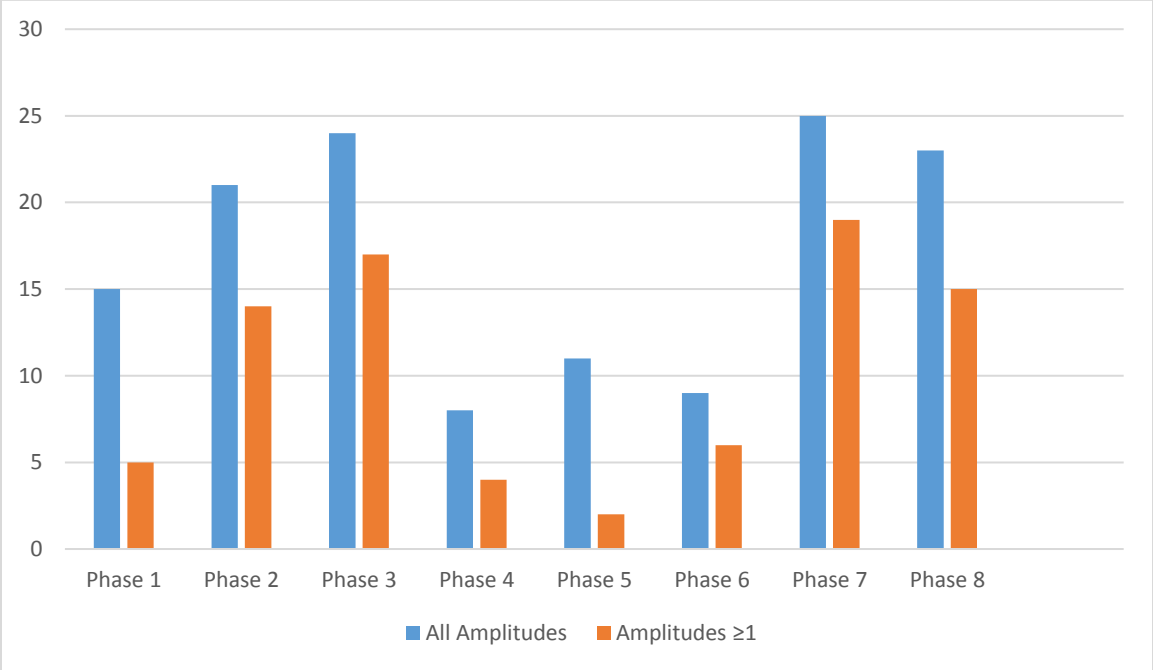


**Figure 3.5** Gulf of Mexico cyclogenesis events by MJO phase for the 1979–2014 period for all MJO amplitudes (blue) and amplitudes ≥1 (red).

A phase-by-phase examination of the mean synoptic pattern and atmospheric anomalies discussed below provide explanation for the results found in this study. More specifically, anomalous patterns of upper-level divergence, mid-tropospheric flow, low-level vorticity, tropospheric moisture and OLR support the results obtained here through Monte Carlo simulations. In most cases, the macro-scale anomalies even support the results only

with a 90% confidence level, adding some measure of certainty even when the statistical correlations are not quite as strong. A more detailed discussion of the synoptic patterns follows in Sections 3.3.1 – 3.3.4 for those MJO phases showing statistically significant associations in Tables 3.2 and 3.3.

To explore the patterns leading to GoM cyclogenesis variability by MJO phase, National Centers for Environmental Prediction/National Center for Atmospheric Research (NCEP/NCAR) Reanalysis 1 daily composite data (Kalnay et al., 1996) was obtained through NOAA's Earth System Research Laboratory (ESRL 2018) online plotting tool (https://www.esrl.noaa.gov/psd/data/composites/day/). The Reanalysis 1 data were chosen primarily because of the availability of the plotting tool which allows for the user to provide a customized series of dates, in this case corresponding to a particular MJO phase, and then download a netCDF file containing the variable of interest for those dates. This project uses anomaly data which is calculated based on a 1981–2010 mean constructed by NCEP/NCAR. Once the data of interest was queried and netCDF files were created, those files were then run though Python scripts to generate the anomaly plots found in the following sections.

### 3.3.1 MJO Phase 4

MJO Phase 4 shows negative associations (i.e., decreased GoM cyclogenesis) for both all MJO amplitudes and only those days when the RMM index was ≥1. Several anomalous atmospheric patterns are noted during Phase 4 that could explain the decrease in GoM cyclogenesis.

Meteorologists often focus on the 500 mb pressure level for a synoptic-scale overview of the key atmospheric features at work on any given day. This level of the atmosphere reveals locations of the longwave troughs and ridges, which in turn can allow a forecaster to deduce much more information about the state of the atmosphere. A plot of 500 mb geopotential height anomalies for all Phase 4 MJO days shows a pattern that suppresses GoM cyclogenesis (Figure 3.6). 500 mb heights are anomalously high over much of the eastern U.S. and the northern GoM. The anomalously strong ridge of high pressure would result in large-scale subsidence or sinking air, a feature known to reduce the likelihood of cyclogenesis. This region would also be expected to

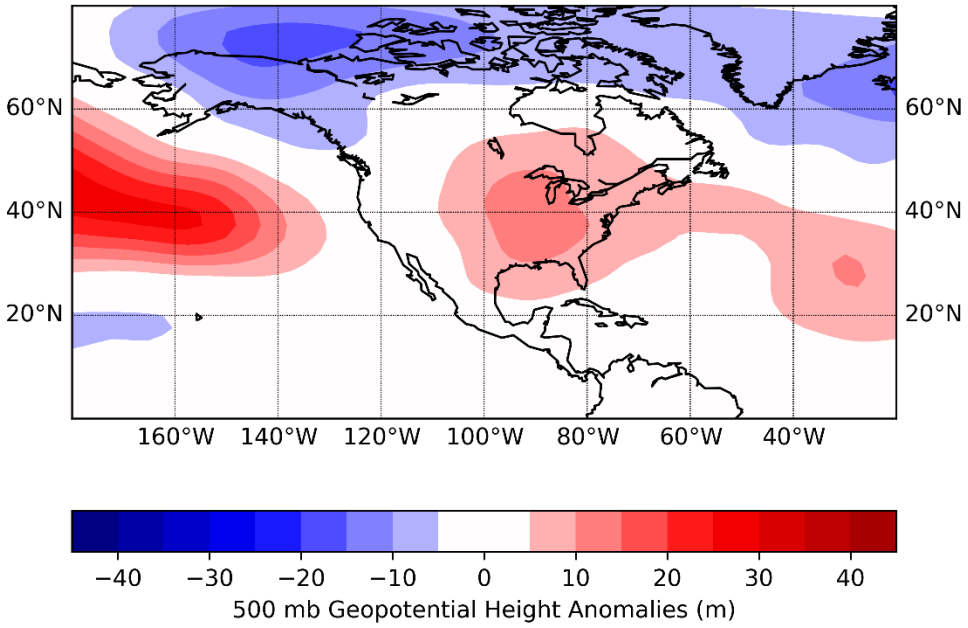


**Figure 3.6** 500 mb geopotential height anomalies for all MJO Phase 4 days during 1979–2014. Anomalies based on the NCEP/NCAR Reanalysis 1981–2010 mean.

have reduced or even negative environmental lapse rates, another negative influence on potential cyclogenesis. Finally, atmospheric moisture levels are

typically reduced in regions of high atmospheric pressure, as the subsidence would move drier air from aloft toward the surface which again would work against cyclogenesis. The lack of humidity would limit the available energy derived through the latent heat released during condensation and deposition, and the lack of liquid water would impair energy released during freezing. Without such energy, an incipient storm would be limited in strength if it could exist at all, as latent heat released is transformed to the kinetic energy that drives winds, as the water changes phase to liquid and solid forms that produce the clouds.

The area of mid-tropospheric high pressure noted by height anomalies in Figure 3.6 is also reflected at the surface when examining sea level pressure (SLP) anomalies. Anomalously high surface pressure extends from the GoM across much of the southeastern U.S. into the western Atlantic during Phase 4 (Figure 3.7). While not identical, this region of higher surface pressures is similar to that of the higher 500 mb heights shown in Figure 3.6. Northern Hemisphere cyclones, by definition, have cyclonic circulations. The region of positive SLP anomalies across most of the GoM represents an anticyclonic circulation pattern and therefore would be supportive of decreased cyclogenesis during MJO Phase 4.Another variable to consider when examining cyclogenesis is the amount of upper-atmospheric wind divergence. Diverging winds result in upward vertical motion which in turn supports the development of convection needed for low pressure development. One indicator of the amount of upper-

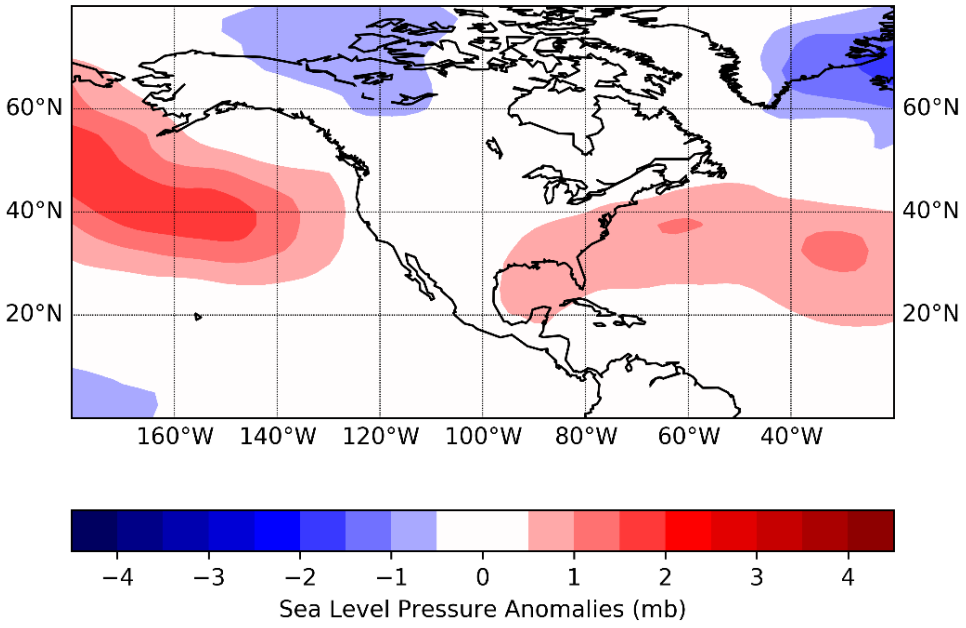


**Figure 3.7** Sea level pressure anomalies for all MJO Phase 4 days during 1979–2014. Anomalies based on the NCEP/NCAR Reanalysis 1981–2010 mean.

atmospheric divergence is velocity potential (Ventrice et al. 2013). Negative (positive) values represent areas of increased divergence (convergence).

The NCEP/NCAR Reanalysis data set provides velocity potential for certain sigma levels instead of the more widely-used pressure levels. Sigma levels are defined as the ratio of the pressure at a given point in the atmosphere to the pressure on the surface of the Earth below it. While somewhat different than pressure levels, the NCEP/NCAR Reanalysis .2101 sigma level analysis can be assumed to correspond roughly to the more commonly-used 200 mb analysis. A plot of the .2101 sigma level velocity potential anomalies shows positive anomalies covering most of North America and the western Atlantic (Figure 3.8). The largest positive anomalies,

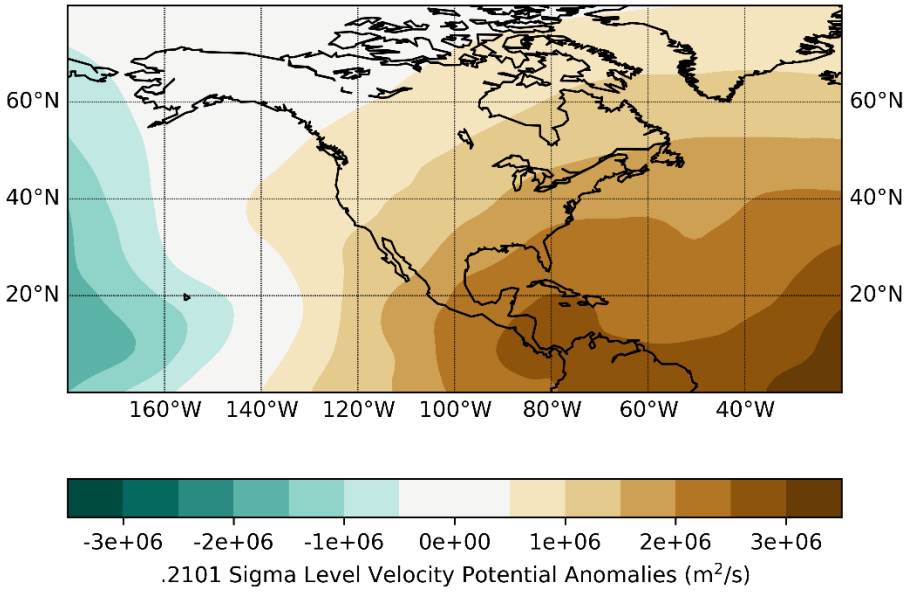


**Figure 3.8** .2101 sigma level velocity potential anomalies for all MJO Phase 4 days during 1979–2014. Anomalies based on the NCEP/NCAR Reanalysis 1981–2010 mean.

corresponding to increased upper-atmospheric convergence and subsiding air, extend from the GoM through Central and South America. This anomalous upper-level convergence would again be expected to be detrimental to cyclone formation in the GoM.

The final variable plotted for large-scale analysis of the atmospheric pattern during MJO Phase 4 days is 850 mb vector wind anomalies. Not surprisingly given the results of the analysis at the other levels, an anomalous anticyclonic circulation extends from the southeastern U.S across the GoM (Figure 3.9). This large area of negative low-level vorticity is yet another factor supportive of reduced cyclogenesis in the GoM during Phase 4.

The Monte Carlo simulations run for this analysis suggest that GoM cyclogenesis rates decrease during MJO Phase 4 days regardless of MJO amplitude. Plotting several NCEP/NCAR reanalysis variables for these

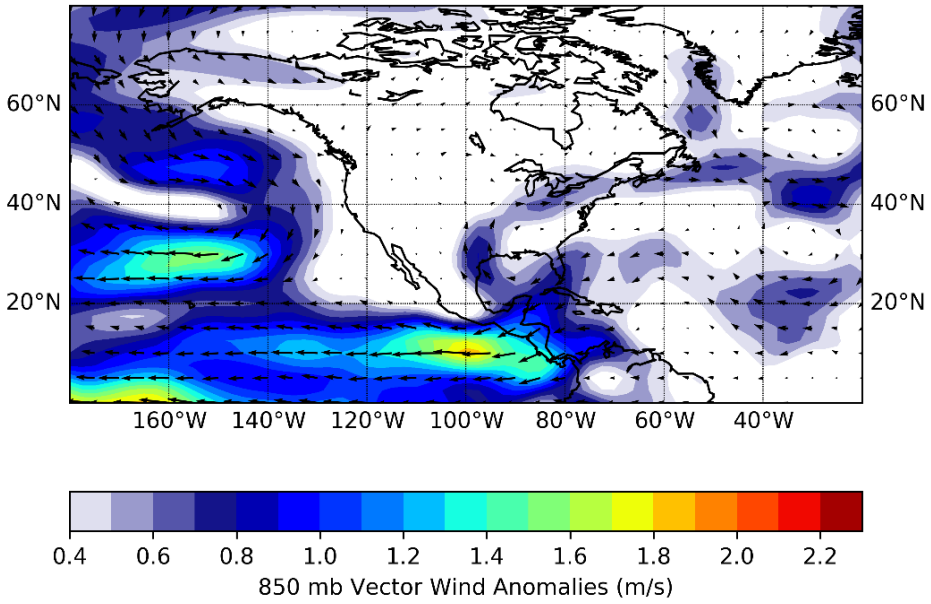


**Figure 3.9** 850 mb vector wind anomalies for all MJO Phase 4 days during 1979–2014. Anomalies based on the NCEP/NCAR Reanalysis 1981–2010 mean.

days verifies that the atmosphere generally suppresses low pressure development in the GoM during RMM MJO Phase 4. In a broad sense, a vertically stacked area of high atmospheric pressure is shown to extend from the western Atlantic into the southeastern U.S. and across the GoM. The resultant anticyclonic circulation, subsiding air, reduced atmospheric moisture, and stable vertical atmospheric profile all support the results obtained through the Monte Carlo simulations.

### 3.3.2 MJO Phase 5

The Monte Carlo simulations revealed no significant associations between MJO Phase 5 and GoM extratropical cyclogenesis when including all MJO amplitude days. However, when narrowing the analysis to days in which the RMM index was ≥1, cyclogenesis rates were shown to decrease at the 95%

confidence level. Analysis of the broad-scale atmospheric pattern during Phase 5 days using NCEP/NCAR Reanalysis data supports the results obtained through the Monte Carlo simulations.

Similar to the pattern shown in Phase 4, an anomalously strong ridge of high pressure is found across the GoM. The positive 500 mb height anomalies for all MJO Phase 5 days are more expansive though, extending from the western Atlantic across most of the U.S. and GoM and into the eastern Pacific (Figure 3.10). This mid-tropospheric area of high pressure suppresses cyclogenesis rates in the GoM.

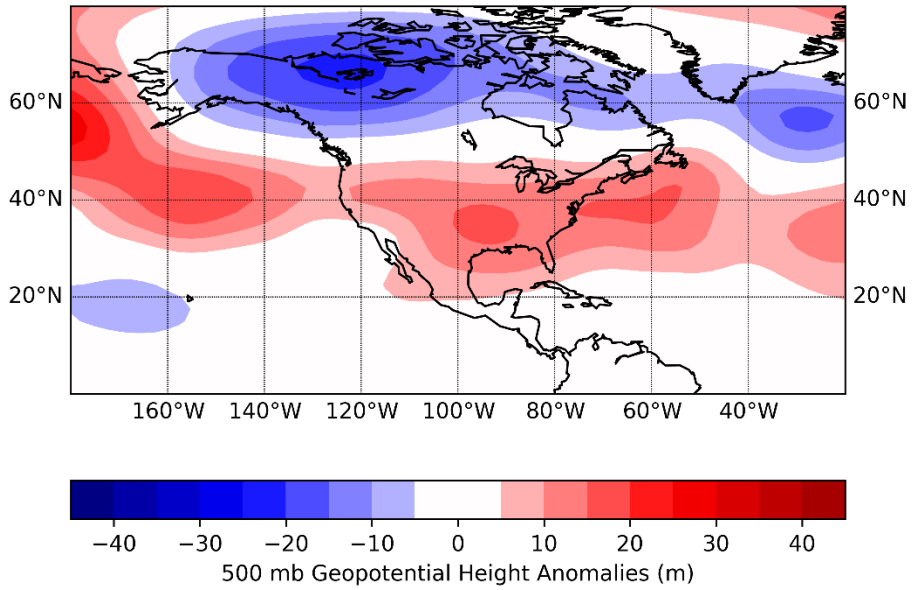


**Figure 3.10** Geopotential height anomalies for all Phase 5 MJO days during 1979–2014. Anomalies based on the NCEP/NCAR Reanalysis 1981–2010 mean.

Phase 5 SLP anomalies show a similar pattern to those found at 500 mb, with an expansive zonal ridge of high pressure extending from the western Atlantic across the continental U.S. into the eastern Pacific (Figure 3.11). A slight break in the anomalies is noted over the western U.S., but anomalously

high surface pressures extend across most of the GoM, indicating a pattern that would likely result in reduced rates of cyclogenesis.

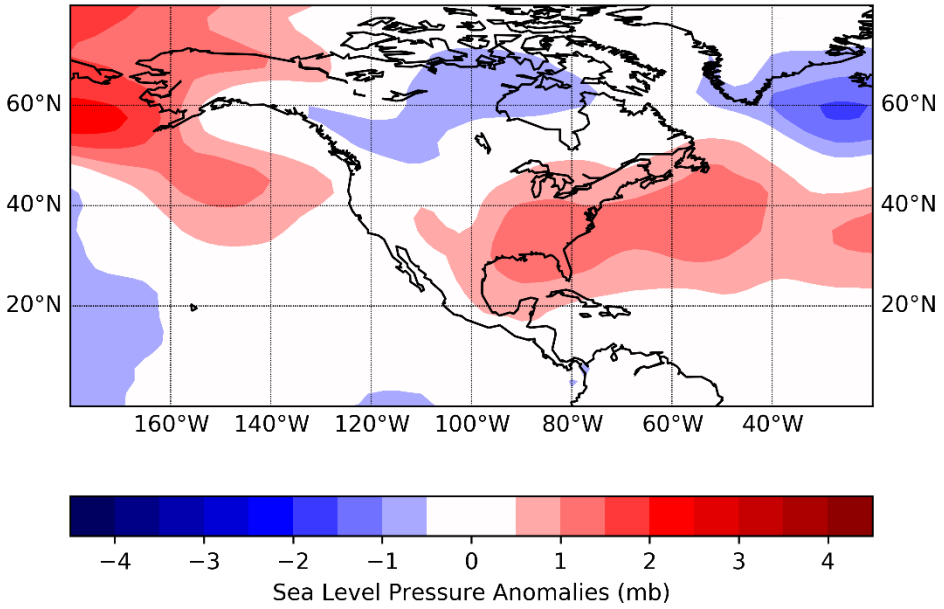


**Figure 3.11** Sea level pressure anomalies for all MJO Phase 5 days during 1979–2014. Anomalies based on the NCEP/NCAR Reanalysis 1981–2010 mean.

While upper-atmospheric divergence, a proxy for rising air, would be identified by negative velocity potential anomalies, positive velocity potential anomalies are instead noted over much of the eastern U.S. and western Atlantic Ocean, but the magnitude of the positive anomalies is lower than that observed in Phase 4 (Figure 3.12). Nevertheless, the positive velocity potential anomalies, representative of upper-level convergence, still suggest sinking motion and suppression of cyclogenesis in the GoM.

Finally, similar to the pattern noted during Phase 4, an anomalous anticyclonic circulation is found at 850 mb over the eastern U.S. and extending across the GoM (Figure 3.13). These low-level wind anomalies and the

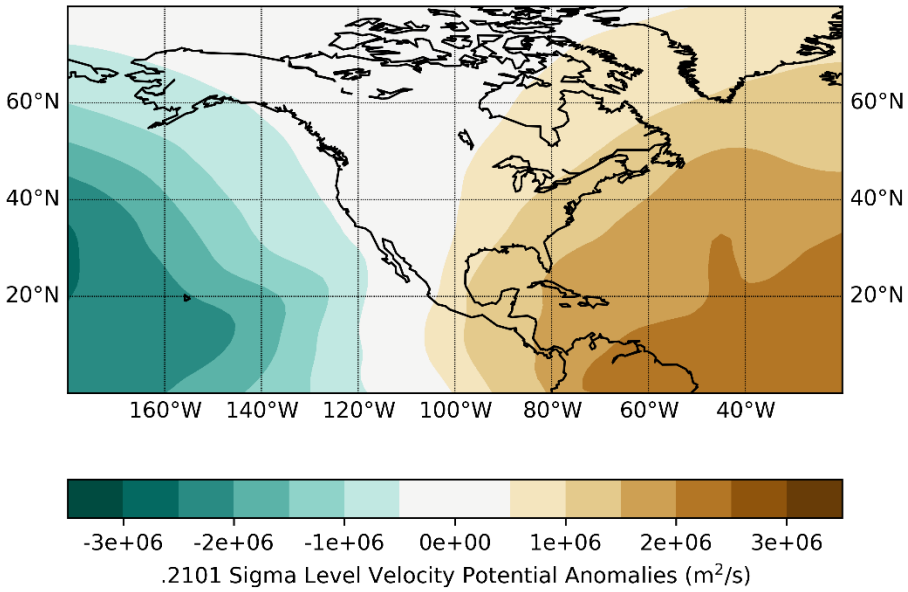


**Figure 3.12** .2101 sigma level velocity potential anomalies for all Phase 5 MJO days during 1979–2014. Anomalies based on the NCEP/NCAR Reanalysis 1981–2010 mean.

associated negative vorticity would tend to suppress cyclone development in the GoM.

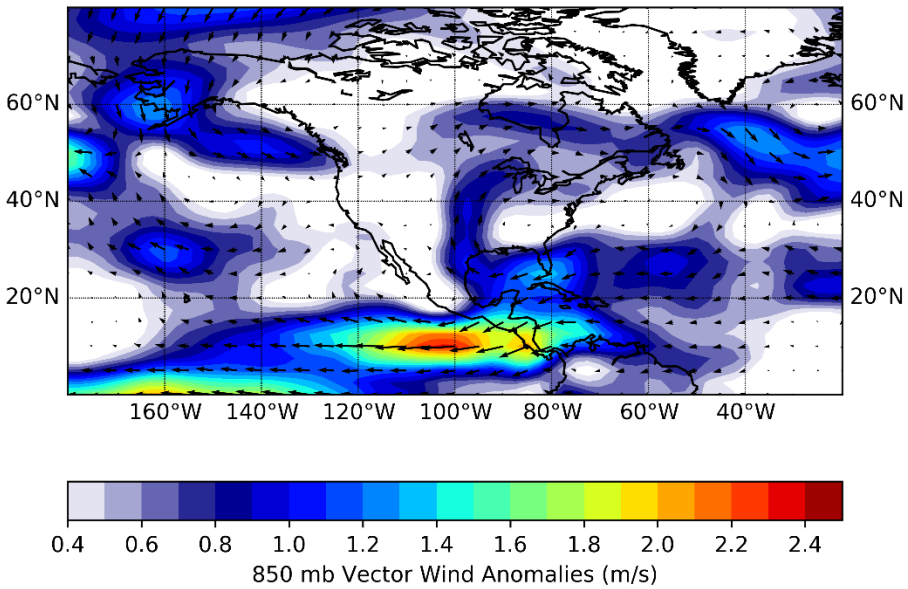


**Figure 3.13** 850 mb vector wind anomalies for all Phase 5 MJO days during 1979–2014. Anomalies based on the NCEP/NCAR Reanalysis 1981–2010 mean.

Collectively, the series of plots of NCEP/NCAR Reanalysis data shown here (Figs. 3.10 – 3.13) support the results obtained from the Monte Carlo simulations. A macro-scale ridge of high pressure centered over the eastern U.S. and its associated anticyclonic circulation would tend to limit GoM cyclogenesis through increased subsidence, increased atmospheric stability, reduced available moisture, and increased low-level negative vorticity.

### 3.3.3 MJO Phase 6

The Monte Carlo simulations suggest a statistically significant decrease in GoM cool season extratropical cyclogenesis at the 95% confidence level during MJO Phase 6 when all MJO amplitudes are included. However, that association disappears when the analysis is restricted to those days when the RMM MJO index is ≥1. Still, though, NCEP/NCAR reanalysis data show an atmospheric pattern that would appear to be marginally supportive of a reduced likelihood of GoM cyclogenesis during Phase 6.

A plot of 500 mb geopotential height anomalies for all Phase 6 days still shows a considerable region of positive anomalies covering much of the U.S. and at least the northern GoM (Figure 3.14). However, when comparing the pattern found during Phase 6 to those found for Phases 4 (Figure 3.6) and 5 (Figure 3.10), the magnitude of positive anomalies is reduced over the GoM and shows a westward shift toward the western U.S. and eastern Pacific.

SLP anomalies show an even weaker signal during Phase 6 relative to the mid-tropospheric ridging depicted in Figure 3.14. A small area of weakly positive SLP anomalies extends from off the southeastern U.S. coastline into

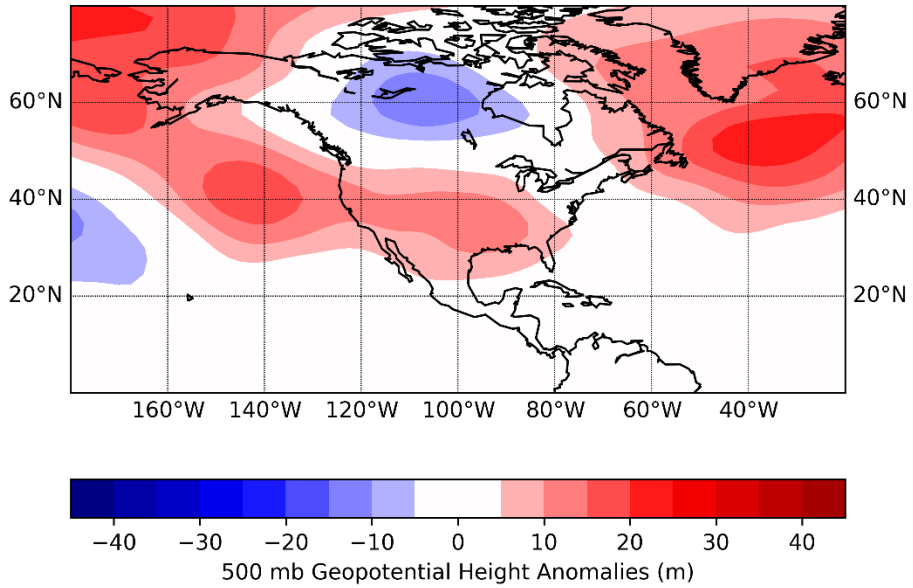


**Figure 3.14** 500 mb geopotential height anomalies for all Phase 6 MJO days during 1979–2014. Anomalies based on the NCEP/NCAR Reanalysis 1981–2010 mean.

the northeastern GoM (Figure 3.15). The relatively weak signature in the SLP anomaly pattern would likely indicate only a minor negative influence on extratropical cyclogenesis in the GoM.

The upper-level divergence signature also shows a significant weakening relative to that associated with Phases 4 (Figure 3.8) and 5 (Figure 3.12). The NCEP/NCAR Reanalysis data reveal no significant anomalies across the GoM, with positive anomalies, indicative of convergence and subsidence, confined eastward over the Atlantic and negative anomalies, indicative of rising motion, spreading eastward from the Pacific basin (Figure 3.16). The lack of any significant anomalies over the GoM indicates no detectable influence from upper-level velocity potential during MJO Phase 6.

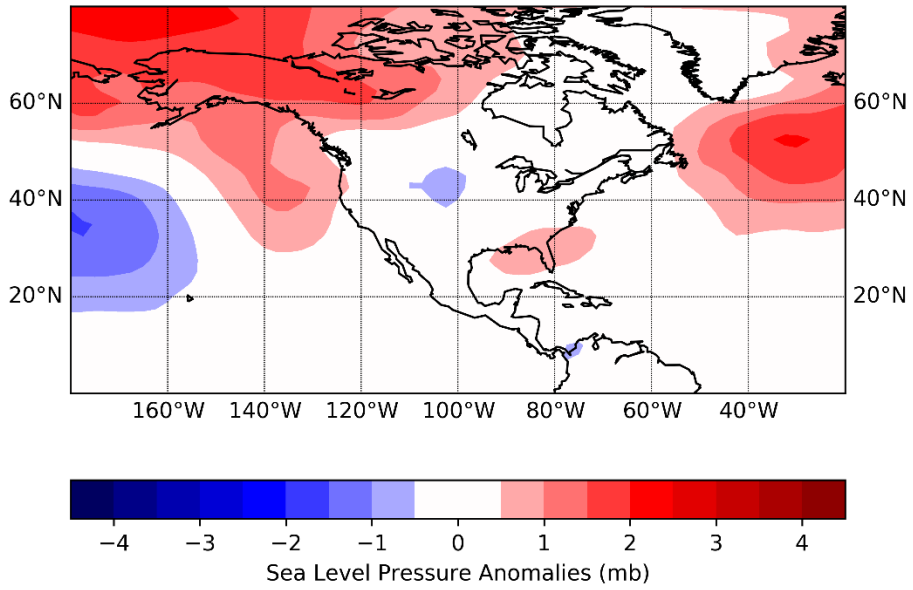


**Figure 3.15** Sea level pressure anomalies for all Phase 6 MJO days during 1979–2014. Anomalies based on the NCEP/NCAR Reanalysis 1981–2010 mean.

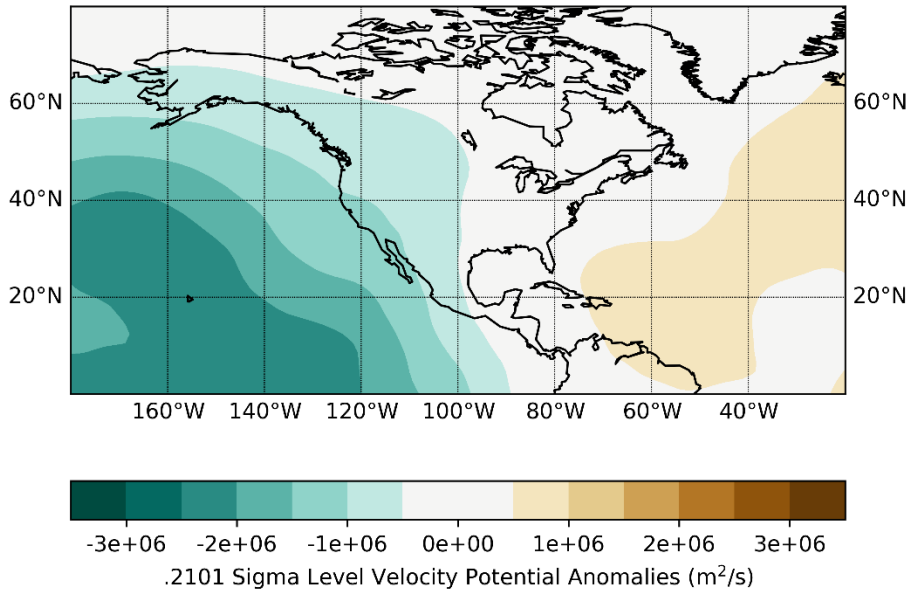


**Figure 3.16** .2101 sigma level velocity potential anomalies for all Phase 6 MJO days during 1979–2014. Anomalies based on the NCEP/NCAR Reanalysis 1981–2010 mean.

One variable that still shows the potential for a significant negative influence on GoM cyclogenesis is the 850 mb vector wind anomaly. An anticyclonic circulation is still evident over the southeastern U.S. and across

the GoM (Figure 3.17). The anomalous negative low-level vorticity resulting from this feature would be a clear detriment to low pressure development.

Contrary to the patterns shown for MJO Phases 4 and 5 which suggest that the majority of atmospheric variables suppress GoM extratropical cyclogenesis, plots for Phase 6 show mixed signals. On the one hand, there is still evidence of high pressure over the eastern U.S. and parts of the GoM,

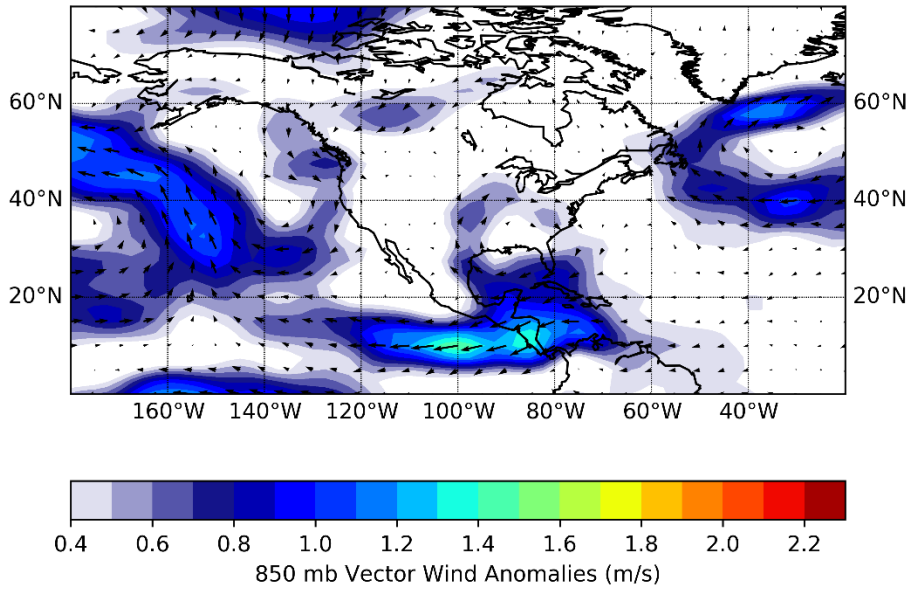


**Figure 3.17** 850 mb vector wind anomalies for all Phase 6 MJO days during 1979–2014. Anomalies based on the NCEP/NCAR Reanalysis 1981–2010 mean.

which would point toward decreased cyclogenesis frequencies. On the other hand, the region of greatest 500 mb height and SLP anomalies is displaced from the GoM. Additionally, measures of upper-level divergence show near-normal values in the region during Phase 6, pointing toward neither increased nor decreased likelihood of cyclogenesis. The strongest signal that carries over from Phases 4 and 5 is that of negative low-level vorticity in and around the GoM. The anticyclonic 850 mb wind anomalies would signal lower probabilities

of cyclone development in the GoM. Overall, the mixed atmospheric signals correspond to the mixed results obtained from the Monte Carlo simulations.

### 3.3.4 MJO Phase 7

The Monte Carlo simulations found no associations between Phase 7 of the MJO and cool season cyclogenesis in the GoM when examining all RMM amplitudes, but narrowing the sample down to those days when the RMM index is ≥1 did show a positive association at the 90% confidence level. It is difficult to determine whether this is a legitimate link or a spurious result since most of the atmospheric variables examined in the previous cases above appear to be nearly neutral during Phase 7. The one notable exception is the amount of upper-level divergence noted in the region.

An examination of 500 mb geopotential height anomalies for all Phase 7 MJO days reveals that most of the continental U.S. and the GoM are devoid of significant deviations from normal. One small area of positive height anomalies, corresponding with higher pressure, is noted over the southeastern U.S. and just offshore of that region (Figure 3.18). In general, high pressure would exert a negative influence on cyclogenesis, but the small spatial coverage and low magnitude of the anomalies suggest they may be an unimportant factor.

SLP patterns during Phase 7 suggest that the majority of the continental U.S. and all of the region of interest for this study are devoid of any significant anomalies (Figure 3.19). In other words, SLP is near-normal in and around the GoM during Phase 7, which would mean that it exerts no significant influence on cyclogenesis variability.

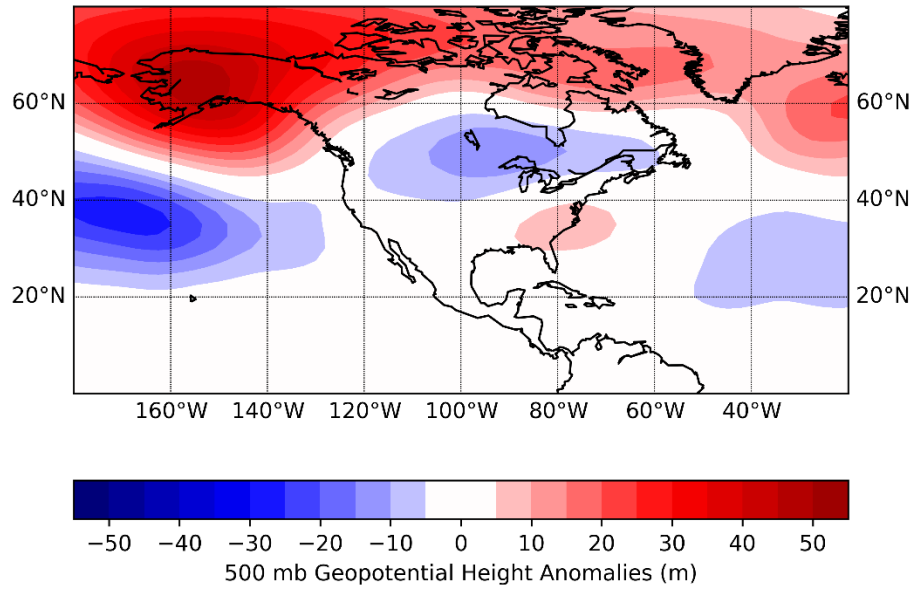


**Figure 3.18** 500 mb geopotential height anomalies for all Phase 7 MJO days during 1979–2014. Anomalies based on the NCEP/NCAR Reanalysis 1981–2010 mean.

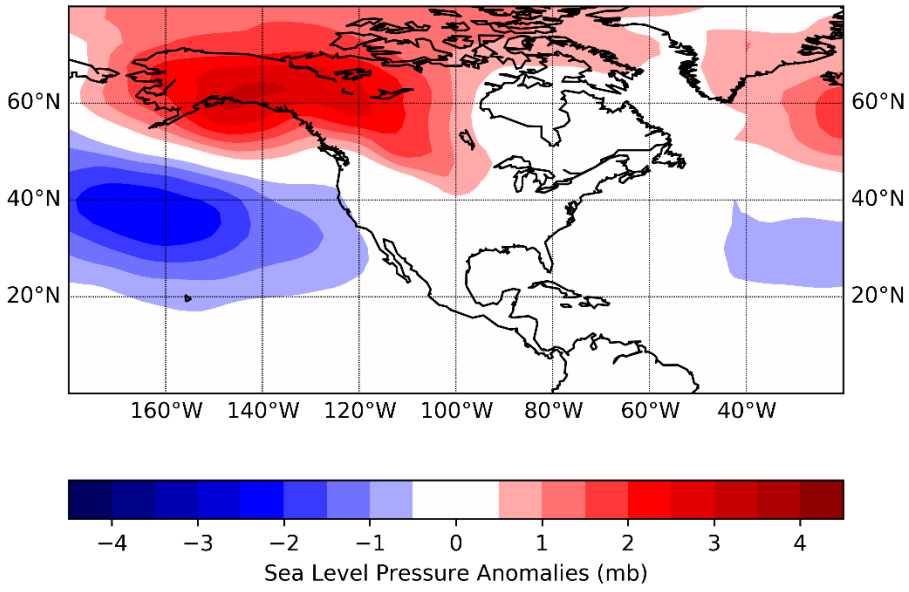


**Figure 3.19** Sea level pressure anomalies for all Phase 7 MJO days during 1979–2014. Anomalies based on the NCEP/NCAR Reanalysis 1981–2010 mean.

While the middle and surface levels of the atmosphere look nearly neutral during Phase 7, the upper atmosphere has properties that would

support GoM extratropical cyclogenesis. In what is likely a continuation of what was noted previously during Phase 6 (Figure 3.16), negative velocity potential anomalies spread eastward across most of North America and into the GoM (Figure 3.20). The largest negative anomalies extend from Mexico southward into the eastern equatorial Pacific. This increase in upper-atmospheric wind divergence is one factor supportive of extratropical cyclogenesis during Phase 7.

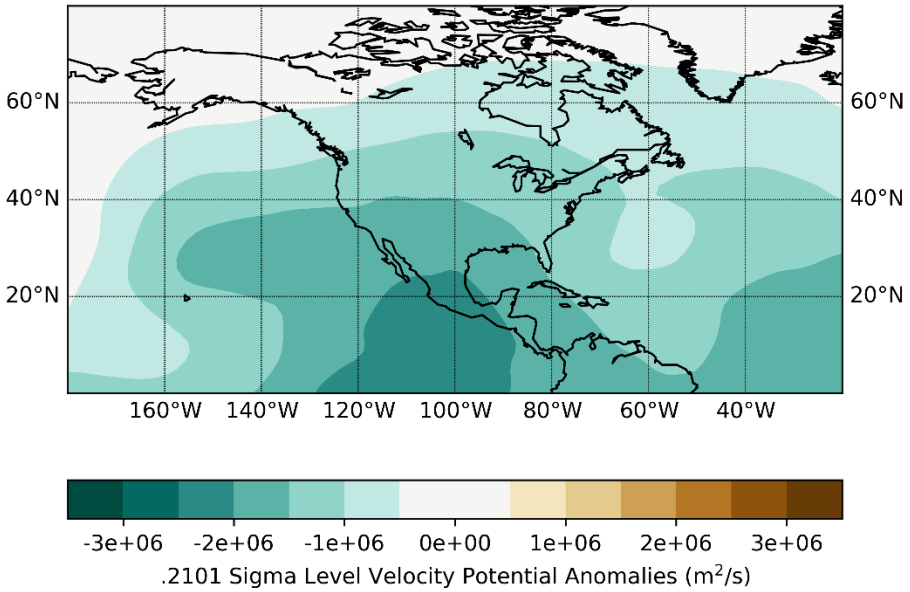


**Figure 3.20** .2101 sigma level velocity potential anomalies for all Phase 7 MJO days during 1979–2014. Anomalies based on the NCEP/NCAR Reanalysis 1981–2010 mean.

Finally, an examination of 850 mb vector wind anomalies provides no definitive evidence pointing toward either increased or decreased cyclogenesis during Phase 7. On the one hand, the weak anticyclonic circulation noted at 500 mb over the southeastern U.S. also appears here, which again would potentially be a weak negating factor for extratropical cyclogenesis in portions of the GoM (Figure 3.21). On the other hand, one might be able to argue that

there are at least some weak signs of convergence in the western and southern GoM as easterly winds cross Central America and Mexico and collide with the westerly flow that is a portion of the anticyclone over the southeastern United

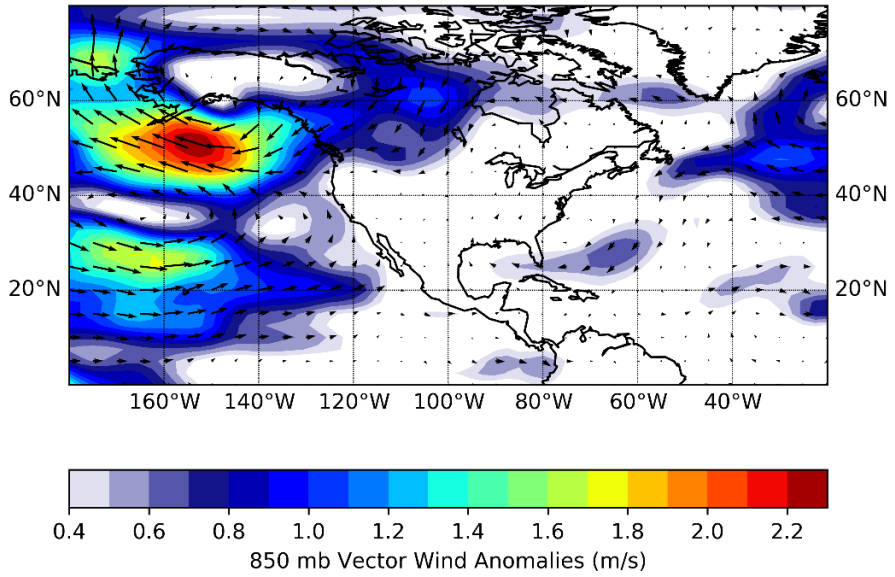


**Figure 3.21** 850 mb vector wind anomalies for all Phase 7 MJO days during 1979–2014. Anomalies based on the NCEP/NCAR Reanalysis 1981–2010 mean.

States. It would likely require further examination and testing to see if a meaningful signal can be gleaned from this pattern.

The mixed atmospheric signals shown by plotting various NCEP/NCAR Reanalysis variables for MJO Phase 7 make it difficult to determine if the results obtained from the Monte Carlo simulations are legitimate. The overall atmospheric pressure pattern appears quasi-neutral during this phase, but there is a notable increase in upper-level divergence. Additionally, the tropical cyclogenesis frequency graph earlier in this chapter (Figure 3.5) suggests that there is a clear increase in extratropical cyclone frequency from MJO Phase 6 to Phase 7. The number of genesis events roughly triples between these phases,

adding some credence to the results obtained through the simulations. Also, previous research has shown a general trend toward increased storminess in and around parts of North America during Phase 7 (Jones et al. 2011; Guo et al. 2017).

### 3.3.5 MJO Phase 8

One might argue that the progression into MJO Phase 8 represents an abrupt transition from a generally more tranquil period to a more active one in and around the GoM. A definitive decrease in cyclogenesis noted during Phases 4 and 5 seems to diminish slowly during Phase 6 and begins to show signs of increasing by Phase 7. By the time Phase 8 arrives, almost all atmospheric variables examined seem to be working in concert toward increased storminess and cyclogenesis around the GoM. Somewhat surprisingly though, the Monte Carlo simulations only show significant positive MJO Phase 8-GoM cyclogenesis association at the 90% confidence level for both all amplitudes and days when the RMM index is ≥1.

The more favorable pattern is clearly evident with a large trough of low pressure over the eastern United States when looking at all Phase 8 MJO days. Significant negative 500 mb height anomalies extend from the Great Lakes southward into the GoM and eastward into the Atlantic (Figure 3.22). This large area of lower heights would be supportive of rising motion, increased environmental lapse rates, and increased wind speeds at many levels, which are all supportive of cyclogenesis.

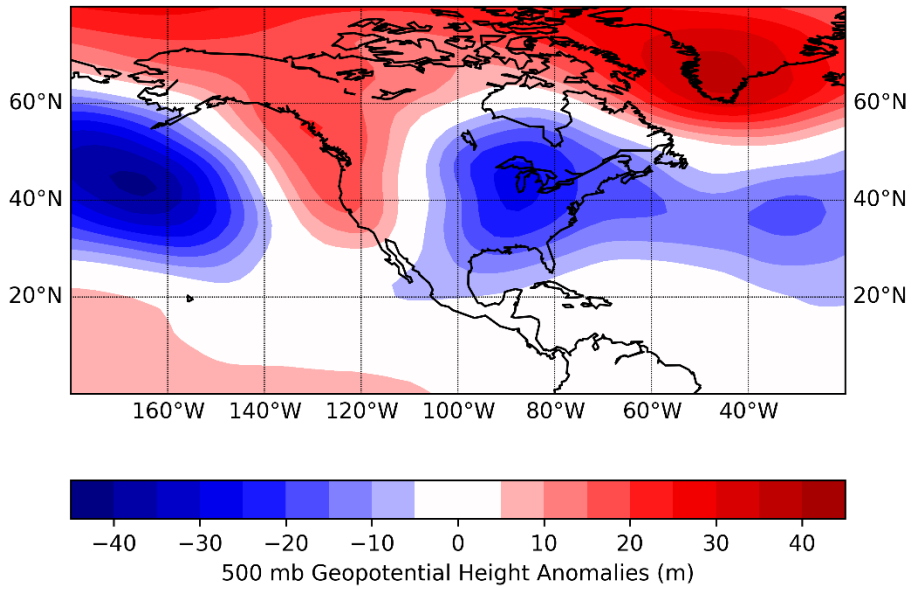


**Figure 3.22** 500 mb geopotential height anomalies for all Phase 8 MJO days during 1979–2014. Anomalies based on the NCEP/NCAR Reanalysis 1981–2010 mean.

The pattern continues to appear conducive for cyclogenesis at the surface. Negative SLP anomalies are also noted over much of the eastern U.S. and GoM but the core of greatest anomalies is over the Atlantic in

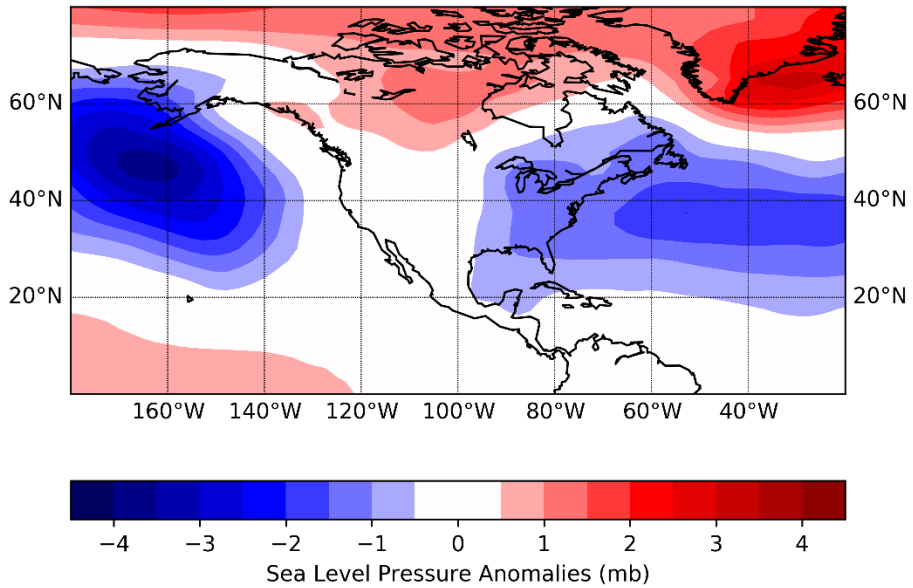


**Figure 3.23** Sea level pressure anomalies for all Phase 8 MJO days during 1979–2014. Anomalies based on the NCEP/NCAR Reanalysis 1981–2010 mean.

the region of the Bermuda-Azores quasi-permanent, subtropical anticyclone (Figure 3.23). Regardless, the below-average SLP values in and around the GoM would certainly favor cyclogenesis.

The atmosphere's tendency to support cyclogenesis during Phase 8 can also be seen aloft. Velocity potential anomalies are largely negative over North America and the GoM, with the greatest negative anomalies extending from the GoM across Central and South America (Figure 3.24). This sprawling region of negative anomalies represents upper-atmospheric wind divergence and promotes the rising motion needed for convection and cyclone development. The trough of low pressure over the eastern U.S. and GoM previously noted at 500 mb (Figure 3.22) and at the surface (Figure 3.23) is also evident at 850 mb (Figure 3.25). The obvious increase in cyclonic turning and positive low-level vorticity in and around the GoM would also be quite supportive of cyclogenesis.

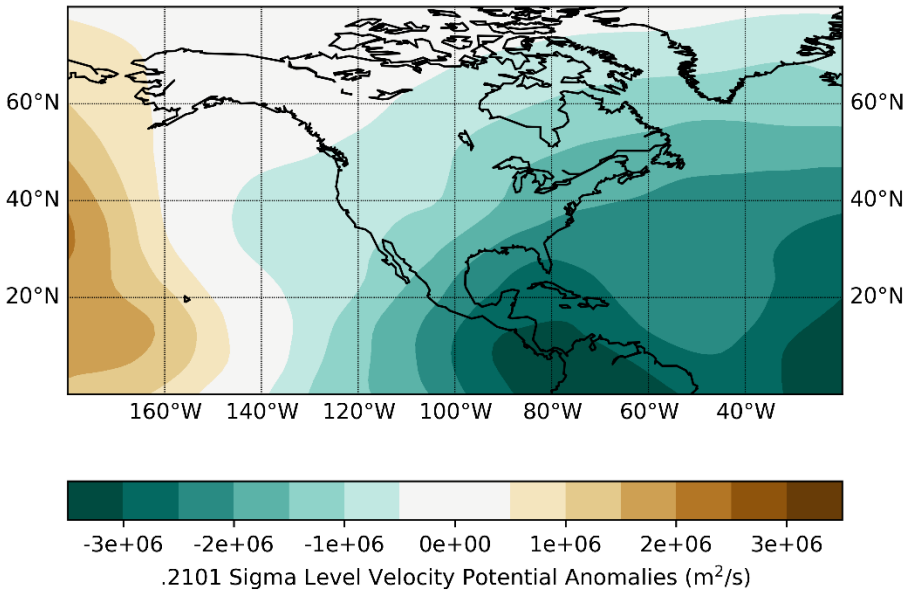


**Figure 3.24** .2101 sigma level velocity potential anomalies for all Phase 8 MJO days during 1979–2014. Anomalies based on the NCEP/NCAR Reanalysis 1981–2010 mean.

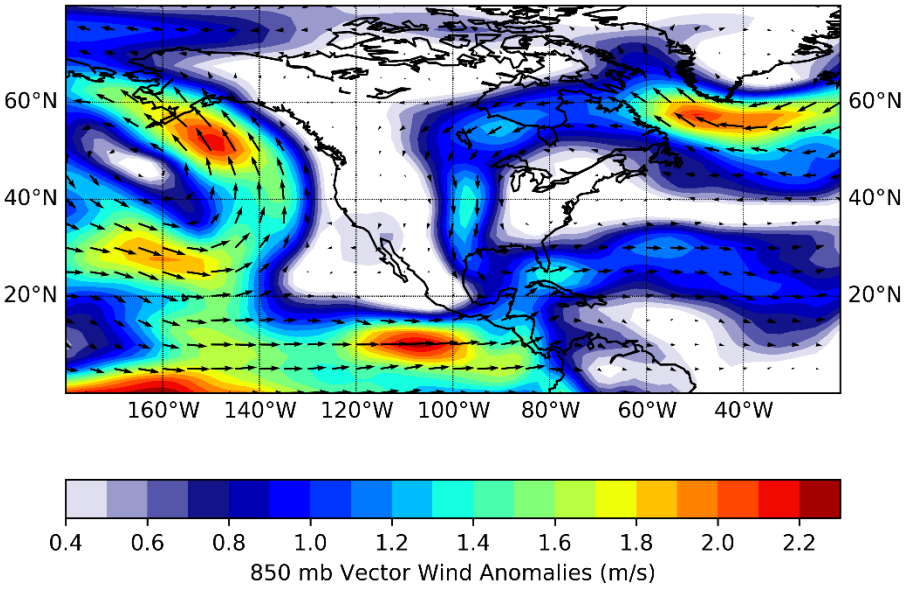


**Figure 3.25** 850 mb vector wind anomalies for all Phase 8 MJO days during 1979–2014. Anomalies based on the NCEP/NCAR Reanalysis 1981–2010 mean.

The Monte Carlo simulations run for MJO Phase 8 fall a little shy of giving a definitive answer on whether cool season cyclogenesis in the GoM is more likely during this phase, but the atmospheric pattern outlined above seems to add a higher measure of certainty to the otherwise uncertain results that only show significance at the 90% level. The NCEP/NCAR Reanalysis variables plotted for this analysis show no factors detrimental to cyclone development and in fact, largely suggest a consensus toward a pattern supportive of cyclogenesis. The combination of a synoptic-scale area of low pressure, increased low-level vorticity, and increased upper-level divergence all point toward a likely connection between Phase 8 and GoM cyclogenesis.

## 3.4 Conclusion

The MJO is shown to have an impact on cool season cyclogenesis in and around the GoM. Cyclone frequencies are found to decrease during MJO Phases 4, 5, and 6 while they increase during Phases 7 and 8. The frequency variability is linked to modifications of the synoptic-scale weather pattern, including 500 mb geopotential heights, SLP, upper-atmospheric wind divergence, and low-level winds and vorticity. Collectively, the anomalous atmospheric patterns found for a particular MJO phase in this study support the results obtained through Monte Carlo simulations.

The results obtained here are supported by prior research that has demonstrated a general trend toward increased storminess in and around parts of North America and the GoM during MJO Phases 7, 8, and 1, with a trend toward more tranquil conditions during Phases 4, 5, and 6. Klotzbach et al. (2016) showed that extratropical cyclones are more frequent just offshore of New England during Phases 7 and 8, and less frequent during Phases 4 and 5. The focus of their work is at higher latitudes but Klotzbach et al. (2016) notes that one of the primary sources of nor'easters is a Miller A type setup (Miller 1946) which involves an intensifying area of low pressure in the GoM tracking northward near or just offshore the U.S. East Coast. And given the extent of positive geopotential height and SLP anomalies during Phases 4 and 5 shown in this study (Figures 3.6–3.7 and 3.10–3.11), it comes as no surprise that both this research and the work of Klotzbach et al. (2016) show a decrease in

extratropical cyclones extending from the GoM northward toward the New England coastline.

The results of this study also corroborate those of the seminal work of Maloney and Hartmann (2000) which focused on GoM tropical cyclones. Maloney and Hartmann (2000) did not have access to the RMM MJO index since it was created four years after their publication (Wheeler and Hendon 2004), but they found a decrease in GoM tropical cyclones during what they called the easterly phases of the MJO and an increase in GoM tropical cyclones during the westerly phases. The easterly and westerly phases that they describe correspond to low-level wind anomalies. While the focus of the current study is on cool season extratropical cyclones, it appears as though those very same low-level wind anomalies noted by Maloney and Hartmann (2000) for tropical cyclones also play a significant role in extratropical cyclone frequency variability in and around the GoM. Maloney and Hartmann (2000) found decreased tropical cyclone frequencies during easterly phases of the MJO and the current study finds decreased extratropical cyclone frequencies during MJO Phases 4, 5, and 6, all of which produce easterly wind anomalies at 850 mb over the GoM (Figures 3.9, 3.13, and 3.17). It is especially interesting to note that the atmospheric pattern during Phase 6 shows mixed signals for extratropical cyclogenesis in the GoM, but the 850 mb easterly (or anticyclonic) wind anomalies remain pronounced. This result suggests that the 850 mb wind anomalies may carry a heavier weight than some of the other variables

discussed in modulating cyclone frequencies. Future research should test this hypothesis.

It is hoped that the links shown here between the MJO and cool season cyclogenesis in and around the GoM will help improve sub-seasonal forecasts around the region. Multiple computer model projections are now available for the MJO through NOAA's Climate Prediction Center (http://www.cpc.ncep.noaa.gov/products/precip/CWlink/MJO/CLIVAR/clivar_wh.shtml), ranging from a lead time of one week to roughly a month. Those MJO forecasts combined with the added knowledge resulting from this study and others that have examined the influence of atmospheric teleconnection patterns may provide forecasters with increased lead time in predicting periods of active or tranquil weather around the GoM. Knowing the far-reaching impacts that cool season extratropical cyclones can produce, the increased lead time could prove invaluable to a number of stakeholders, including the oil and gas, fisheries, shipping, and other industries.

## 3.5 References

Aiyyer, A., and J. Molinari, 2008: MJO and tropical cyclogenesis in the Gulf of Mexico and eastern Pacific: Case study and idealized numerical modeling. Journal of the Atmospheric Sciences, 65(8), 2691–2704.

Bove, M.C., J.B. Elsner, C.W. Landsea, X.F. Niu, and J.J. O'Brien, 1998: Effect of El Niño on US landfalling hurricanes, revisited. Bulletin of the American Meteorological Society, 79(11), 2477–2482.

Centre for Australian Weather and Climate Research (CAWCR), 2018: An All-season Real-time Multivariate MJO Index. Available online at http://www.bom.gov.au/climate/mjo/graphics/rmm.74toRealtime.txt. Last accessed: 5/23/2018.

Colle, B.A., J.F. Booth, and E.K. Chang, 2015: A review of historical and future

changes of extratropical cyclones and associated impacts along the US East Coast. Current Climate Change Reports, 1(3), 125–143.

Crawford, A.D., and M.C. Serreze, 2016: Does the summer Arctic frontal zone influence Arctic Ocean cyclone activity? Journal of Climate, 29(13), 4977–4993.

Earth System Research Laboratory (ESRL), 2018: Daily Mean Composites. Available online at: https://www.esrl.noaa.gov/psd/data/composites/day/. Last accessed: 5/23/2018.

Gray, W.M., 1984: Atlantic seasonal hurricane frequency. 1. El-Niño and 30-mb quasi-biennial oscillation influences. Monthly Weather Review, 112(9), 1649–1668.

Guo, Y., T. Shinoda, J. Lin, and E.K. Chang, 2017: Variations of northern hemisphere storm track and extratropical cyclone activity associated with the Madden–Julian Oscillation. Journal of Climate, 30(13), 4799–4818.

Jones, C., 2000: Occurrence of extreme precipitation events in California and relationships with the Madden-Julian oscillation. Journal of Climate, 13(20), 3576–3587.

Jones, C., J. Gottschalck, L.M. Carvalho, and W. Higgins, 2011: Influence of the Madden-Julian oscillation on forecasts of extreme precipitation in the contiguous United States. Monthly Weather Review, 139(2), 332–350.

Kaiser, M.J., and A.G. Pulsipher, 2007: The impact of weather and ocean forecasting on hydrocarbon production and pollution management in the Gulf of Mexico. Energy Policy, 35(2), 966–983.

Kalnay, E., M. Kanamitsu, R. Kistler, W. Collins, D. Deaven, L. Gandin, M. Iredell, S. Saha, G. White, J. Woollen, Y. Zhu, M. Chelliah, W. Ebisuzaki, W. Higgins, J. Janowiak, K. C. Mo, C. Ropelewski, J. Wang, A. Leetmaa, R. Reynolds, Roy Jenne, and Dennis Joseph, 1996: The NCEP/NCAR 40-year reanalysis project. Bulletin of the American Meteorological Society, 77(3), 437–471.

Klotzbach, P.J., 2014: The Madden-Julian Oscillation's impacts on worldwide tropical cyclone activity. Journal of Climate, 27(6), 2317–2330.

Klotzbach, P.J., and E.C. Oliver, 2015: Modulation of Atlantic basin tropical cyclone activity by the Madden–Julian Oscillation (MJO) from 1905 to 2011. Journal of Climate, 28(1), 204–217.

Klotzbach, P.J., E.C. Oliver, R.D. Leeper, and C.J. Schreck III, 2016: The Relationship between the Madden–Julian Oscillation (MJO) and southeastern New England snowfall. Monthly Weather Review, 144(4), 1355–1362.

Lewis, M.S., 2009: Temporary wholesale gasoline price spikes have long-lasting retail effects: The aftermath of Hurricane Rita. The Journal of Law and Economics, 52(3), 581–605.

Lin, H., G. Brunet, and J. Derome, 2009: An observed connection between the North Atlantic Oscillation and the Madden-Julian oscillation. Journal of Climate, 22(2), 364–380.

Lott, N., 1993: The Big One!: A review of the March 12–14, 1993," Storm of the Century". National Climatic Data Center, Research Customer Service Group.

Lyle, D., 2005: Experience blunts Katrina's wrath. Exploration & Production, 78(10), 17–19.

Madden, R.A., and P.R. Julian, 1994: Observations of the 40-50-day tropical oscillation – A review. Monthly Weather Review, 122(5), 814–837.

Maloney, E.D., and D.L. Hartmann, 2000: Modulation of hurricane activity in the Gulf of Mexico by the Madden-Julian oscillation. Science, 287(5460), 2002–2004.

Miller, J.E., 1946: Cyclogenesis in the Atlantic coastal region of the United States. Journal of Meteorology, 3(2), 31–44.

Mo, K.C., 1999: Alternating wet and dry episodes over California and intraseasonal oscillations. Monthly Weather Review, 127(12), 2759–2776.

——, 2000: Intraseasonal modulation of summer precipitation over North America. Monthly Weather Review, 128(5), 1490–1505.

Mo, K.C., and R. Higgins, 1998: Tropical convection and precipitation regimes in the western United States. Journal of Climate, 11(9), 2404–2423.

Mooney, C.Z., 1997: Monte Carlo simulation (Vol. 116). Sage Publications.

NOAA CPC, 2018: Dynamical Model MJO Forecasts. Available online at: http://www.cpc.ncep.noaa.gov/products/precip/CWlink/MJO/CLIVAR/clivar_wh.shtml. Last accessed: 5/23/2018.

Paganie, D., and P. Buschee, 2005: Operators begin cleanup, repair from Katrina, Rita. Offshore, 65(10), 24–35.

Patricola, C.M., R. Saravanan, and P. Chang, 2014: The impact of the El Niño–Southern Oscillation and Atlantic Meridional Mode on seasonal Atlantic tropical cyclone activity. Journal of Climate, 27(14), 5311–5328.

Pattiaratchi, C.B., and E.M.S. Wijeratne, 2015: Are meteotsunamis an underrated hazard? Philosophical Transactions of the Royal Society A, 373(2053), Art. No. 20140377.

Schreck, C., and D. Margolin, 2012: An MJO index for the Western Hemisphere. AGU Fall Meeting Abstracts, 0220.

Schumann, S.A., J. Moser, G.A. Johnson, N.D. Walker, and S.A. Hsu, 1995: An overview of a strong winter low in the Gulf of Mexico 12–13 March 1993. National Weather Digest, 20(1), 11–25.

Tang, B.H., and J.D. Neelin, 2004: ENSO influence on Atlantic hurricanes via tropospheric warming. Geophysical Research Letters, 31(24), Art. No. L24204.

Thompson, D.B., and P.E. Roundy, 2013: The relationship between the Madden-Julian oscillation and US violent tornado outbreaks in the spring. Monthly Weather Review, 141(6), 2087–2095.

Ventrice, M.J., M.C. Wheeler, H.H. Hendon, C.J. Schreck III, C.D. Thorncroft, and G.N. Kiladis, 2013: A modified multivariate Madden–Julian oscillation index using velocity potential. Monthly Weather Review, 141(12), 4197–4210.

Wheeler, M.C., and H.H. Hendon, 2004: An all-season real-time multivariate MJO index: Development of an index for monitoring and prediction. Monthly Weather Review, 132(8), 1917–1932.

Wheeler, M.C., H.H. Hendon, S. Cleland, H. Meinke, and A. Donald, 2009: Impacts of the Madden–Julian oscillation on Australian rainfall and circulation. Journal of Climate, 22(6), 1482–1498.

# CHAPTER 4. DAILY PRECIPITAITON VARIABILITY ALONG THE U.S. GULF COAST AND THE MADDEN-JULIAN OSCILLATION

## 4.1 Introduction

The Gulf Coast is among the wettest regions of the continental U.S. in terms of annual average precipitation, particularly the area extending from southeast Texas eastward to the Florida panhandle (Figure 4.1). This region along the northern Gulf Coast has minimal seasonal variability in precipitation with a maximum during boreal summer but no distinct dry season easily detectable (Figure 4.2). The rainy pattern can be explained by a number of factors, including high amounts of specific humidity for much of the year, the influence of the sea breeze front in the warm season, precipitation generated by

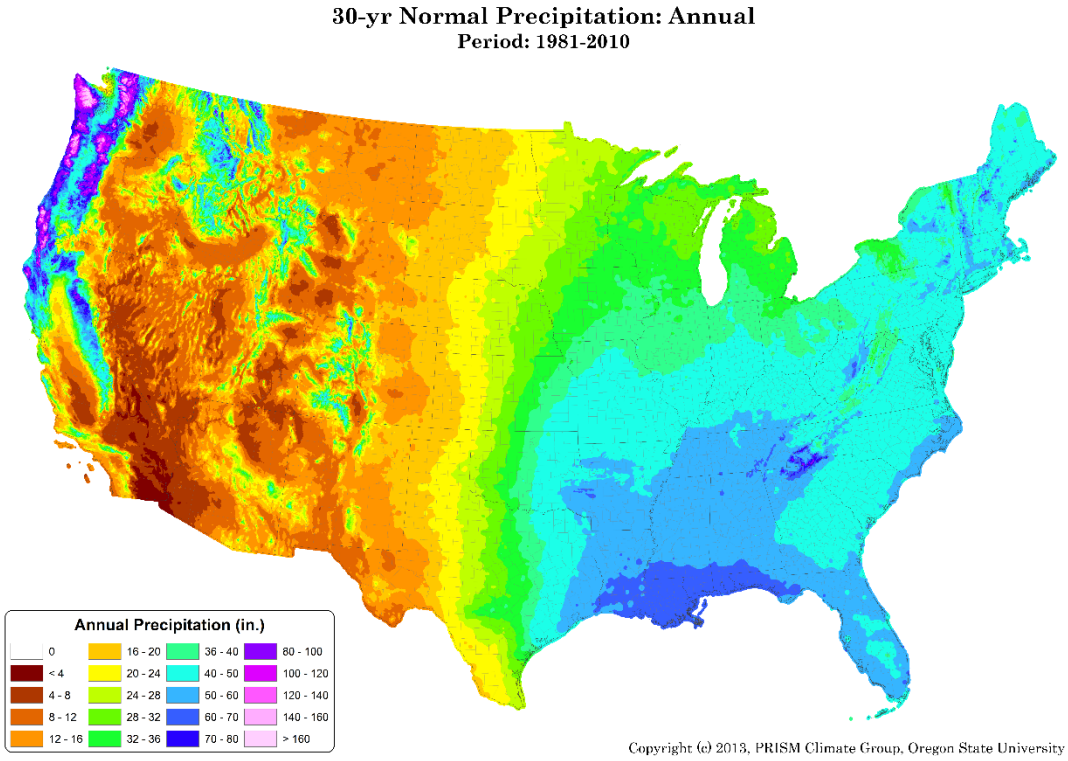


**Figure 4.1** Mean annual precipitation (in.) for the period 1981-2010. Map created April 3, 2018. Credit: PRISM Climate Group, Oregon State University.

both tropical and extratropical cyclones, and regular cold front passages in the cool season (Vega et al. 2013). Abundant rainfall makes it important to understand the mechanisms driving daily rainfall variability along the Gulf Coast.

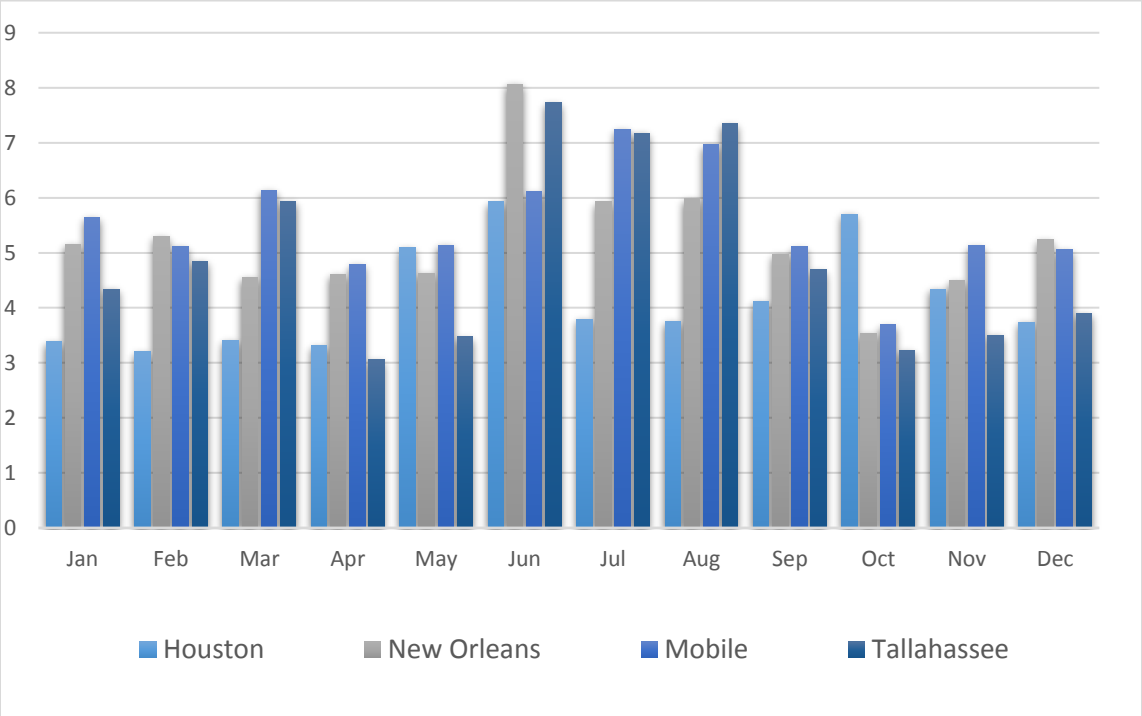


**Figure 4.2** Mean annual precipitation (1981-2010) for select sites along the U.S. Gulf Coast. Data via SC ACIS (http://scacis.rcc-acis.org/).

The importance of understanding U.S. Gulf Coast precipitation variability has been underscored by two extreme rainfall events within the last few years. An historic rain event unfolded over the course of several days over South Louisiana in August 2016. Rainfall totals topped 76 cm (30 in) in some locations (Di Liberto 2018), an estimated 30,000 people were rescued, at least 60,000 homes were impacted by rising waters, and 13 deaths were attributed to the record flood (van der Wiel et al. 2017). The financial toll is estimated to

be around $10 billion, making it the costliest flood event in the U.S. since Superstorm Sandy struck the Northeast in 2012 (NOAA NCEI 2018).

Only a year later in August 2017, Hurricane Harvey devastated parts of southeastern Texas and a small area in western Louisiana with record rainfall. The worst of the damage was centered around Houston and Beaumont, Texas, where widespread multi-day rain totals of 100–130 cm (40–50 in) were reported, with maxima of just over 150 cm (60 in) of rainfall measured in Nederland and Groves, Texas. Those values, along with five others, all surpassed the previous U.S. tropical cyclone storm total rainfall record of 132 cm (52 in) set in Hawaii by Hurricane Hiki in 1950 (Blake and Zelinsky 2018). Accounting for inflation, the estimated $125 billion in damages produced by Harvey ranks it as the second costliest U.S. tropical cyclone on record, trailing only the $160 billion in damages produced by Hurricane Katrina in 2005 (National Hurricane Center 2018). Harvey is also responsible for 68 fatalities, making it the deadliest U.S. tropical system since Sandy (2012) and the deadliest tropical cyclone in Texas since 1919 (Blake and Zelinsky 2018).

The August 2016 flooding in Louisiana and Hurricane Harvey's flooding in Texas and Louisiana are two extreme examples of the impacts of rainfall variability along the U.S. Gulf Coast, but even the more common, less extreme events are important to the climate in this region. The lack of a distinct dry season and the generally low elevations above sea-level make many larger population centers prone to recurring flooding. Rainfall variability also has important impacts in a number of arenas, including those with agricultural

interests, and the Gulf Coast's thriving fisheries, shipping, and energy industries.

## 4.2 Data and Methods

An analysis of daily precipitation variability along the U.S. Gulf Coast during the cool season is conducted to examine possible links to the Madden-Julian Oscillation (MJO). The period of analysis is 1918–2014, with the starting point corresponding to the earliest available continuous records for select sites along the Gulf Coast with no more than 10% missing data for a particular year. Precipitation data were queried for the period of interest and downloaded from the State Climatologists Applied Climate Information System (SC ACIS 2018; http://scacis.rcc-acis.org/) in comma-separated values (CSV) file format for each station. The canonical Real-time Multivariate MJO (RMM) index (Wheeler and Hendon 2004) used in the Chapter 3 study is only available to 1974, so the Oliver-Thompson (OT) index is used instead because it provides reliable data back to 1905. Oliver and Thompson (2011) demonstrated that their index was consistent with the RMM index when compared during the 1979–2008 period. Klotzbach and Oliver (2015) also found consistency between the indices when examining the impact of the MJO on Atlantic tropical cyclone variability.

The OT index uses 20$^{th}$ Century Reanalysis (20CR) surface pressure data from 12 sites located in the tropics. Values are calculated by performing multiple linear regression of these pressure time series onto the RMM index (Oliver and Thompson 2011). The OT daily index is available for download (OT Index 2018; https://ecjoliver.weebly.com/mjo-reconstruction.html) in three

different formats: a single index based on the 20CR version 2c (V2c) ensemble mean pressure, a version that has an ensemble of 54 indices based on each of the 20CR V2c ensemble members, and the original OT index presented in the *Journal of Climate* (Oliver and Thompson 2011). This study uses the index based on the ensemble mean because the original OT index is only available through 2008.

Daily precipitation data were obtained for 12 sites near the U.S. Gulf Coast ranging from Brownsville, Texas, to Key West, Florida (Figure 4.3).

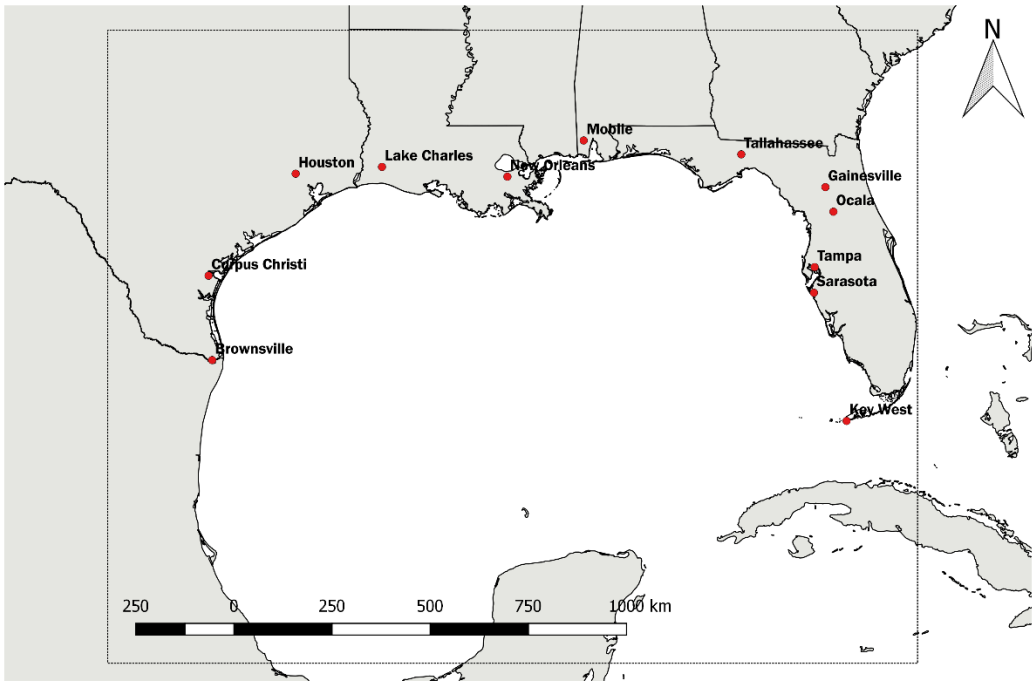


**Figure 4.3** Sites located along the U.S. Gulf Coast used for this study.

The initial study examined eight locations with Tampa, Florida, being the southernmost in that state, but four additional sites – Gainesville, Sarasota, Ocala and Key West – were added when the initial results suggested there may be some stronger MJO-precipitation relationships in the Florida Peninsula. Additional information on those results can be found in Section 4.3.

Daily precipitation amounts for each of the 12 study sites were then assigned a value of 1–8 corresponding to the MJO phase on those dates as shown by the OT index. Subsequently, mean daily precipitation values were calculated for each site and MJO phase. Once those calculations were completed, statistical testing for MJO-daily precipitation associations was conducted by running Monte Carlo simulations.

The Monte Carlo techniques used in this study largely follow those first introduced in a study examining MJO links to Australian rainfall and circulation (Wheeler et al. 2009) that were subsequently used to explore MJO associations with snowfall in the northeastern U.S. (Klotzbach et al. 2016). The techniques involve establishing two vectors of equal length; in this case, the vectors are composite averages of daily precipitation by MJO phase and the daily MJO phase as defined by the OT index. A new estimated response of the first vector (daily precipitation composites) to the second vector (daily MJO phase) is then created by shifting the second vector by some random amount in time. The shift is not completely random in that a certain number of values are moved from the bottom of the time series to the top. In the case of using this technique with the MJO, it is known that the MJO decorrelates in less than 50 days (Salby and Hendon 1994) so the minimum number of values that must be shifted to preserve the autocorrelation structure of the MJO is 50. In this study, 1,000 Monte Carlo simulations were run for each site, producing 1,000 estimated responses to a random climate. Those 1,000 responses then allow for the construction of confidence intervals, with the 2.5$^{th}$ and 97.5$^{th}$ percentiles

representing the limits of a 95% confidence interval. A 90% confidence interval is represented by the 5$^{th}$ and 95$^{th}$ percentiles as calculated by the Monte Carlo simulations. Any composite precipitation average calculated in the original vector falling outside of those limits holds statistical significance at that particular level.

The Monte Carlo simulations are constructed by running a programming script in Python. The script was provided by Dr. Eric Oliver and was created for some of his own research, including published work on the MJO and Northeast U.S. snowfall (Klotzbach et al. 2016). A few minor modifications had to be made to account for the use of a newer version of Python than the one used for the original script and for some of the particular needs of this study. The script rejects any days on which the OT MJO index has an amplitude <1, as the MJO is considered to be weak in this range.

The Monte Carlo simulations are run for all 12 sites using Dr. Oliver's script to test for associations between daily precipitation and MJO phase. Very similar Python scripts are then constructed and run to test for associations between MJO phase the frequency of days producing at least 2.5 cm and 5.0 cm of precipitation at each of the 12 sites. Thus, three sets of simulations are run for each site or a total of 36 sets for all locations selected along the U.S. Gulf Coast. As a final measure of confidence, Monte Carlo simulations are constructed and run for a small sample of those 36 using a slightly different method. In all cases, the results were the same even with the use of slightly different techniques.

## 4.3 Results

The Monte Carlo simulations were constructed for daily precipitation totals, the number of days with precipitation totals ≥ 2.5 cm, and the number of days with precipitation totals ≥ 5.0 cm for select sites along the U.S. Gulf Coast only for those days when the MJO amplitude was ≥ 1. Additionally, results were obtained using both 90% and 95% confidence intervals in each scenario. The use of 90% confidence intervals was included in this analysis to remain consistent with the methods used in Study 1 but also because MJO phases as identified by the OT index are discrete, suggesting that there is the potential in some occasions for a lag between a particular phase and an impact on precipitation frequencies. It is recognized that there is an increased chance for spurious results when using a 90% confidence interval since Type I error increases to .10. A summary of the final results for both the 90% and 95% confidence intervals is shown in Tables 4.1 – 4.6 below. The Gulf Coast stations used for this study are identified in the tables below by their 4-letter METAR identifiers which in many but not all cases equates to the International Civil Aviation Organization (ICAO) codes for those cities. The station abbreviations include: KBRO (Brownsville), KCRP (Corpus Christi), KIAH (Houston), KLCH (Lake Charles), KAUD (New Orleans/Audubon), KMOB (Mobile), KTLH (Tallahassee), KGNV (Gainesville), KOCF (Ocala), KTPA (Tampa), KSRQ (Sarasota), and KEYW (Key West).

**Table 4.1** Daily precipitation averages for each MJO phase. Green (red) shading indicates a positive (negative) association from the Monte Carlo simulations using a 90% confidence interval.

| Phase | KBRO | KCRP | KIAH | KLCH | KAUD | KMOB | KTLH | KGNV | KOCF | KTPA | KSRQ | KEYW |
|---|---|---|---|---|---|---|---|---|---|---|---|---|
| 1 | 0.070 | 0.085 | 0.157 | 0.131 | 0.150 | 0.175 | 0.157 | 0.156 | 0.157 | 0.134 | 0.162 | 0.211 |
| 2 | 0.052 | 0.084 | 0.105 | 0.130 | 0.126 | 0.156 | 0.105 | 0.086 | 0.153 | 0.083 | 0.089 | 0.070 |
| 3 | 0.030 | 0.052 | 0.115 | 0.165 | 0.136 | 0.166 | 0.115 | 0.126 | 0.130 | 0.095 | 0.099 | 0.060 |
| 4 | 0.044 | 0.056 | 0.136 | 0.169 | 0.116 | 0.158 | 0.136 | 0.072 | 0.139 | 0.060 | 0.075 | 0.072 |
| 5 | 0.068 | 0.053 | 0.120 | 0.145 | 0.152 | 0.115 | 0.120 | 0.076 | 0.121 | 0.045 | 0.039 | 0.035 |
| 6 | 0.043 | 0.059 | 0.122 | 0.123 | 0.140 | 0.159 | 0.122 | 0.074 | 0.127 | 0.046 | 0.056 | 0.075 |
| 7 | 0.062 | 0.065 | 0.159 | 0.164 | 0.192 | 0.202 | 0.159 | 0.102 | 0.126 | 0.066 | 0.061 | 0.070 |
| 8 | 0.063 | 0.088 | 0.164 | 0.182 | 0.197 | 0.216 | 0.164 | 0.112 | 0.150 | 0.092 | 0.100 | 0.113 |

The Monte Carlo simulation results elicit three regional groupings with associations that are often found to be consistent across the western Gulf Coast, the northern Gulf Coast, and the eastern Gulf Coast. In the case of the 90% confidence interval for daily precipitation, the most prevalent associations include a positive connection with Phase 1 along the eastern Gulf Coast and a positive association with Phase 8 along portions of both the western and eastern Gulf Coast. Several negative associations appear with Phases 5 and 6 along the eastern Gulf Coast. Elsewhere, there are a few sporadic associations found using the 90% confidence interval, but it is interesting to note that the northern Gulf Coast is largely devoid of any apparent MJO-daily rainfall connections with none found from KAUD to KMOB and only the positive Phase 8 association occurring for KLCH.

Not surprisingly, the number of associations is reduced when using a 95% confidence interval but the most prevalent regional patterns noted in Table 4.1 remain in Table 4.2. Phase 1 shows a positive association with daily rainfall along

the eastern Gulf Coast as does Phase 8 for parts of both the eastern and western Gulf Coast. The negative associations persist for Phases 5 and 6 along the eastern Gulf Coast. A few other isolated associations are noted including a positive connection with Phase 1 for KBRO, a negative for KEYW during Phase 3, and a negative for KSRQ during Phase 7. It is possible that these are spurious or could suggest only localized impacts from those specific MJO phases. The positive association for KBRO during Phase 1 is interesting because it is plausible that it represents a lag or overlap from Phase 8 when considering that the MJO most often progresses from Phase 8 to Phase 1. Further exploration is needed to determine whether that is the case.

**Table 4.2** As in Table 4.1 for a 95% confidence interval.

| Phase | KBRO | KCRP | KIAH | KLCH | KAUD | KMOB | KTLH | KGNV | KOCF | KTPA | KSRQ | KEYW |
|---|---|---|---|---|---|---|---|---|---|---|---|---|
| 1 | 0.070 | 0.085 | 0.157 | 0.131 | 0.150 | 0.175 | 0.157 | 0.156 | 0.157 | 0.134 | 0.162 | 0.211 |
| 2 | 0.052 | 0.084 | 0.105 | 0.130 | 0.126 | 0.156 | 0.105 | 0.086 | 0.153 | 0.083 | 0.089 | 0.070 |
| 3 | 0.030 | 0.052 | 0.115 | 0.165 | 0.136 | 0.166 | 0.115 | 0.126 | 0.130 | 0.095 | 0.099 | 0.060 |
| 4 | 0.044 | 0.056 | 0.136 | 0.169 | 0.116 | 0.158 | 0.136 | 0.072 | 0.139 | 0.060 | 0.075 | 0.072 |
| 5 | 0.068 | 0.053 | 0.120 | 0.145 | 0.152 | 0.115 | 0.120 | 0.076 | 0.121 | 0.045 | 0.039 | 0.035 |
| 6 | 0.043 | 0.059 | 0.122 | 0.123 | 0.140 | 0.159 | 0.122 | 0.074 | 0.127 | 0.046 | 0.056 | 0.075 |
| 7 | 0.062 | 0.065 | 0.159 | 0.164 | 0.192 | 0.202 | 0.159 | 0.102 | 0.126 | 0.066 | 0.061 | 0.070 |
| 8 | 0.063 | 0.088 | 0.164 | 0.182 | 0.197 | 0.216 | 0.164 | 0.112 | 0.150 | 0.092 | 0.100 | 0.113 |

Monte Carlo testing shows that the MJO has a definitive impact on Gulf Coast daily precipitation depending on location and phase, so further testing was conducted to examine whether days producing heavy precipitation were more or less likely during particular phases. Testing for the frequency of days producing at least 2.5 cm of rainfall provides results that in some cases resemble those in Tables 4.1 and 4.2. Using a 90% confidence interval, positive

associations for Phase 1 along the eastern Gulf Coast and Phase 8 along the western Gulf Coast are very similar to those found for daily precipitation (Tables 4.1 and 4.2). Negative associations shown at Phases 5 and 6 are also quite similar to those found for daily rainfall. Several other associations are

**Table 4.3** Average rates of days producing ≥2.5 cm of precipitation for each MJO phase. Green (red) shading indicates a positive (negative) association from the Monte Carlo simulations using a 90% confidence interval.

| Phase | KBRO | KCRP | KIAH | KLCH | KAUD | KMOB | KTLH | KGNV | KOCF | KTPA | KSRQ | KEYW |
|---|---|---|---|---|---|---|---|---|---|---|---|---|
| 1 | 0.024 | 0.022 | 0.034 | 0.050 | 0.052 | 0.054 | 0.057 | 0.049 | 0.044 | 0.049 | 0.051 | 0.034 |
| 2 | 0.017 | 0.019 | 0.037 | 0.039 | 0.052 | 0.054 | 0.048 | 0.044 | 0.046 | 0.045 | 0.045 | 0.027 |
| 3 | 0.019 | 0.022 | 0.037 | 0.044 | 0.044 | 0.054 | 0.048 | 0.039 | 0.038 | 0.040 | 0.036 | 0.024 |
| 4 | 0.012 | 0.017 | 0.035 | 0.053 | 0.047 | 0.060 | 0.047 | 0.031 | 0.040 | 0.037 | 0.037 | 0.030 |
| 5 | 0.019 | 0.021 | 0.041 | 0.048 | 0.048 | 0.050 | 0.042 | 0.032 | 0.032 | 0.034 | 0.037 | 0.020 |
| 6 | 0.018 | 0.022 | 0.039 | 0.049 | 0.057 | 0.063 | 0.038 | 0.035 | 0.035 | 0.032 | 0.042 | 0.024 |
| 7 | 0.019 | 0.017 | 0.042 | 0.050 | 0.055 | 0.059 | 0.052 | 0.039 | 0.034 | 0.032 | 0.036 | 0.023 |
| 8 | 0.024 | 0.029 | 0.048 | 0.061 | 0.058 | 0.060 | 0.050 | 0.041 | 0.040 | 0.040 | 0.049 | 0.032 |

identified sporadically by region and phase, but one other similarity with these results to those of daily rainfall is that the MJO signal appears weak along the northern Gulf Coast for days producing at least 2.5 cm of precipitation, although a negative association does appear for Phase 3 at KAUD.

Restricting the results to a 95% confidence interval reduces the noise and provides a better look at the broadest MJO associations with heavy daily precipitation along the Gulf Coast. Much like the results in Tables 4.1 and 4.2, positive associations appear for Phase 8 along the western Gulf Coast and Phase 1 along the eastern Gulf Coast. Elsewhere, the associations are much more sporadic geographically, but there is some minor agreement with previous results for the negative associations shown for Phase 5 at KEYW (see Table 4.1)

and Phase 6 at KTLH (see Tables 4.1 and 4.2). The negative associations for KLCH during Phase 2 and KBRO for Phase 4 require further study. One other

**Table 4.4** As in Table 4.3 for a 95% confidence interval.

| Phase | KBRO | KCRP | KIAH | KLCH | KAUD | KMOB | KTLH | KGNV | KOCF | KTPA | KSRQ | KEYW |
|---|---|---|---|---|---|---|---|---|---|---|---|---|
| 1 | 0.024 | 0.022 | 0.034 | 0.050 | 0.052 | 0.054 | 0.057 | 0.049 | 0.044 | 0.049 | 0.051 | 0.034 |
| 2 | 0.017 | 0.019 | 0.037 | 0.039 | 0.052 | 0.054 | 0.048 | 0.044 | 0.046 | 0.045 | 0.045 | 0.027 |
| 3 | 0.019 | 0.022 | 0.037 | 0.044 | 0.044 | 0.054 | 0.048 | 0.039 | 0.038 | 0.040 | 0.036 | 0.024 |
| 4 | 0.012 | 0.017 | 0.035 | 0.053 | 0.047 | 0.060 | 0.047 | 0.031 | 0.040 | 0.037 | 0.037 | 0.030 |
| 5 | 0.019 | 0.021 | 0.041 | 0.048 | 0.048 | 0.050 | 0.042 | 0.032 | 0.032 | 0.034 | 0.037 | 0.020 |
| 6 | 0.018 | 0.022 | 0.039 | 0.049 | 0.057 | 0.063 | 0.038 | 0.035 | 0.035 | 0.032 | 0.042 | 0.024 |
| 7 | 0.019 | 0.017 | 0.042 | 0.050 | 0.055 | 0.059 | 0.052 | 0.039 | 0.034 | 0.032 | 0.036 | 0.023 |
| 8 | 0.024 | 0.029 | 0.048 | 0.061 | 0.058 | 0.060 | 0.050 | 0.041 | 0.040 | 0.040 | 0.049 | 0.032 |

consistency is found along the northern Gulf Coast (KAUD, KMOB) with no associations found between days producing at least 2.5 cm of precipitation and MJO phase.

Not surprisingly, doubling the heavy precipitation threshold to 5.0 cm reduces the number of associations found with the MJO, even when using a 90% confidence interval (Table 4.5). A few similarities remain when compared to previous results, including positive associations with Phase 8 along the western Gulf Coast and negative associations for Phases 5 and 6 along the eastern Gulf Coast. Additionally, the overriding theme of little connection between the MJO and northern Gulf Coast precipitation continues as a broad region from KLCH eastward to KTLH produces no significant associations.

The MJO association with heavy precipitation along the Gulf Coast becomes even more difficult to detect when using a 95% confidence interval for days with ≥5.0 cm of precipitation. Only seven associations are found out of a

possible 96 (12 sites * 8 phases) in this round of Monte Carlo simulations (Table 4.6). The most familiar links that appear are the positive associations for

**Table 4.5** Average rates of days producing ≥5.0 cm of precipitation for each MJO phase. Green (red) shading indicates a positive (negative) association from the Monte Carlo simulations using a 90% confidence interval.

| Phase | KBRO | KCRP | KIAH | KLCH | KAUD | KMOB | KTLH | KGNV | KOCF | KTPA | KSRQ | KEYW |
|---|---|---|---|---|---|---|---|---|---|---|---|---|
| 1 | 0.007 | 0.009 | 0.013 | 0.017 | 0.012 | 0.020 | 0.015 | 0.012 | 0.012 | 0.013 | 0.016 | 0.009 |
| 2 | 0.008 | 0.006 | 0.011 | 0.013 | 0.017 | 0.019 | 0.014 | 0.012 | 0.015 | 0.015 | 0.016 | 0.008 |
| 3 | 0.006 | 0.007 | 0.011 | 0.017 | 0.015 | 0.019 | 0.010 | 0.012 | 0.008 | 0.009 | 0.010 | 0.006 |
| 4 | 0.004 | 0.006 | 0.011 | 0.014 | 0.014 | 0.020 | 0.015 | 0.010 | 0.012 | 0.011 | 0.010 | 0.010 |
| 5 | 0.005 | 0.008 | 0.016 | 0.016 | 0.016 | 0.015 | 0.014 | 0.010 | 0.007 | 0.007 | 0.012 | 0.007 |
| 6 | 0.004 | 0.005 | 0.013 | 0.017 | 0.019 | 0.017 | 0.010 | 0.006 | 0.006 | 0.006 | 0.010 | 0.006 |
| 7 | 0.007 | 0.003 | 0.009 | 0.015 | 0.018 | 0.019 | 0.014 | 0.009 | 0.008 | 0.008 | 0.009 | 0.008 |
| 8 | 0.010 | 0.010 | 0.015 | 0.019 | 0.014 | 0.019 | 0.014 | 0.011 | 0.013 | 0.014 | 0.014 | 0.013 |

Phase 8 at KBRO and KEYW and the negative associations for Phase 6 at KGNV and KTPA. Comparing Table 4.5 to Table 4.6 makes it clear that the MJO-precipitation signal becomes increasingly difficult to detect at increasing thresholds, likely because the sample size decreases as the stringency for rejecting the null hypotheses increases.

**Table 4.6** As in Table 4.5 for a 95% confidence interval.

| Phase | KBRO | KCRP | KIAH | KLCH | KAUD | KMOB | KTLH | KGNV | KOCF | KTPA | KSRQ | KEYW |
|---|---|---|---|---|---|---|---|---|---|---|---|---|
| 1 | 0.007 | 0.009 | 0.013 | 0.017 | 0.012 | 0.020 | 0.015 | 0.012 | 0.012 | 0.013 | 0.016 | 0.009 |
| 2 | 0.008 | 0.006 | 0.011 | 0.013 | 0.017 | 0.019 | 0.014 | 0.012 | 0.015 | 0.015 | 0.016 | 0.008 |
| 3 | 0.006 | 0.007 | 0.011 | 0.017 | 0.015 | 0.019 | 0.010 | 0.012 | 0.008 | 0.009 | 0.010 | 0.006 |
| 4 | 0.004 | 0.006 | 0.011 | 0.014 | 0.014 | 0.020 | 0.015 | 0.010 | 0.012 | 0.011 | 0.010 | 0.010 |
| 5 | 0.005 | 0.008 | 0.016 | 0.016 | 0.016 | 0.015 | 0.014 | 0.010 | 0.007 | 0.007 | 0.012 | 0.007 |
| 6 | 0.004 | 0.005 | 0.013 | 0.017 | 0.019 | 0.017 | 0.010 | 0.006 | 0.006 | 0.006 | 0.010 | 0.006 |
| 7 | 0.007 | 0.003 | 0.009 | 0.015 | 0.018 | 0.019 | 0.014 | 0.009 | 0.008 | 0.008 | 0.009 | 0.008 |
| 8 | 0.010 | 0.010 | 0.015 | 0.019 | 0.014 | 0.019 | 0.014 | 0.011 | 0.013 | 0.014 | 0.014 | 0.013 |

The results thus far indicate that the MJO has statistically significant associations with Gulf Coast precipitation variability during specific phases for

specific thresholds. In the following sections, these associations will be explored further on a region-by-region scale around the GoM with a look at the atmospheric mechanisms that are likely to be responsible for these connections. The analysis is restricted to the results produced by the 95% confidence intervals (Tables 4.2, 4.4, and 4.6).

A phase-by-phase examination of the mean synoptic pattern and atmospheric anomalies provides additional explanation for the results identified in this study. In general terms, anomalous patterns of mid-tropospheric geopotential heights, SLP, atmospheric moisture, and surface precipitation rates support the results obtained here through Monte Carlo simulations. In most cases, the broad-scale anomalies are even supportive of the results only reported with a 90% confidence level, adding some measure of certainty even when the statistical correlations are not quite as strong. The results shown here also suggest many similarities to those of Study 1 which should not be surprising since cyclone variability would be expected to have an impact on precipitation variability. A more detailed discussion of the synoptic patterns follows in Sections 4.3.1 – 4.3.8 relating to the statistically significant associations found in Tables 4.2, 4.4, and 4.6.

In order to display the patterns leading to GoM cyclogenesis variability, NCEP/NCAR Reanalysis daily composite data were obtained through NOAA's Earth System Research Laboratory (ESRL 2018) online plotting tool (https://www.esrl.noaa.gov/psd/data/composites/day/). This tool allows for the user to provide a custom series of dates, which in this case corresponds to

a particular MJO phase, and then download a netCDF file containing the variable of interest for those dates. This project uses anomaly data which is calculated based on a 1981–2010 mean constructed by NCEP/NCAR. Once the data of interest were queried and netCDF files were created, those files were then run though Python scripts to generate the anomaly plots found in the following sections.

### 4.3.1 MJO Phase 1

MJO Phase 1 shows several positive associations with precipitation, particularly along the eastern Gulf Coast. Both daily precipitation and the number of days with at least 2.5 cm of precipitation show increases for most sites near the Florida coastline. KBRO also has a positive association with daily rainfall but it does not show up for days with ≥2.5 cm or ≥5.0 cm of precipitation. Several anomalous atmospheric patterns are noted during Phase 1 that might explain the increased precipitation noted in these regions.

An examination of both 500 mb geopotential height and sea level pressure (SLP) patterns shows that the majority of the GoM experiences negative anomalies during Phase 1, with the maximum noted near and north of the northern Gulf Coast. The pattern seems to suggest a weakening of the semi-permanent subtropical high (Bermuda-Azores high) that typically extends across much of the Atlantic and to varying degrees into the eastern United States. Any weakening of the Bermuda-Azores high would support an increase in the vertical motion that is one of the key components needed for the generation of precipitation. The closer proximity of Florida than other regions of

the GoM to this semi-permanent high might suggest that it is more strongly influenced by any fluctuations in its strength.

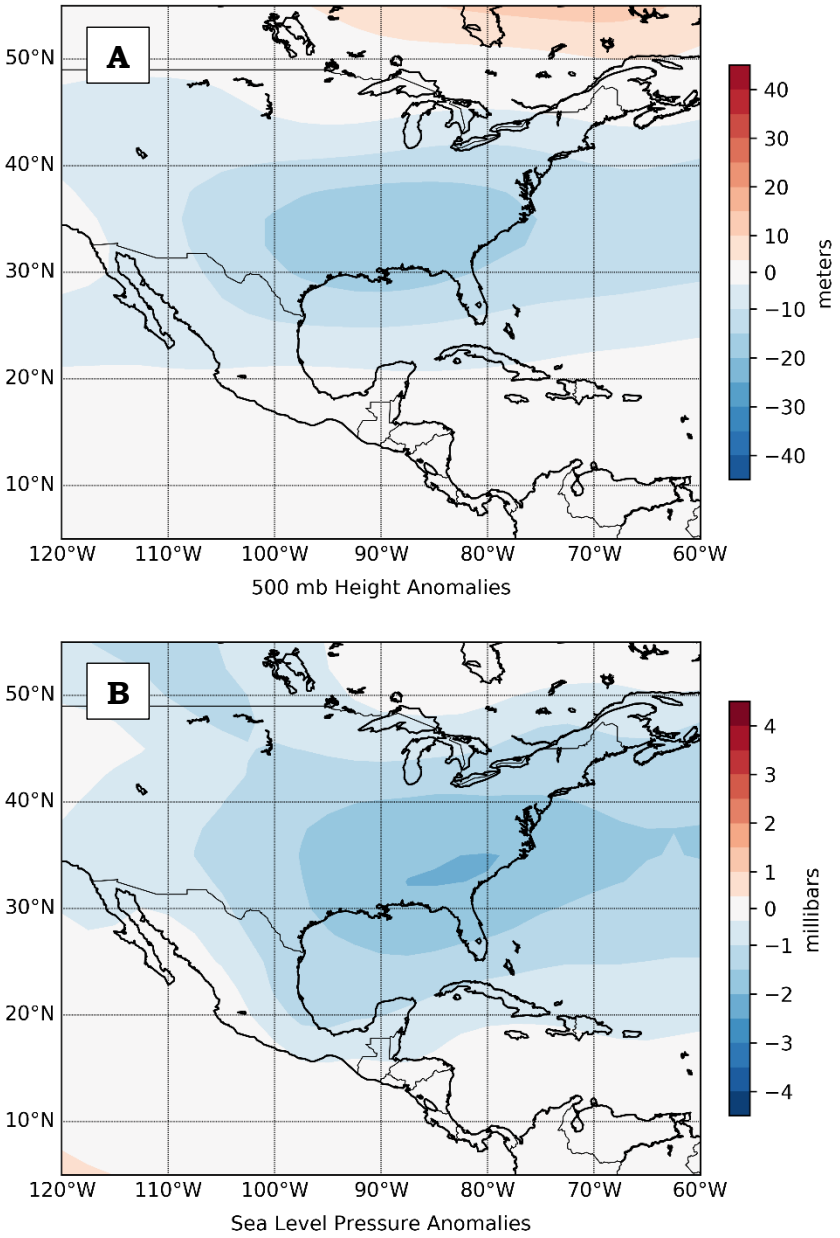


**Figure 4.4** MJO Phase 1 500 mb geopotential height anomalies (A) and sea level pressure anomalies (B) for 1979–2014. Anomalies based on the NCEP/NCAR Reanalysis 1981–2010 mean.

Measures of atmospheric moisture content during MJO Phase 1 also support the results found in Tables 4.2, 4.4, and 4.6. Relative humidity is a

measure of atmospheric moisture content, particularly as it relates to the saturation vapor pressure. A plot of 700 mb relative humidity anomalies during Phase 1 shows a large area of mid-tropospheric positive anomalies extending from the southwestern GoM into Florida, with the greatest positive anomalies over the Florida Peninsula (Figure 4.5). These positive anomalies would be supportive of increased cloud cover and precipitation.

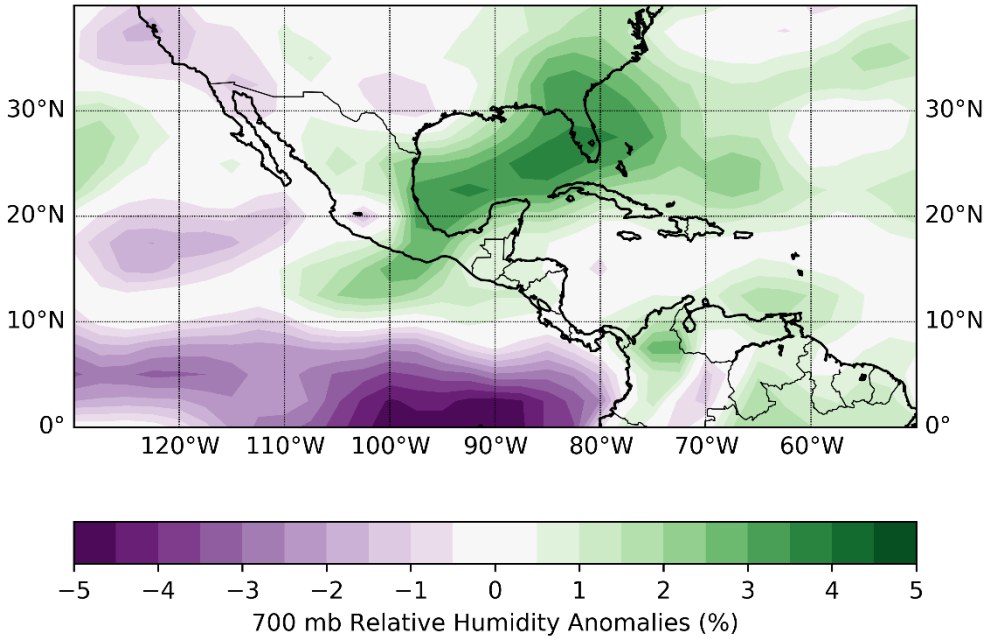


**Figure 4.5** MJO Phase 1 700 mb relative humidity anomalies for 1979–2014. Anomalies based on the NCEP/NCAR Reanalysis 1981–2010 mean.

Figure 4.5 displays a proxy for atmospheric moisture and saturation at a single level in the mid troposphere but precipitable water (PW) provides a way to examine the integrated moisture content throughout the entire atmospheric column. Not surprisingly, a plot of PW anomalies (Figure 4.6) displays a pattern similar to that shown in Figure 4.5, with anomalously high PW content noted from the southwestern GoM into Florida. Once again, the greatest positive anomalies are near and over portions of the Florida Peninsula. Increased PW

values would aid in the development of precipitation and are supportive of the results found in Tables 4.2, 4.4, and 4.6.

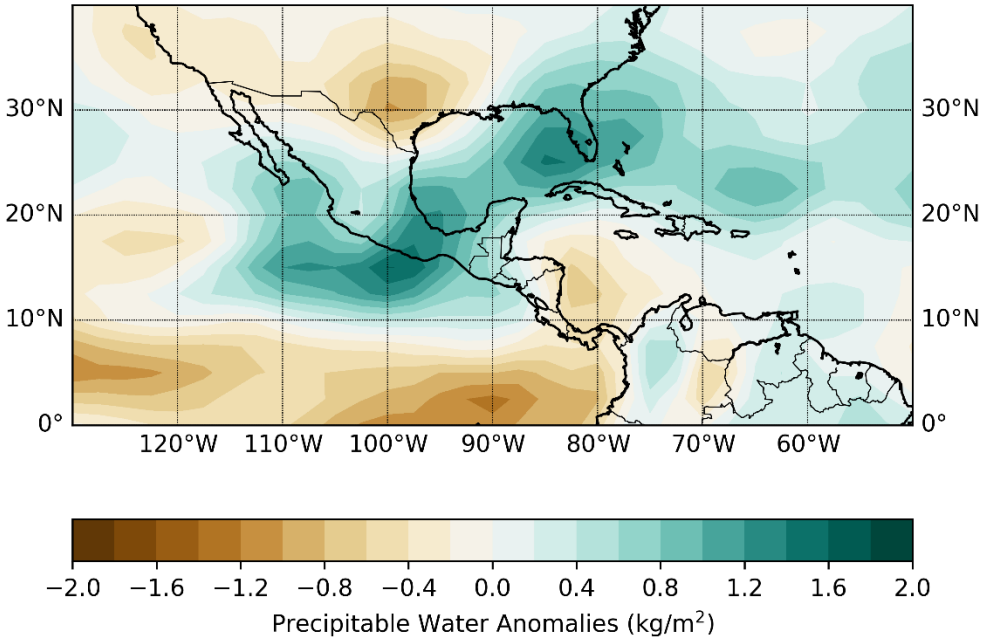


**Figure 4.6** MJO Phase 1 precipitable water anomalies for 1979–2014. Anomalies based on the NCEP/NCAR Reanalysis 1981–2010 mean.

A final and perhaps more direct way to explore the associations between MJO Phase 1 and precipitation along the U.S. Gulf Coast is through the use of precipitation rate anomalies. Figure 4.7 displays some similarities to Figures 4.5 and 4.6 with a generally moist pattern noted over the eastern GoM, but the moisture signal over the western and southwestern GoM becomes more difficult to discern. Anomalously high precipitation rates near and over the Florida Peninsula are once again supportive of the results found from the Monte Carlo simulations. At first glance, it might appear that Figure 4.7 does not support the positive association found with daily rainfall at KBRO, but Figures 4.4, 4.5, and 4.6 show a pattern that is generally supportive of precipitation near South Texas. Additionally, no associations were found at

KBRO with the heavier precipitation days (2.5 cm and 5.0 cm), so it is possible that MJO Phase 1 produces an increase in daily precipitation at KBRO but not in the frequency of heavy rain events at this location. Figure 4.7 lends credence to this notion because no significant change in precipitation rates is noted.

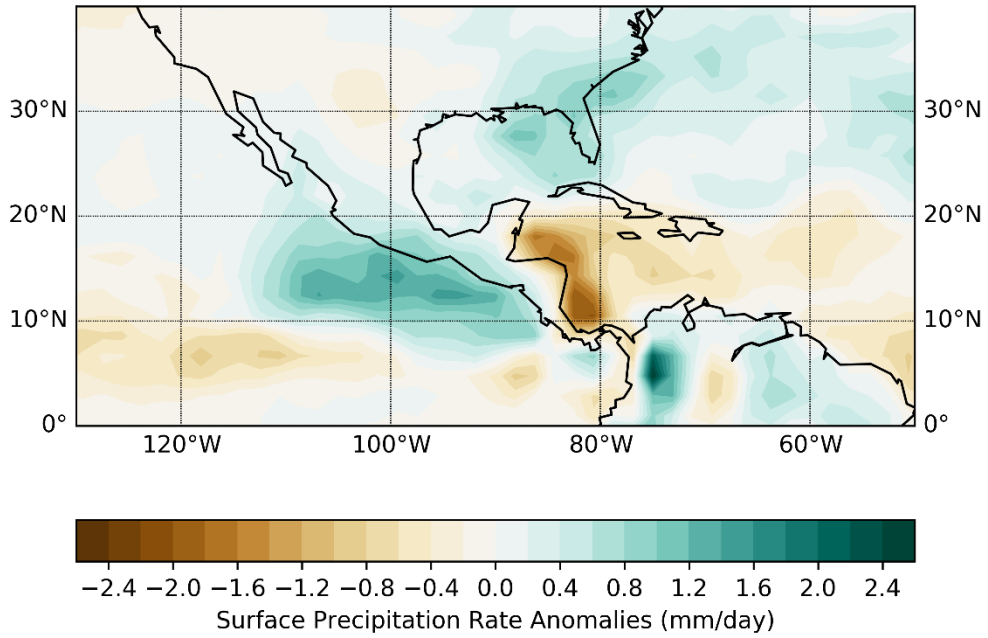


**Figure 4.7** MJO Phase 1 precipitation rate anomalies for 1979–2014. Anomalies based on the NCEP/NCAR Reanalysis 1981–2010 mean.

The Monte Carlo simulations run for this analysis show that MJO Phase 1 results in increased precipitation for much of the eastern GoM but also for portions of South Texas. The increase appears to be linked to a broad area of reduced atmospheric pressures over the eastern U.S., both in the mid-troposphere and near the surface. Additionally, tropical moisture is funneled into portions of the GoM, producing an increase in atmospheric moisture content, particularly from northern Mexico eastward to the Florida Peninsula. These patterns shown in Figures 4.4 – 4.7 collectively support the results obtained through Monte Carlo simulations in Tables 4.2, 4.4, and 4.6.

### 4.3.2 MJO Phase 2

Monte Carlo simulations only show a few associations between MJO Phase 2 and Gulf Coast precipitation when limiting the results to a 95% confidence interval. Tables 4.2, 4.4, and 4.6 do indicate some additional possible linkages when broadening the results to a 90% confidence interval, but this discussion will limit analysis to those connections meeting the more stringent criteria. No associations are found for any of the sites when examining daily precipitation, but a negative link is found between MJO Phase 2 and days producing ≥2.5 cm of precipitation at KLCH, whereas a positive link is found for days producing ≥5.0 cm of precipitation at KOCF and KTPA. Examining NCEP/NCAR reanalysis data for Phase 2 shows an atmospheric pattern that falls short of demonstrating a clear-cut connection to these results, but some clues are still found in the figures that follow.

Plots of 500 mb geopotential height anomalies and SLP anomalies for MJO Phase 2 (Figure 4.8) still show some lowering of atmospheric pressure over the eastern U.S., but both the magnitude and the coverage of these anomalies are greatly reduced from Phase 1 (Figure 4.4). Lower-than-normal 500 mb geopotential heights are centered near the U.S. Midwest with some weak negative anomalies extending southward to the northern and eastern Gulf Coast. SLP is largely found to be near-normal in and around the GoM but some weak negative anomalies are apparent just east of the Florida Peninsula. It cannot be stated conclusively whether this pattern alone is enough to support the positive associations found for 5.0 cm precipitation days at KOCF

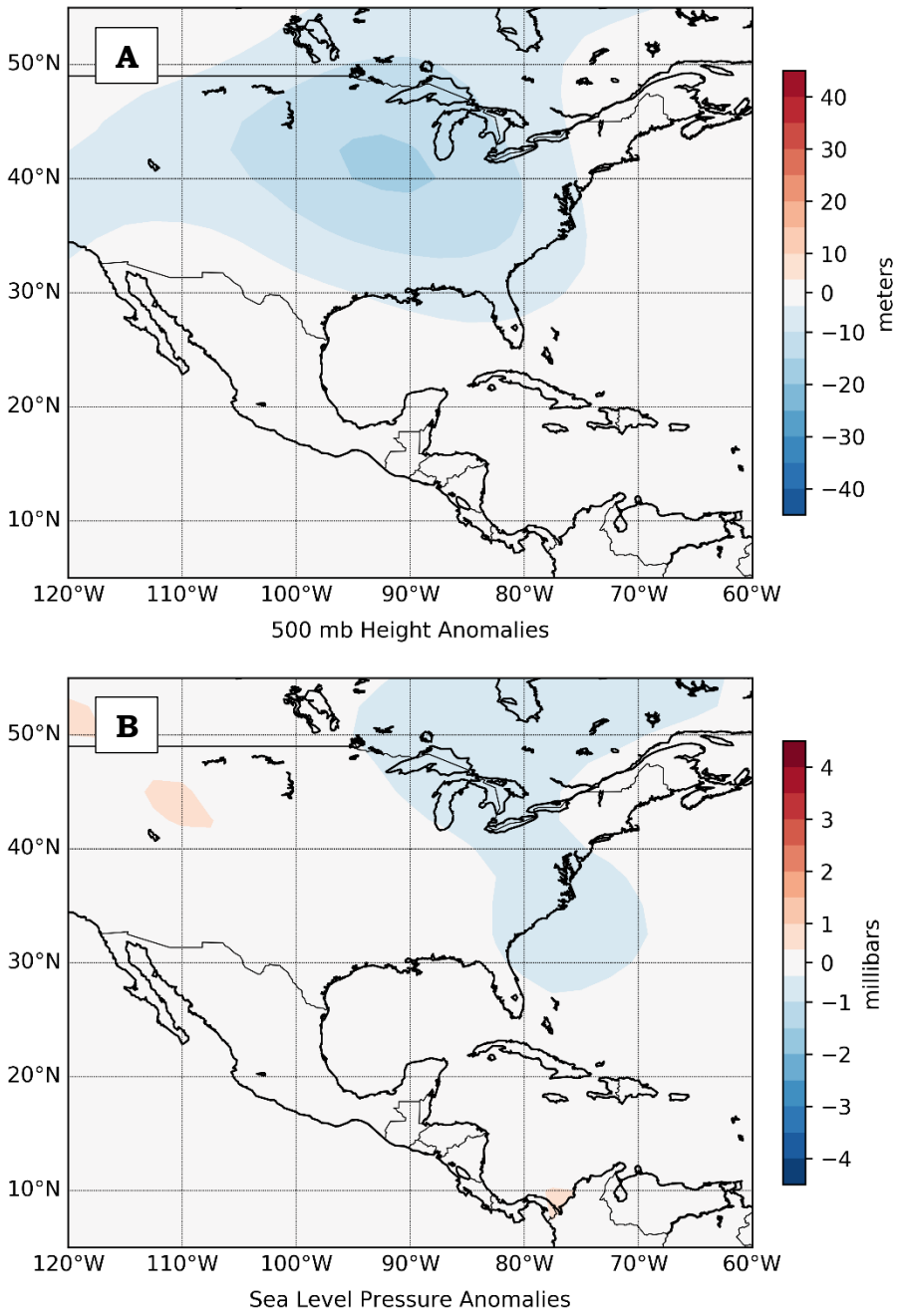


**Figure 4.8** MJO Phase 2 500 mb geopotential height anomalies (A) and sea level pressure anomalies (B) for 1979–2014. Anomalies based on the NCEP/NCAR Reanalysis 1981–2010 mean.

and KTPA, but the pattern does not seem to show a clear link to the negative association found for 2.5 cm precipitation days at KLCH.

Examination of 700 mb relative humidity anomalies (Figure 4.9) begins to show some signs of the atmosphere supporting the results obtained in Tables 4.2, 4.4, and 4.6. A large area of negative anomalies, indicative of drier-than-normal mid-tropospheric air, covers much of the western and north-central Gulf Coast. Somewhat weaker positive anomalies, indicative of a more humid mid-troposphere, are noted over the Florida Peninsula. These patterns would lend credence to the results obtained through the Monte Carlo simulations showing a decrease in days producing ≥2.5 cm of precipitation and KLCH and an increase in days with ≥5.0 cm of precipitation at KOCF and KTPA.

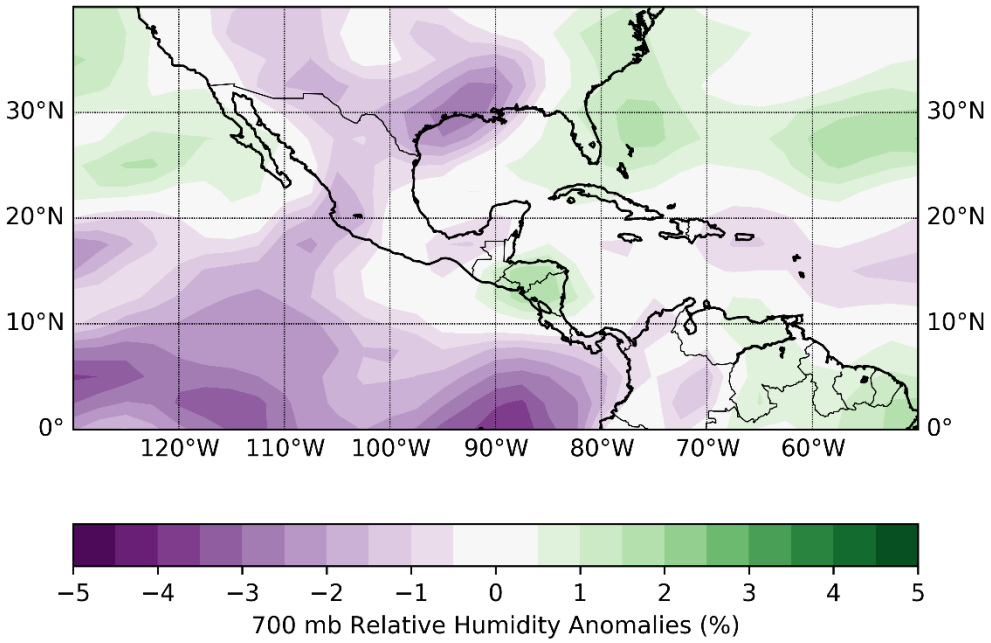


**Figure 4.9** MJO Phase 2 700 mb relative humidity anomalies for 1979–2014. Anomalies based on the NCEP/NCAR Reanalysis 1981–2010 mean.

Examination of PW anomalies during Phase 2 (Figure 4.10) shows a negative maximum very near KLCH with some weak positive anomalies over the southeastern GoM and South Florida. Since PW is representative of the

moisture content through the entire column of the atmosphere, Figure 4.10 supports the negative association found at KLCH between Phase 2 and days producing ≥2.5 cm of precipitation. The signal is less clear for the association between the PW anomalies and the results found for KOCF and KTPA indicating an increase in days with ≥5.0 cm of precipitation during Phase 2, but it can at least be seen that there are some small positive anomalies near and just south of this region.

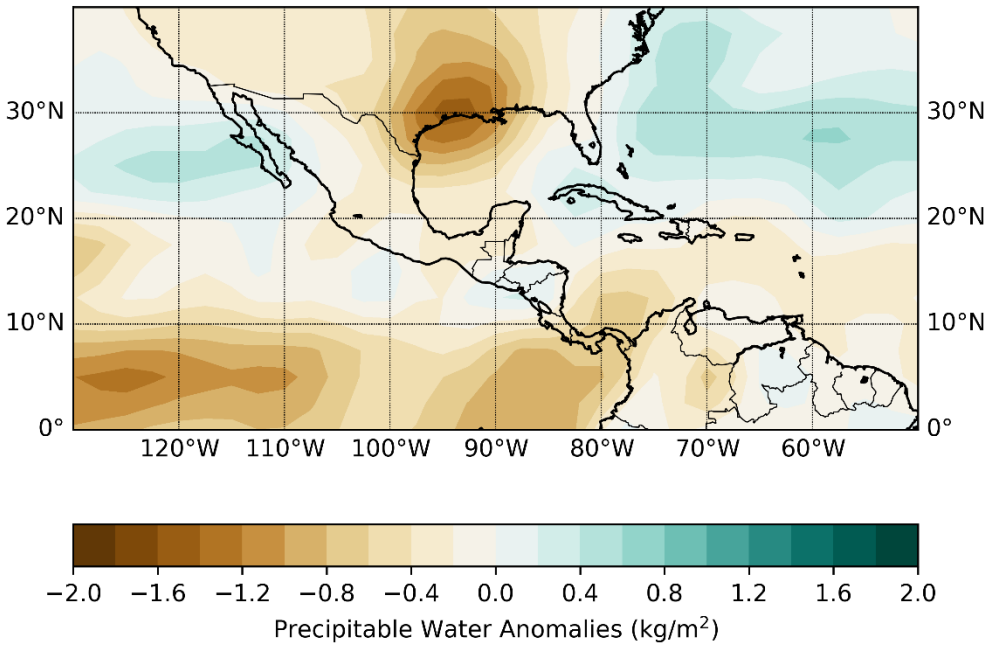


**Figure 4.10** MJO Phase 2 precipitable water anomalies for 1979–2014. Anomalies based on the NCEP/NCAR Reanalysis 1981–2010 mean.

A plot of MJO Phase 2 surface precipitation rate anomalies (Figure 4.11) shows some resemblance to the patterns found in Figures 4.9 and 4.10. Positive anomalies are located over the Florida Peninsula with an area of negative anomalies over the western and north-central GoM. The magnitudes of the both anomalies are somewhat small but still supportive of the results found

in the Monte Carlo simulations with reduced precipitation rates in the vicinity of KLCH and increased rates in the vicinity of KOCF and KTPA.

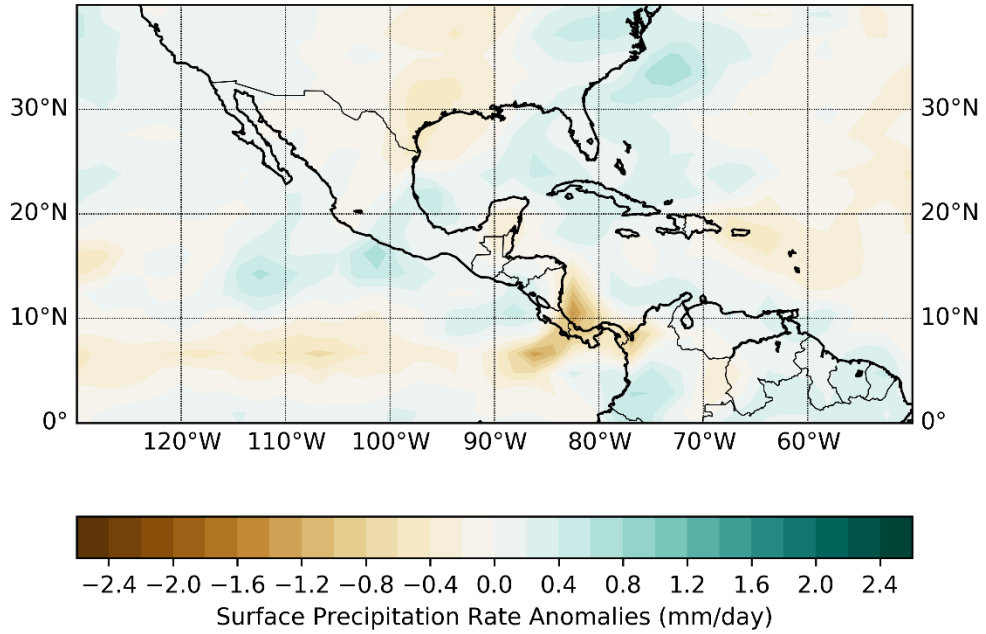


**Figure 4.11** MJO Phase 2 precipitation rate anomalies for 1979–2014. Anomalies based on the NCEP/NCAR Reanalysis 1981–2010 mean.

The Monte Carlo simulation results for MJO Phase 2 show only a few associations with location-specific precipitation along the Gulf Coast. Days producing at least 2.5 cm of precipitation are found to be less common at KLCH while days producing at least 5.0 cm of precipitation are more common at KOCF and KTPA. The atmospheric pattern may not show robust support for these results, but Figures 4.8 – 4.11 do show modestly lower pressures and somewhat greater amounts of moisture in the region around KOCF and KTPA, lending some credence to those results. The pressure pattern fails to show a discernable signal around KLCH, but measures of atmospheric moisture show a clear decrease during Phase 2, supporting the reduction in 2.5 cm precipitation days found in the Monte Carlo simulations.

### 4.3.3 MJO Phase 3

The Monte Carlo simulations conducted for MJO Phase 3 indicate that it has little impact on precipitation along the U.S. Gulf Coast. When looking at the results at a 95% confidence level (Tables 4.2, 4.4, and 4.6), the only significant association found is a decrease in daily precipitation for KEYW (Table 4.2). Given the limited impact of MJO Phase 3, only a brief discussion follows on its associated atmospheric anomalies.

The pressure pattern fails to identify a clear signal that would reduce precipitation at KEYW, but measures of atmospheric moisture do show some support. A plot of 700 mb relative humidity anomalies (Figure 4.12) shows lower-than-normal mid-tropospheric humidity through most of the GoM,

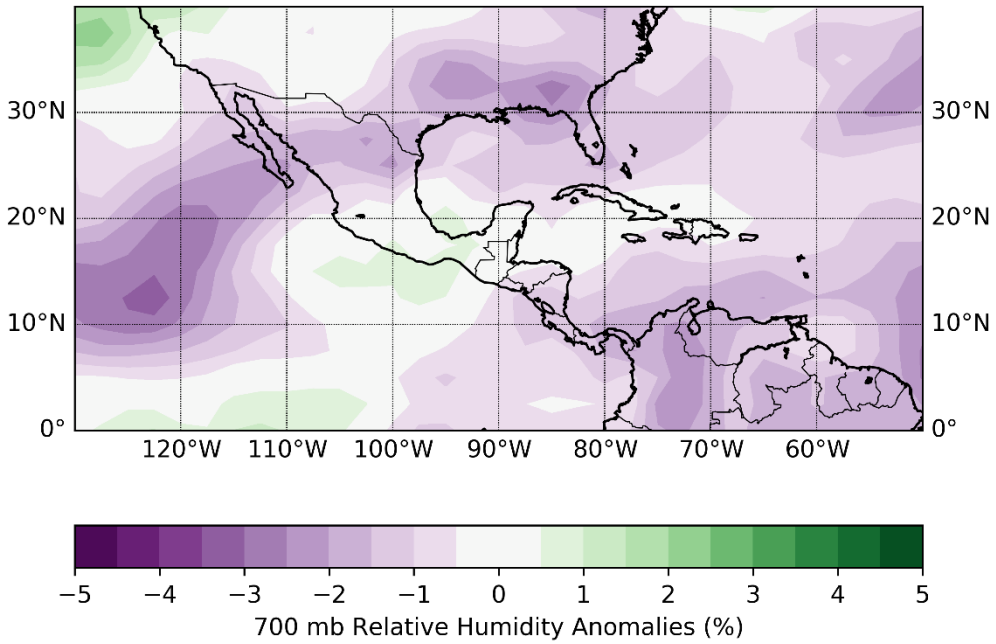


**Figure 4.12** MJO Phase 3 700 mb relative humidity anomalies for 1979–2014. Anomalies based on the NCEP/NCAR Reanalysis 1981–2010 mean.

including KEYW. Reduced relative humidity levels in the mid-troposphere of the atmosphere would likely support a reduction in rainfall, but it should be

noted that with negative anomalies prevailing over the majority of the GoM, there are likely other factors influencing the reduction in daily precipitation at KEYW since the negative associations fail to show up with any of the other sites along the Gulf Coast.

Similarly, negative PW anomalies are found over most of the GoM during Phase 3 (Figure 4.13), representing a pattern that would support a reduction in precipitation. But as with 700 mb relative humidity, the lone negative association at KEYW indicates other factors are influencing the reduction and further study would be needed to identify those features.

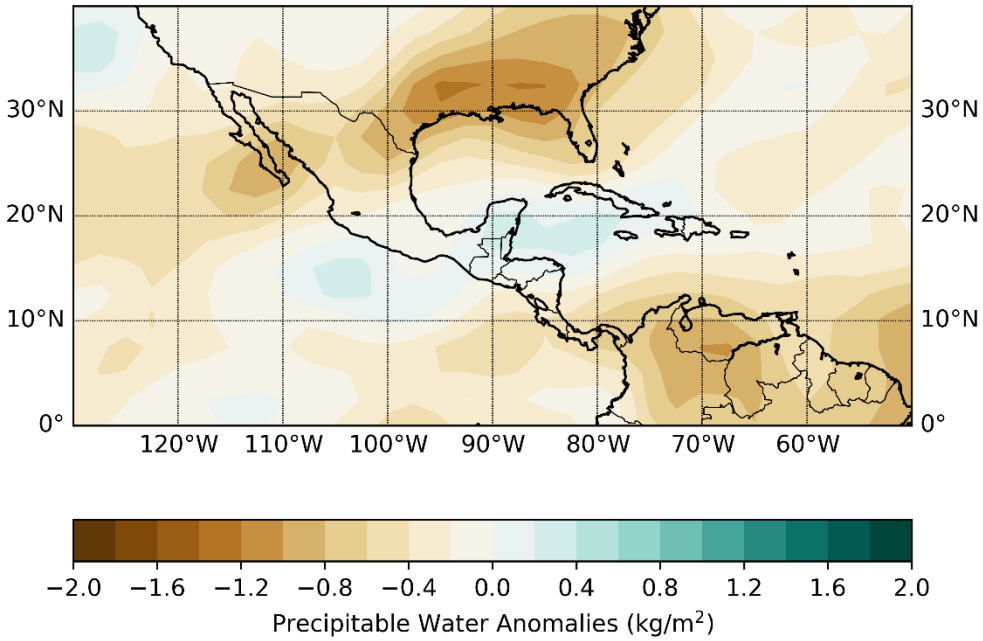


**Figure 4.13** MJO Phase 3 precipitable water anomalies for 1979–2014. Anomalies based on the NCEP/NCAR Reanalysis 1981–2010 mean.

MJO Phase 3 has a minimal impact on precipitation in and around the GoM as indicated by the Monte Carlo simulations conducted for this study. A reduction in daily precipitation is found for KEYW but it is not clear why the negative association is limited to this one site. Measures of atmospheric

moisture show a large-scale reduction throughout the region with some of the largest negative anomalies along the northern Gulf Coast. So even though this reduction in moisture is supportive of the results found for KEYW, further study is needed to determine why precipitation is not reduced along other areas of the Gulf Coast during Phase 3.

### 4.3.4 MJO Phase 4

Similar to Phase 3, MJO Phase 4 appears to have a limited impact on precipitation in and around the GoM. Monte Carlo simulations only suggest negative associations between Phase 3 and the number of days producing at least 2.5 cm of precipitation at KBRO and KGNV. The results in Tables 4.2, 4.4, and 4.6 are somewhat surprising since the atmospheric pattern seems to support an overall reduction in precipitation across much of the region. As with Phase 3, the discussion that follows will be somewhat limited since minimal associations were found.

The reduction in days producing ≥2.5 cm of precipitation at KGNV is supported by a number of anomalies in the atmosphere, including a general increase in atmospheric pressure and a reduction in moisture. Focusing on the moisture, a plot of PW anomalies (Figure 4.14) shows levels that are well below-normal for much of the eastern GoM during Phase 3, with a maximum reduction centered near KGNV.

Surface precipitation rate anomalies (Figure 4.15) show a similar pattern although the maximum negative anomalies are located over the eastern GoM

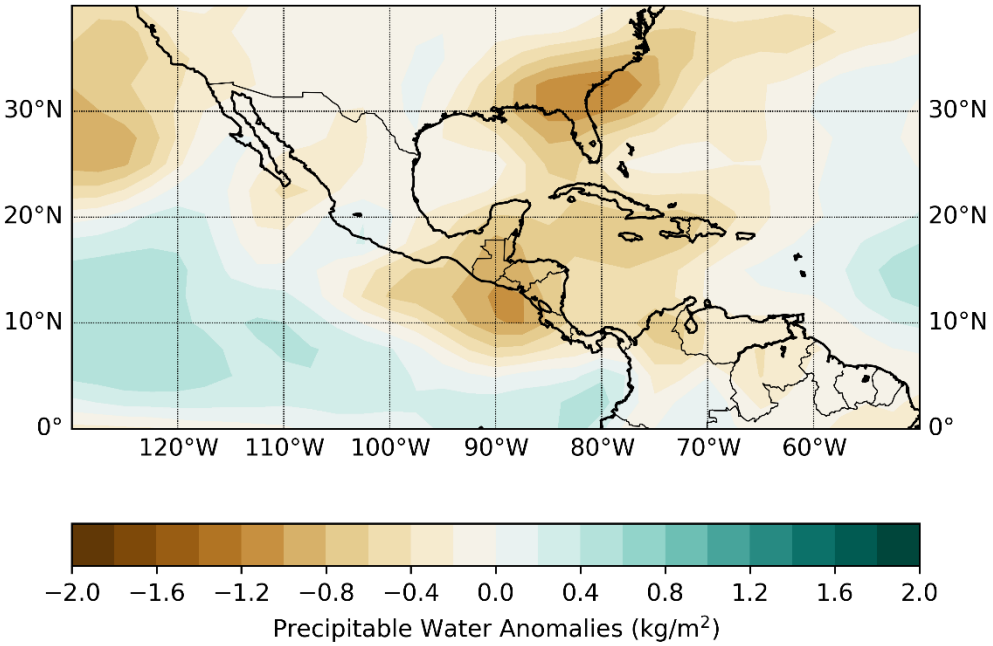


**Figure 4.14** MJO Phase 4 precipitable water anomalies for 1979–2014. Anomalies based on the NCEP/NCAR Reanalysis 1981–2010 mean.

and just east of Jacksonville, FL. However, both Figures 4.14 and 4.15 identify patterns that support a reduction in precipitation at KGNV.

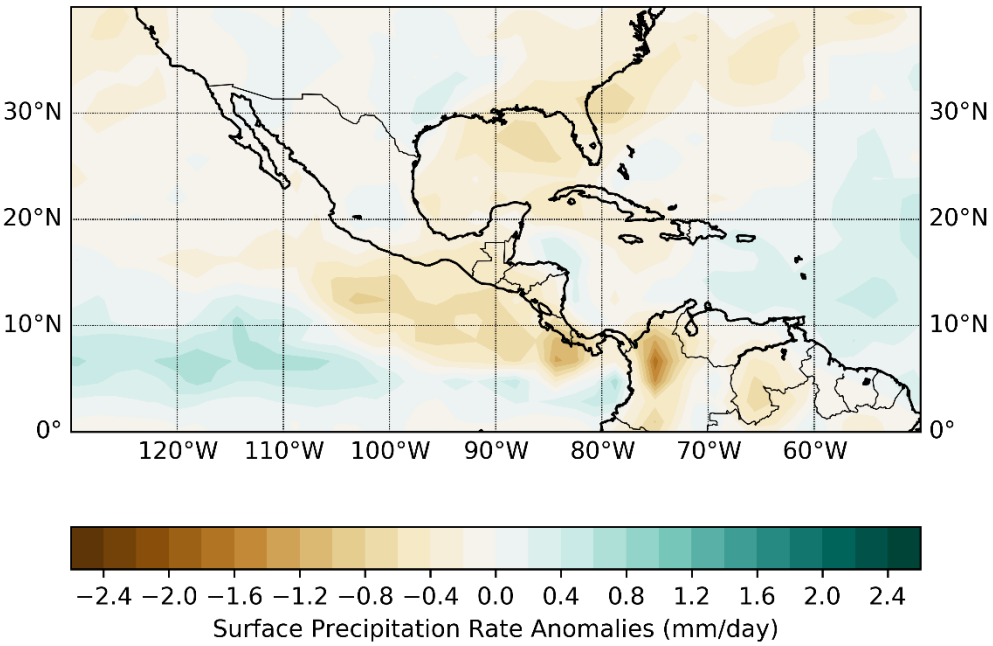


**Figure 4.15** MJO Phase 4 precipitation rate anomalies for 1979–2014. Anomalies based on the NCEP/NCAR Reanalysis 1981–2010 mean.

The negative association found for KBRO with days producing at least 2.5 cm of precipitation is more curious when examining Figures 4.14 and 4.15. Both PW and surface precipitation rates appear to be near-normal in this general region. While not pictured here, 500 mb geopotential heights are slightly above-normal in the western GoM and this would at least provide some support for the results at KBRO.

MJO Phase 4 appears to have a minimal impact on precipitation along the U.S. Gulf Coast, but negative associations are found at KBRO and KGNV when looking at the number of days with at least 2.5 cm of precipitation. A reduction in atmospheric moisture over the eastern GoM during this phase, along with increased atmospheric pressures, supports the results at KGNV. The cause of the reduction at KBRO is more difficult to pinpoint but an increase in 500 mb geopotential heights could be at least partially responsible.

### 4.3.5 MJO Phase 5

The results of the Monte Carlo simulations indicate that MJO Phase 5 is most influential on precipitation over the Florida Peninsula. Using a 95% confidence interval, daily precipitation is shown to decrease at KGNV and KOCF, while the number of days producing at least 2.5 cm of precipitation is reduced at KEYW. Examination of atmospheric pressure anomalies, along with measures of atmospheric moisture and precipitation rates, all support the Phase 5 Monte Carlo simulation results.

Plots of atmospheric heights and SLP indicate that high pressure becomes more prevalent over much of the U.S. and GoM during Phase 5

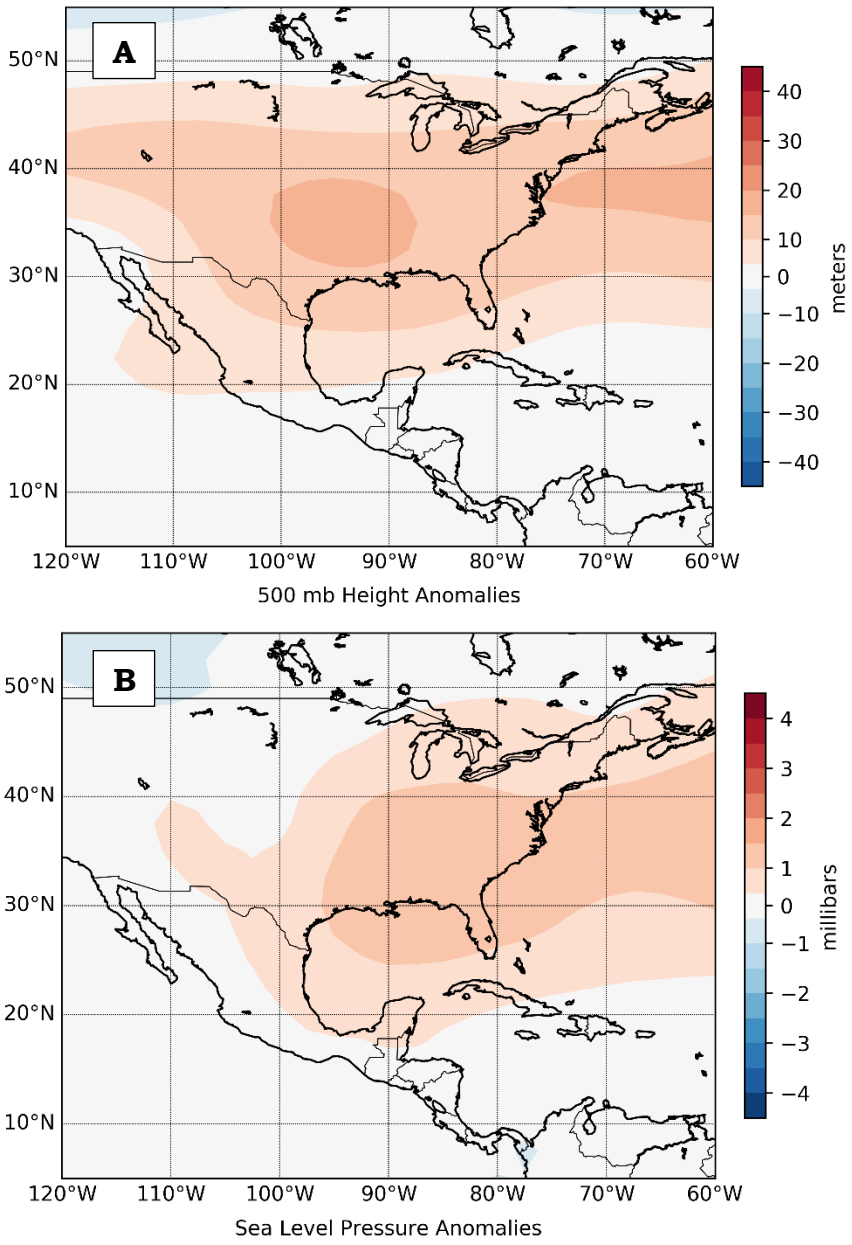


**Figure 4.16** MJO Phase 5 500 mb geopotential height anomalies (A) and sea level pressure anomalies (B) for 1979–2014. Anomalies based on the NCEP/NCAR Reanalysis 1981–2010 mean.

(Figure 4.16). Anomalously high pressures would tend to increase subsidence and atmospheric stability while reducing moisture. All of these factors would support a reduction in precipitation.

The reduction in atmospheric moisture can be seen more clearly when examining anomalies of 700 mb relative humidity and PW. Lower-than-normal mid-tropospheric relative humidity is noted across much of the GoM during Phase 5 (Figure 4.17), with the greatest negative anomalies extending from the eastern GoM across portions of the Florida Peninsula. PW anomalies (Figure 4.18) show a very similar pattern and both of these taken together would support a reduction in precipitation in the vicinity of KGNV, KOCF, and KEYW.

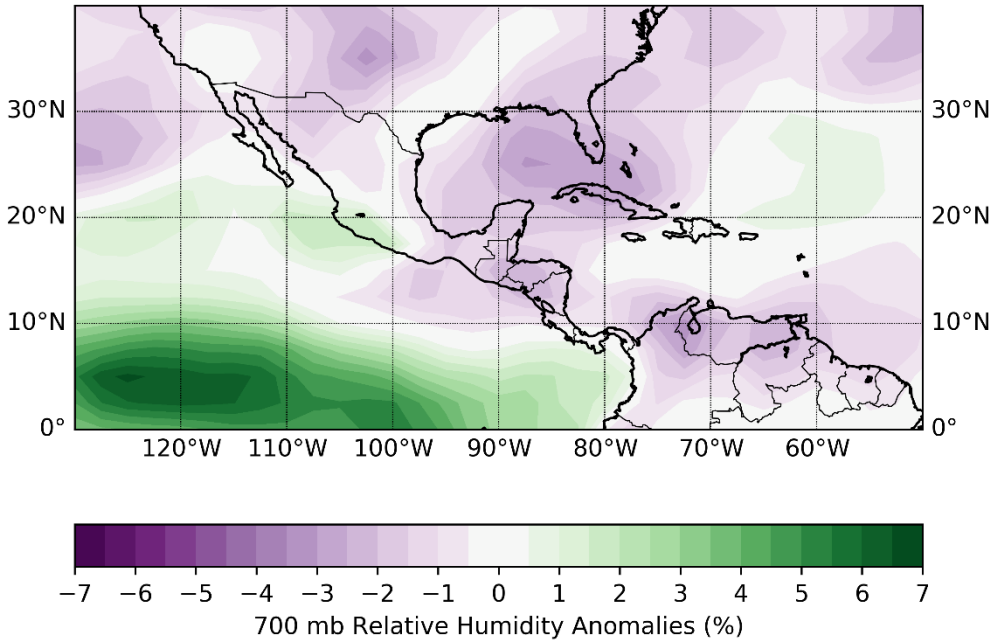


**Figure 4.17** MJO Phase 5 700 mb relative humidity anomalies for 1979–2014. Anomalies based on the NCEP/NCAR Reanalysis 1981–2010 mean.

Finally, an examination of surface precipitation rate anomalies (Figure 4.19) lends further support to the reduction in precipitation over the Florida Peninsula found in the Monte Carlo simulations. A large area of negative precipitation rate anomalies covers the eastern two-thirds of the GoM, including KGNV, KOCF, and KEYW.

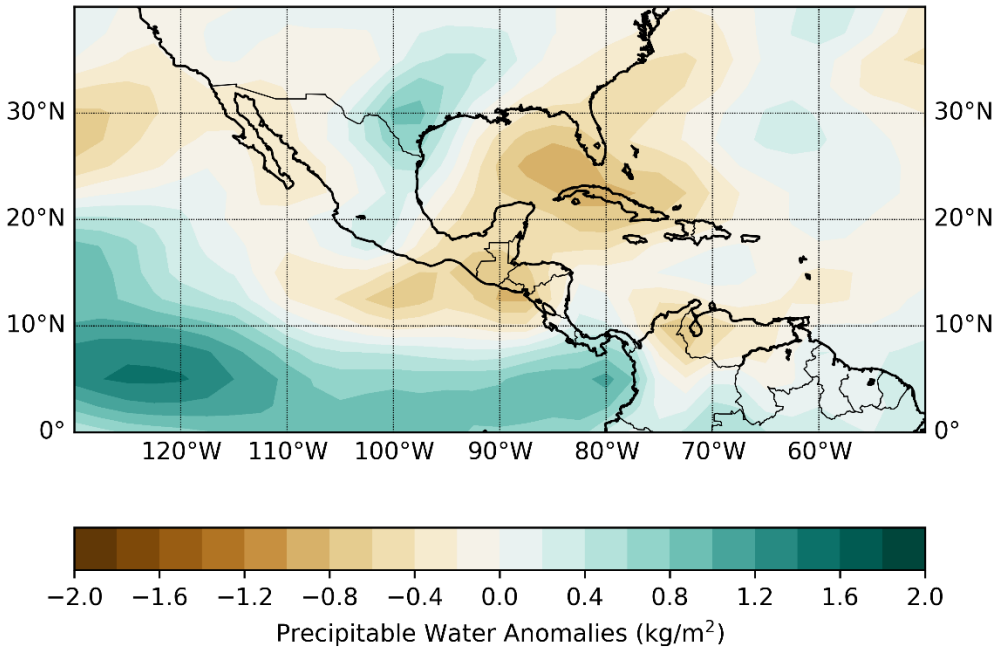


**Figure 4.18** MJO Phase 5 precipitable water anomalies for 1979–2014. Anomalies based on the NCEP/NCAR Reanalysis 1981–2010 mean.

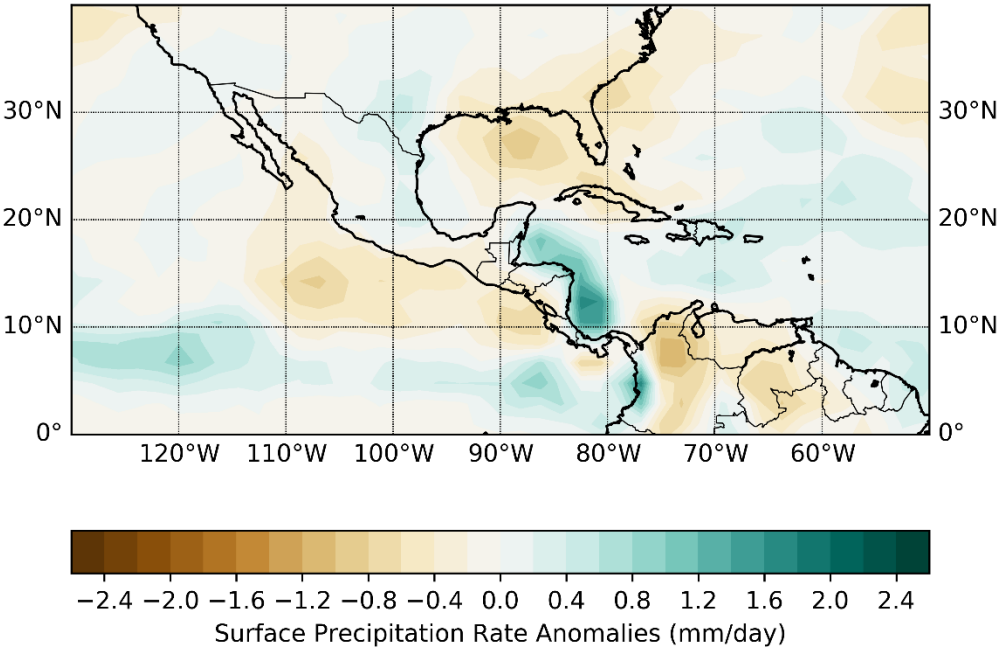


**Figure 4.19** MJO Phase 5 surface precipitation rate anomalies for 1979–2014. Anomalies based on the NCEP/NCAR Reanalysis 1981–2010 mean.

MJO Phase 5 exerts its greatest influence on U.S. Gulf Coast precipitation over the Florida Peninsula. The results obtained in the Monte

Carlo simulations (Tables 4.2 and 4.4) indicate that the daily precipitation is reduced at KGNV and KOCF, while days producing at least 2.5 cm of precipitation are less frequent at KEYW. The atmosphere is shown to support these reductions through anomalously high pressure and anomalously low moisture in this region.

### 4.3.6 MJO Phase 6

The negative associations that first appear in MJO Phases 4 and 5 for parts of the eastern Gulf Coast persist in this general region for Phase 6. The Monte Carlo simulations indicate negative associations with daily precipitation at KTLH and KTPA, days producing at least 2.5 cm of precipitation at KTLH, and days producing at least 5.0 cm of precipitation at KGNV and KTPA. Atmospheric anomalies during Phase 6 include a pattern that is supportive of reduced precipitation in the area of the Florida Peninsula.

A plot of 500 mb geopotential height anomalies (Figure 4.20) shows above-normal heights, corresponding with high atmospheric pressure, covering a large portion of the U.S., including much of the Gulf Coast. SLP anomalies only show a small region of positive anomalies but those anomalously high values are centered over the Florida Peninsula (Figure 4.20). High pressure promotes increased atmospheric stability and the SLP anomalies in particular lend support to the Monte Carlo results in Tables 4.2, 4.4, and 4.6 indicating a reduction in precipitation during Phase 6 for parts of the Florida Peninsula.

Figure 4.20 shows a pressure pattern that is somewhat supportive of reduced precipitation over the Florida Peninsula, but measures of atmospheric

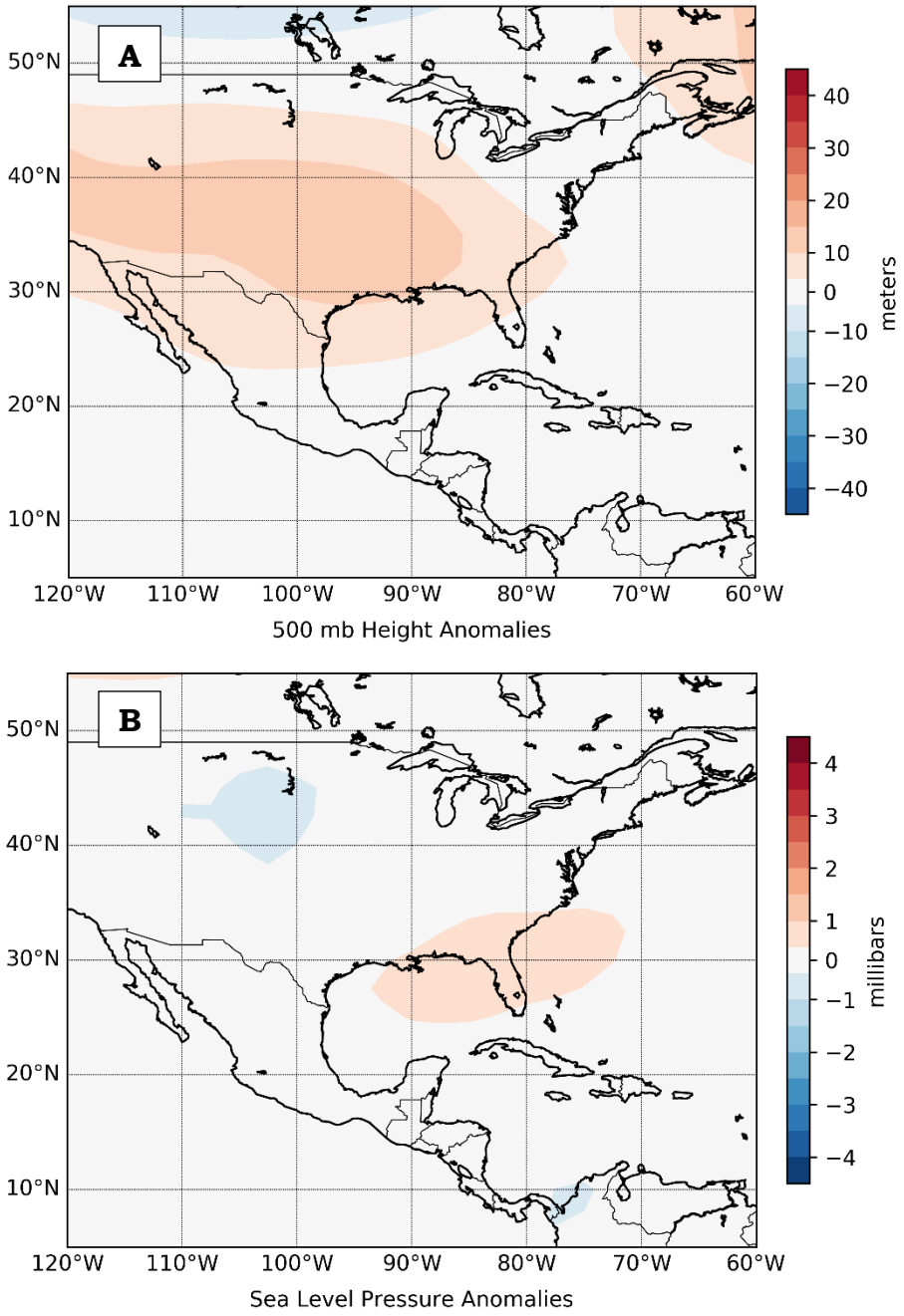


**Figure 4.20** MJO Phase 6 500 mb geopotential height anomalies (A) and sea level pressure anomalies (B) for 1979–2014. Anomalies based on the NCEP/NCAR Reanalysis 1981–2010 mean.

moisture provide a much stronger signal for this reduction. Relative humidity anomalies at 700 mb (Figure 4.21) are negative across most of the GoM with the greatest anomalies noted from the central GoM across the Florida

Peninsula. This area of anomalously low mid-tropospheric relative humidity is supportive of a reduction in precipitation.

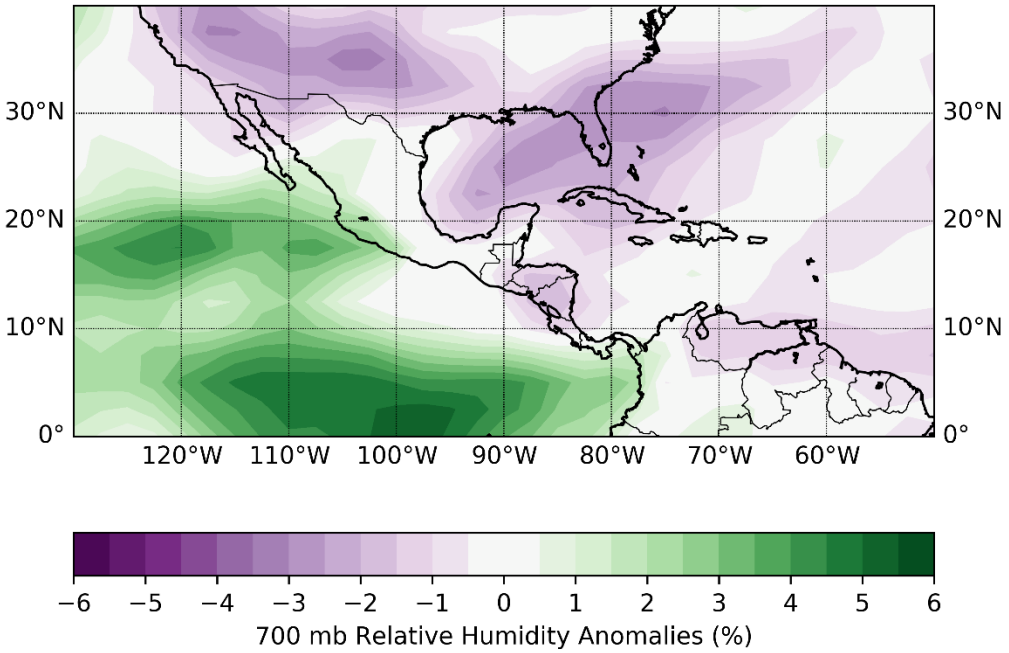


**Figure 4.21** MJO Phase 6 700 mb relative humidity anomalies for 1979–2014. Anomalies based on the NCEP/NCAR Reanalysis 1981–2010 mean.

PW anomalies (Figure 4.22) show a very similar pattern to Figure 4.21 with a large region of negative anomalies extending from the central GoM across the Florida Peninsula. The negative anomalies with the greatest magnitude are located near and just east of the Florida Peninsula. The anomalously low values of available moisture through the atmospheric column support the decrease in precipitation noted at several sites in this region.

The Monte Carlo results from Tables 4.2, 4.4, and 4.6 get a final measure of support from a plot of surface precipitation rate anomalies (Figure 4.23). Negative anomalies are once again noted in the general region extending from the central GoM across the Florida Peninsula, although the magnitude of the anomalies is somewhat lower. However, Figure 4.23 provides one more piece of

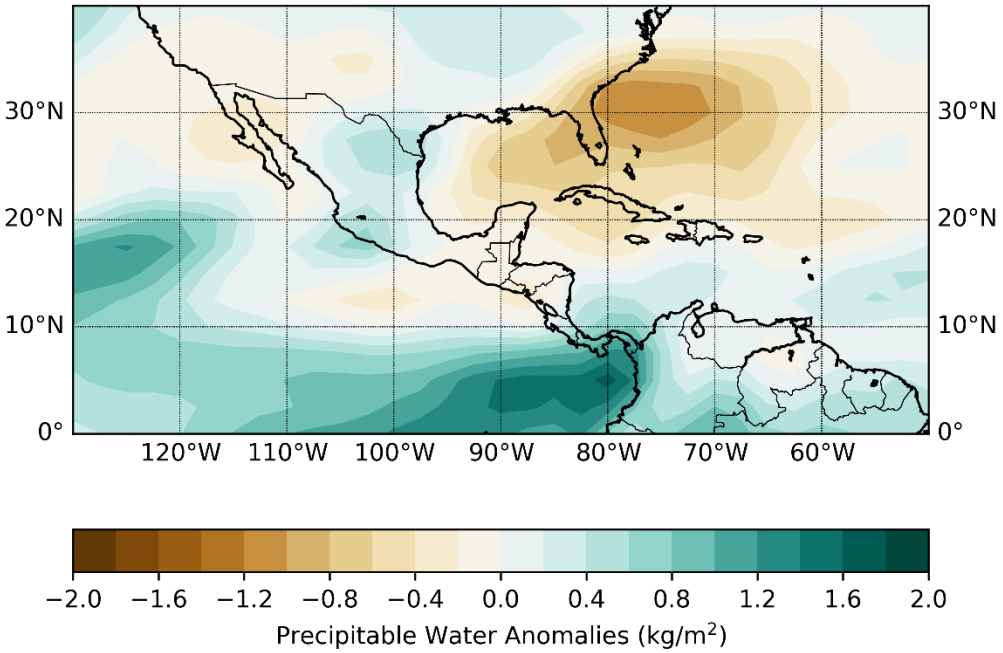


**Figure 4.22** MJO Phase 6 700 precipitable water anomalies for 1979–2014. Anomalies based on the NCEP/NCAR Reanalysis 1981–2010 mean.

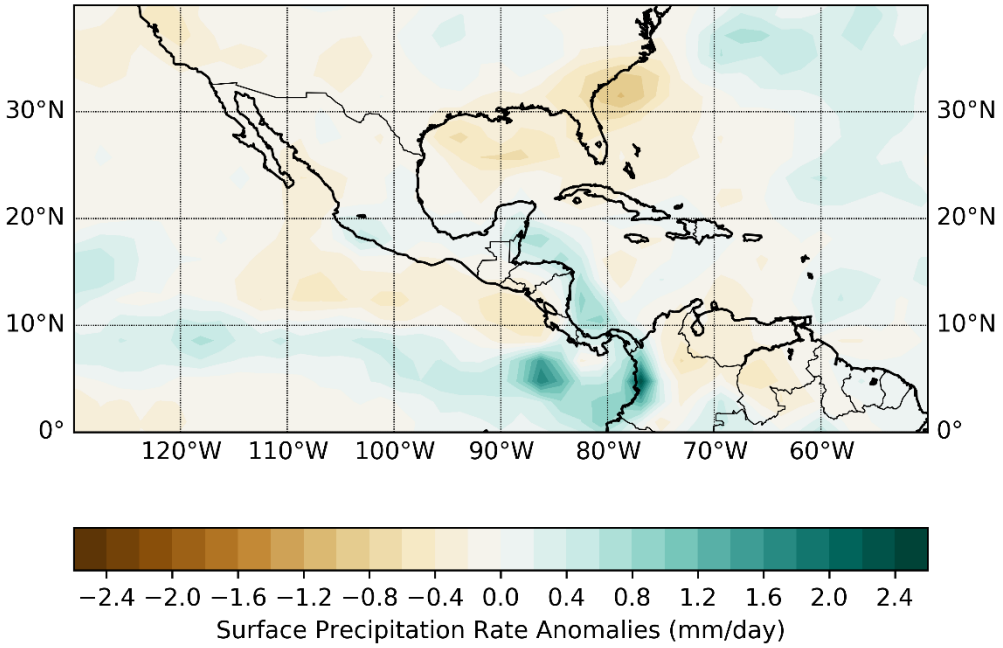


**Figure 4.23** MJO Phase 6 surface precipitation rate anomalies for 1979–2014. Anomalies based on the NCEP/NCAR Reanalysis 1981–2010 mean.

evidence as to why several sites in Florida see a reduction in precipitation during MJO Phase 6.

MJO Phase 6 continues a pattern of reduced precipitation that begins in Phases 4 and 5 for portions of the Florida Peninsula. The reduction is linked to multiple changes in the synoptic scale weather pattern, including increased atmospheric pressure, increased stability, reduced levels of moisture, and reduced precipitation rates. The extent of the impacts also appears to be a bit greater than those noted in Phases 4 and 5.

### 4.3.7 MJO Phase 7

MJO Phase 7 appears to be a transitional time in and around the GoM as the pattern shifts from a relatively stable one during Phases 4-6 to a more active one heading into Phases 8 and 1. Monte Carlo simulations for this phase only reveal a pair of isolated negative associations with precipitation along the Gulf Coast. When limiting the results to a 95% confidence interval, daily precipitation is shown to be reduced at KSRQ while the number of days producing at least 5.0 cm of precipitation is reduced at KCRP. Phase 7 proves to be the most confounding when examining atmospheric links to the reductions in precipitation at these locations since some variables seemingly point toward a likelihood of increased precipitation.

Measures of atmospheric moisture show a distinct increase during MJO Phase 7 relative to the prior phases. A plot of 700 mb relative humidity anomalies (Figure 4.24) shows anomalously high levels of mid-tropospheric saturation across most of the GoM with the greatest anomalies noted from the northeastern GoM into northern Florida. This would seem to conflict with the negative association found with daily precipitation for KSRQ. Near-normal

levels of 700 mb relative humidity are noted near KCRP where the Monte Carlo simulations indicate a reduction in days producing at least 5.0 cm of precipitation.

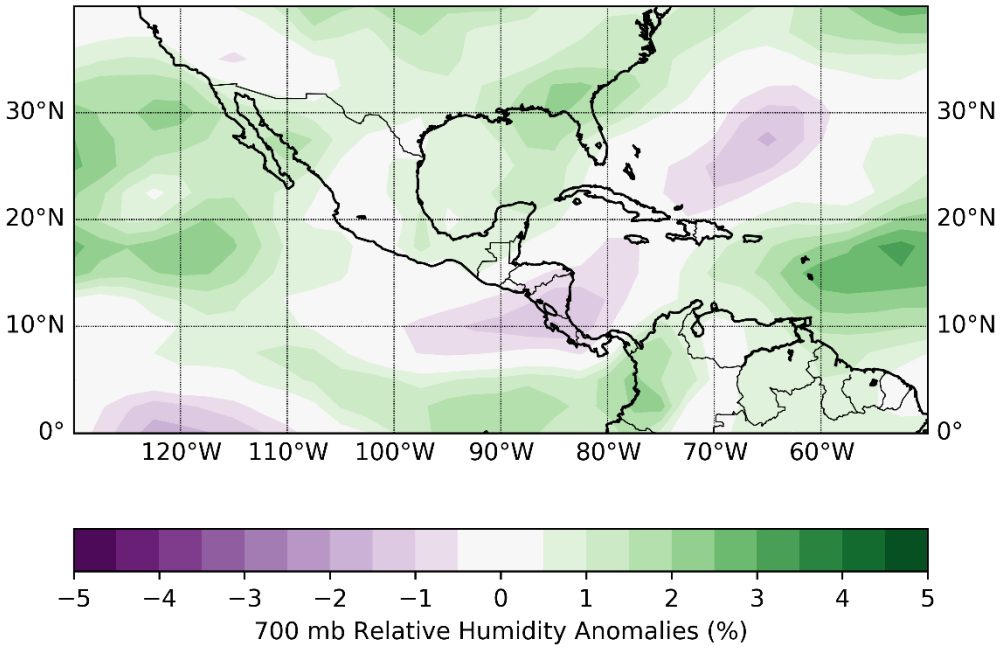


**Figure 4.24** MJO Phase 7 700 mb relative humidity anomalies for 1979–2014. Anomalies based on the NCEP/NCAR Reanalysis 1981–2010 mean.

PW anomalies (Figure 4.25) show a pattern similar to that in Figure 4.24 but positive anomalies cover nearly the entire GoM region. The greatest anomalies are once again noted from the northeastern GoM into northern Florida with the magnitude of those anomalies being a bit greater than those of 700 mb relative humidity (Figure 4.24). Increased moisture levels through the atmospheric column again make the results at KSRQ surprising. While the magnitude of the anomalies is low around KCRP, the PW anomaly pattern also fails to provide any support for the reduction in 5.0 cm precipitation days at this site.

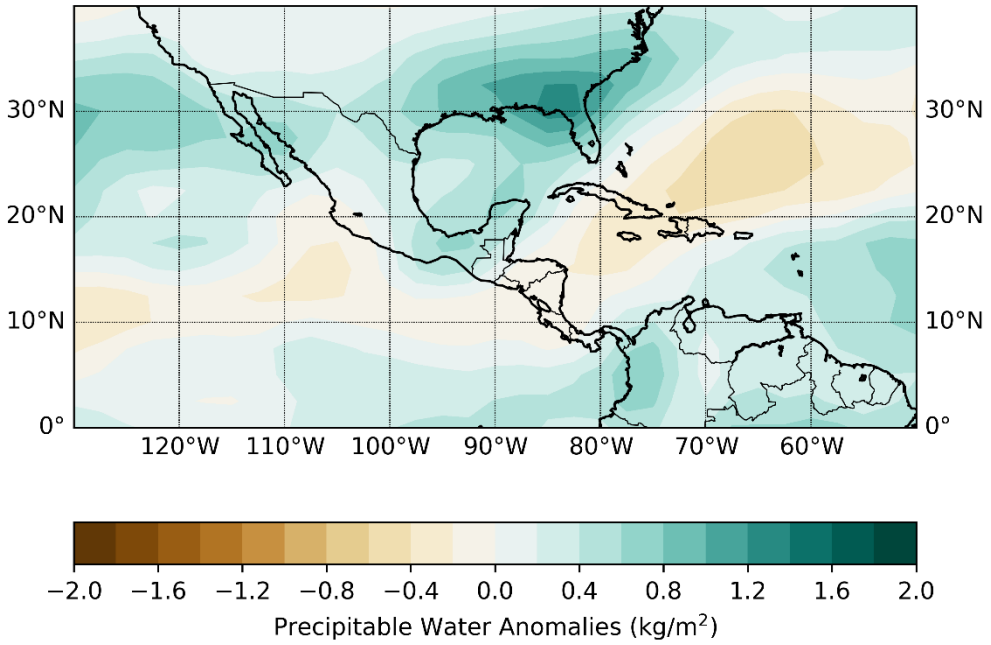


**Figure 4.25** MJO Phase 7 precipitable water anomalies for 1979–2014. Anomalies based on the NCEP/NCAR Reanalysis 1981–2010 mean.

Surface precipitation rate anomalies are less distinct than those shown in Figures 4.24 and 4.25, with near-normal rates covering most of the eastern

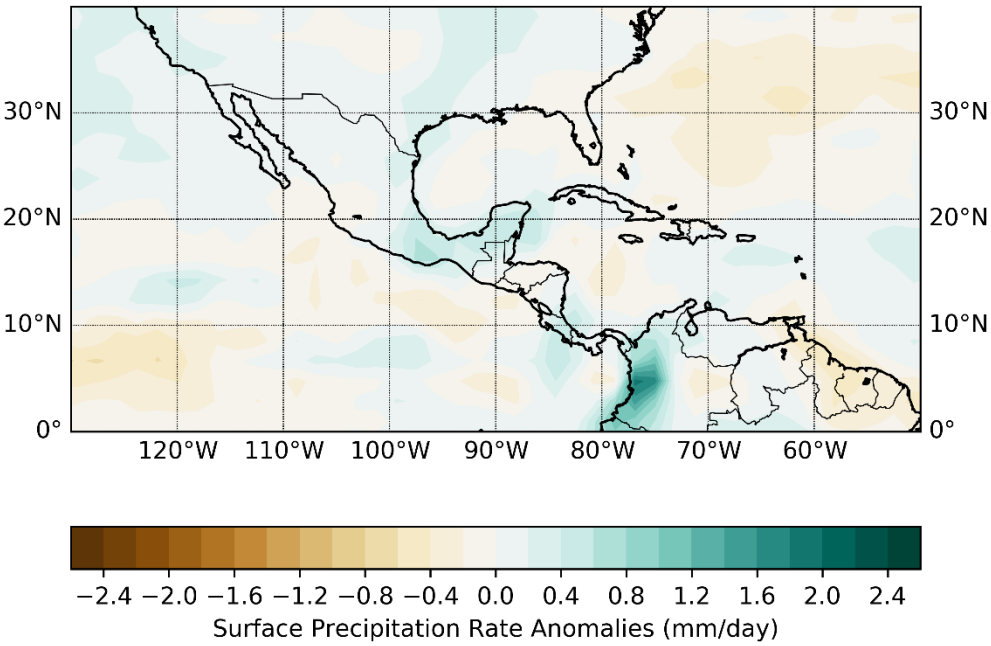


**Figure 4.26** MJO Phase 7 surface precipitation rate anomalies for 1979–2014. Anomalies based on the NCEP/NCAR Reanalysis 1981–2010 mean.

GoM and small positive anomalies over the western GoM (Figure 4.26). The pattern over the eastern GoM appears a bit neutral when considered against the results at KSRQ, but the positive anomalies near the Texas coastline are again somewhat confounding when considering the reduction in 5.0 cm precipitation days at KCRP.

MJO Phase 7 appears to be a transitional time in the GoM with minimal impacts on precipitation in the region. However, Monte Carlo simulations do suggest negative relationships between this phase and daily precipitation at KSRQ and the number of days producing at least 5.0 cm of precipitation at KCRP. The results are a bit surprising because plots of atmospheric anomalies fail to show any clear signals that would support these relationships. The pressure pattern is near-normal during Phase 7 while measures of atmospheric moisture tend to increase during this phase. More than any of the other relationships found from the Monte Carlo simulations, Phase 7 requires further study to explain the results obtained for KSRQ and KCRP.

### 4.3.8 MJO Phase 8

MJO Phase 8 shows the most widespread associations with Gulf Coast precipitation as evidenced by Monte Carlo simulation results in Tables 4.2, 4.4, and 4.6. Portions of both the western and eastern GoM are shown to have positive associations with Phase 8, with daily precipitation showing an increase all the way from KBRO northward to KLCH in the west and from KTPA southward to KEYW in the east. The western Gulf Coast also shows an increase in days producing at least 2.5 cm of precipitation while the number of days

producing at least 5.0 cm of precipitation increases at KBRO and KEYW. Analysis of atmospheric anomalies during Phase 8 reveals a pattern that is generally supportive of increased precipitation in the region.

Plots of 500 mb geopotential height and SLP anomalies (Figure 4.27) reveal a tendency for a trough to be in place over the eastern U.S. during Phase 8. The greatest negative anomalies at 500 mb are centered near the Great Lakes but lower-than-normal heights extend southward across the majority of the GoM. The greatest SLP anomalies are in the vicinity of the Bermuda-Azores high in the Atlantic, but negative anomalies extend westward into the eastern U.S. and across most of the GoM. This pattern of anomalously low atmospheric pressure is supportive of increased precipitation in and around the GoM. Ingredients necessary for the development of precipitation such as instability and vertical motion would be expected to increase in such a pattern.

Measures of atmospheric moisture during Phase 8 show mixed signals in terms of supporting the results obtained through the Monte Carlo simulations. On the one hand, mid-tropospheric relative humidity is above normal across the entire GoM region (Figure 4.28), with the greatest positive anomalies noted from Mexico across the southern GoM to near South Florida. Increased levels of mid-tropospheric saturation would be supportive of increased precipitation. On the other hand, positive PW anomalies (Figure 4.29) are only found across the southern GoM, with near-normal values along the northern Gulf Coast and some negative anomalies noted along the Texas coastline. The PW anomaly

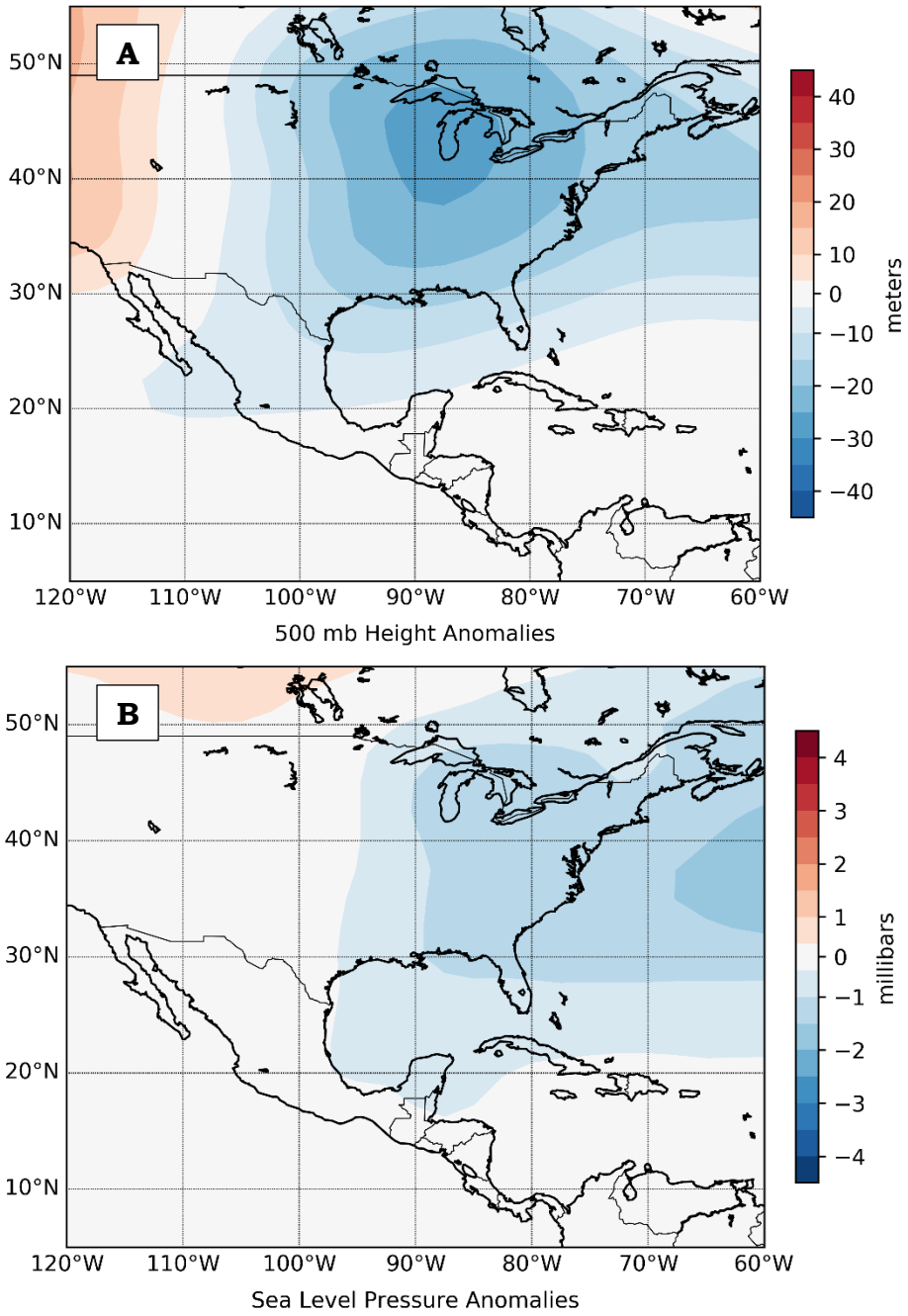


**Figure 4.27** MJO Phase 8 500 mb geopotential height anomalies (A) and sea level pressure anomalies (B) for 1979–2014. Anomalies based on the NCEP/NCAR Reanalysis 1981–2010 mean.

pattern is supportive of the results found from KTPA to KEYW but would seem to conflict with the increased precipitation observed at several sites in the western GoM.

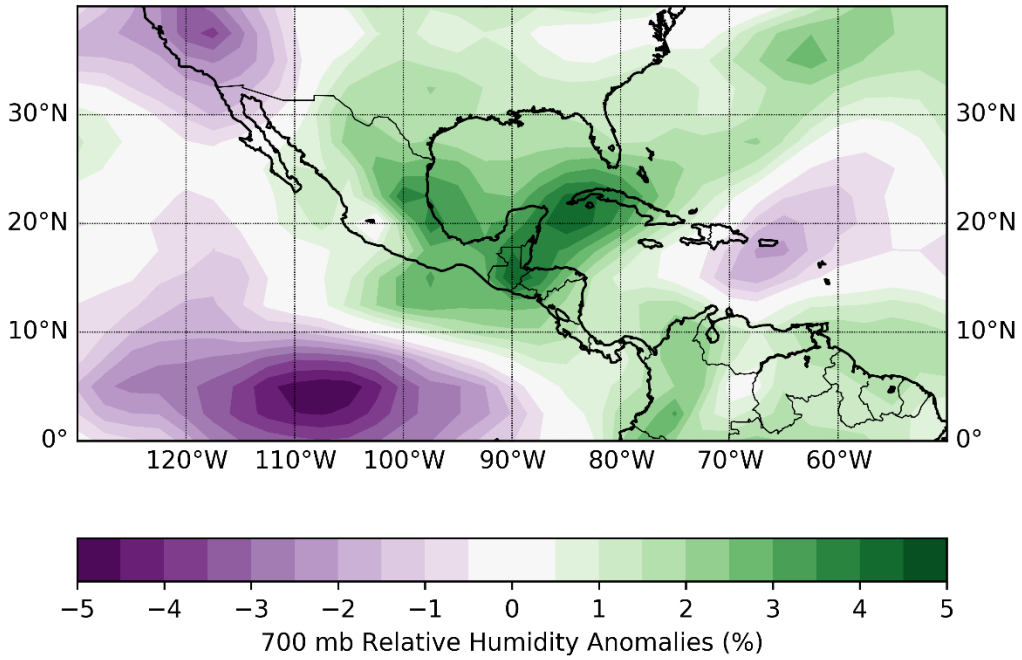


**Figure 4.28** MJO Phase 8 700 mb relative humidity anomalies for 1979–2014. Anomalies based on the NCEP/NCAR Reanalysis 1981–2010 mean.

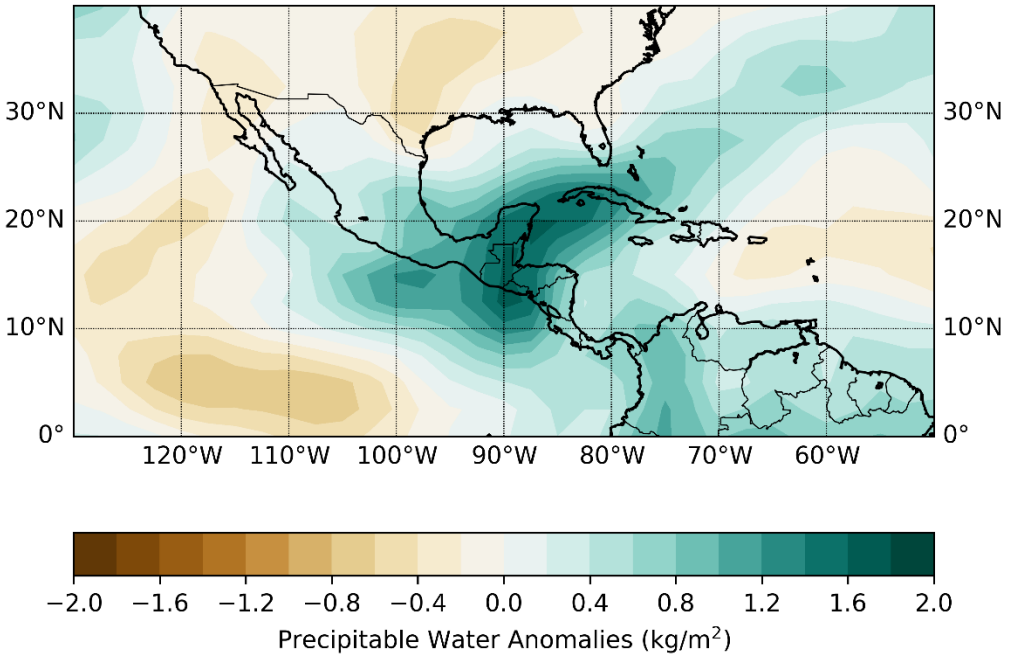


**Figure 4.29** MJO Phase 8 700 precipitable water anomalies for 1979–2014. Anomalies based on the NCEP/NCAR Reanalysis 1981–2010 mean.

Finally, a plot of surface precipitation rate anomalies (Figure 4.30) falls short of either definitively supporting the idea that certain measures of

precipitation increase along portions of the U.S. Gulf Coast during Phase 8, but the pattern shows a general increase in precipitation rates with the greatest anomalies noted from the central GoM northward to the northern Gulf Coast. Smaller positive anomalies are observed around most but not all of the sites, showing positive associations with Phase 8 in the Monte Carlo simulations.

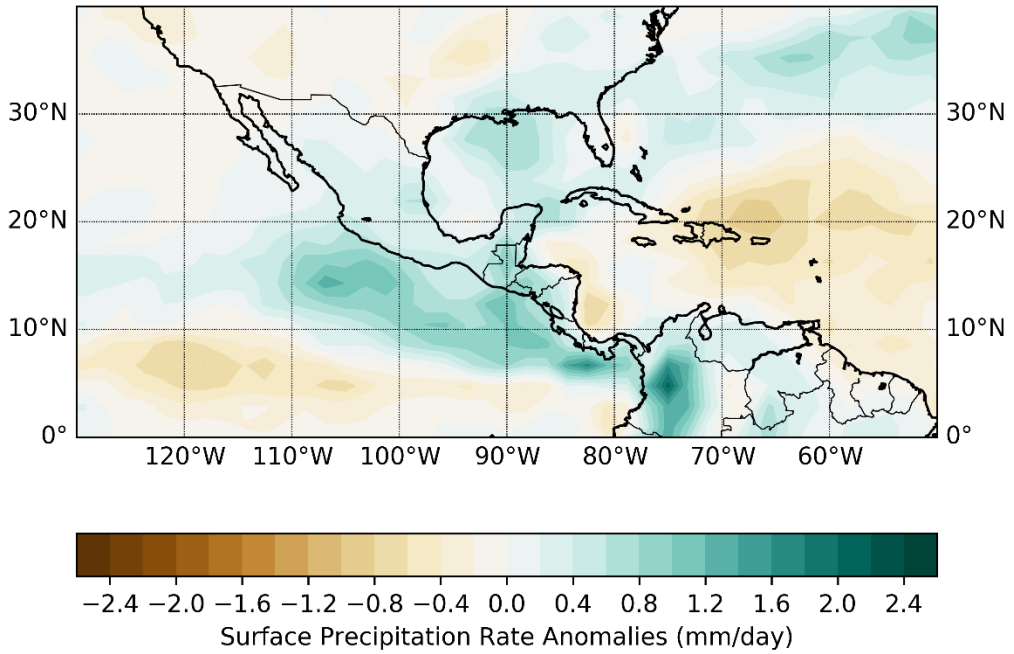


**Figure 4.30** MJO Phase 8 surface precipitation rate anomalies for 1979–2014. Anomalies based on the NCEP/NCAR Reanalysis 1981–2010 mean.

Monte Carlo simulations indicate several positive associations between single-site precipitation along the Gulf Coast and MJO Phase 8. Analysis of atmospheric anomalies during this phase shows a pattern that would be conducive to increased precipitation, including lowered atmospheric pressure, increased levels of atmospheric moisture, and modest increases in surface precipitation rates. Phase 8, along with Phase 1, stand out as producing the most widespread associations with precipitation along the Gulf Coast. Those

results align with the fact that Phases 8 and 1 represent the times when the convective clusters associated with the MJO are closest to the GoM.

## 4.4 Conclusion

The MJO is shown to have an impact on daily precipitation in and around the GoM. In general terms, precipitation is found to be more likely and at times heavier during MJO Phases 8, 1, and 2 while it is found to be less likely and at times lighter during Phases 4, 5, and 6. The precipitation variability is linked to modifications of the synoptic-scale weather pattern by the MJO, including 500 mb geopotential heights, SLP, mid-tropospheric relative humidity, PW, and surface precipitation rates. The anomalous atmospheric patterns shown for each MJO phase largely support the results obtained through the Monte Carlo simulations, with a few minor exceptions. As is noted in Section 4.3, further study is required to understand those instances where MJO-precipitation associations are found but atmospheric anomalies fail to explain adequately the mechanisms behind the variability.

The results obtained here are supported by prior research that has demonstrated a general trend toward increased storminess in and around parts of the southeastern U.S. and the GoM during MJO Phases 8, and 1, with a trend toward more tranquil conditions during Phases 4, 5, and 6. A previous study examining cold season precipitation in the U.S. and MJO influences (Becker et al. 2011) found that daily precipitation was generally reduced near the Gulf Coast during Phases 5, 6, and 7. Those authors attribute this drier pattern to a northward shift in the jet stream that results in the primary storm

track being farther inland across the central U.S. Their study also shows portions of the U.S. Gulf Coast receiving increased precipitation during MJO Phases 8 and 1. Some differences appear when comparing their work to this study, but that is to be expected since Becker et al. (2011) focused solely on precipitation during Nov-Mar while this study analyzes daily precipitation for the entire calendar year.

The work of Klotzbach et al. (2016) also lends some support to the results found in this study. Similar to the idea of jet stream variability noted by Becker et al. (2011), their examination of MJO-related snowfall variability in the northeastern U.S. concluded that a key component is the modification of the tracks of winter extratropical (ET) cyclones. Specifically, they found a decrease in frequency of ET cyclone tracks over the southern U.S., including near the Gulf Coast, during MJO Phases 4 and 5. Fewer cyclones would support the results found here by showing a general decrease in precipitation around the GoM during those phases. Conversely, they show that ET cyclone track frequencies increase by Phase 7, but especially Phase 8 in the region around the GoM. This increased cyclone frequency would aid in the increased precipitation amounts found in this study.

It is hoped that the links shown here between the MJO and cool season precipitation in and around the GoM will improve sub-seasonal forecasts around the region. Multiple computer model projections are now available for the MJO through NOAA's Climate Prediction Center (NOAA CPC 2018; http://www.cpc.ncep.noaa.gov/products/precip/CWlink/MJO/CLIVAR/clivar_

wh.shtml) ranging from a lead time of a week to roughly a month. Those MJO forecasts combined with the added knowledge of this study and other known teleconnection patterns may provide forecasters with increased lead time in predicting periods of increased or decreased precipitation around the GoM. Understanding the region's vulnerability to precipitation variability and in particular, heavy precipitation, the increased lead time potentially provided from these sub-seasonal predictions could prove invaluable to forecasters, emergency planners, those with commercial interests dependent on the weather, and others.

## 4.5 References


Becker, E.J., E.H. Berbery, and R.W. Higgins, 2011: Modulation of cold-season U.S. daily precipitation by the Madden–Julian Oscillation. Journal of Climate, 24(19), 5157-5166.

Blake, E.S., and D.A. Zelinsky, 2018: Hurricane Harvey Tropical Cyclone Report. Available online at: https://www.nhc.noaa.gov/data/tcr/AL092017_Harvey.pdf. Last accessed: 5/23/2018.

Di Liberto, T., 2018: August 2016 extreme rain and floods along the Gulf Coast. Available online at: https://www.climate.gov/news-features/event-tracker/august-2016-extreme-rain-and-floods-along-gulf-coast. Last accessed: 5/23/2018.

Earth System Research Laboratory (ESRL), 2018: NCEP/NCAR Reanalysis Daily Mean Composites Plotting Tool, https://www.esrl.noaa.gov/psd/data/composites/day/. Last accessed: 5/23/2018.

Klotzbach, P.J., and E.C. Oliver, 2015: Modulation of Atlantic basin tropical cyclone activity by the Madden–Julian Oscillation (MJO) from 1905 to 2011. Journal of Climate, 28(1), 204–217.

Klotzbach, P.J., E.C. Oliver, R.D. Leeper, and C.J. Schreck III, 2016: The relationship between the Madden–Julian Oscillation (MJO) and

southeastern New England snowfall. Monthly Weather Review, 144(4), 1355–1362.

National Hurricane Center, 2018: Costliest U.S. tropical cyclones tables updated. Available online at: https://www.nhc.noaa.gov/news/UpdatedCostliest.pdf. Last accessed: 5/23/2018.

NOAA CPC, 2018: Dynamical Model MJO Forecasts. Available online at: http://www.cpc.ncep.noaa.gov/products/precip/CWlink/MJO/CLIVAR/clivar_wh.shtml. Last accessed: 5/23/2018.

NOAA NCEI, 2018: U.S. Billion-Dollar Weather and Climate Disasters 1980-2018. Available online at: https://www.ncdc.noaa.gov/billions/events.pdf. Last accessed: 5/23/2018.

Oliver, E.C., and K.R. Thompson, 2011: A reconstruction of Madden–Julian oscillation variability from 1905 to 2008. Journal of Climate, 25(6), 1996–2019.

OT Index, 2018: Historical Reconstruction of the Madden-Julian Oscillation Index. Available online at: https://ecjoliver.weebly.com/mjo-reconstruction.html. Last accessed: 5/23/2018.

Salby, M.L., and H.H. Hendon, 1994: Intraseasonal behavior of clouds, temperature, and motion in the Tropics. Journal of the Atmospheric Sciences, 51(15), 2207–2224.

SC ACIS, 2018: State Climatologists Applied Climate Information System. Available online at: http://scacis.rcc-acis.org/. Last accessed: 5/23/2018.

van der Wiel, K., S.B. Kapnick, G.J. van Oldenborgh, K. Whan, S. Philip, G. Vecchi, … and H. Cullen, 2017: Rapid attribution of the August 2016 flood-inducing extreme precipitation in south Louisiana to climate change. Hydrology and Earth System Sciences, 21(2), 897–921.

Vega, A.J., J.M. Grymes, and R.V. Rohli, 2013: Louisiana Weather and Climate. Jones and Bartlett Publishers, Burlington, MA, 360 pp.

Wheeler, M.C., and H.H. Hendon, 2004: An all-season real-time multivariate MJO index: Development of an index for monitoring and prediction. Monthly Weather Review, 132(8), 1917–1932.

Wheeler, M.C., H.H. Hendon, S. Cleland, H. Meinke, and A. Donald, 2009: Impacts of the Madden–Julian oscillation on Australian rainfall and circulation. Journal of Climate, 22(6), 1482–1498.

# CHAPTER 5. DAILY COOL SEASON SEVERE WEATHER VARIABILITY ALONG THE U.S. GULF COAST AND THE MADDEN-JULIAN OSCILLATION

## 5.1 Introduction

Severe weather is often most closely associated with the Great Plains and Midwest regions of the U.S., with meteorologists and the general public alike commonly referring to this area as "Tornado Alley." However, recent years have seen an increased focus on a region in the southern and southeastern U.S. as a potential rival to the so-called "Tornado Alley." Allen Pearson, a former director of the National Severe Storms Forecast Center (NSSFC), is credited with first using the phrase "Dixie Alley" in 1971 to describe the area of the southern U.S. that is most prone to frequent and powerful tornadoes (Gagan et al. 2010). But the phrase "Dixie Alley" only began to appear regularly in published literature over the last 10–15 years (e.g., Dixon et al. 2011; Standohar-Alfono and van de Lindt 2014; Agee et al. 2016). A 2010 study proposed a formal definition for "Dixie Alley" that would include all of Arkansas, Louisiana, Mississippi, and Alabama, along with parts of Tennessee and Georgia (Gagan et al. 2010). A sizeable portion of the proposed "Dixie Alley" overlaps with the region examined in this study.

The U.S. Storm Prediction Center (SPC) published an analysis of the frequency of severe weather days – defined as days with reports of tornadoes, severe wind, and/or hail – for the continental U.S. during 2003–2012 (Figure 5.1). That analysis provides support for the idea of "Dixie Alley" as a rival to "Tornado Alley," with some of the highest frequencies of severe weather noted

in portions of Louisiana, Mississippi, Alabama, and Tennessee. Interestingly, the region with the largest number of severe weather reports is shown to be in the Carolinas and falls outside of both “Tornado Alley” and “Dixie Alley” as defined by Gagan et al. (2010). This severe weather hot spot also falls outside of the current study area which focuses on the Gulf of Mexico (GoM) region, but future research may want to explore possible relationships with the MJO. Nonetheless, the SPC analysis demonstrates that severe weather is frequent in the states bordering the Gulf of Mexico (GoM).

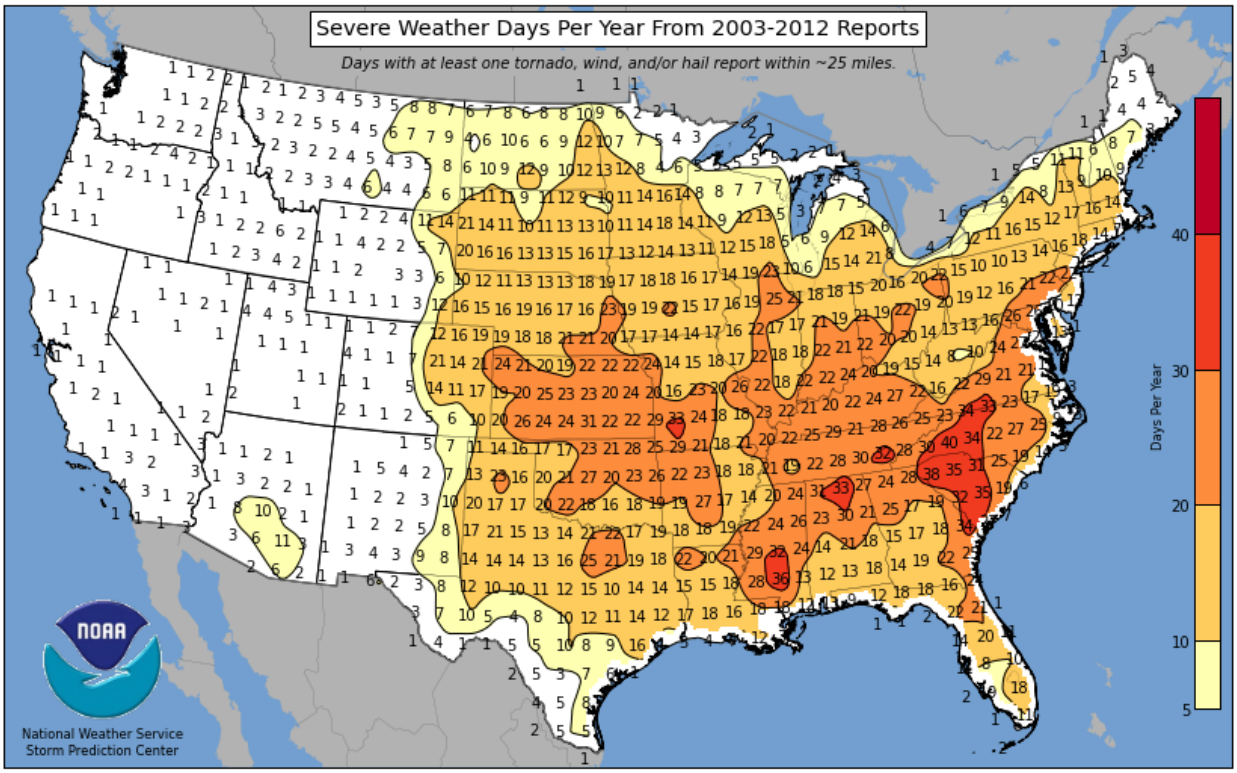


**Figure 5.1** Frequency of severe weather days for the continental U.S. during 2003–2012. Credit: NWS Storm Prediction Center.

History also provides examples of significant severe weather events near and just inland from the GoM Coast. For example, a three-day outbreak of severe weather, including dozens of tornadoes, first began near Houston,

Texas, on November 21, 1992, and went on to impact areas in 12 additional states in the eastern U.S. (Figure 5.2). At least 94 tornadoes occurred in the outbreak, along with 26 fatalities and more than 600 injuries (NWS Jackson 2018). The 1992 event has been described as one of the longest continuous tornado outbreaks on record in the U.S. (Grazulis 2001).

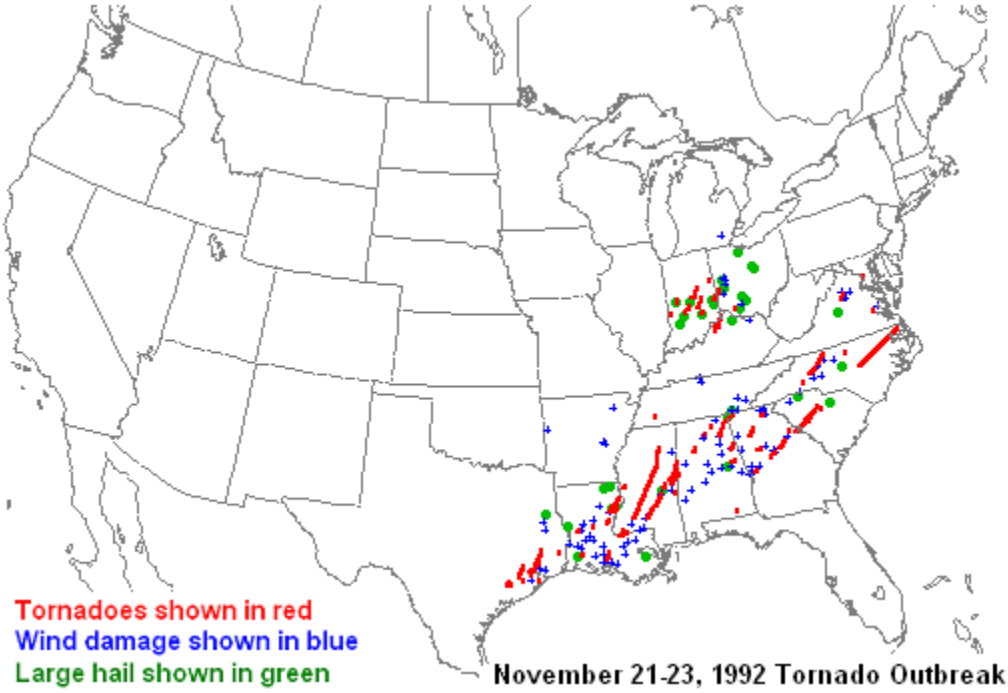


**Figure 5.2** Areas impacted by the severe weather outbreak of November 1992. Credit: NWS Raleigh.

Tornadoes are often the focus of severe weather discussions, but non-tornadic severe thunderstorm winds can sometimes produce impacts and damage similar to weak tornadoes. In the case of a severe wind event known as a derecho, impacts can be far more widespread than a typical individual tornado. The definition of the term *derecho* has changed several times through the years, but the most recent glossary by the American Meteorological Society (AMS) defines it this way:

A widespread convectively induced straight-line windstorm. Specifically, the term is defined as any family of particularly damaging downburst clusters produced by a mesoscale convective system. Such systems have sustained bow echoes with book-end vortices and/or rear-inflow jets and can generate considerable damage from straight-line winds over a long broad swath.

One notable derecho impacted areas from the Ohio Valley to the Southern Plains to the GoM on April 4–5, 2011. A line of severe thunderstorms trekked more than 1300 km (800 miles) in a 24-hour period, producing nearly

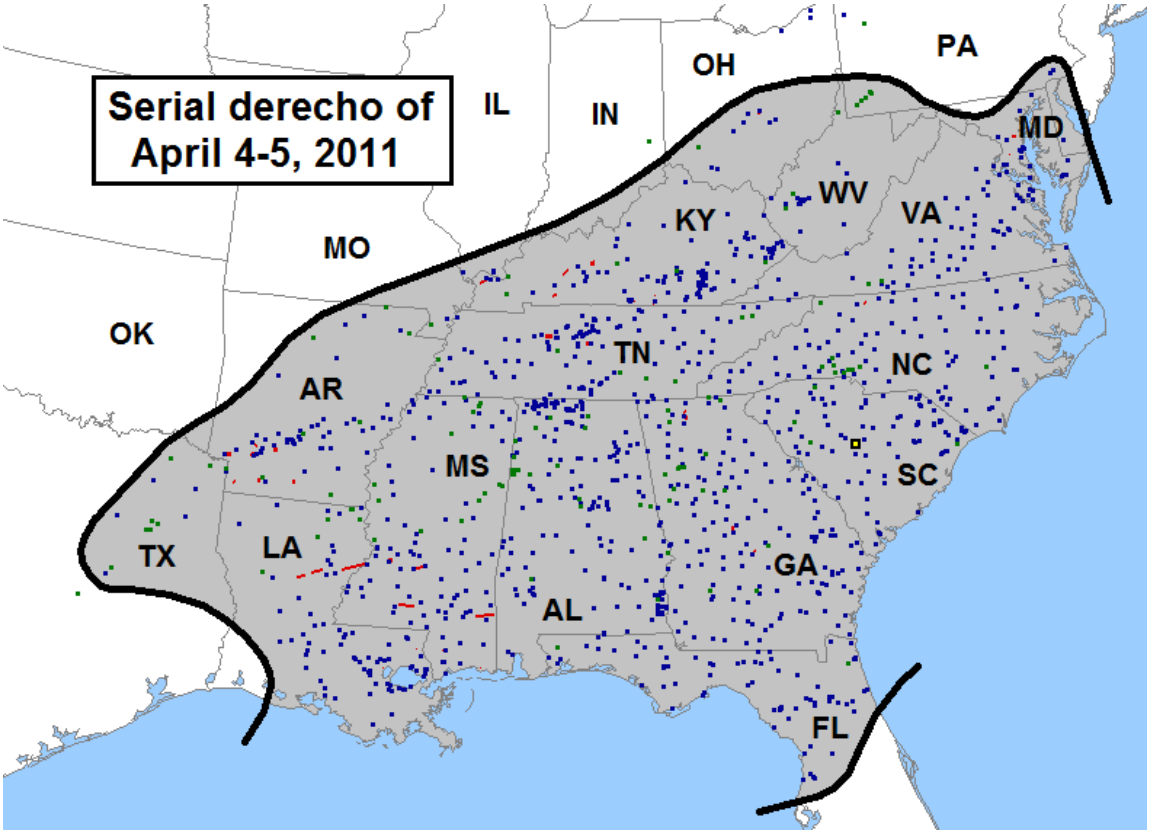


**Figure 5.3** Approximate area (gray shading) impacted by April 4–5, 2011 derecho and severe weather reports (wind, blue squares; estimated or measured wind gust ≥ 65 kts (74 mph), large black square with yellow center; hail, green squares; tornadoes, red squares and tracks). Credit: Storm Prediction Center.

1,100 reports of wind damage, several fatalities, and at least 30 injuries (Figure 5.3; SPC 2018). The event is best remembered for the breadth of its wind

damage, but it also produced dozens of tornadoes, including at least four that were confirmed in southern Louisiana (NWS New Orleans 2018).

Several factors likely contribute to daily severe weather variability near the GoM but when looking at sub-seasonal trends, the Madden-Julian Oscillation (MJO) warrants significant attention. The MJO is the leading mode of intraseasonal variability in the tropics (Madden and Julian 1994) but was long ago shown to influence weather into the midlatitudes (Anderson and Rosen 1983). Recent work has made the link between the MJO and severe weather frequencies in the U.S., including tornadoes (Thompson and Roundy 2013; Barrett and Gensini 2013; Dixon and Moore 2015) and hail (Barrett and Henley 2015). Collectively, these studies demonstrate that as the MJO progresses through its different phases as defined by the Real-time Multivariate (RMM) index developed by Wheeler and Hendon (2004), severe weather frequencies in the U.S. are impacted through modification of the Rossby wave train. The established connections between the MJO and U.S. severe weather variability, along with the known vulnerability of states bordering the GoM to all modes of severe weather, support the need to investigate the relationships between the MJO and daily severe weather variability along the U.S. GoM Coast.

## 5.2 Data and Methods

An analysis of daily severe weather variability along the U.S. GoM Coast during the cool season is conducted to examine possible links to the MJO. The period of analysis is 1979–2014, corresponding with the start and end dates

used in Study 1. Severe weather for the purposes of this study includes reports of hail, strong/damaging winds, and tornadoes. The data used for the analysis are obtained from NOAA's National Centers for Environmental Information (NCEI 2018) Storm Events Database (https://www.ncdc.noaa.gov/stormevents/ftp.jsp). Annual files containing severe weather reports are then filtered temporally for the cool season (October-March) and spatially for the area of interest (Figure 5.4). It is acknowledged that while Figure 5.4 covers the GoM along with parts of Mexico and Cuba, severe weather reports are largely limited to terrestrial

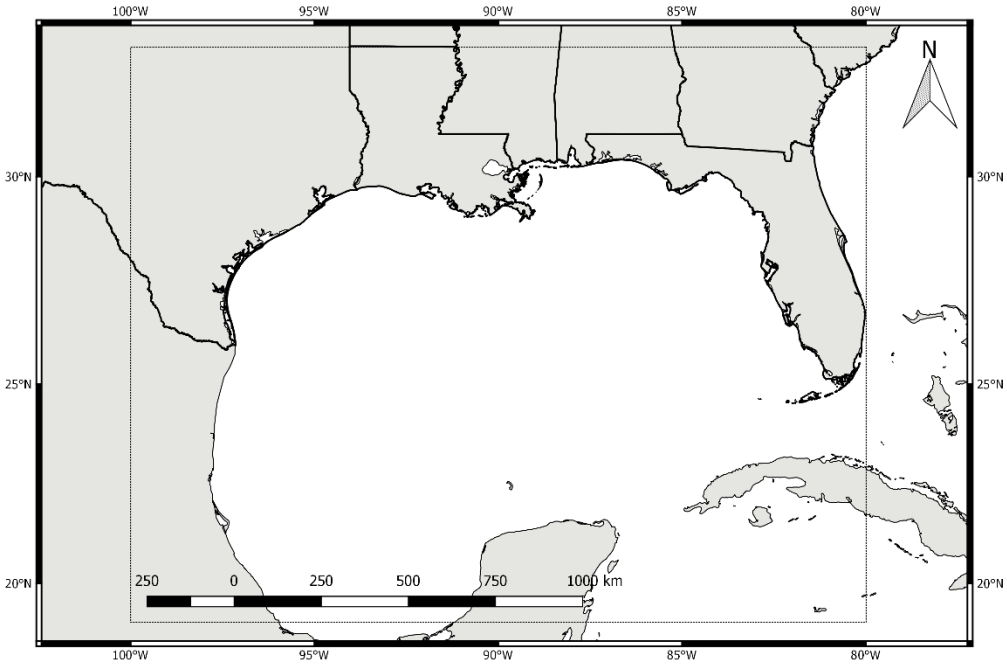


**Figure 5.4** Bounding box (19°N–33°N, 100°W–80°W) showing the region of interest for this study.

areas of the U.S. within the box, with a much smaller number of reports from U.S. marine areas due to limited storm detection capabilities and therefore data availability.

Daily frequencies of severe weather reports are tallied and assigned a value of 1–8 corresponding with the MJO phase for that particular date as shown by the RMM index. An online archive of the index is available from 1974 to present via the Centre for Australian Weather and Climate Research (CAWCR; http://www.bom.gov.au/climate/mjo/graphics/rmm.74toRealtime.txt). The RMM MJO index is derived through empirical orthogonal function (EOF; Wheeler and Hendon 2004) techniques based on the analysis of 850-hPa zonal (east-west) winds, 200-hPa zonal winds, and outgoing longwave radiation (OLR) data (Wheeler and Hendon 2004). Monte Carlo simulations are then run to test for statistical significance between specific phases of the MJO and daily severe weather frequencies along the U.S. GoM Coast.

The Monte Carlo techniques used in this study largely follow those first introduced in a study examining MJO links to Australian rainfall and circulation (Wheeler et al. 2009) that were subsequently used to also explore MJO associations with snowfall in the northeastern U.S. (Klotzbach et al. 2016). The techniques involve establishing two vectors of equal length; in this case, the vectors are composite averages of daily severe weather frequencies by MJO phase and the daily MJO phase as defined by the RMM index. A new estimated response of the first vector (daily severe weather frequencies) to the second vector (daily MJO phase) is then created by shifting the second vector by some random amount in time. The shift is not completely random, as a certain number of values are moved from the bottom of the time series to the

top. In the case of using this technique with the MJO, it is known that the MJO decorrelates in less than 50 days (Salby and Hendon 1994) so the minimum number of values that must be shifted is 50 to preserve the autocorrelation structure of the MJO. In this study, 1,000 Monte Carlo simulations are run for each site, producing 1,000 estimated responses to a random climate. Those 1,000 responses then allow for the construction of confidence intervals, with the 2.5th and 97.5th percentiles representing the 95% confidence interval limits. A 90% confidence interval is represented by the 5th and 95th percentiles as calculated by the Monte Carlo simulations. Any averaged severe weather frequency calculated in our original vector falling outside of those limits holds statistical significance at that particular level.

The Monte Carlo simulations are constructed by running a programming script in Python. The script was provided by Dr. Eric Oliver for some of his own research, including published work on the MJO and northeastern U.S. snowfall (Klotzbach et al. 2016). A few minor modifications are made to account for the use of a newer version of Python than that used for the original script and for some of the particular needs of this study. The script rejects any days on which the RMM MJO index has an amplitude <1 since the MJO is considered to be weak in this range.

The Monte Carlo simulations are run for all modes of severe weather collectively and then individually for tornado days, hail days, and wind days. In total, four sets of simulations are run for each RMM phase, using a 90% confidence interval approach, and then repeated for more stringent statistical

testing at a 95% confidence interval. Those results and their potential influences are presented in Section 5.3 below.

## 5.3 Results

The Monte Carlo simulations were constructed separately for reported frequencies of tornadoes, hail, and strong/damaging winds, with an additional round of simulations for all three modes of severe weather combined. The simulations only included days when the RMM MJO index was ≥1 and results were obtained for both 90% and 95% confidence intervals. The 90% confidence interval was included to remain consistent with Studies 1 and 2, but also because the daily RMM MJO phases are discrete by definition whereas severe weather events and the mechanisms responsible for them may include more than one MJO phase. The results for both the 90% and 95% confidence intervals are presented in Table 5.1 below.

The Monte Carlo results (Table 5.1) suggest that only MJO Phases 1 and 6 have statistically significant associations with severe weather frequencies for areas near the GoM. Tornadoes were found to be more frequent during RMM Phase 1, while hail, wind, and all modes of severe weather combined were less frequent during RMM Phase 6. All four of those associations were significant at the 95% level.

The results in Table 5.1 show some consistency with the results for cyclogenesis and precipitation found in Studies 1 and 2. Results from Study 1 suggest that cyclogenesis rates in the GoM decrease during Phase 6 when all

**Table 5.1** Monte Carlo simulation results for daily severe weather frequencies when MJO amplitude ≥1. Green (red) shading indicates a significant positive (negative) association at the 90% level (*) or 95% level (**) between severe weather frequencies and that particular MJO phase.

| Phase | Tornado | Hail | Wind | All |
|---|---|---|---|---|
| 1 | 0.878** | 2.024 | 3.311 | 6.167 |
| 2 | 0.518 | 2.214 | 3.258 | 5.970 |
| 3 | 0.585 | 2.092 | 2.132 | 4.787 |
| 4 | 0.514 | 1.852 | 2.039 | 4.388 |
| 5 | 0.601 | 1.627 | 2.337 | 4.514 |
| 6 | 0.569 | 1.034** | 1.929** | 3.475** |
| 7 | 0.560 | 1.028 | 2.825 | 4.398 |
| 8 | 0.630 | 2.102 | 3.069 | 5.756 |

MJO days are included, while Study 2 found that precipitation increases for many locations along the U.S. GoM Coast during Phase 1. In short, there appears to be an increase in storminess around the GoM during Phase 1 and a decrease during Phase 6.

An examination of the synoptic-scale weather pattern during RMM Phases 1 and 6 provided insight into the mechanisms responsible for the associations found in Table 5.1. The analysis was conducted by constructing anomaly plots of several atmospheric variables based on NCEP/NCAR Reanalysis data (Kalnay et al. 1996). Daily anomaly composites, based on the NCEP/NCAR 1981–2010 mean, were downloaded through NOAA's Earth System Research Laboratory (ESRL 2018) online plotting tool (https://www.esrl.noaa.gov/psd/data/composites/day/). The tool allows users

to provide a custom list of dates, which in this case allowed for the calculation of anomalies specific to each MJO phase. The data were then downloaded in netCDF format and plots of the anomalies were generated using scripts in Python. A discussion of the synoptic-scale weather patterns during MJO Phases 1 and 6 follows in Sections 5.3.1 and 5.3.2., with a spatial analysis of GoM severe weather frequencies by MJO phase in Sections 5.3.3–5.3.10.

### 5.3.1 Synoptic Weather Pattern during MJO Phase 1

Analysis of synoptic-scale atmospheric anomalies during MJO Phase 1 showed a pattern clearly supportive of an increase in storminess and modestly supportive of an increase in tornadoes. Plots of anomalies of both 500 mb geopotential height (Figure 5.5) and sea level pressure (SLP; Figure 5.6) showed a large area of negative anomalies across much of the U.S. and extending into the western Atlantic. These negative anomalies indicate lower-than-normal atmospheric pressure and also appear to represent a weakening of the semi-permanent Bermuda-Azores High. In both cases, the greatest negative anomalies were located over the southeastern U.S. and into the northern GoM. This broad area of lower-than-normal atmospheric pressure would support conditions needed to produce thunderstorms, including increased vertical motion and instability.

A plot of 500 mb temperature anomalies during Phase 1 (Figure 5.7) showed a small region of cooler-than-normal mid tropospheric temperatures over portions of the northern and western GoM Coast. Below-normal

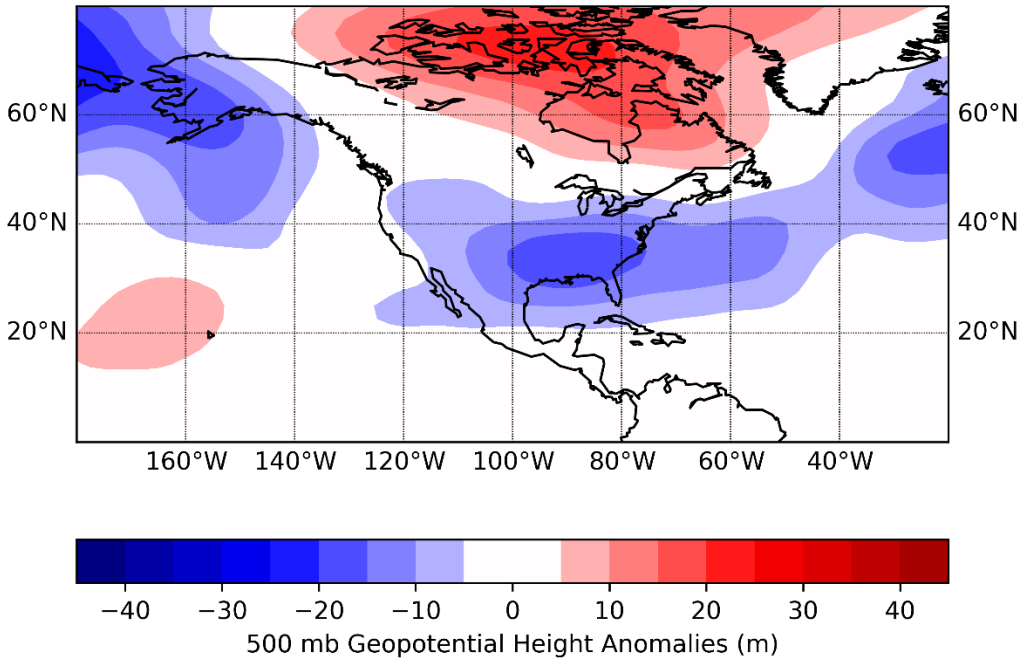


**Figure 5.5** MJO Phase 1 500 mb geopotential height anomalies for 1979–2014. Anomalies are based on the NCEP/NCAR Reanalysis 1981–2010 mean.

temperatures at this level of the atmosphere are typically associated with increased instability, something known to support thunderstorm development.

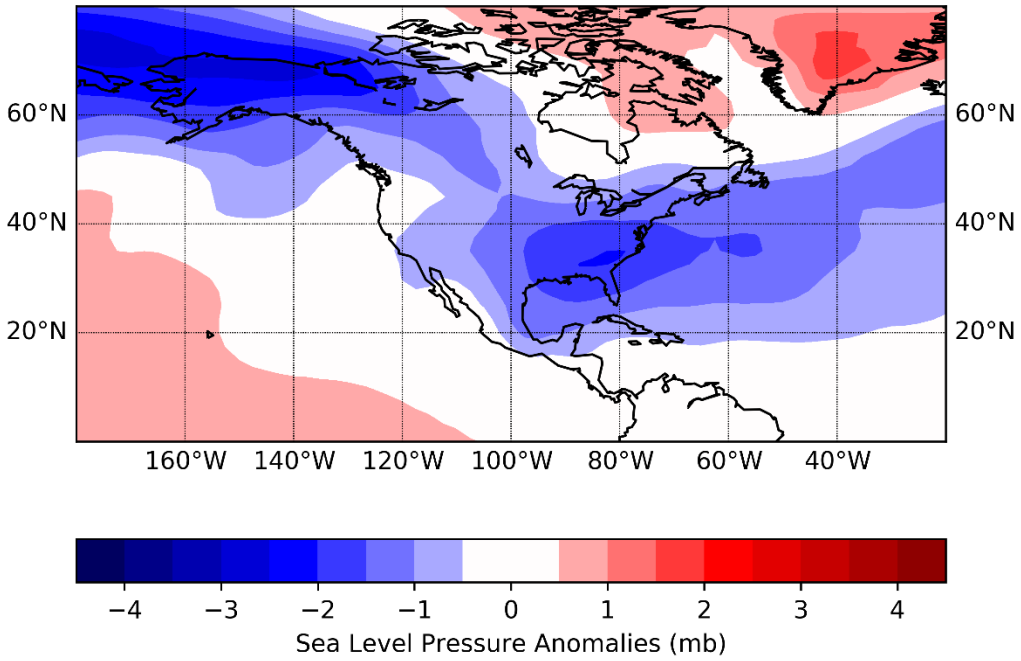


**Figure 5.6** MJO Phase 1 sea level pressure anomalies for 1979–2014. Anomalies are based on the NCEP/NCAR Reanalysis 1981–2010 mean.

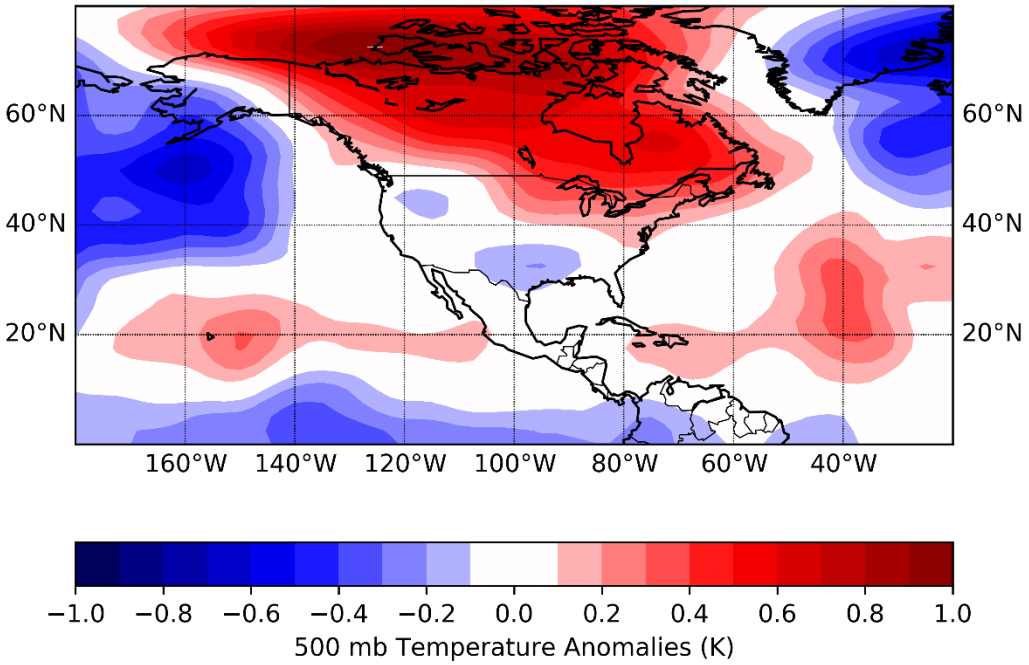


**Figure 5.7** MJO Phase 1 500 mb temperature anomalies for 1979–2014. Anomalies are based on the NCEP/NCAR Reanalysis 1981–2010 mean.

More specifically, severe weather is favored when warm air near the surface is overlain by a much colder layer of static air aloft; this allows a parcel of rising air to remain warmer than its surrounding environment as it rises, and therefore enhances its buoyancy. Moreover, the colder air aloft during a thunderstorm could be indicative of the evaporative cooling that occurs in association with downdrafts of air in the incipient thunderstorm.

The small spatial extent of the negative temperature anomalies shown in Figure 5.7 was somewhat surprising given the much larger region of negative height anomalies at 500 mb shown in Figure 5.5. However, a geospatial analysis of tornado formation locations (to be described more completely in Section 5.3.3) found that tornadoes were most frequent during Phase 1 over southern portions of Louisiana and Mississippi, with another maximum located near Tampa, Florida. The negative mid-tropospheric temperature anomalies in

Figure 5.7 covered a small spatial area but it does overlap with the Phase 1 tornado maximum in Louisiana and Mississippi.

Among the atmospheric variables analyzed for Phase 1, 300 mb vectorized wind anomalies (Figure 5.8) provided the greatest support for an increase in tornado frequency near the U.S. GoM Coast. The 300 mb level of the atmosphere is often considered to be a good representation during the cool season of the high-altitude river of fast-moving air known as the polar front jet stream, which separates air masses of tropical from those of polar origin. The polar front jet stream is important for a number of reasons in the realm of synoptic meteorology, but as it relates to severe weather, the position of its core reveals regions that are more favorable for the increased vertical motion necessary for the development of severe thunderstorms. Specifically, a four-quadrant model of a jet stream maximum or jet streak shows that the right-

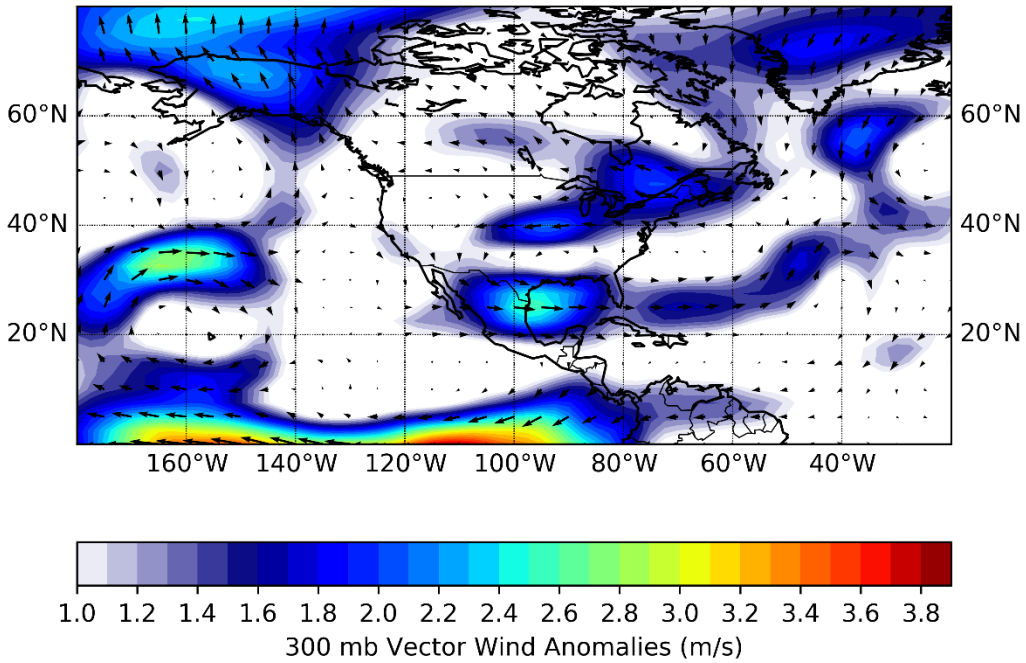


**Figure 5.8** MJO Phase 1 300 mb vector wind anomalies for 1979–2014. Anomalies based on the NCEP/NCAR Reanalysis 1981–2010 mean.

entrance and left-exit regions are the areas favorable for upward vertical motion. This is because air that accelerates through the rear of the jet streak (i.e., the entrance region) possesses increasing velocity, and therefore an increasing Coriolis effect. But the velocity and momentum initially in the air stream is associated with a weaker Coriolis effect, which temporarily leaves the other force involved – the pressure gradient force – to dominate the Coriolis effect. The result is that the air stream in the entrance region tends to move slightly down the pressure gradient, which in this upper tropospheric altitude is toward the pole, since the colder polar air has sunk, leaving less atmospheric mass aloft with proximity to the pole. Thus, in the entrance region, the upper-tropospheric air (as represented by the 300 mb level) converges slightly on the poleward (i.e., left-entrance) side and diverges slightly on the equatorward (i.e., right-entrance) side. The upper-level convergence side would support sinking motion and reduced thunderstorm activity, while the divergence side would support rising motion and enhanced thunderstorm activity. The opposite effect happens in the "front" of the jet streak. As air decelerates past the jet streak core, its velocity decreases and therefore the Coriolis effect weakens. But the initially strong velocity allows the Coriolis effect to be stronger than the pressure gradient force, which results in a slightly rightward motion (in the Northern Hemisphere) – toward the equatorward side of the jet streak. This produces convergence aloft (and decreased storm likelihood) on the right-exit side of the jet streak, and divergence aloft (and enhanced storm likelihood) on the left-exit side of the jet streak.

Figure 5.8 reveals an anomalously strong jet streak near the western GoM during Phase 1 that places much of the study area in the favored left-exit region of the polar front jet stream. Furthermore, it has been previously shown that the left-exit region is the most favorable quadrant for tornado formation (Rose et al. 2004). The jet stream also provides an approximation of the storm track at any given point in time. The enhanced polar front jet noted over the GoM would likely result in the more frequent passage of midlatitude atmospheric disturbances and cyclones, which would in turn enhance the storminess in the region. The results obtained here indicate the stronger-than-normal polar front jet stream found over the GoM during Phase 1 is likely a key factor in the increased tornado frequencies near the U.S. GoM Coast.

### 5.3.2 Synoptic Weather Pattern during MJO Phase 6

Analysis of synoptic-scale atmospheric anomalies during MJO Phase 6 showed a pattern supportive of a decrease in storminess near the GoM and therefore a decrease in severe weather. Plots of both 500 mb geopotential height anomalies (Figure 5.9) and SLP anomalies (Figure 5.10) showed a general trend toward higher-than-normal atmospheric pressure over portions of the study region. The 500 mb analysis (Figure 5.9) revealed positive anomalies extending into the northern GoM, with the greatest U.S. anomalies from the northern GoM Coast extending westward to the Pacific Coast. The SLP pattern (Figure 5.10) showed an area of positive anomalies that was smaller both spatially and in magnitude, centered near Florida. The SLP pattern suggested a small-scale area of surface high pressure extending from the

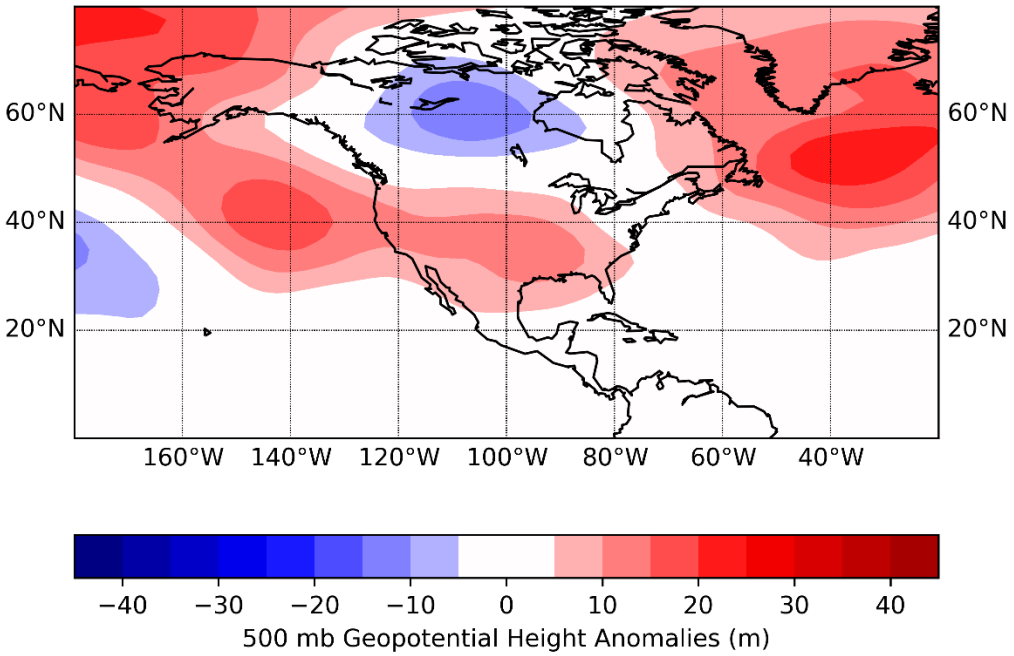


**Figure 5.9** MJO Phase 6 500 mb geopotential height anomalies for 1979–2014. Anomalies are based on the NCEP/NCAR Reanalysis 1981–2010 mean.

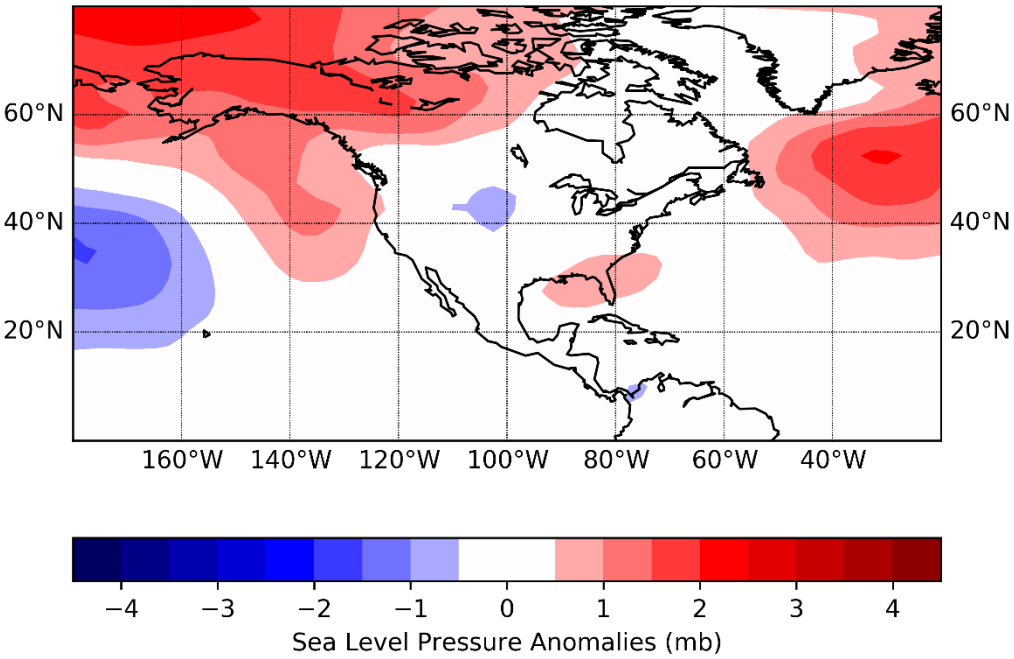


**Figure 5.10** MJO Phase 6 sea level pressure anomalies for 1979–2014. Anomalies are based on the NCEP/NCAR Reanalysis 1981–2010 mean.

central GoM into the western Atlantic. Collectively, this noted trend toward higher-than-normal pressures over much of the study area would support

increased subsidence, reduced atmospheric instability, and therefore a reduction in thunderstorm activity.

A plot of 500 mb temperature anomalies (Figure 5.11) during Phase 6 provided some stronger support for the reduction in severe weather frequencies near the U.S. GoM Coast. Above-normal temperatures in the mid-troposphere were noted over the majority of the U.S., including the GoM Coast and portions

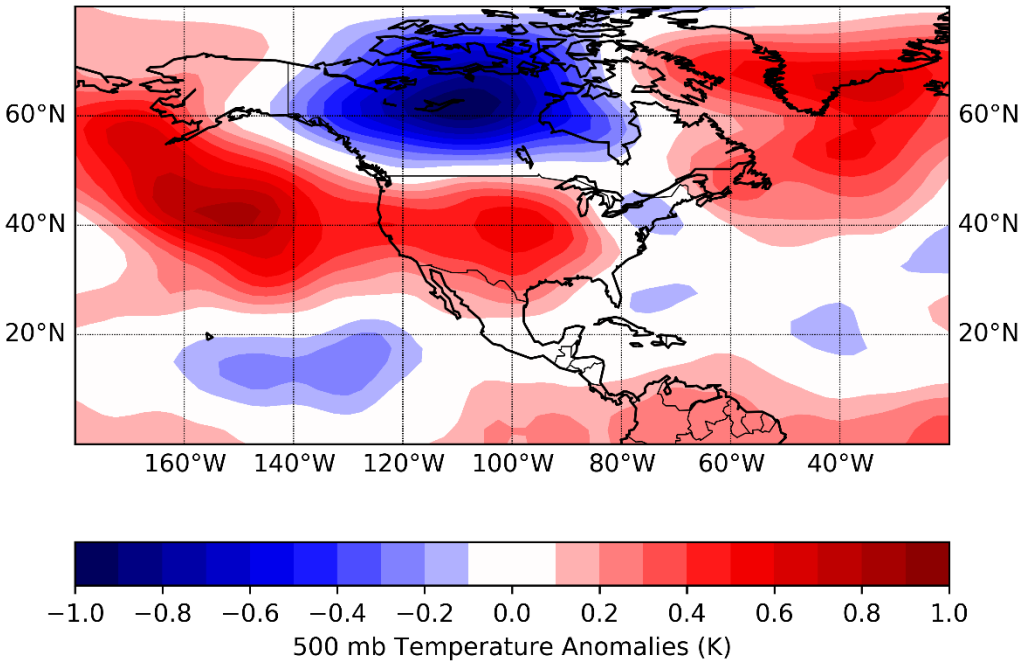


**Figure 5.11** MJO Phase 1 500 mb temperature anomalies for 1979–2014. Anomalies are based on the NCEP/NCAR Reanalysis 1981–2010 mean.

of the northern GoM. Warmer-than-normal temperatures at 500 mb are indicative of increased stability and would be supportive of a reduction in the thunderstorm activity necessary for the generation of severe weather. This is because, with a warm mid- to upper-troposphere, a rising parcel of air associated with an incipient thunderstorm would be less likely to remain warmer than the surrounding static environment, thereby limiting its development.

Analysis of 300 mb vector wind anomalies (Figure 5.12) also provided support for the decrease in severe weather near the U.S. GoM Coast noted during Phase 6. A synoptic-scale anticyclone was noted over most of the U.S. with its southern flank extending into the northern GoM. This upper-tropospheric anticyclone would produce increased subsidence and a decrease in thunderstorm activity. Additionally, the subtropical jet stream, a conveyor belt for atmospheric disturbances and increased storminess, was displaced well southward of the GoM and near the equator. The southern displacement of the jet stream, along with the easterly wind anomalies, would tend to limit the

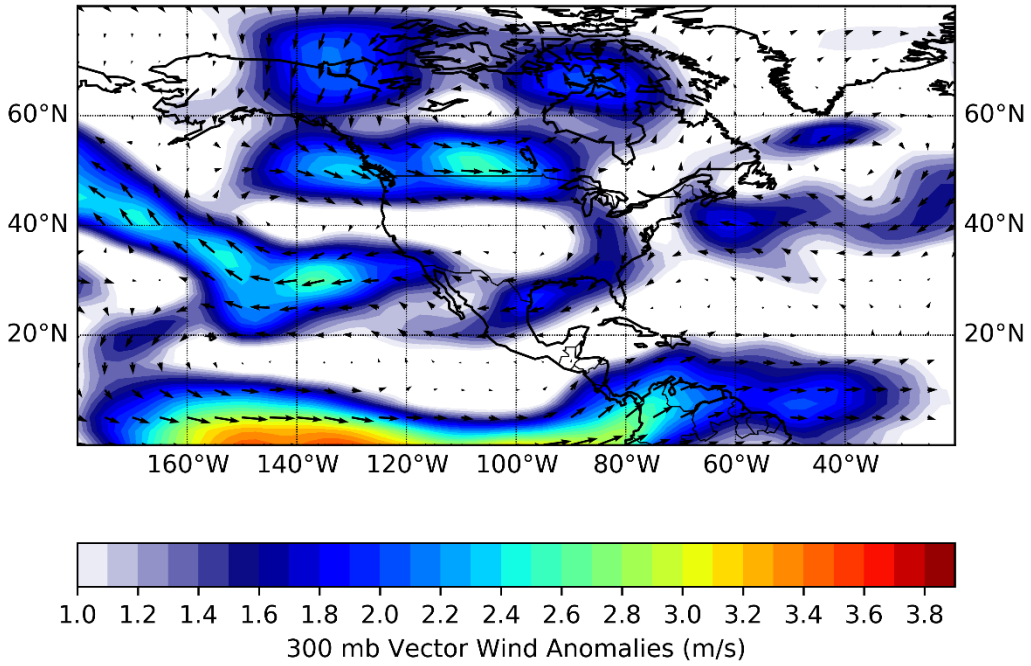


**Figure 5.12** MJO Phase 1 300 mb vector wind anomalies for 1979–2014. Anomalies are based on the NCEP/NCAR Reanalysis 1981–2010 mean.

frequency of storm systems near the GoM since these features typically arrive in the region during the cool season via the midlatitude westerlies.

### 5.3.3 Geospatial Patterns during MJO Phase 1

Reports of severe weather obtained through the NCEI Storm Events Database (NCEI 2018; https://www.ncdc.noaa.gov/stormevents/ftp.jsp) were filtered spatially for the study domain, temporally to cover 1979–2014, and by type (tornado/wind/hail) for further analysis. Once sorted by type, individual files were created and imported into Quantum GIS (QGIS) for a closer examination of spatial patterns. Plots of report locations were created first and an additional level of investigation was performed through kernel density analysis to identify regions where particular types of severe weather were most frequent.

Figure 5.13 provides a broad overview of reports of tornadoes, hail, strong/damaging winds, and all modes of severe weather combined. Figure 5.14 identifies spatial trends of severe weather modes during MJO Phase 1. Tornadoes were found to be most frequent in southern Mississippi, with secondary maxima noted near central Florida and in southwestern Louisiana. Hail was found to be most prevalent farther inland in a region extending from near Dallas, Texas, to Shreveport, Louisiana. Hail minima are noted in both southern Florida and southern Texas, which may in part be attributable to the fact that these regions are closer to the tropics and generally have warmer temperature profiles through the troposphere that would be less supportive of hail. Reports of strong and damaging winds were most common in southern Mississippi in an area that looks very similar to the hot spot for tornadoes. It also appeared as though wind reports were more common in the eastern half of

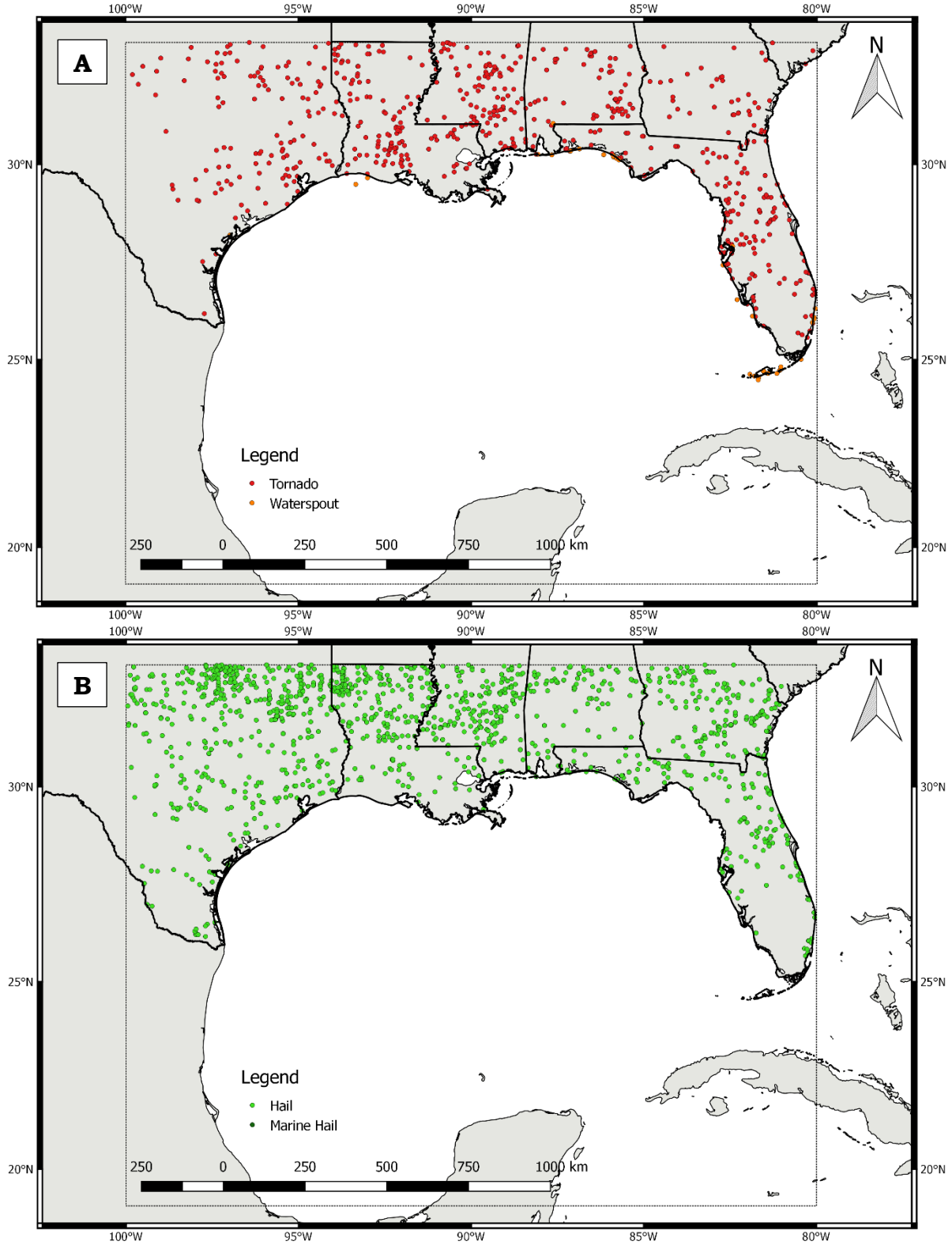


**Figure 5.13** MJO Phase 1 reports of tornadoes (A), hail (B), strong/damaging winds (C), and all severe weather types combined (D).
(figure continued)

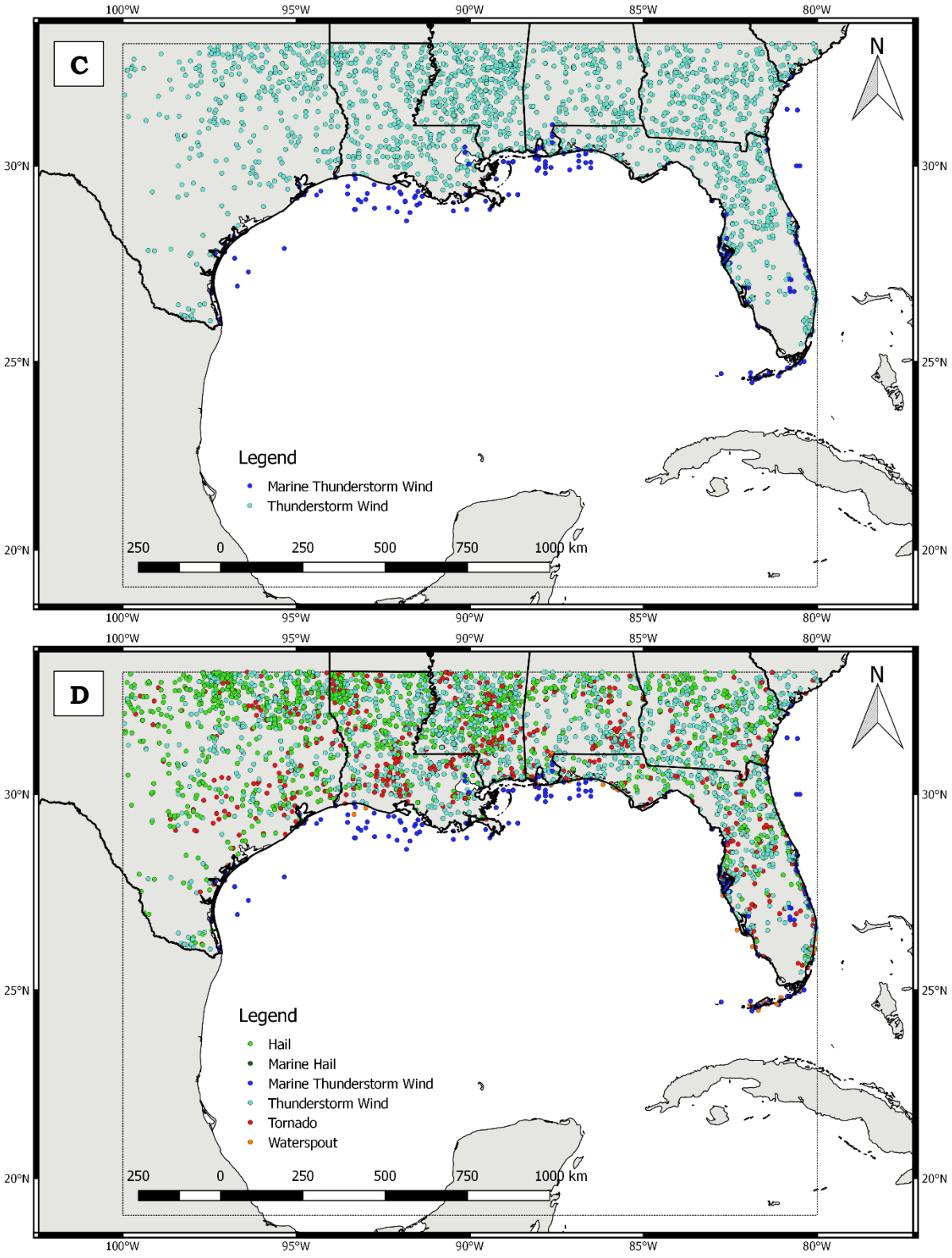
C
N
100°W
95°W
90°W
85°W
80°W
30°N
25°N
20°N
Legend
Marine Thunderstorm Wind
Thunderstorm Wind
250
0
250
500
750
1000 km
D
N
Legend
Hail
Marine Hail
Marine Thunderstorm Wind
Thunderstorm Wind
Tornado
Waterspout
250
0
250
500
750
1000 km

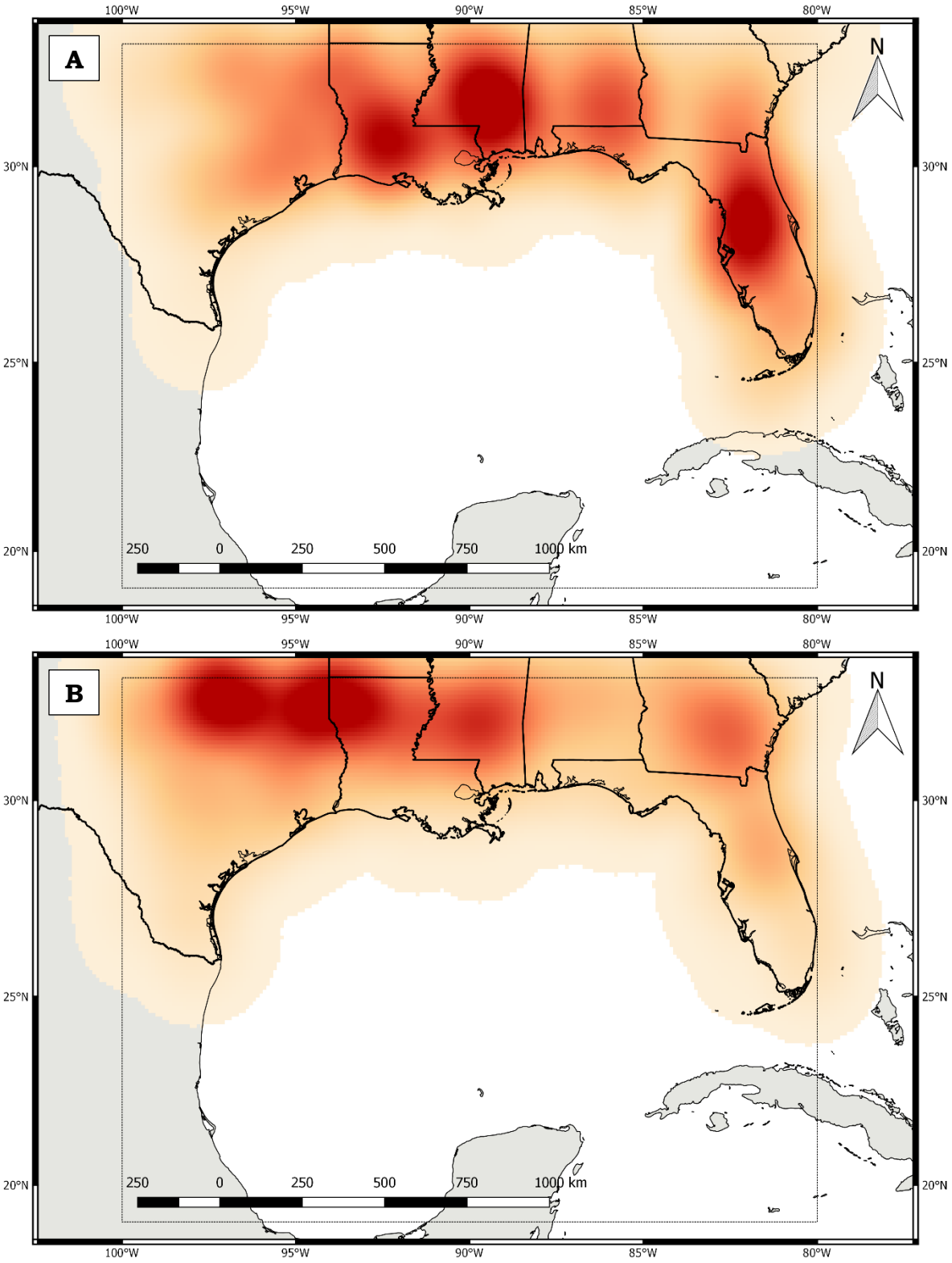


**Figure 5.14** MJO Phase 1 kernel density maps for reports of tornadoes (A), hail (B), strong/damaging winds (C), and all severe weather types combined (D). (figure continued)

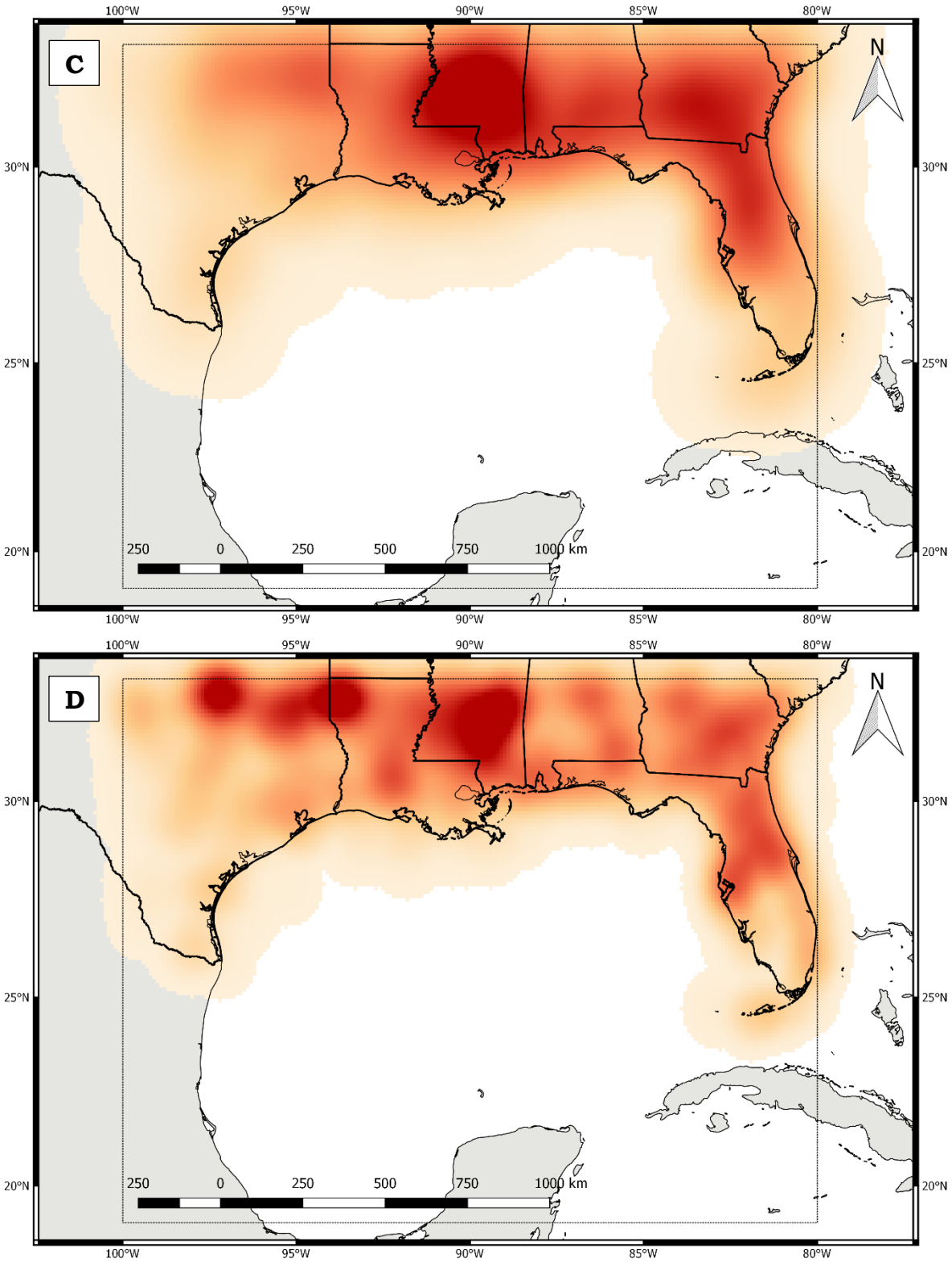


the GoM region than in the western half. For all reports combined, Phase 1 severe weather was most common in a region stretching from northern Texas

east-southeastward to southern Mississippi. Severe weather was least frequent in southern Texas and southern Florida, which again may be attributable to closer proximity to the tropics. southern Florida also is likely to have a data gap in the region of the Everglades swamp.

### 5.3.4 Geospatial Patterns during MJO Phase 2

Figure 5.15 provides a broad overview of reports of tornadoes, hail, strong/damaging winds, and all modes of severe weather combined during MJO Phase 2. Spatial trends in severe weather reports can be examined using the kernel density maps in Figure 5.16. In particular, tornadoes were found to be most common in an area covering central and southern portions of Mississippi and Alabama, with a secondary maximum noted from western Louisiana into southeastern Texas. This pattern resembled that of Phase 1 (Figure 5.14) but the primary tornado hot spot showed an eastward shift while the secondary maximum was shifted slightly westward. The tornado hot spot noted near Orlando, Florida, in Phase 1 (Figure 5.14) was no longer apparent for Phase 2. Hail appeared to be most frequent in an area in Texas extending from near Dallas to Austin. Additional maxima were noted near Shreveport, Louisiana, and Hattiesburg, Mississippi. The hail hot spots were similar to those for Phase 1 (Figure 5.14) with a notable southern extension of the maximum near Dallas, Texas. Phase 2 wind reports were found to be most frequent from near Jackson, Mississippi, to near New Orleans, Louisiana. This hot spot appeared to dominate but there were suggestions of a much smaller

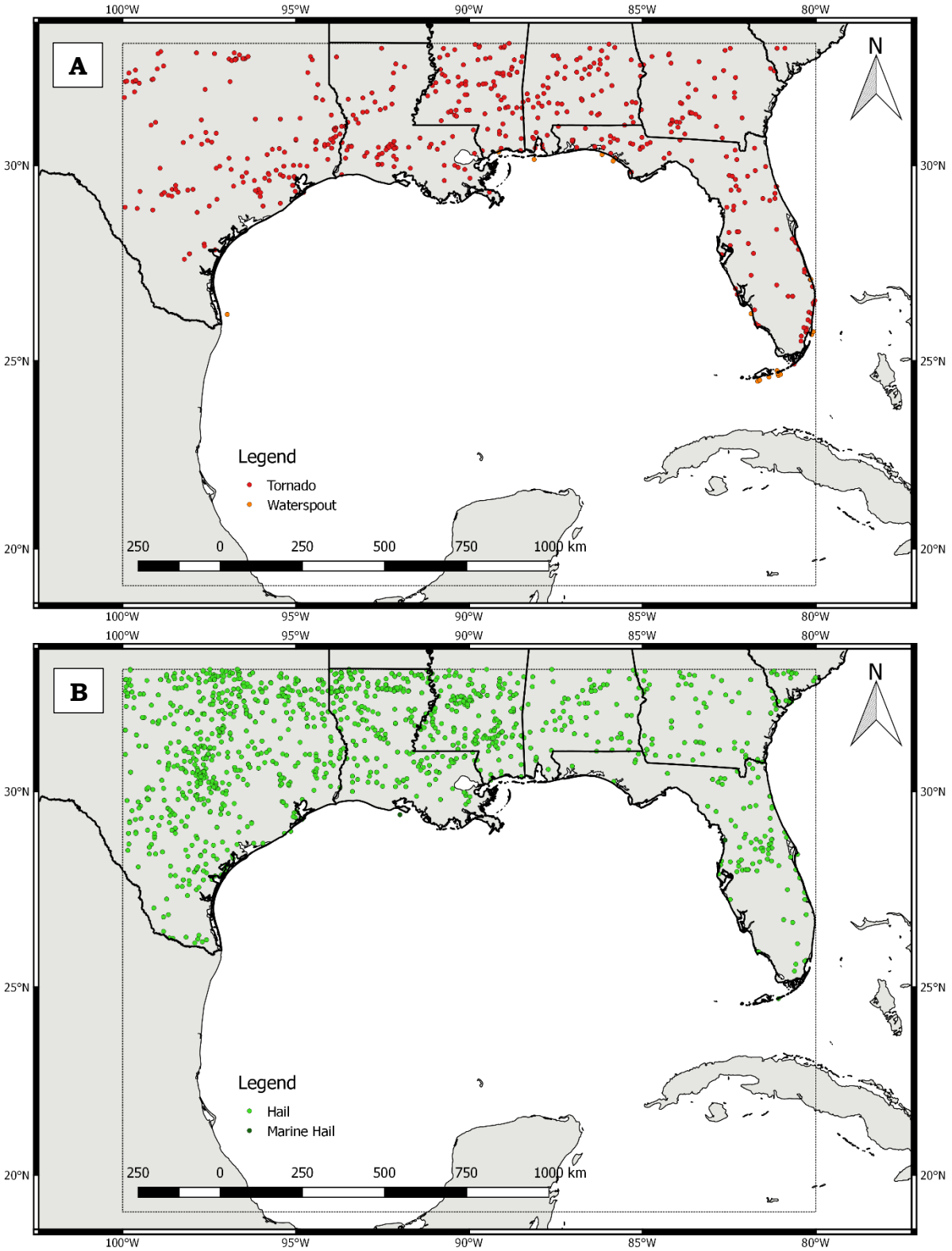


**Figure 5.15** MJO Phase 2 reports of tornadoes (A), hail (B), strong/damaging winds (C), and all severe weather types combined (D).
(figure continued)

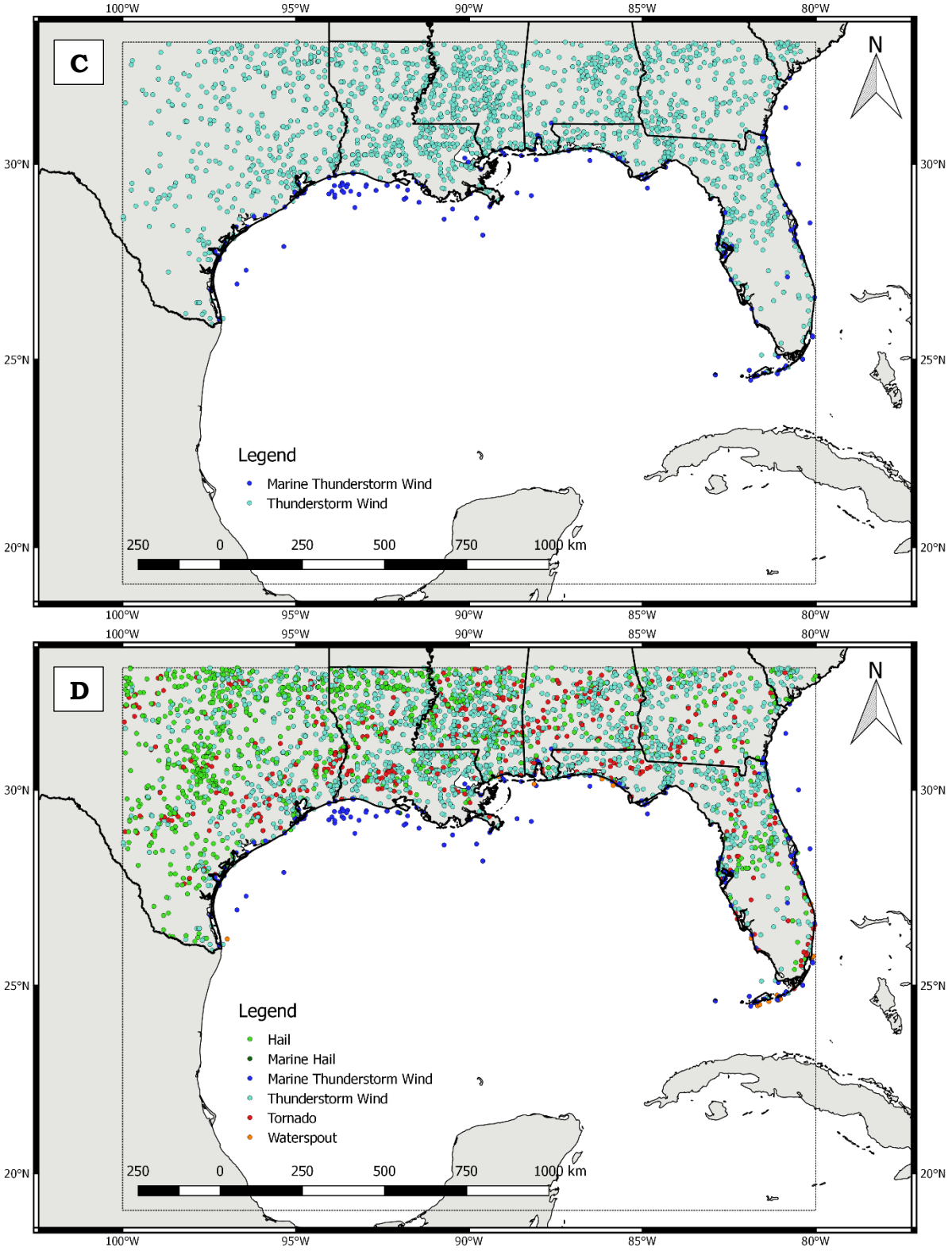
C
N
100°W
95°W
90°W
85°W
80°W
30°N
25°N
20°N
Legend
Marine Thunderstorm Wind
Thunderstorm Wind
250
0
250
500
750
1000 km
D
N
Legend
Hail
Marine Hail
Marine Thunderstorm Wind
Thunderstorm Wind
Tornado
Waterspout
250
0
250
500
750
1000 km

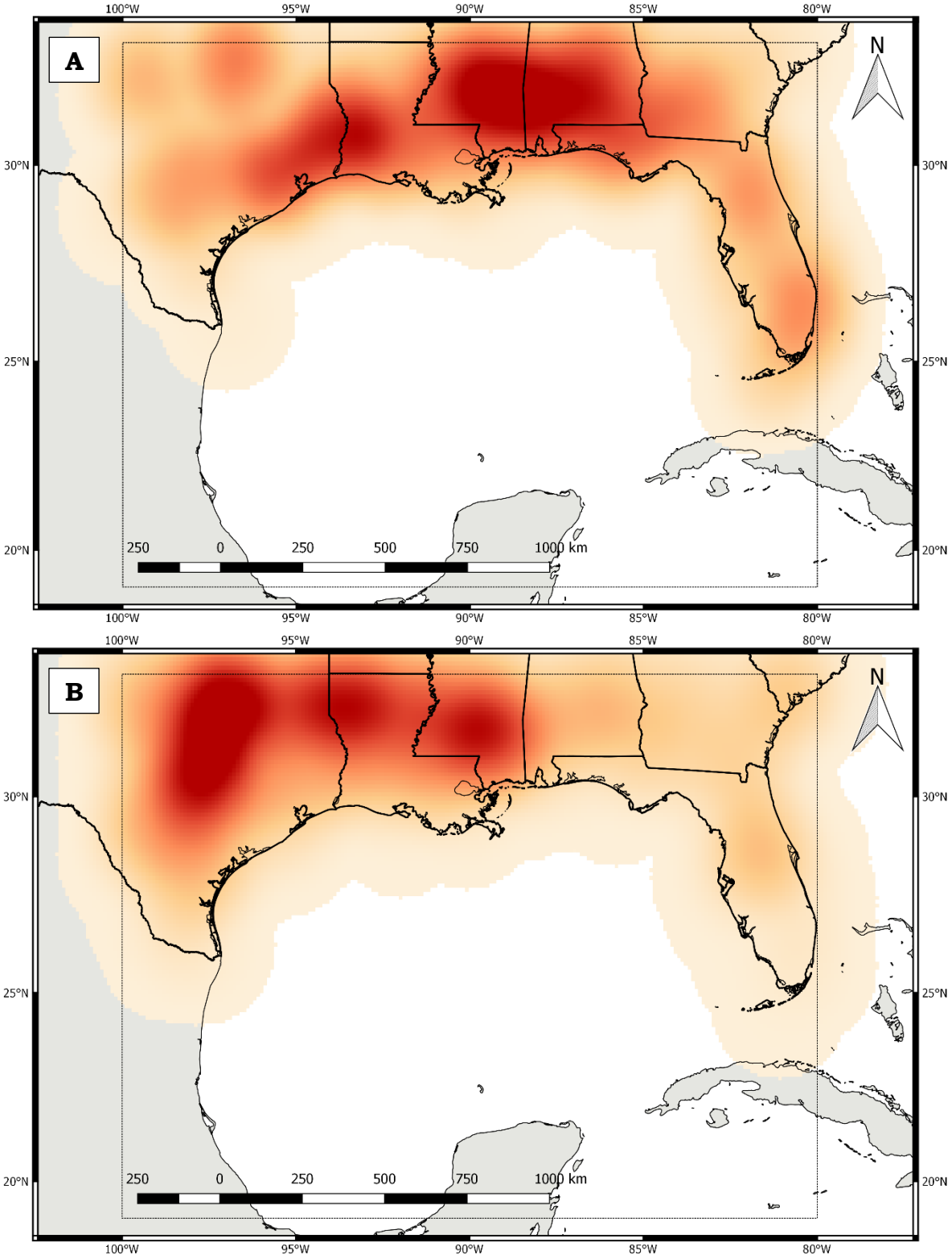


**Figure 5.16** MJO Phase 2 kernel density maps for reports of tornadoes (A), hail (B), strong/damaging winds (C), and all severe weather types combined (D). (figure continued)

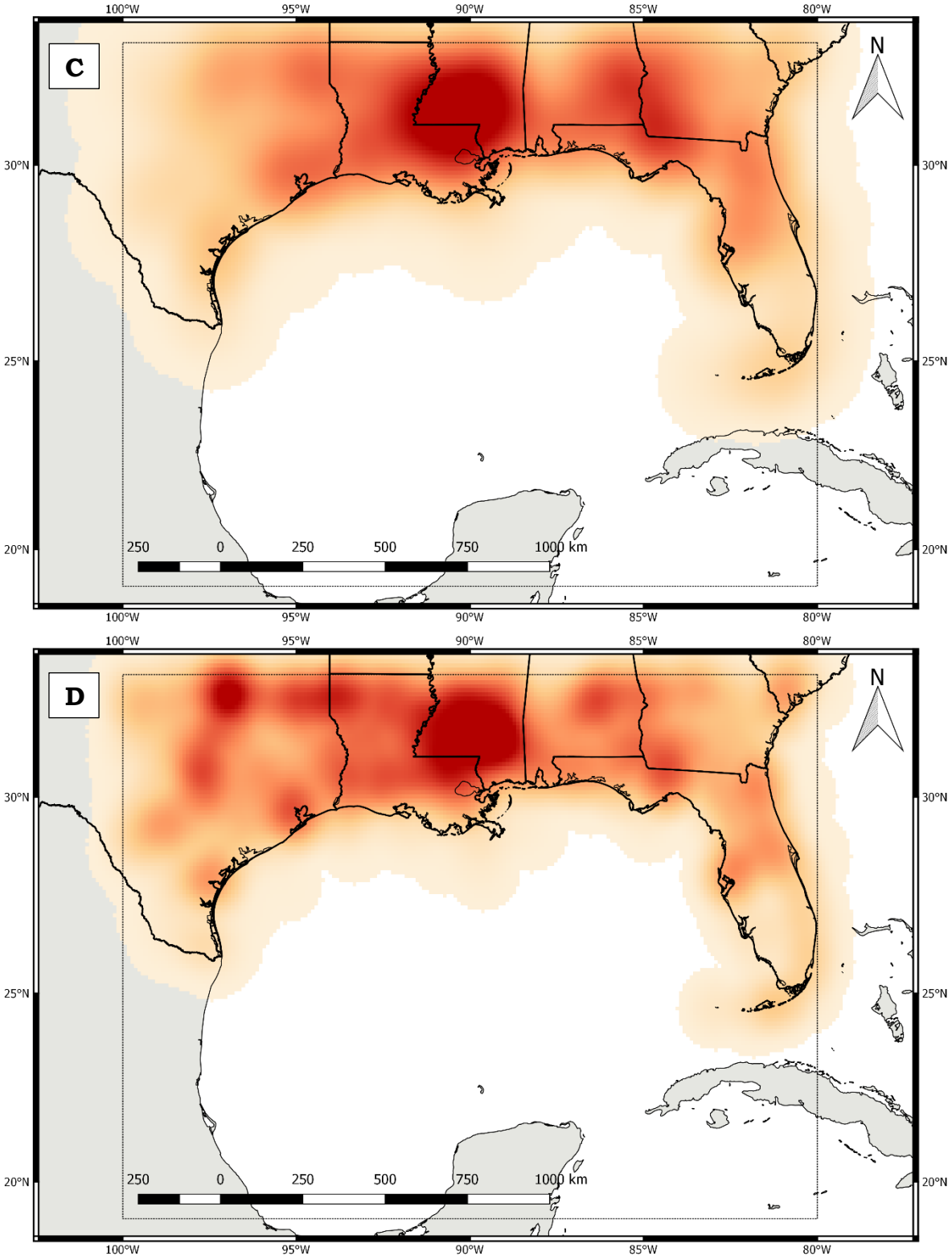
C
D
N
100°W
95°W
90°W
85°W
80°W
30°N
25°N
20°N
250
0
250
500
750
1000 km

magnitude maximum near the Alabama-Georgia state line. The primary maximum was very similar to the one shown in Phase 1 (Figure 5.14). The kernel density map for all reports combined showed a maximum that was geographically very similar to that for wind reports, but this was also likely aided by portions of this region showing relatively frequent reports of tornadoes and hail.

### 5.3.5 Geospatial Patterns during MJO Phase 3

Figure 5.17 provides a broad overview of reports of tornadoes, hail, strong/damaging winds, and all modes of severe weather combined during MJO Phase 3. Spatial trends in severe weather reports can be examined using the kernel density maps in Figure 5.18. Tornadoes were found to be most common in a region covering much of the southern half of Mississippi extending into parts of central and southeastern Louisiana. This represented a slight westward shift from the Phase 2 maximum (Figure 5.16). Hail trends remained similar to those noted in Phases 1 and 2 with a maximum extending from near Dallas, Texas, to Shreveport, Louisiana. A smaller magnitude maximum was located in southern Mississippi while a hail minimum again appeared in southern Florida. Reports of strong and damaging winds showed similar regional trends to Phases 1 and 2, with a clear maximum extending from central Mississippi into southeastern Louisiana. Broader, weaker maxima were found over much of western Louisiana and eastern Texas, and also in the area extending from southern Georgia to near Tampa, Florida. Kernel density plots of all severe weather modes combined reflected a triple maxima pattern

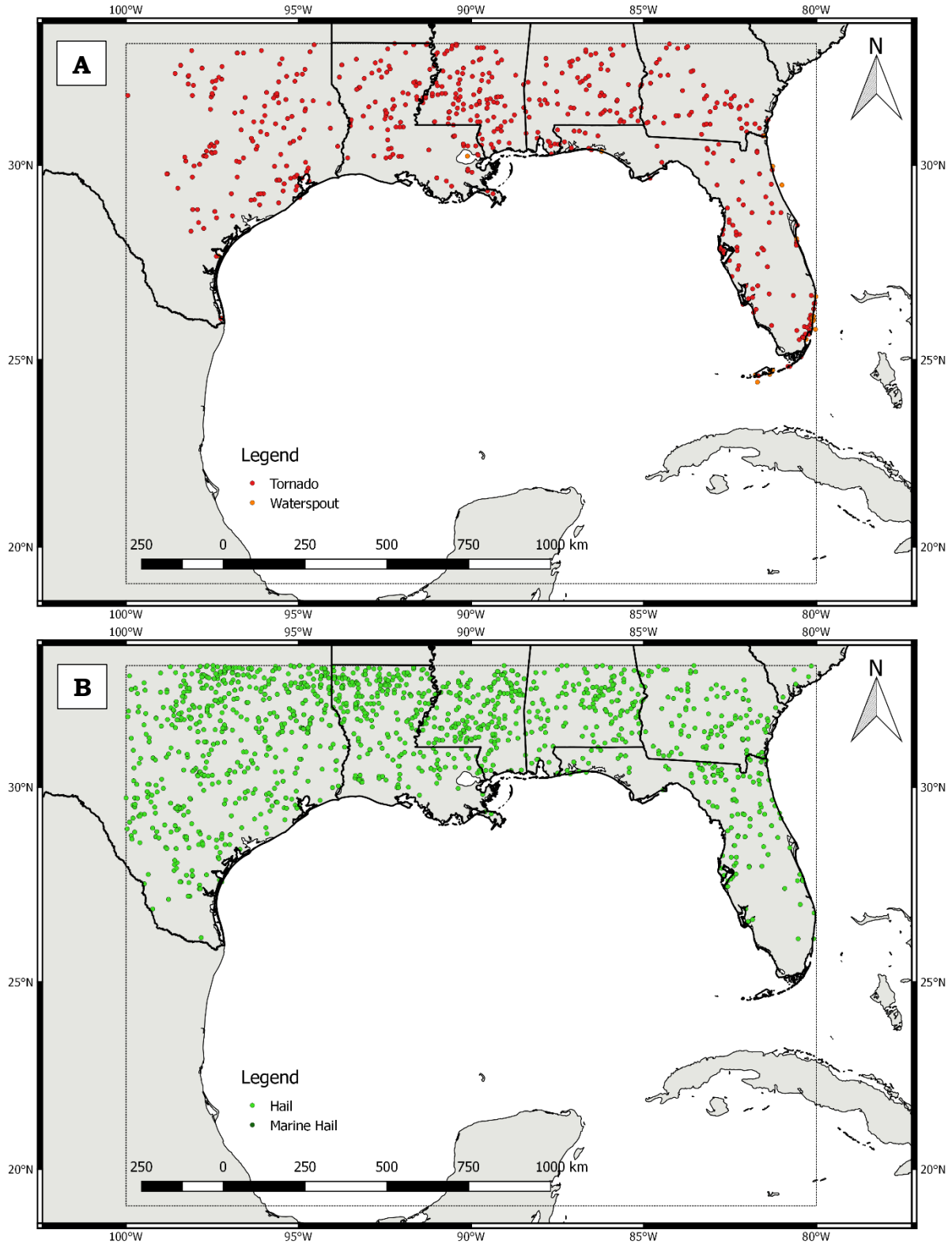


**Figure 5.17** MJO Phase 3 reports of tornadoes (A), hail (B), strong/damaging winds (C), and all severe weather types combined (D).
(figure continued)

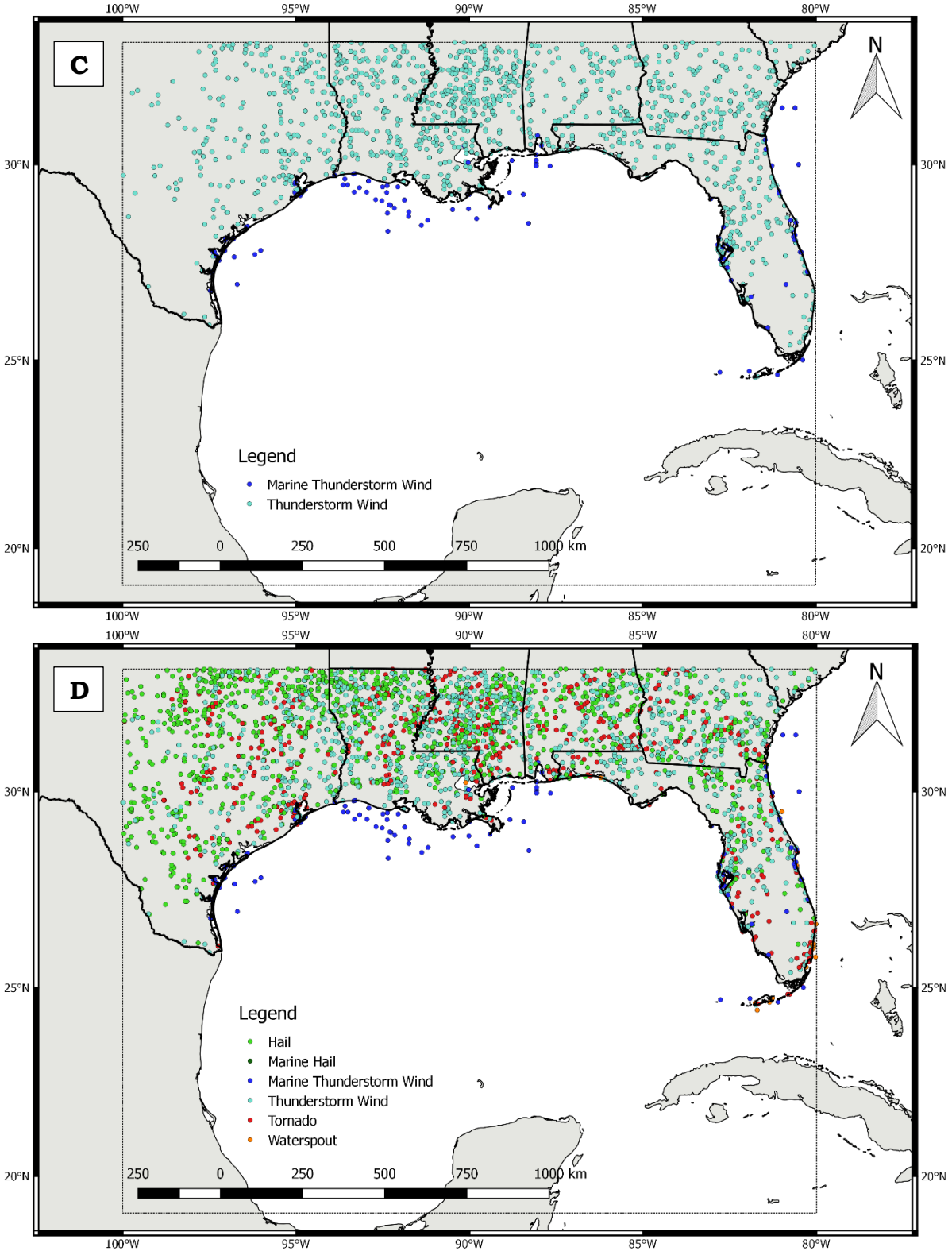
C
N
100°W
95°W
90°W
85°W
80°W
30°N
25°N
20°N
Legend
Marine Thunderstorm Wind
Thunderstorm Wind
250
0
250
500
750
1000 km
D
N
Legend
Hail
Marine Hail
Marine Thunderstorm Wind
Thunderstorm Wind
Tornado
Waterspout
250
0
250
500
750
1000 km

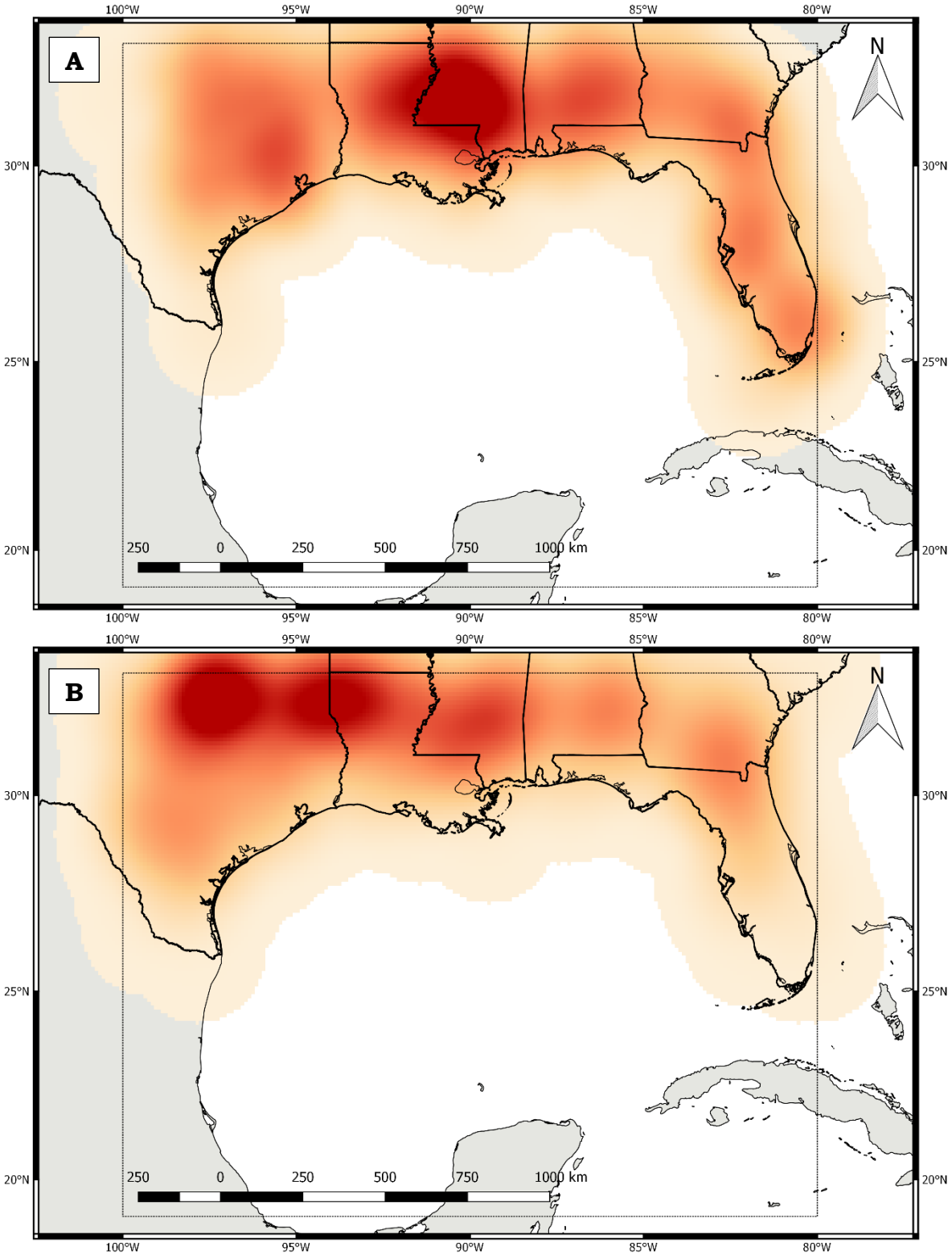


**Figure 5.18** MJO Phase 3 kernel density maps for reports of tornadoes (A), hail (B), strong/damaging winds (C), and all severe weather types combined (D). (figure continued)

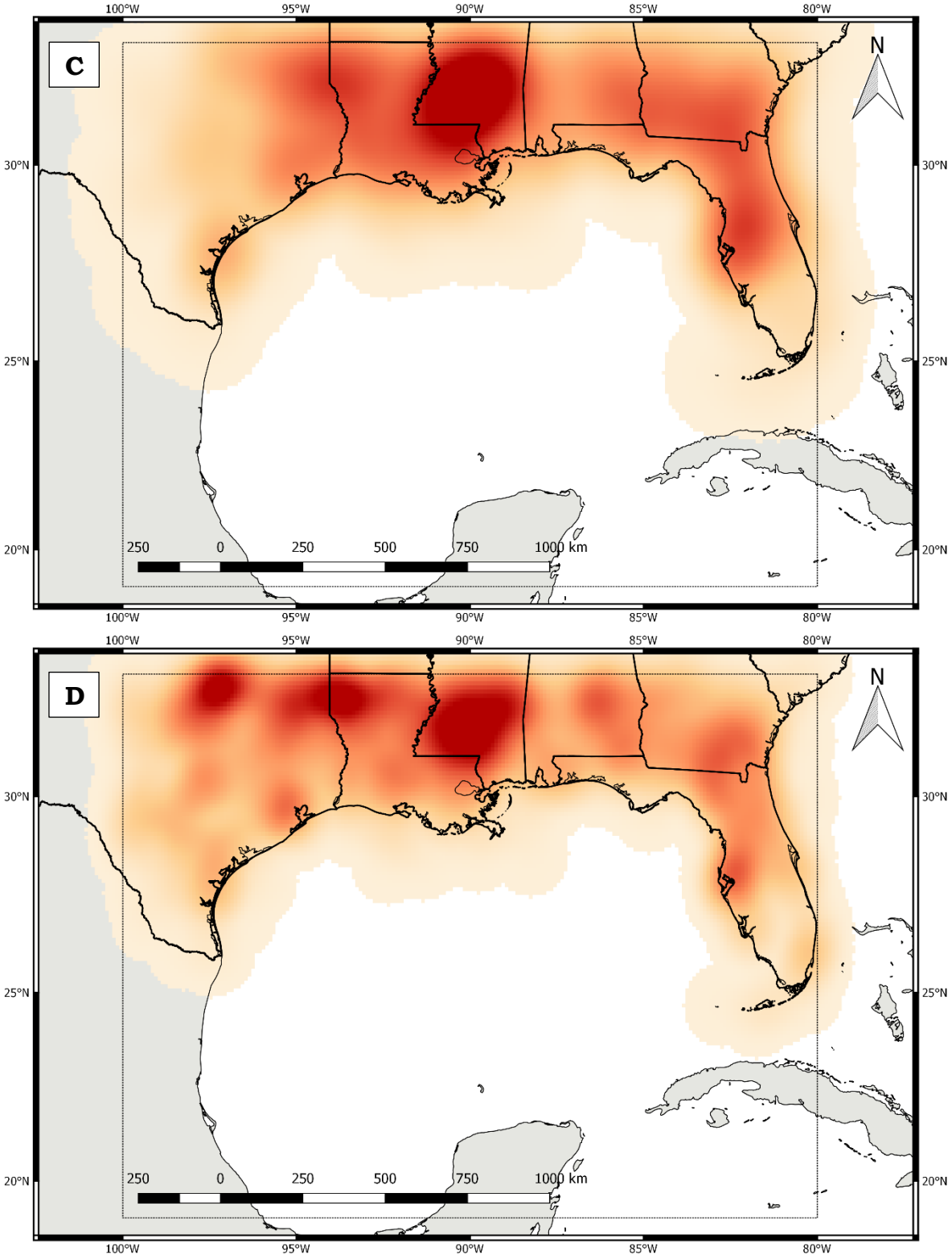
C
D
N
100°W
95°W
90°W
85°W
80°W
30°N
25°N
20°N
250
0
250
500
750
1000 km

similar to Phases 1 and 2, with hot spots noted near Dallas, Shreveport, , and over southern Mississippi.

### 5.3.6 Geospatial Patterns during MJO Phase 4

Figure 5.19 provides a broad overview of reports of tornadoes, hail, strong/damaging winds, and all modes of severe weather combined during MJO Phase 4. Spatial trends in severe weather reports can be examined using the kernel density maps in Figure 5.20. Tornadoes displayed a triple maxima pattern, with the greatest maximum noted in eastern Texas, a second maximum in southern Mississippi, and a somewhat lower magnitude maximum in central Florida between Tampa and Orlando. The trio of tornado hot spots was notable for the large geographic spread ranging from the northwestern GoM Coast to the Florida Peninsula. Hail reports continued the spatial trends noted during Phases 1–3, with the highest frequencies shown in northeastern Texas, a small part of northwestern Louisiana, and much of southern Mississippi. Reports of strong and/or damaging winds again showed a preference for southern Mississippi but the maximum was slightly different from previous phases, arcing from near Baton Rouge, Louisiana, to Jackson, Mississippi, and southeastward toward Mobile, Alabama. A second maximum was also noted near Shreveport, Louisiana. When all modes of severe weather were combined, the pattern that emerged was very similar to that for Phases 1–3. Severe weather report maxima were noted near Dallas, Texas, Shreveport, Louisiana, and Jackson, Mississippi. Other smaller maxima were found near Houston, Texas, and in central Florida.

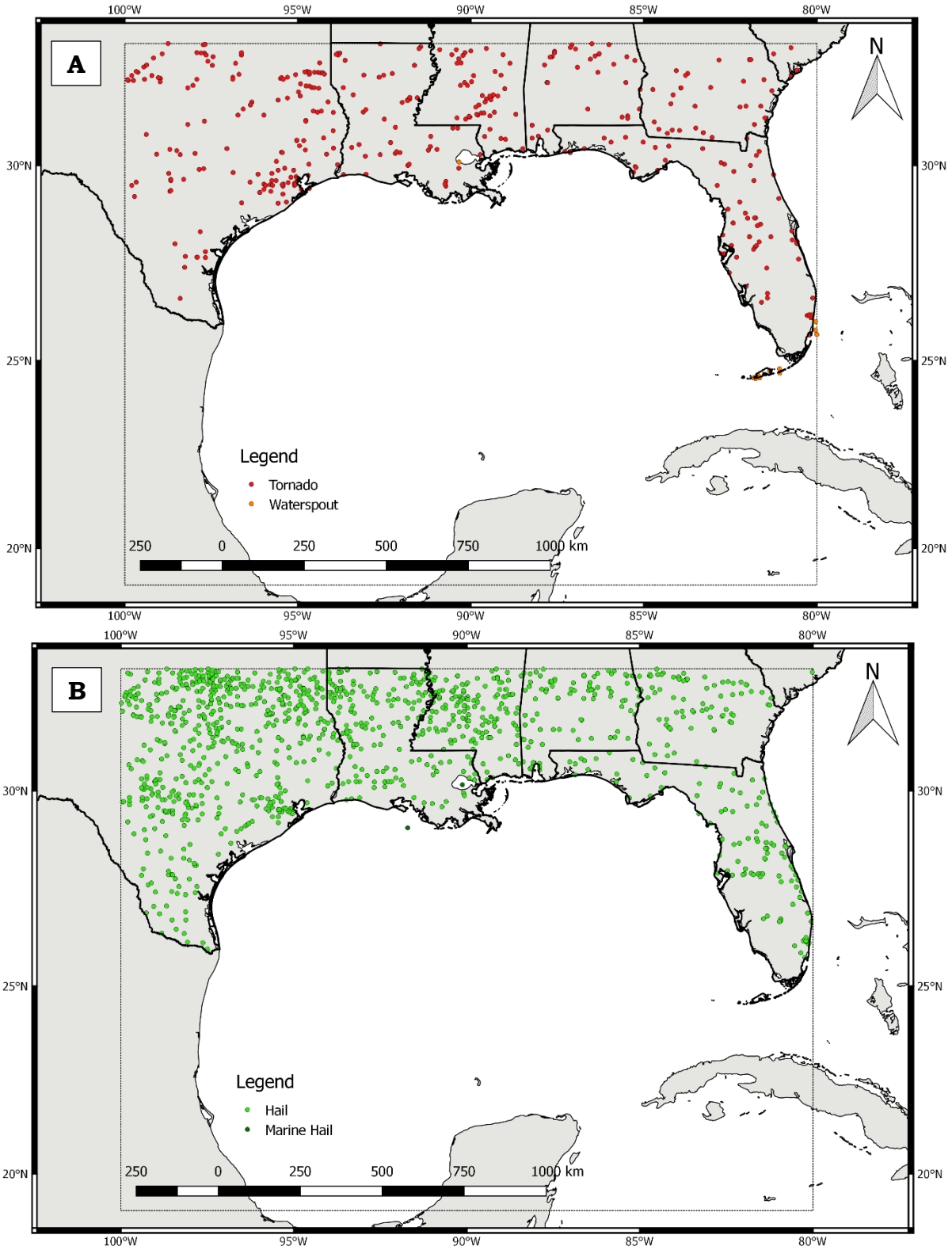


**Figure 5.19** MJO Phase 4 reports of tornadoes (A), hail (B), strong/damaging winds (C), and all severe weather types combined (D).
(figure continued)

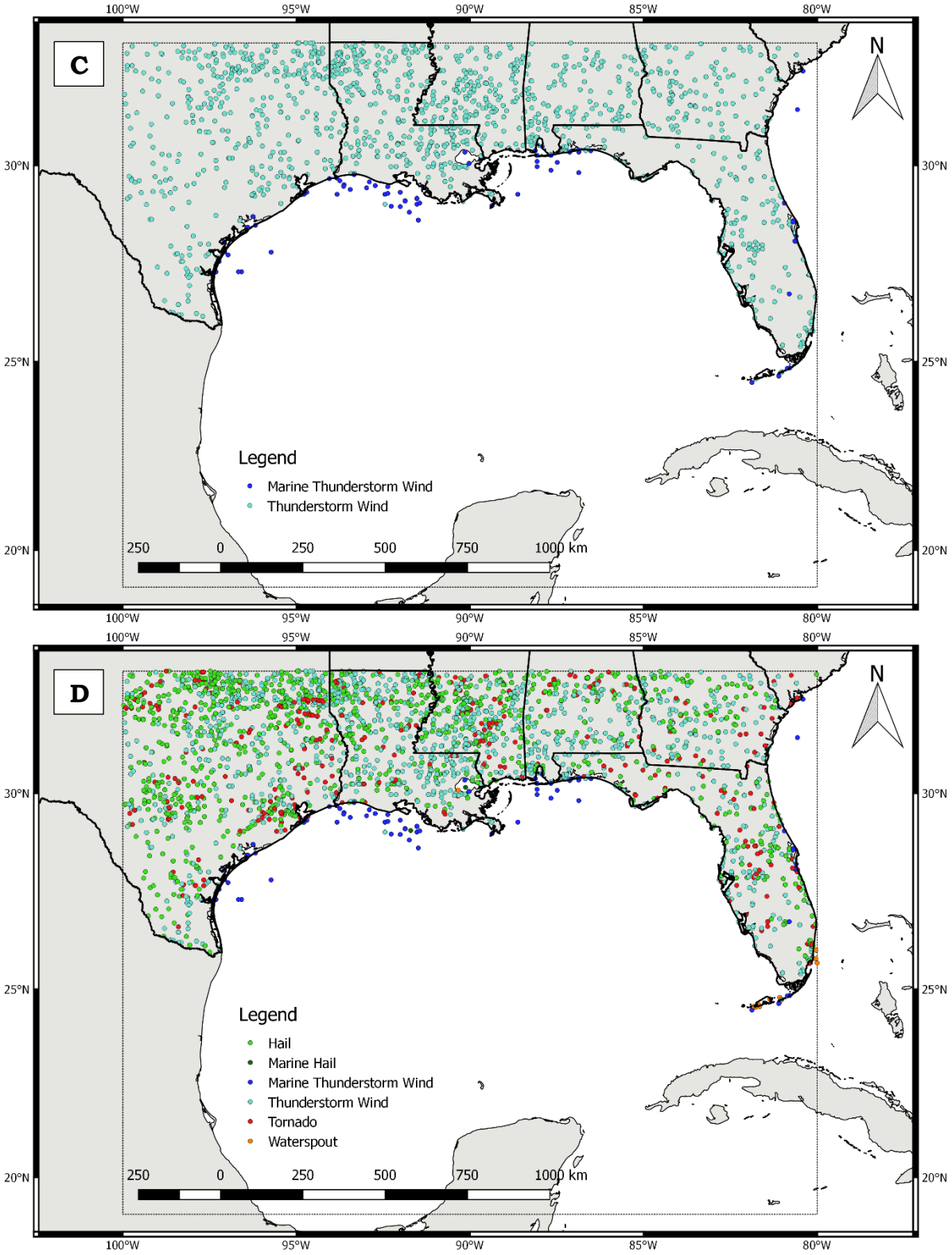
C
N
100°W
95°W
90°W
85°W
80°W
30°N
25°N
20°N
Legend
Marine Thunderstorm Wind
Thunderstorm Wind
250
0
250
500
750
1000 km
D
Legend
Hail
Marine Hail
Marine Thunderstorm Wind
Thunderstorm Wind
Tornado
Waterspout

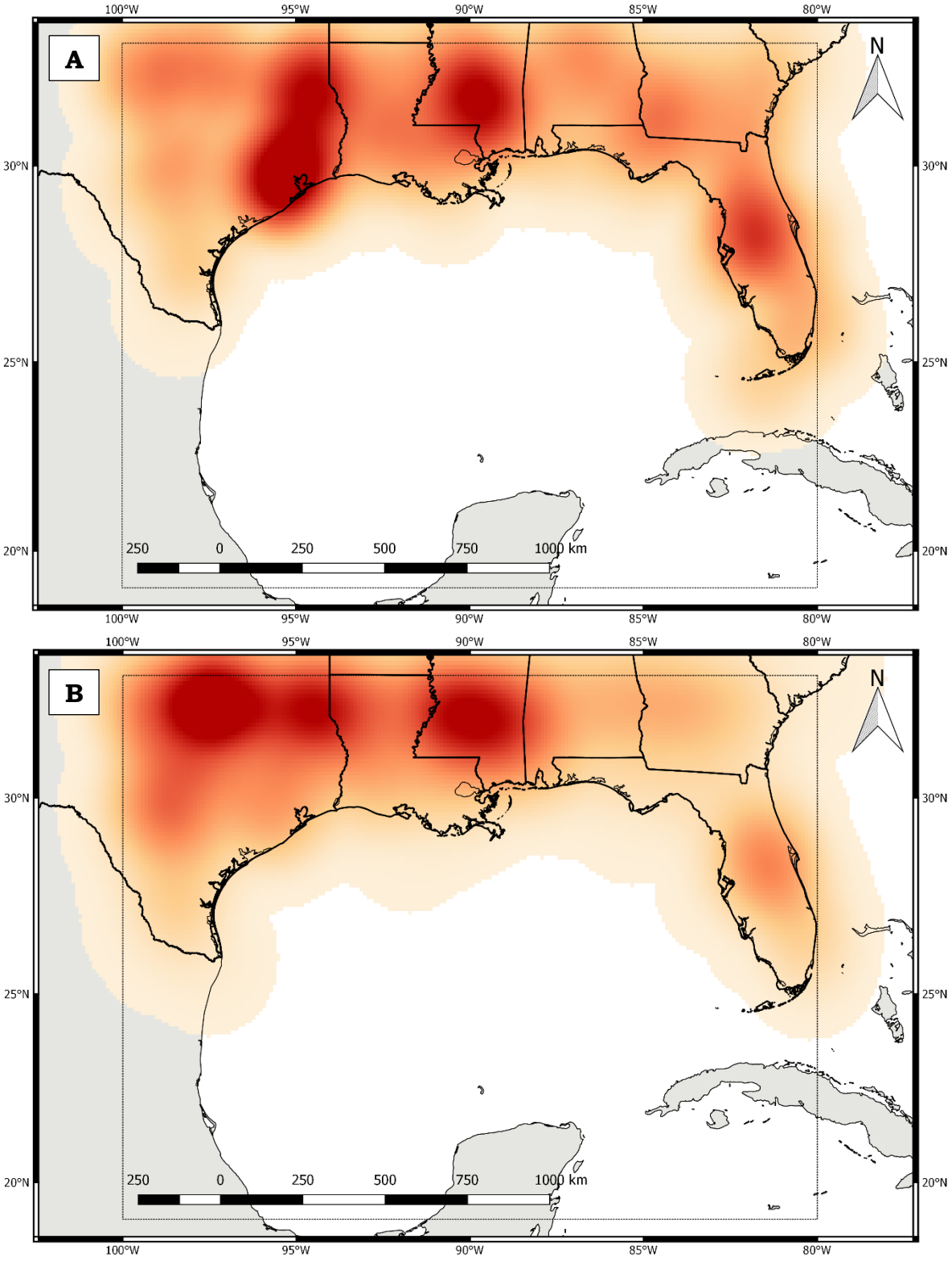


**Figure 5.20** MJO Phase 4 kernel density maps for reports of tornadoes (A), hail (B), strong/damaging winds (C), and all severe weather types combined (D). (figure continued)

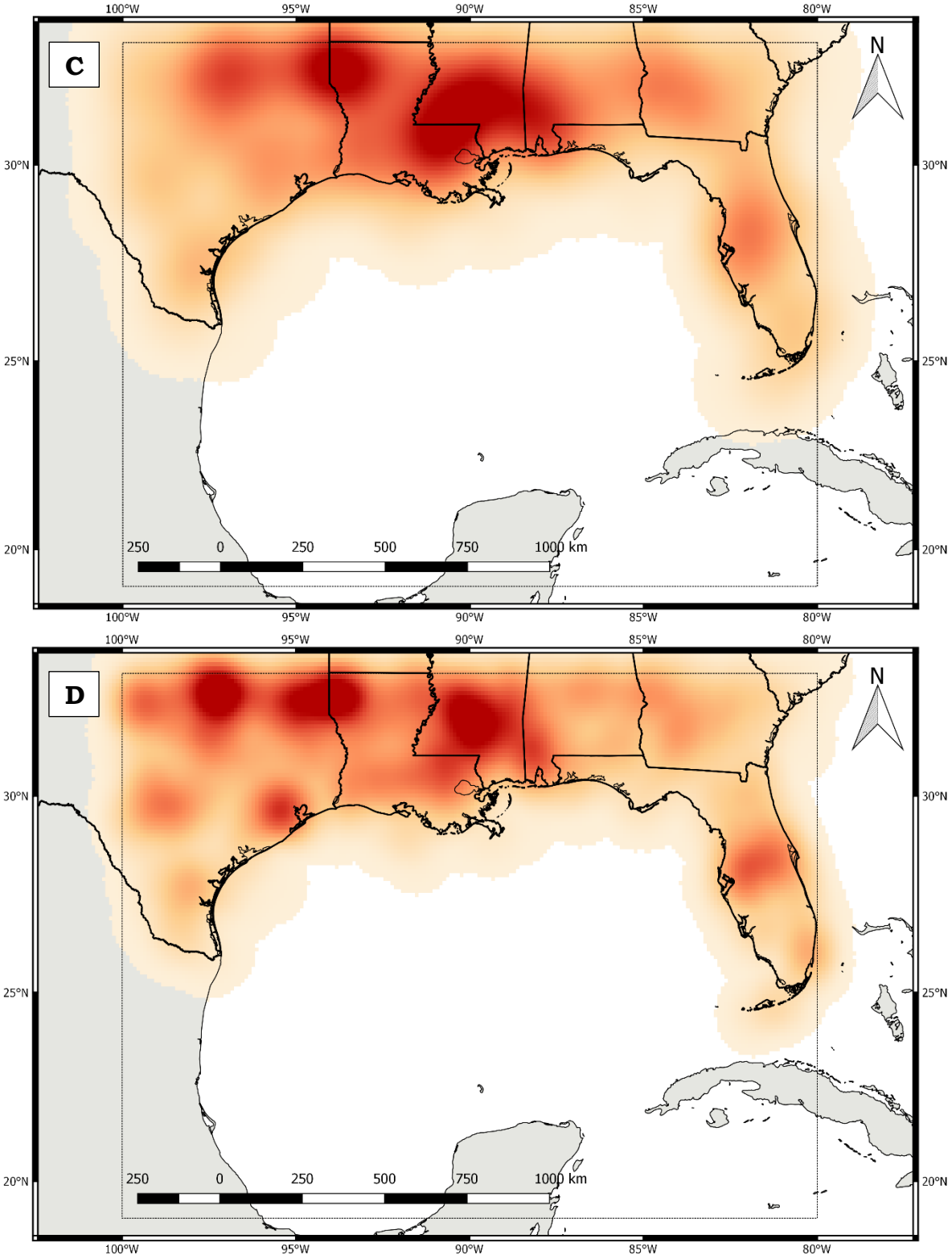
C
D
N
100°W
95°W
90°W
85°W
80°W
30°N
25°N
20°N
250
0
250
500
750
1000 km

### 5.3.7 Geospatial Patterns during MJO Phase 5

Figure 5.21 provides a broad overview of reports of tornadoes, hail, strong/damaging winds, and all modes of severe weather combined during MJO Phase 5. Spatial trends in severe weather reports can be examined using the kernel density maps in Figure 5.22. Tornadoes during Phase 6 were most frequent in a triangular region bounded by Shreveport, Houston, and Lake Charles. A smaller secondary maximum was noted just near and south of Jackson, Mississippi. The geographic distribution resembled the one noted during Phase 4 (Figure 5.20). Frequencies of hail, strong/damaging winds, and all modes of severe weather combined showed similar kernel density patterns as during Phase 5. Once again, a triple maxima pattern was noted, with the hot spots centered around Dallas, Shreveport, and Jackson. Hail frequencies were again low in much of the Florida Peninsula, with the lowest number of reports over southern Florida. Local maxima for reports of strong/damaging winds and all types of severe weather combined were observed near Tampa, Florida. Spatial trends in severe weather during MJO Phase 5 appeared very similar to those observed during Phase 4.

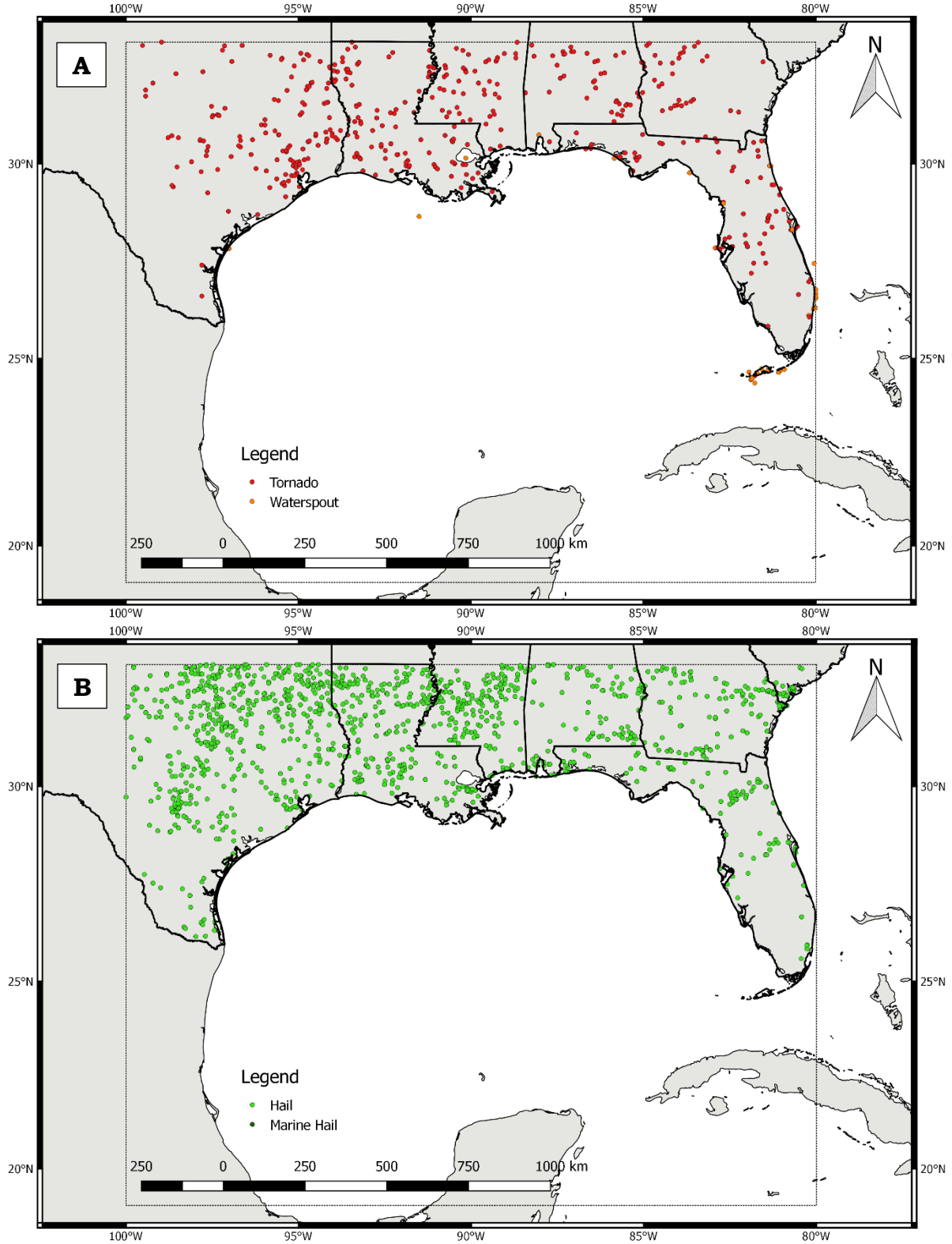


**Figure 5.21** MJO Phase 5 reports of tornadoes (A), hail (B), strong/damaging winds (C), and all severe weather types combined (D).
(figure continued)

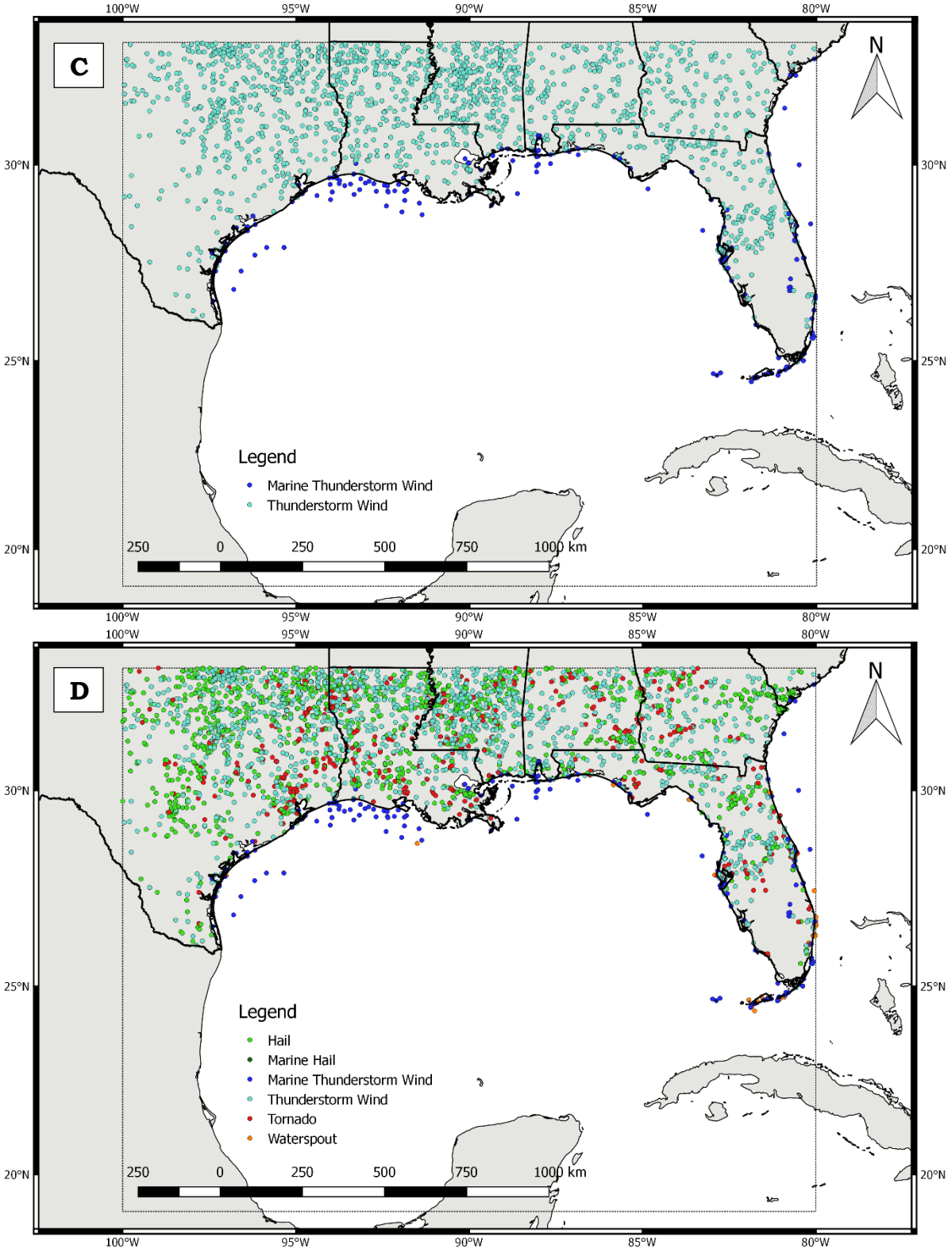
C
N
100°W
95°W
90°W
85°W
80°W
30°N
25°N
20°N
Legend
Marine Thunderstorm Wind
Thunderstorm Wind
250 0 250 500 750 1000 km
D
N
Legend
Hail
Marine Hail
Marine Thunderstorm Wind
Thunderstorm Wind
Tornado
Waterspout
250 0 250 500 750 1000 km

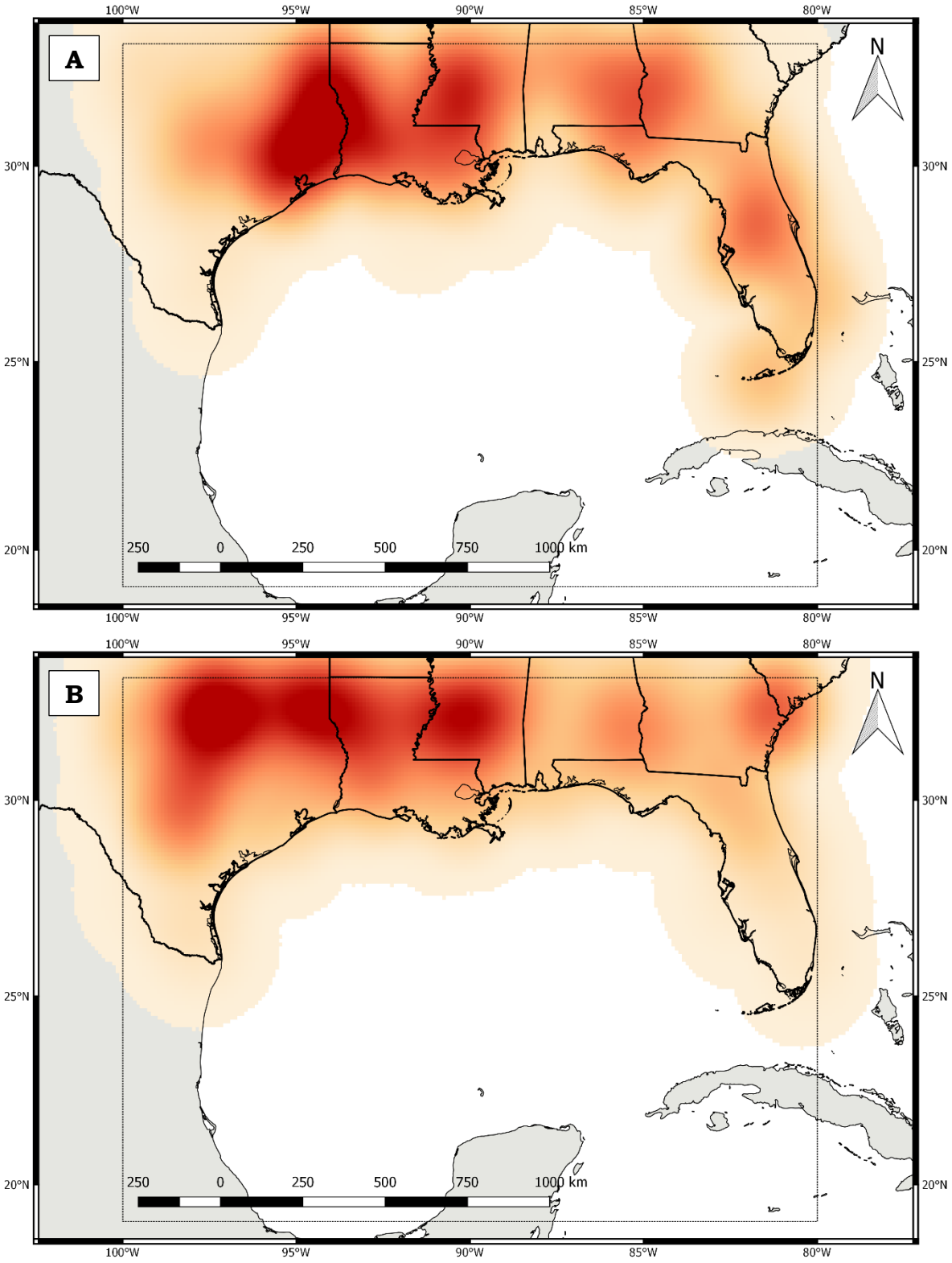


**Figure 5.22** MJO Phase 5 kernel density maps for reports of tornadoes (A), hail (B), strong/damaging winds (C), and all severe weather types combined (D). (figure continued)

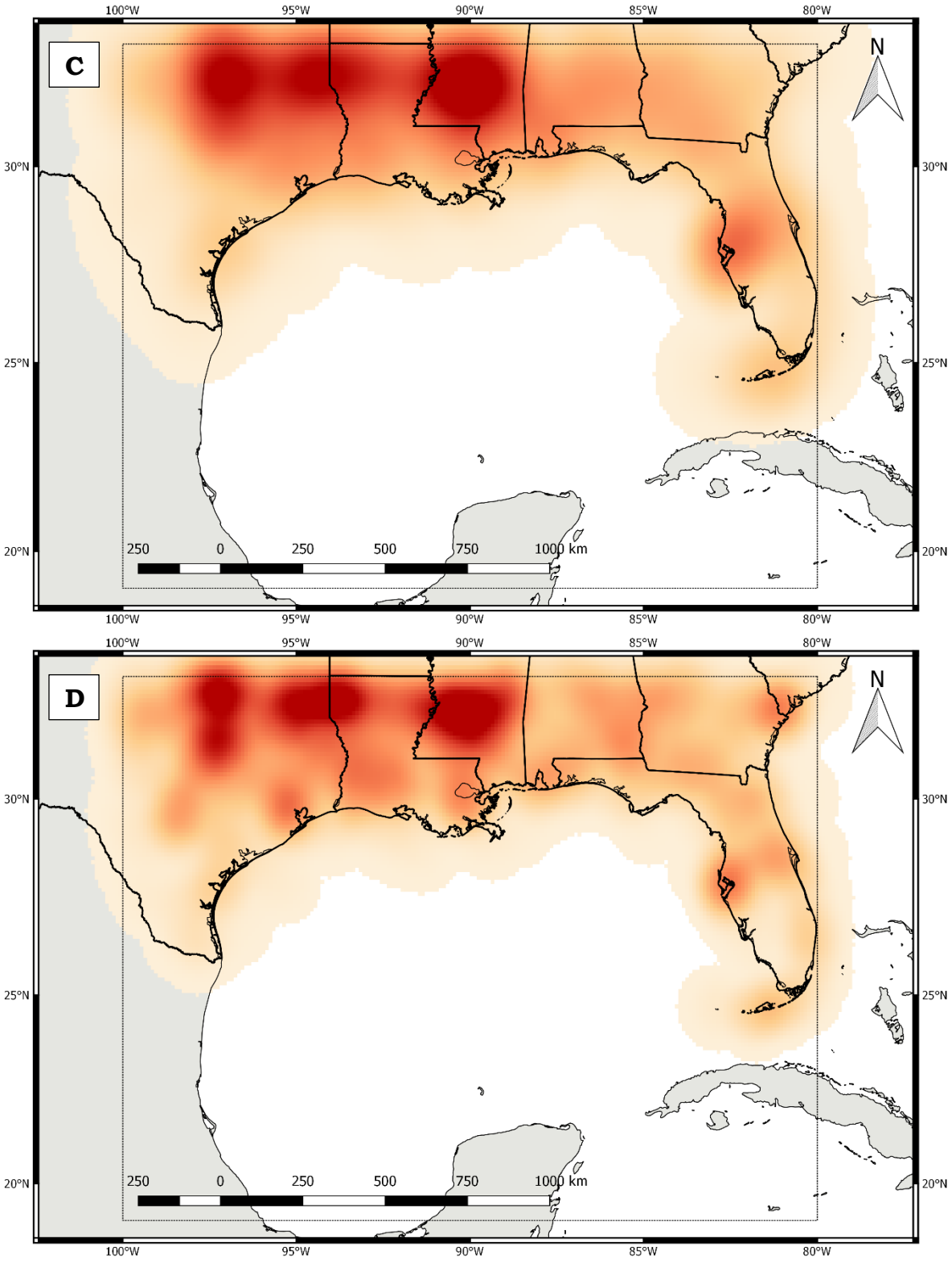
C
D
N
100°W
95°W
90°W
85°W
80°W
30°N
25°N
20°N
250
0
250
500
750
1000 km

### 5.3.8 Geospatial Patterns during MJO Phase 6

Figure 5.23 provides a broad overview of reports of tornadoes, hail, strong/damaging winds, and all modes of severe weather combined during MJO Phase 6. Spatial trends in severe weather reports can be examined using the kernel density maps in Figure 5.24. Phase 6 showed a preference for severe weather over the western half of the study area, with nearly all clustering of reports noted from Mississippi westward. A primary tornado maximum was noted over much of southern Mississippi, with a much smaller maximum, both spatially and in magnitude, over the northwestern Florida Panhandle into southeastern Alabama. Hail reports were most frequent from Shreveport to Dallas, with relatively high frequencies noted over much of eastern Texas. A smaller secondary maximum was over southern Mississippi but also notable was the sparsity of hail reports east of Mississippi, particularly over Georgia and Florida. Analysis of wind reports produced a pattern not seen in any of the previous phases, with an east-west oriented maximum extending from near Jackson, Mississippi, across northern Louisiana. As with hail reports, strong/damaging wind frequencies were low over the eastern half of the GoM study region. The kernel density plots for all modes of severe weather combined displayed two report maxima centered near Jackson and Shreveport. The most notable pattern during MJO Phase 6 was the clear trend toward lower frequencies of severe weather over the eastern half of the study area in Alabama, Georgia, Florida, and a small part of South Carolina.

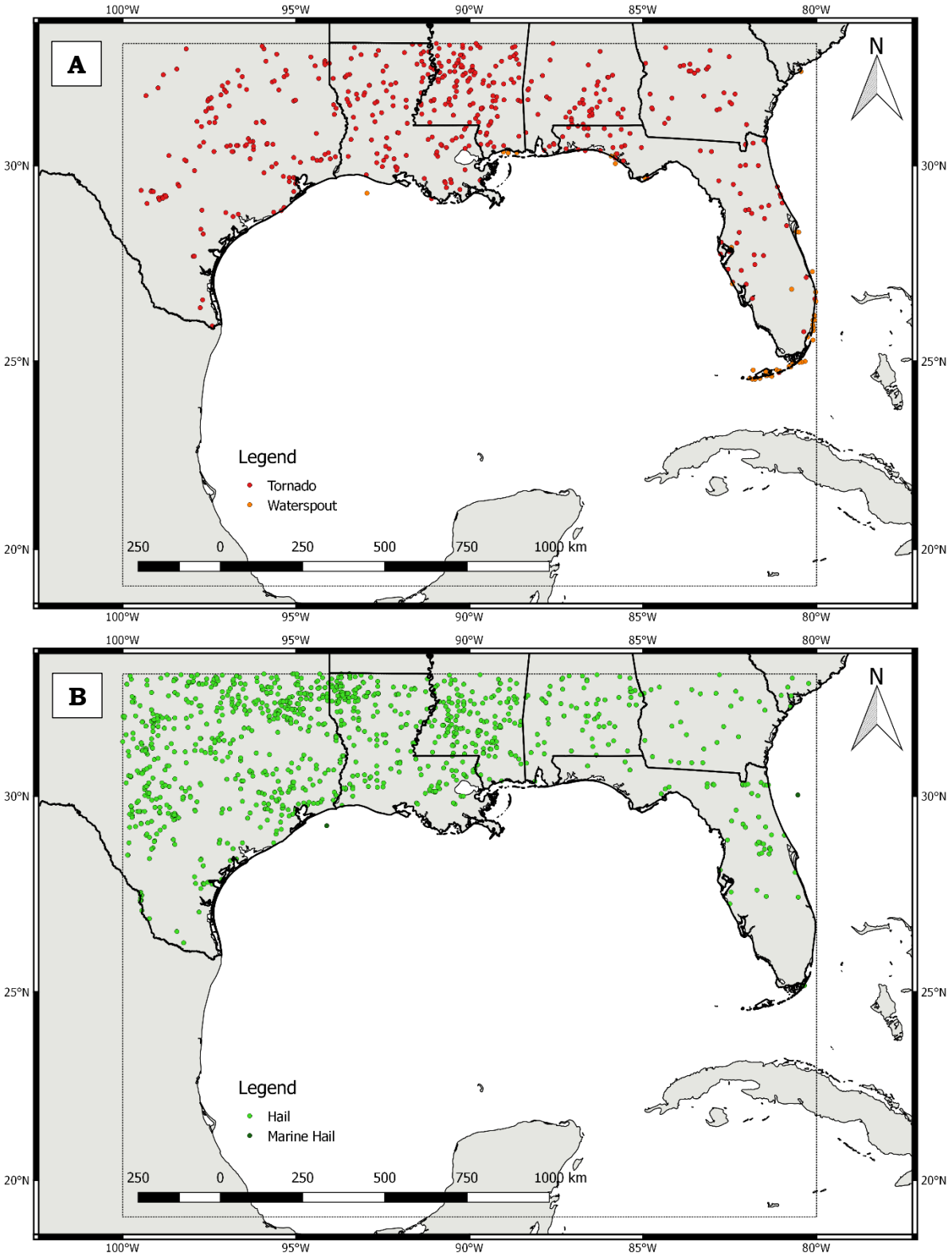


**Figure 5.23** MJO Phase 6 reports of tornadoes (A), hail (B), strong/damaging winds (C), and all severe weather types combined (D).
(figure continued)

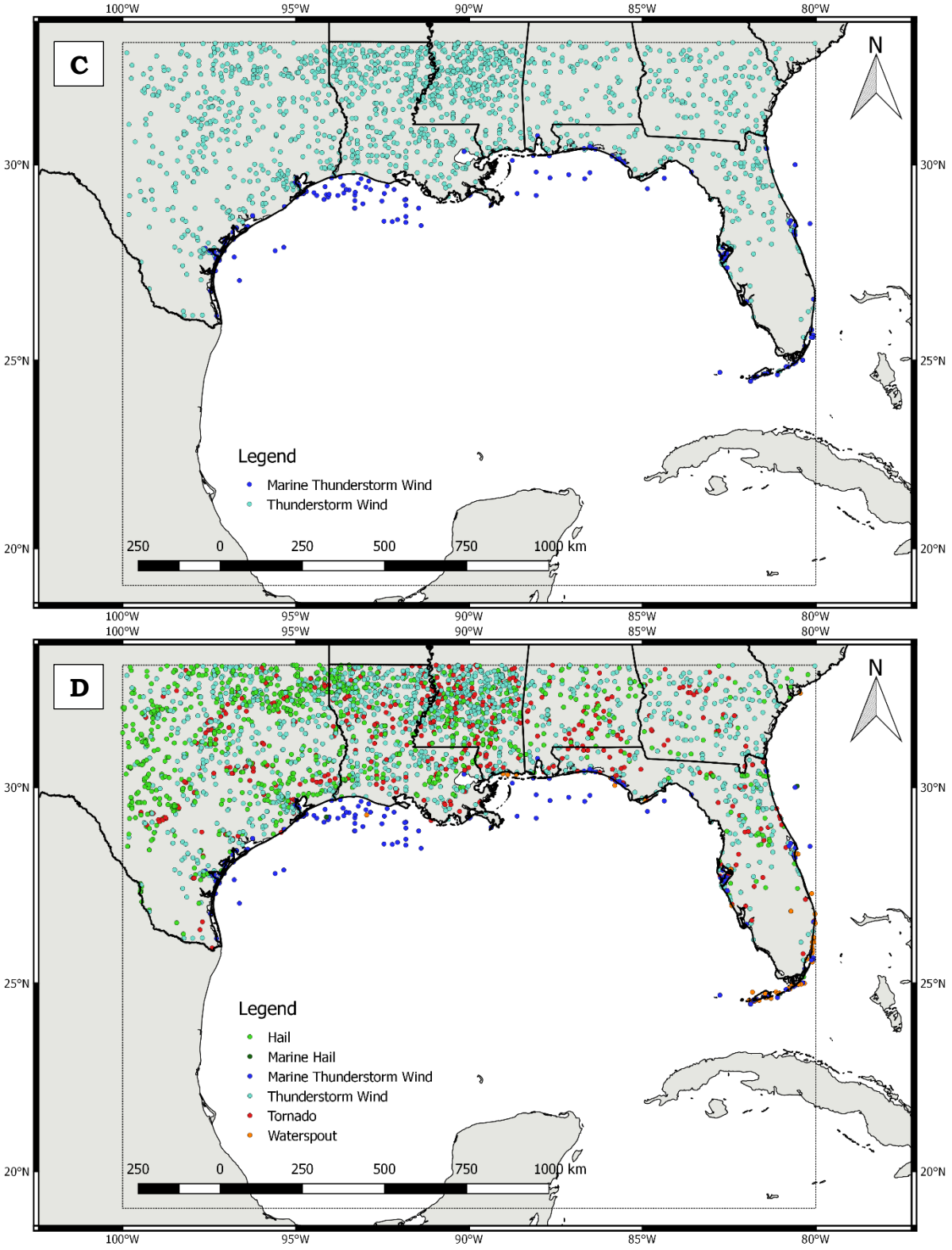
C
N
100°W
95°W
90°W
85°W
80°W
30°N
25°N
20°N
Legend
Marine Thunderstorm Wind
Thunderstorm Wind
250
0
250
500
750
1000 km
D
Legend
Hail
Marine Hail
Marine Thunderstorm Wind
Thunderstorm Wind
Tornado
Waterspout

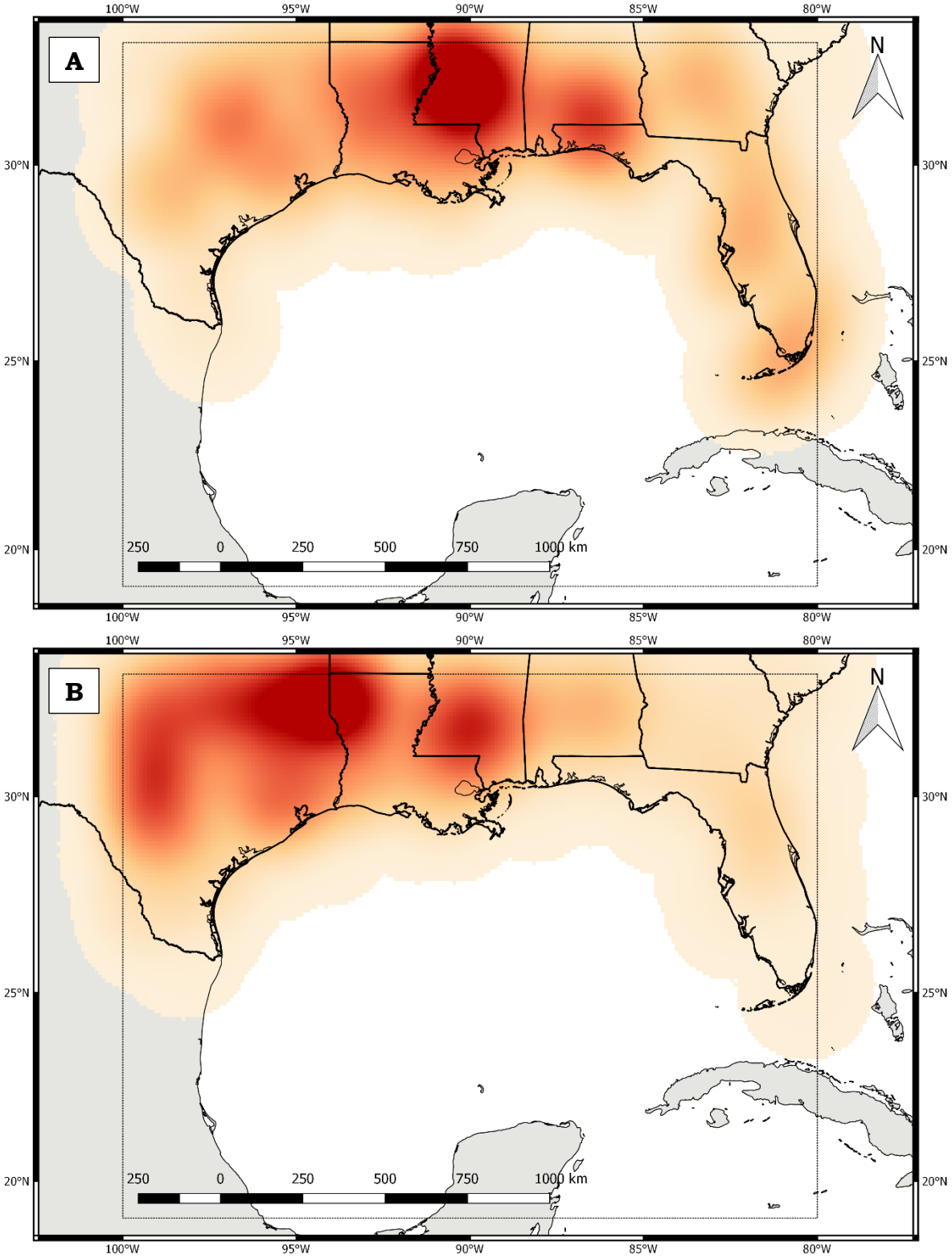


**Figure 5.24** MJO Phase 6 kernel density maps for reports of tornadoes (A), hail (B), strong/damaging winds (C), and all severe weather types combined (D). (figure continued)

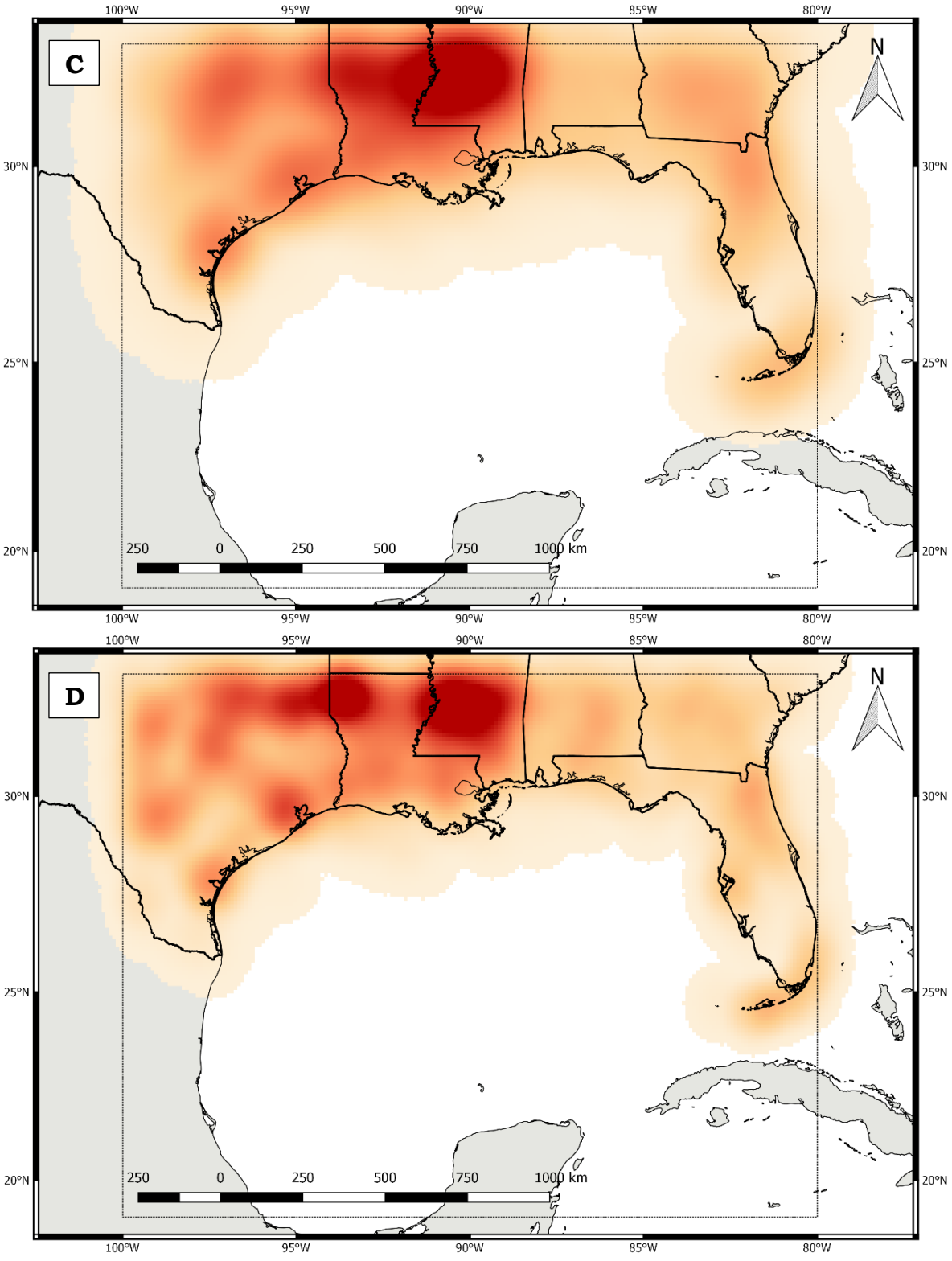
C
D
N
100°W
95°W
90°W
85°W
80°W
30°N
25°N
20°N
250
0
250
500
750
1000 km

### 5.3.9 Geospatial Patterns during MJO Phase 7

Figure 5.25 provides a broad overview of reports of tornadoes, hail, strong/damaging winds, and all modes of severe weather combined during MJO Phase 7. Spatial trends in severe weather reports can be examined using the kernel density maps in Figure 5.26. The trend toward lower severe weather frequencies over the eastern GoM study region noted in Phase 6 appears to come to a halt during Phase 7. The greatest maximum in tornado reports was noted from Jackson to Baton Rouge, but a secondary maximum was found in the Alabama, Georgia, and Florida triple point. A third, much smaller maximum, both spatially and in magnitude, was centered near Houston. Reports of hail showed two relative hot spots, with one maximum noted southwest of Dallas and another west-east oriented maximum from Shreveport, Louisiana, to Hattiesburg, Mississippi. Similar to Phase 6, hail frequencies were low east of Mississippi, particularly in Georgia and Florida. Strong/damaging wind reports showed the greatest change from Phase 6 to 7. While a maximum still appeared over Mississippi, a broader scale enhanced band of wind reports stretched from eastern Texas into Georgia. Kernel density analysis of all modes of severe weather combined produced familiar results, with the maximum frequencies extending across northern Louisiana into Mississippi. Sporadic hot spots that were smaller both in magnitude and coverage were noted elsewhere but the most notable trend during Phase 7 was the tendency toward increasing severe weather frequencies over the eastern GoM relative to Phase 6.

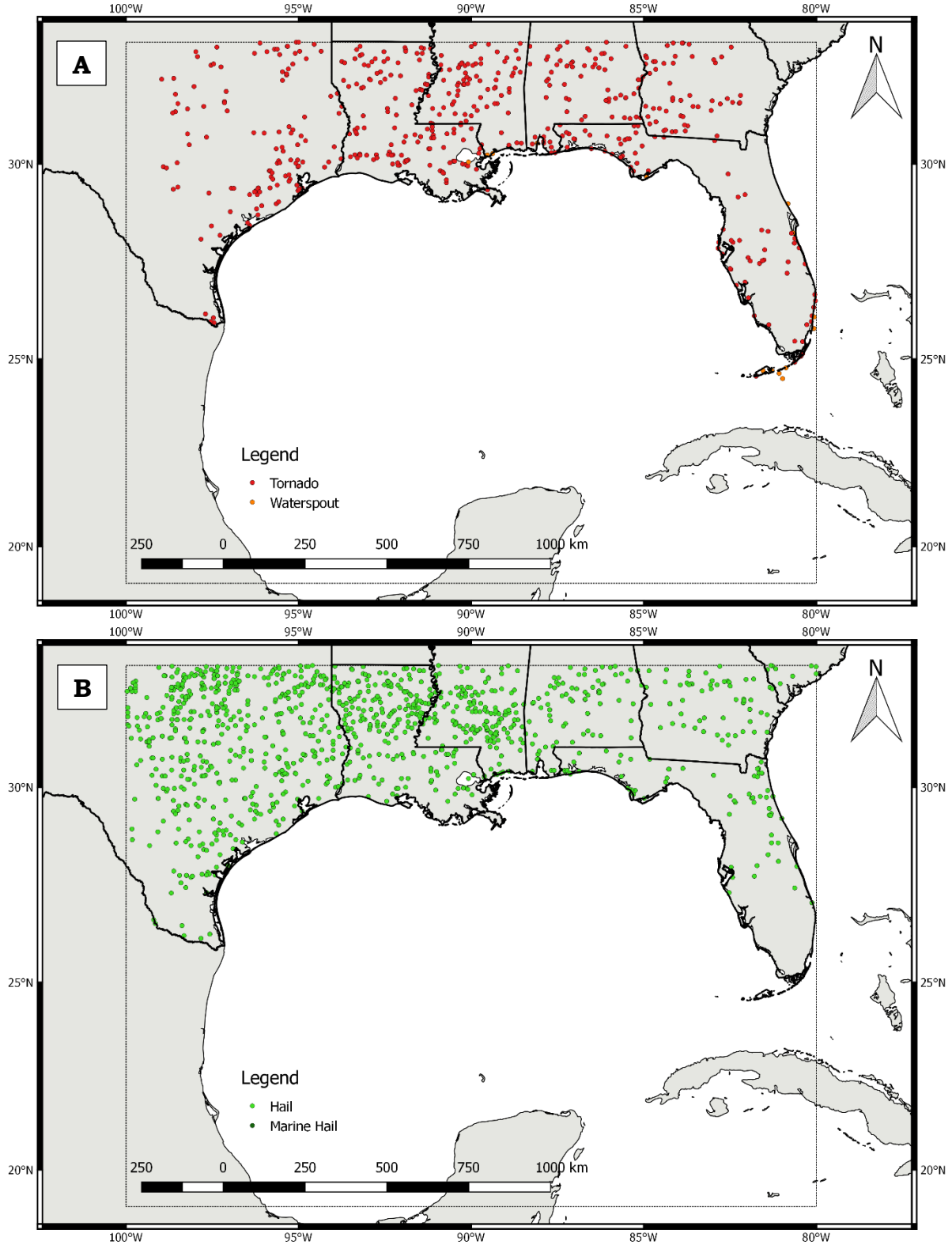


**Figure 5.25** MJO Phase 7 reports of tornadoes (A), hail (B), strong/damaging winds (C), and all severe weather types combined (D).
(figure continued)

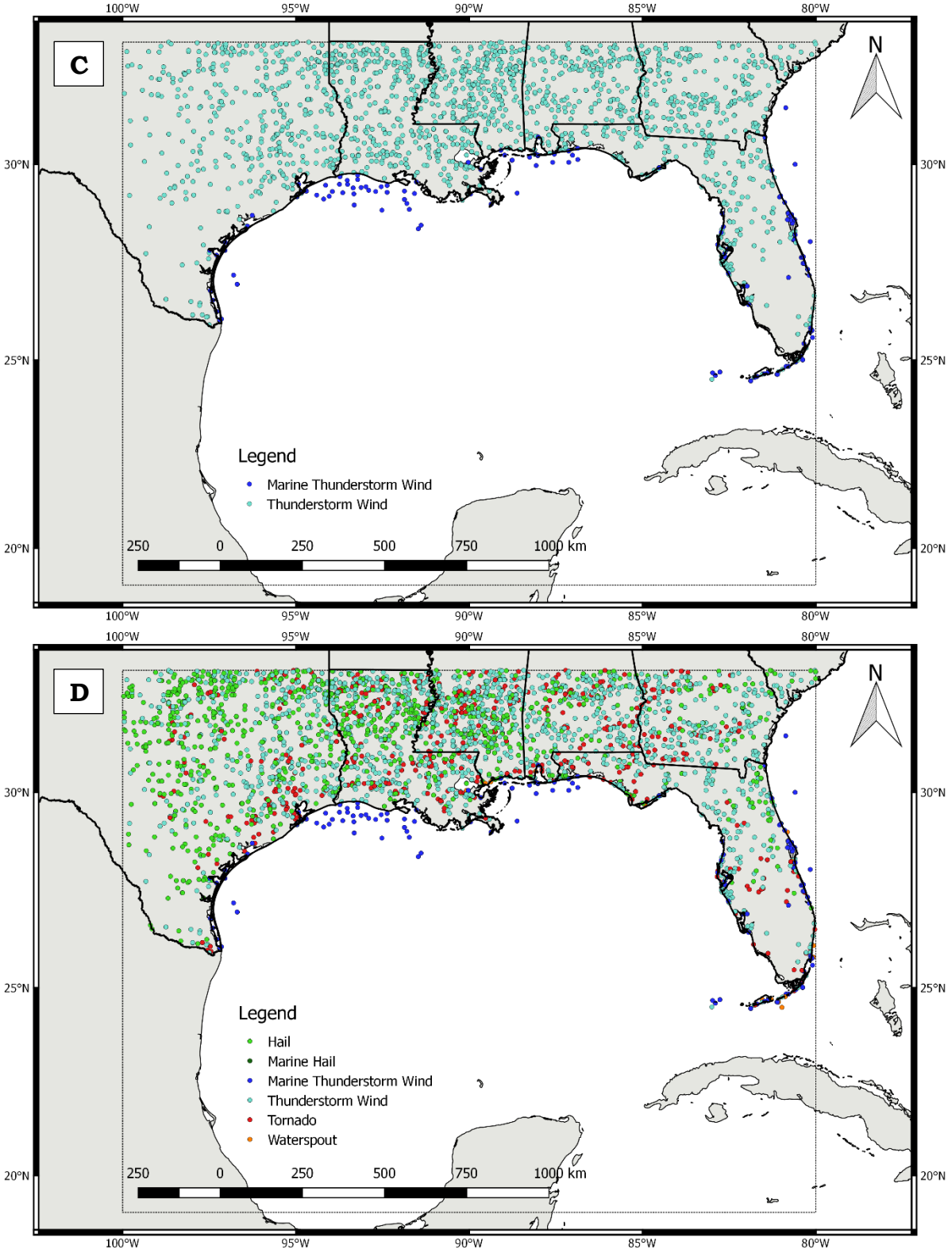
C
N
100°W
95°W
90°W
85°W
80°W
30°N
25°N
20°N
Legend
Marine Thunderstorm Wind
Thunderstorm Wind
250
0
250
500
750
1000 km
D
N
Legend
Hail
Marine Hail
Marine Thunderstorm Wind
Thunderstorm Wind
Tornado
Waterspout
250
0
250
500
750
1000 km

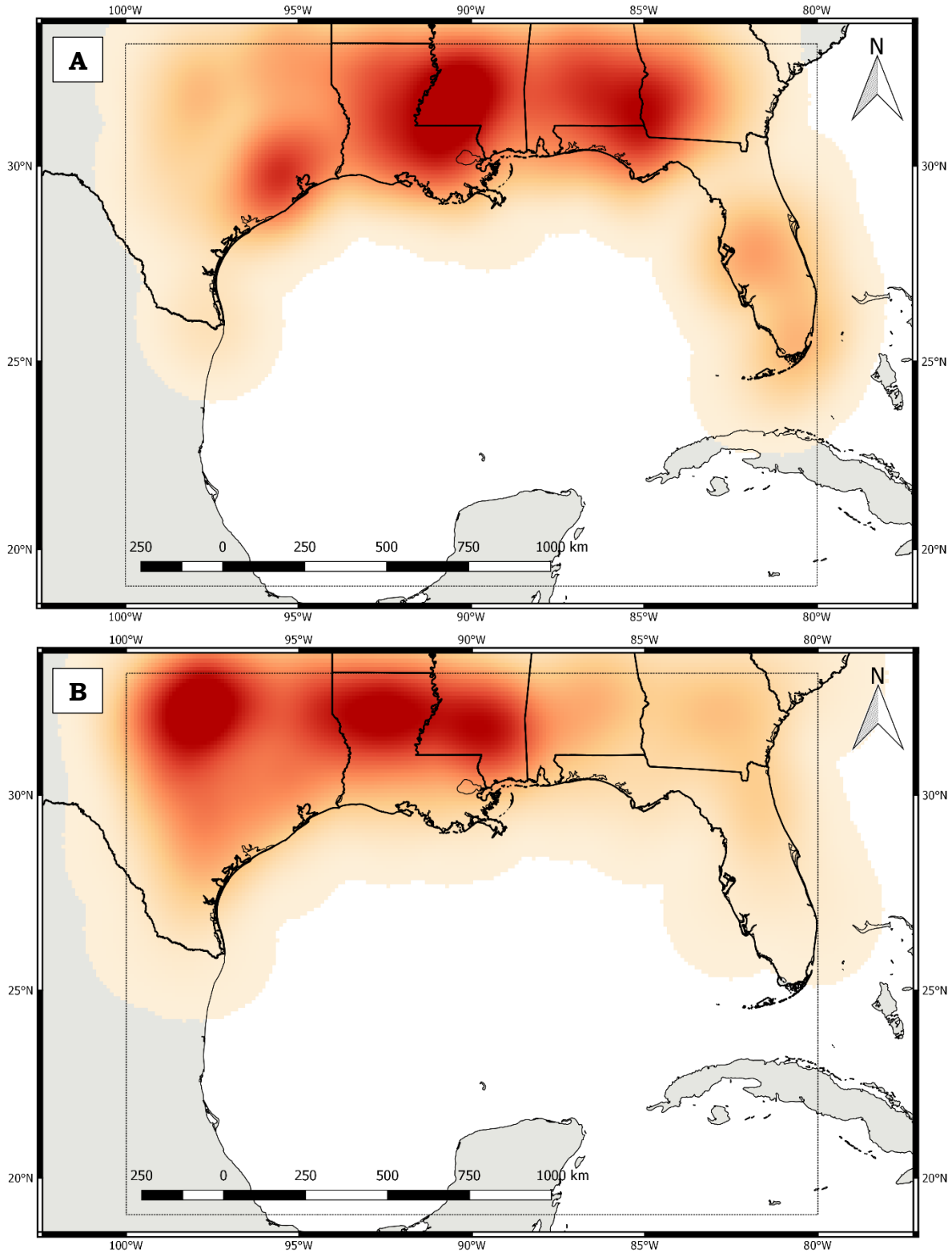


**Figure 5.26** MJO Phase 7 kernel density maps for reports of tornadoes (A), hail (B), strong/damaging winds (C), and all severe weather types combined (D). (figure continued)

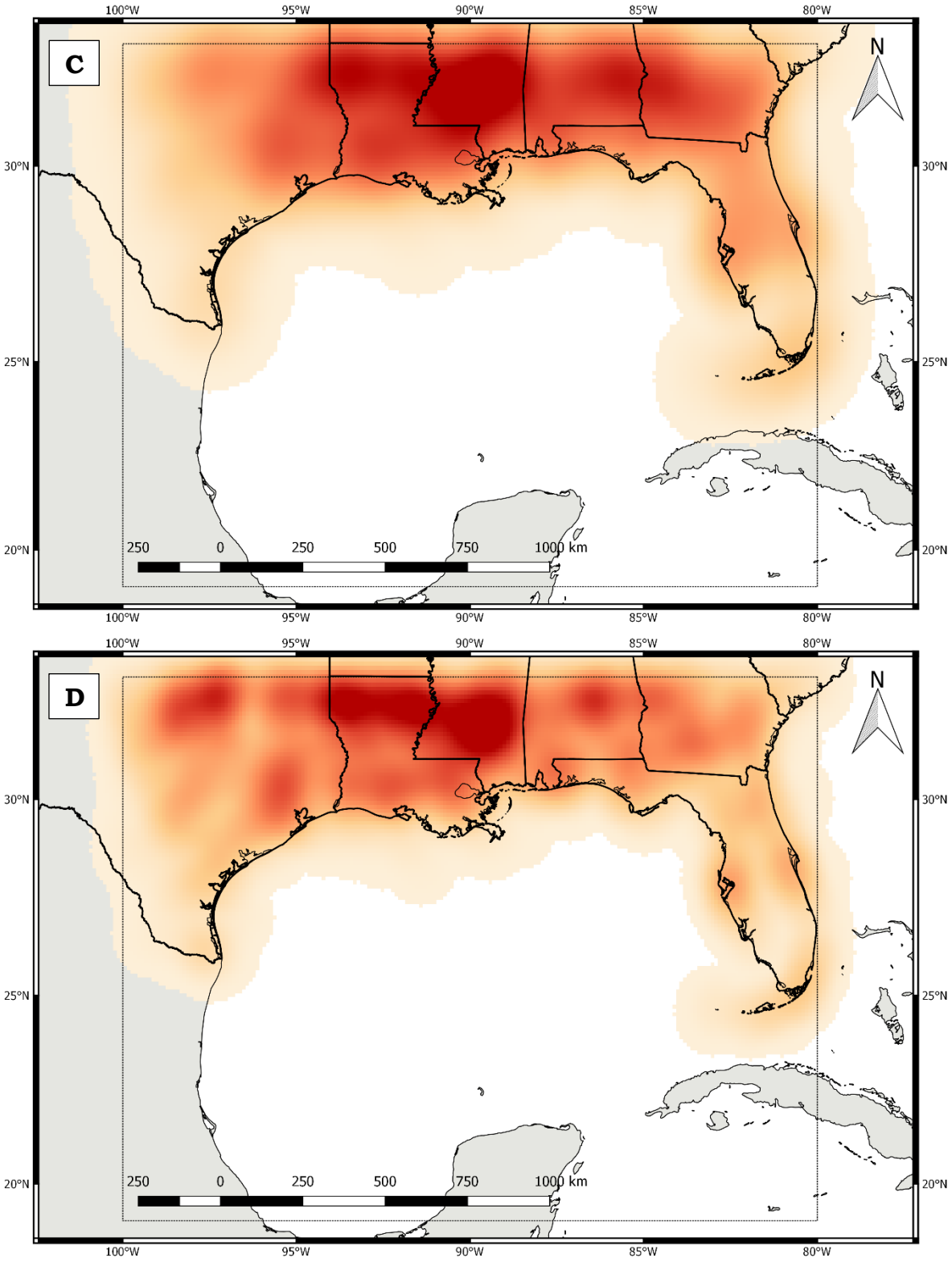
C
D
N
100°W
95°W
90°W
85°W
80°W
30°N
25°N
20°N
250
0
250
500
750
1000 km

### 5.3.10 Geospatial Patterns during MJO Phase 8

Figure 5.27 provides a broad overview of reports of tornadoes, hail, strong/damaging winds, and all modes of severe weather combined during MJO Phase 8. Spatial trends in severe weather reports can be examined using the kernel density maps in Figure 5.28. Phase 8 continued the trend first noted in Phase 7 of increasing severe weather frequencies over the eastern half of the study region. Conversely, Phase 8 is also linked to decreasing number of severe weather reports over the western half of the region relative to previous phases. Phase 8 tornado reports produced a pair of notable spatial features: 1) hot spots were located closer to the coast, and 2) a relative maximum was noted for the first time over southern Florida. In total, four maxima were found centered near Tampa, the northwestern Florida Panhandle, Hattiesburg, and from Lake Charles to Houston. Hail trends were more similar to previous phases, with the primary maximum over Mississippi and northern Louisiana. However, a secondary maximum was noted near Austin, a geospatial trend not found in any of the other phases. Wind reports showed a notable eastward trend, with a west-east maximum displayed from Jackson to near Savannah, Georgia. There was also a clear downward trend in wind reports over much of Texas. When all modes of severe weather were combined, the highest frequency of reports still appeared over Mississippi and parts of northern Louisiana, but other sporadic maxima were spotted throughout the region. Most notably, the kernel density plots showed the clear eastward shift in severe weather reports during Phase 8.

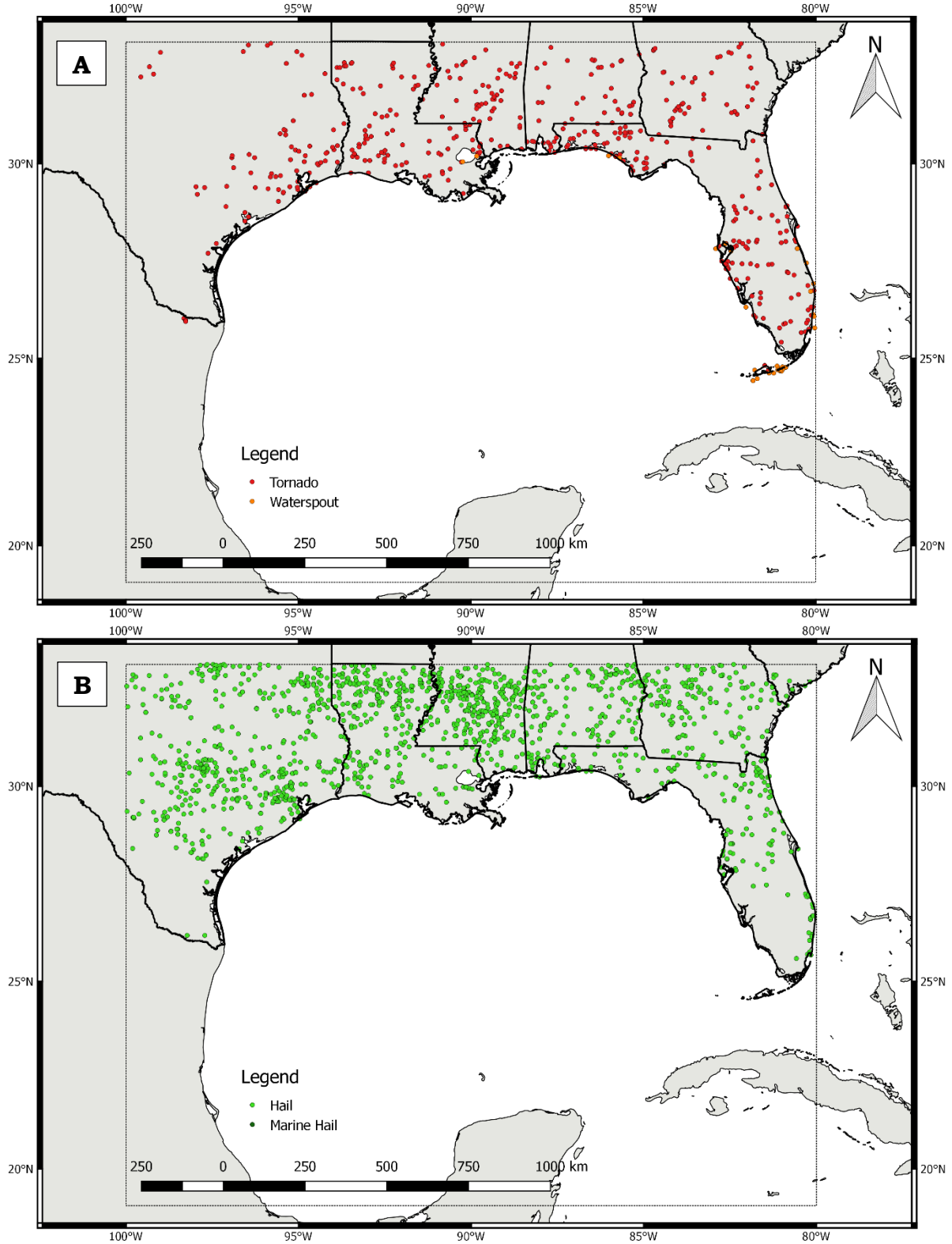


**Figure 5.27** MJO Phase 8 reports of tornadoes (A), hail (B), strong/damaging winds (C), and all severe weather types combined (D).
(figure continued)

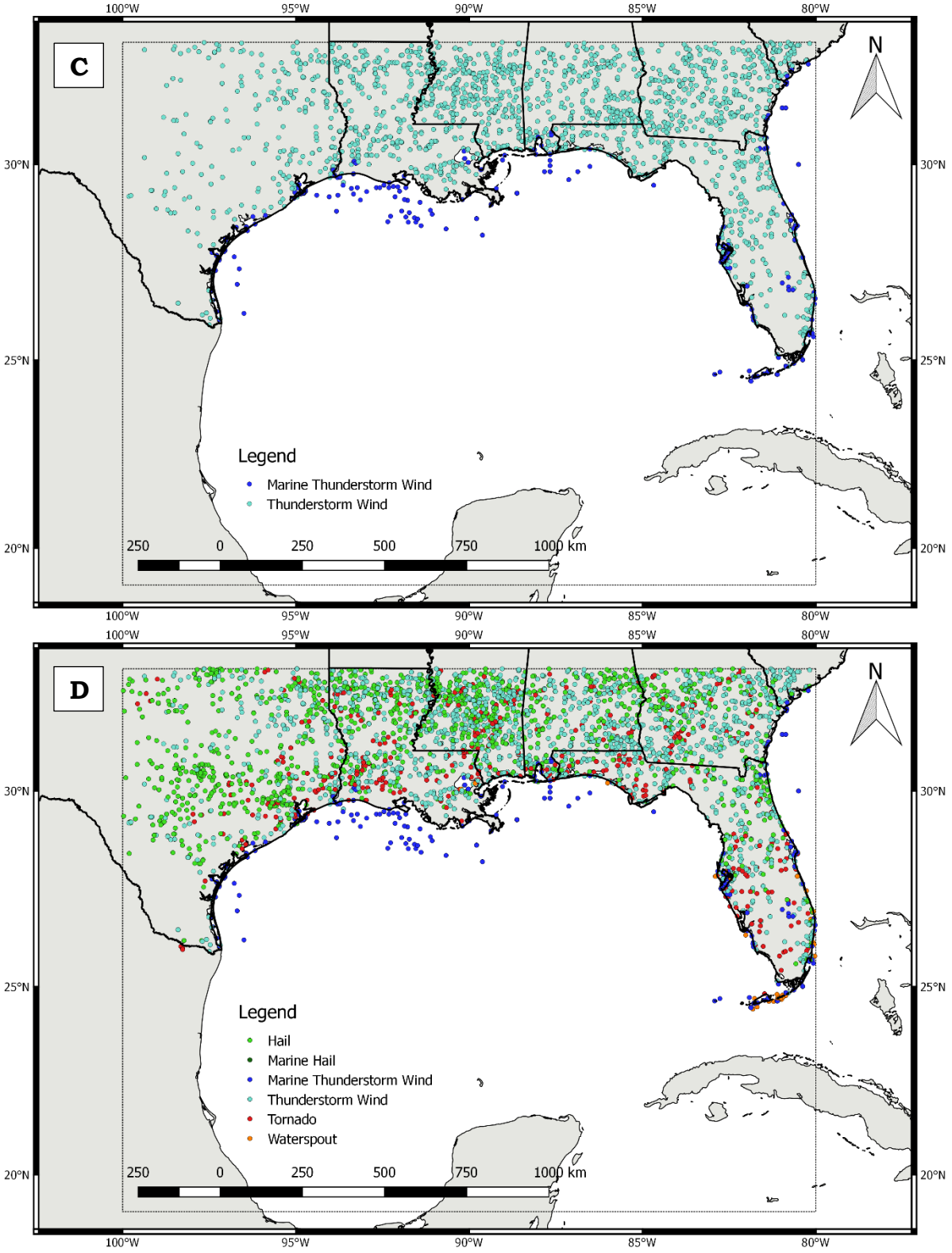
C
N
100°W
95°W
90°W
85°W
80°W
30°N
25°N
20°N
Legend
Marine Thunderstorm Wind
Thunderstorm Wind
250
0
250
500
750
1000 km
D
N
Legend
Hail
Marine Hail
Marine Thunderstorm Wind
Thunderstorm Wind
Tornado
Waterspout
250
0
250
500
750
1000 km

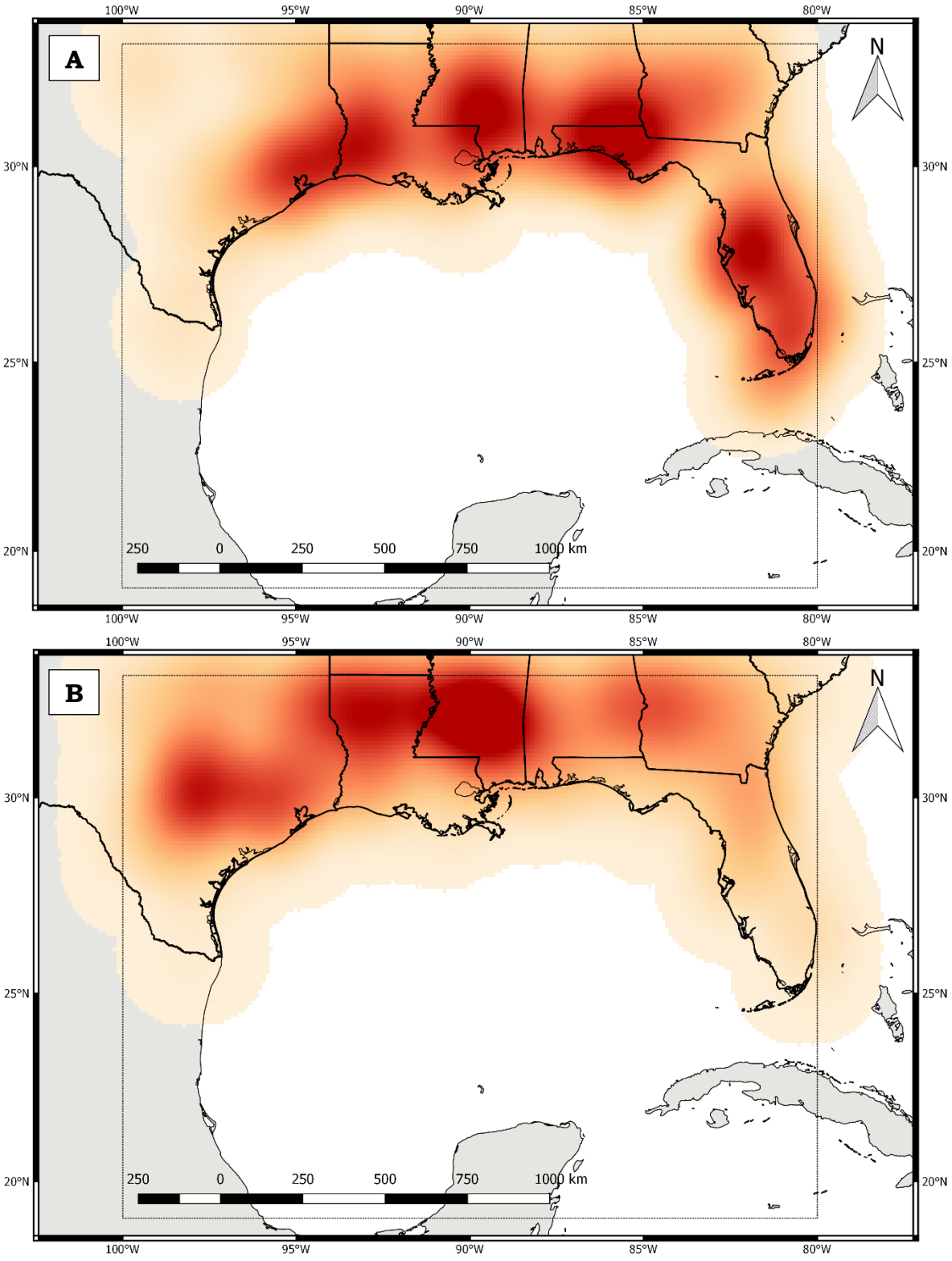


**Figure 5.28** MJO Phase 8 kernel density maps for reports of tornadoes (A), hail (B), strong/damaging winds (C), and all severe weather types combined (D). (figure continued)

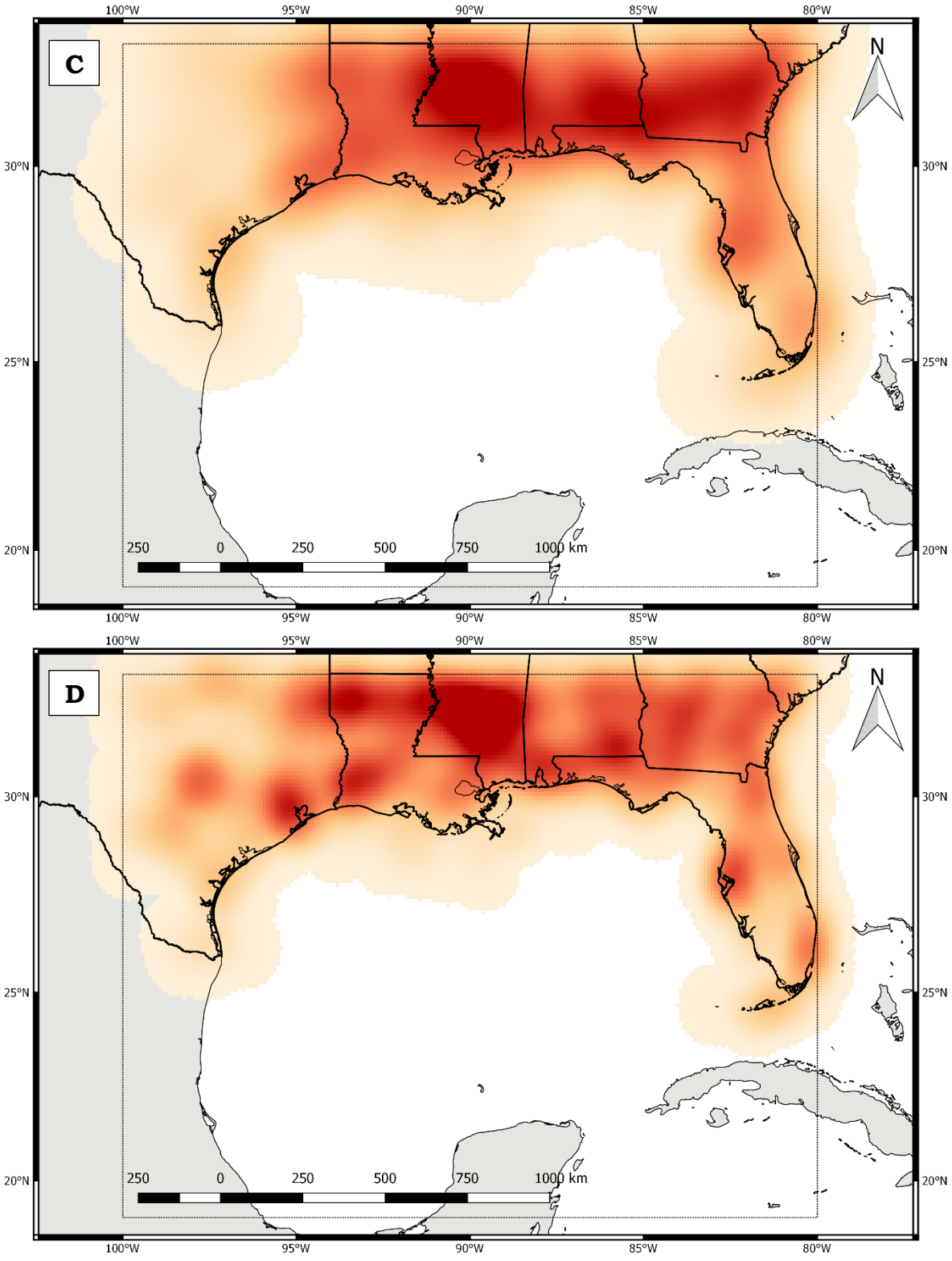
C
D
N
100°W
95°W
90°W
85°W
80°W
30°N
25°N
20°N
250
0
250
500
750
1000 km

## 5.4 Interpretation and Conclusion

The MJO was shown to influence severe weather frequencies in areas near the U.S. GoM Coast. Specifically, tornadoes were found to be more common during Phase 1, while Phase 6 saw a reduction in hail, strong/damaging winds, and all modes of severe weather (tornado/wind/hail) combined. The synoptic scale weather pattern was shown to be supportive of the results found through Monte Carlo simulations in Table 5.1. Phase 1 was shown to have generally low atmospheric pressures, increased instability, and a strengthened polar front jet stream in a favorable position for the formation of tornadoes near the GoM Coast. Phase 6 was shown to have anomalously high atmospheric pressures, lower instability, and a polar front jet stream pattern that was less favorable for the development of severe weather in the GoM region. Nonetheless, further research beyond the scope of this study is necessary to understand more fully the mechanisms responsible for the severe weather frequency variability found here.

The results obtained here also corroborate those of Studies 1 and 2 which showed a general increase in storminess around the GoM during MJO Phase 1 and a trend toward a more tranquil weather pattern during Phase 6. The association between the MJO and cyclogenesis explored in Study 1 failed to produce statistically significant results for RMM Phase 1, but the cyclogenesis rate was only slightly outside of the 90% confidence interval. It would be interesting to determine whether this remained the case if a larger sample size of GoM cool season cyclones were available. Study 2, on the other

hand, did have several statistically significant positive correlations between rainfall and RMM Phase 1. The aforementioned alteration of the synoptic scale pattern during this phase is apparently supportive of both an increase in precipitation and an increase in tornadoes near the GoM.

A prior study that investigated the relationship between the MJO and violent tornado outbreaks in the U.S. found that those outbreaks were more likely during RMM Phase 2 (Thompson and Roundy 2013), which may seem to conflict with the results shown here. However, that study had some key differences, not the least of which was the use of the entire continental U.S. versus the much narrower region around the GoM used here. Thompson and Roundy (2013) also focused on tornadoes that were EF2 or stronger on the Enhanced Fujita scale, while this study examined tornadoes of all magnitudes. Finally, the Thompson and Roundy study (2013) focused exclusively on spring while here both fall and spring were examined. One point of agreement between the two studies was that modification of the Rossby wave pattern by the MJO and the resultant polar front jet stream pattern seemed to play a key role in altering regional tornado frequencies.

Only a few other studies have examined the relationships between the MJO and severe weather in the United States. Barrett and Gensini (2013) limited their analysis to tornadoes in the central U.S. during April and May. Barrett and Henley (2015) focused on hail in the contiguous U.S. for the April – June period. Each study found somewhat different results when examining MJO impacts on U.S. severe weather. The broad range of results and lack of a

consensus can certainly be attributed to the varying methods, variables, and study regions used, but it also emphasizes that MJO impacts like vary region-to-region and season-to-season.

Kernel density analysis also revealed some geospatial trends in severe weather frequencies near the GoM when analyzed by MJO phase. Most notable was the general maximum in severe weather reports that extended from northeastern Texas through northern Louisiana into Mississippi during several MJO phases. It was also noted that severe weather was generally less frequent farther south in the study region used here, which can likely be at least partially attributed to reduced atmospheric lapse rates and a more saturated vertical profile in these regions. The western half of the study area most often had more frequent severe weather reports when compared to the eastern half, but there was a notable upswing in severe weather activity across the eastern GoM during MJO Phases 7 and 8.

Forecasts of severe weather outbreaks show significant skill in most instances within a few days of the event. However, it is often beyond the current level of forecast skill to make any prognostications about severe weather potential beyond a five to seven day lead time. It is hoped that the trends discovered here, along with other ongoing research, will improve our ability to issue subseasonal risk outlooks for severe weather that extend beyond a week. The increasing predictability of the MJO should aid in this effort.

## 5.5 References


Agee, E., J. Larson, S. Childs, and A. Marmo, 2016: Spatial redistribution of US tornado activity between 1954 and 2013. Journal of Applied Meteorology and Climatology, 55(8), 1681–1697.

Anderson, J.R., and R. D. Rosen, 1983: The latitude-height structure of 40-50 day variations in atmospheric angular-momentum. Journal of the Atmospheric Sciences, 40(6), 1584–1591.

Barrett, B.S., and V.A. Gensini, 2013: Variability of central United States April–May tornado day likelihood by phase of the Madden-Julian Oscillation. Geophysical Research Letters, 40(11), 2790–2795.

Barrett, B.S., and B.N. Henley, 2015: Intraseasonal variability of hail in the contiguous United States: Relationship to the Madden–Julian Oscillation. Monthly Weather Review, 143(4), 1086–1103.

Centre for Australian Weather and Climate Research (CAWCR), 2018: An All-season Real-time Multivariate MJO Index. Available online at http://www.bom.gov.au/climate/mjo/graphics/rmm.74toRealtime.txt.

Dixon, P.G., A.E. Mercer, J. Choi, and J.S. Allen, 2011: Tornado risk analysis: Is Dixie Alley an extension of Tornado Alley? Bulletin of the American Meteorological Society, 92(4), 433–441.

Dixon, R.W., and T.W. Moore, 2015: The relationship between the Madden–Julian Oscillation and tropical cyclone tornado clusters. Papers in Applied Geography, 1(1), 86–89.

Earth System Research Laboratory (ESRL), 2018: NCEP/NCAR Reanalysis Daily Mean Composites Plotting Tool, https://www.esrl.noaa.gov/psd/data/composites/day/. Last accessed: 5/23/2018.

Gagan, J.P., A. Gerard, and J. Gordon, 2010: A historical and statistical comparison of “Tornado Alley” to “Dixie Alley.” National Weather Digest, 34(2), 145–155.

Grazulis, T.P., 2001: The Tornado: Nature's Ultimate Windstorm. University of Oklahoma Press.

Kalnay, E., M. Kanamitsu, R. Kistler, W. Collins, D. Deaven, L. Gandin, M. Iredell, S. Saha, G. White, J. Woollen, Y. Zhu, M. Chelliah, W. Ebisuzaki, W. Higgins, J. Janowiak, K. C. Mo, C. Ropelewski, J. Wang, A. Leetmaa,

R. Reynolds, Roy Jenne, and Dennis Joseph, 1996: The NCEP/NCAR 40-year reanalysis project. Bulletin of the American Meteorological Society, 77(3), 437–471.

Klotzbach, P.J., E.C. Oliver, R.D. Leeper, and C.J. Schreck III, 2016: The relationship between the Madden–Julian Oscillation (MJO) and southeastern New England snowfall. Monthly Weather Review, 144(4), 1355–1362.

Madden, R.A., and P.R. Julian, 1994: Observations of the 40-50-day tropical oscillation-A review. Monthly Weather Review, 122(5), 814–837.

National Centers for Environmental Information (NCEI), 2018: Storm Events Database (https://www.ncdc.noaa.gov/stormevents/ftp.jsp, last accessed 5/23/2018.

NWS Jackson, 2018: November 21–22,1992 Tornado Outbreak. Available online at: https://www.weather.gov/jan/1992_11_21_22_tor. Last accessed: 05/13/2018.

NWS New Orleans, 2018: Tornadoes and Strong Straight Line Winds Impact Southeast Louisiana and Coastal Mississippi April 4, 2011. Available online at: https://www.weather.gov/lix/040411severe. Last accessed: 05/13/2018.

Rose, S.F., P.V. Hobbs, J.D. Locatelli, and M.T. Stoelinga, 2004: A 10-yr climatology relating the locations of reported tornadoes to the quadrants of upper-level jet streaks. Weather and Forecasting, 19(2), 301–309.

Salby, M.L., and H.H. Hendon, 1994: Intraseasonal behavior of clouds, temperature, and motion in the Tropics. Journal of the Atmospheric Sciences, 51(15), 2207–2224.

SPC, 2018: The Southeast U.S. 'Derecho' of April 4-5, 2011. Available online at: http://www.spc.noaa.gov/misc/AbtDerechos/casepages/apr042011page.htm. Last accessed: 05/13/2018.

Standohar-Alfano, C.D., and J.W. van de Lindt, 2014: Empirically based probabilistic tornado hazard analysis of the United States using 1973–2011 data. Natural Hazards Review, 16(1), 04014013.

Thompson, D.B., and P.E. Roundy, 2013: The relationship between the Madden–Julian Oscillation and US violent tornado outbreaks in the spring. Monthly Weather Review, 141(6), 2087–2095.

Wheeler, M.C., and H.H. Hendon, 2004: An all-season real-time multivariate MJO index: Development of an index for monitoring and prediction. Monthly Weather Review, 132(8), 1917–1932.

Wheeler, M.C., H.H. Hendon, S. Cleland, H. Meinke, and A. Donald, 2009: Impacts of the Madden–Julian Oscillation on Australian rainfall and circulation. Journal of Climate, 22(6), 1482–1498.

# CHAPTER 6. CONCLUSIONS

## 6.1 General Conclusions

The Madden-Julian Oscillation (MJO) was shown to have significant associations with weather in the Gulf of Mexico (GoM) region, including cool season cyclogenesis, daily precipitation through all seasons, and cool season severe weather frequencies. Weather variability around the GoM was linked to specific phases of the MJO as defined by the Real-time Multivariate (RMM) index (Wheeler and Hendon 2004) or the Oliver-Thompson (OT) index (Oliver and Thompson 2011) where appropriate. In general, the convective clusters associated with the MJO were shown to modify synoptic-scale weather patterns into the midlatitudes through alteration of the Rossby wave train. The GoM region saw a general increase in storminess as the MJO convective clusters progressed from the eastern Pacific into the Western Hemisphere (Phases 7, 8, and 1), while there was a trend toward more tranquil conditions as the clusters propagated from near the Maritime Continent to the central Pacific (Phases 4, 5, and 6). In other words, the a more active pattern was more likely in the GoM region when the clusters were in closest proximity, and a quieter pattern was more likely in the GoM region when the clusters were more distant.

In all three studies, Monte Carlo simulations were constructed to test for statistical significance. The techniques used here largely followed those first introduced in a study relating Australian precipitation to the MJO (Wheeler et al. 2009). The simulations involved creating two vectors of equal length, with the weather variable of choice being the first (i.e., cyclogenesis, precipitation,

severe weather) and the MJO phase representing the second. A chosen number of simulated responses (in this case 1,000) was then collected by shifting the second vector some random amount in time. Once the simulations were completed, confidence intervals were established, allowing for the identification of statistically significant associations between the MJO and the GoM variable of choice. Advantages of using Monte Carlo simulations in these studies included preserving the correlation structure of the MJO, avoiding assumptions about normality, and accounting for the variable number of days in each MJO phase (Wheeler et al. 2009).

The mechanisms responsible for the results obtained in all three studies were explored by plotting a set of atmospheric temperature, humidity, pressure, and circulation anomalies as depicted by NCEP/NCAR Reanalysis data (Kalnay et al. 1996). Increases in GoM cyclogenesis, daily precipitation, and severe weather frequencies were largely associated with anomalously low atmospheric pressure, anomalously high tropospheric moisture, and anomalously strong atmospheric instability. The opposite was found during times of reduced storminess around the GoM, with a trend toward above-normal atmospheric pressures, below-normal tropospheric moisture, and weaker-than-normal instability.

A summary of the key conclusions from each study is found in the sections that follow. It is hoped that the data presented here will further our understanding of how the MJO modulates synoptic-scale weather patterns and variability on a subseasonal scale in the GoM region.

## 6.2 Study 1 Conclusions

Study 1 focused on associations between the MJO and cool season (October-March) cyclogenesis in the GoM. The study period was 1979 – 2014, coincident with an available dataset of surface cyclones obtained from researchers at the National Snow and Ice Data Center (NSIDC; Crawford and Serreze 2016). Cyclogenesis events were analyzed for both all MJO amplitude days (136 cyclones) and only those days when the MJO amplitude was ≥1 (82 cyclones). Monte Carlo simulations were constructed to test for significance of associations between MJO phase and cyclogenesis rates in the GoM.

Study 1 concluded that cyclogenesis was encouraged during MJO phases 7 and 8. During Phase 7, atmospheric pressures showed no significant anomalies in the GoM region and low-level vorticity was weak relative to normal, but upper-tropospheric divergence as depicted by velocity potential anomalies showed a pattern supportive of the increased vertical motion necessary for the generation of convection. Phase 7 also represents a time when the MJO convective clusters are passing from the central to the eastern Pacific and it is possible that increasing proximity to the GoM may aid in greater rates of cyclogenesis.

Phase 8 provided much clearer evidence of the atmospheric mechanisms responsible for increased cyclogenesis rates in the GoM. Atmospheric pressures were anomalously low over the eastern U.S. and much of the GoM, while upper-tropospheric divergence was greater-than-normal. Low-level vorticity as depicted by 850 mb vector wind anomalies showed increased positive vorticity

which would favor increased frequency of cyclogenesis. The increased cyclogenesis frequencies found for Phases 7 and 8 in Study 1 parallel results found by Klotzbach et al. (2016) for extratropical cyclones near the coast of the northeastern United States.

By contrast, cyclogenesis frequencies were shown to decrease in the GoM during MJO Phases 4, 5, and 6. These phases were dominated by higher-than-normal atmospheric pressures over the eastern U.S. and the GoM, increased upper-tropospheric subsidence, and anomalous levels of negative lower-tropospheric vorticity. Collectively, these synoptic-scale anomalies were supportive of decreased cyclogenesis rates during the GoM cool season. The results obtained here were also again similar to those of Klotzbach et al. (2016), who found that extratropical cyclones were less frequent in the vicinity of the northeastern U.S. coastline during MJO Phases 4 and 5. Additional corroboration comes from the seminal work of Maloney and Hartmann (2000), who focused on tropical cyclones in the GoM. Their work found that tropical cyclone frequencies were reduced when low-level wind anomalies were easterly in the GoM. Plots of 850 vector wind anomalies in this this study showed that low-level wind anomalies were largely easterly over the GoM during Phases 4, 5, and 6, coincident with the times when cool season cyclogenesis rates were reduced in the GoM as indicated by the Monte Carlo simulations.

## 6.3 Study 2 Conclusions

Study 2 focused on associations between the MJO and daily precipitation for sites near the U.S. GoM Coast. Precipitation data were obtained for 12 sites

stretching from Texas to Florida through the State Climatologists Applied Climate Information System (SC ACIS 2018; http://scacis.rcc-acis.org/). The analysis was restricted to days when the magnitude of the OT MJO index was ≥1 since the MJO is considered to be weak when values are <1. Monte Carlo simulations were then constructed to test for statistical significance between the MJO and daily precipitation, the number of days producing at least 2.5 cm of precipitation, and the number of days producing at least 5.0 cm of precipitation.

Daily precipitation was found to have positive associations with MJO Phases 8, 1, and 2 at several of the selected sites along the U.S. GoM coast. Specifically, Phase 8 associations were noted both in western portions of the GoM study region and parts of the Florida Peninsula. Phase 1 associations were mostly confined to the Florida Peninsula, but Brownsville, Texas, was also shown to have increased daily precipitation during this phase. The positive Phase 2 associations were limited to two sites – Ocala and Sarasota, Florida. Another noteworthy result was that New Orleans and Mobile were the only two sites that failed to produce a positive association between daily precipitation and any of the eight MJO phases. Negative associations were confined largely to Phases 4, 5, and 6 and almost exclusively to the Florida Panhandle. A couple of outliers were noted, with Key West shown to have a negative association with Phase 3 and Sarasota shown to have a negative association with Phase 7.

The Monte Carlo simulations that focused on the number of days generating at least 2.5 cm of precipitation produced similar results to those for

daily precipitation. Phase 8 once again had positive associations both in western portions of the GoM region and in the Florida Peninsula. Phase 1 positive associations were confined to Florida, extending eastward across the Florida Panhandle from Tallahassee and then southward for nearly the entire length of the Florida Peninsula from Gainesville to Key West, with an isolated gap in the associations at Ocala. Positive associations for Phase 2 were confined to a small area in the Florida Peninsula extending from Ocala to Tampa. Negative associations between the MJO and the number of days with at least 2.5 cm of precipitation were again most prevalent during Phases 4, 5, and 6. However, a few negative associations were found during Phases 2 and 3, most notably for Lake Charles and New Orleans. These results along the northern GoM coast were unique since most of the statistical testing in Study 2 failed to reveal significant associations in this region.

Finally, and not surprisingly, testing for associations between the MJO and the number of days producing at least 5.0 cm of precipitation produced the fewest significant results. The higher precipitation threshold resulted in smaller sample sizes across the entire region and is the likely explanation for the reduction in the number of associations. Even with that reduction, some of the trends remained, with all but one of the positive associations restricted to Phases 8, 1, and 2. The negative associations were also similar with all but one of those found during Phases 5 and 6. The geographic distribution was also similar, with associations most frequent in the Florida Peninsula, followed by a lower number in the western GoM region.

Analysis of synoptic-scale atmospheric anomalies provided support for the results obtained in Study 2. During MJO Phases 8, 1, and 2, atmospheric pressures were largely found to be lower-than-normal, atmospheric moisture higher-than-normal, and surface precipitation rates higher-than-normal in the GoM region. Collectively, these anomalous patterns corroborated the Monte Carlo simulation results showing a number of positive associations between daily precipitation and those MJO phases. Conversely, a reversal of most of those anomalies was noted during Phases 4, 5, and 6, when several negative associations were found with daily precipitation near the U.S. GoM coast.

### 6.4 Study 3 Conclusions

Study 3 focused on associations between the MJO and daily severe weather frequencies near the U.S. GoM coast. Reports of tornadoes, hail, and strong/damaging winds were obtained from the National Centers for Environmental Information (NCEI, 2018) Storm Events Database (https://www.ncdc.noaa.gov/stormevents/ftp.jsp). The analysis was restricted to days when the magnitude of the RMM index was ≥1 since the MJO is considered to be weak when values are <1. Monte Carlo simulations were then constructed to test for statistical significance between the MJO and the frequency of daily tornado reports, hail reports, strong/damaging wind reports, and all severe weather modes (tornado/wind/hail) combined.

The Monte Carlo simulation results indicated that tornadoes were more frequent during MJO Phase 1, while reports of hail, damaging winds, and all modes of severe weather combined were less frequent during Phase 6. All of

those results were significant at the 95% level. The results also showed consistency with those of Studies 1 and 2, which pointed toward an increase in storminess around the GoM during Phase 1 and a decrease in storminess around the GoM during Phase 6.

The increased tornado frequencies found during Phase 1 were supported by an analysis of synoptic-scale atmospheric anomalies using NCEP/NCAR Reanalysis data (Kalnay et al. 1996). Anomaly plots indicated that atmospheric pressure was lower-than-normal region-wide, mid-tropospheric temperatures were below-normal in the portion of the study area producing the most tornadoes, and most importantly, a strengthened polar front jet stream was found in the GoM in a location that was favorable for the development of tornadoes. Collectively, these anomalous patterns supported the Monte Carlo simulation results that indicated tornadoes were more frequent in the GoM region during Phase 1.

Atmospheric anomaly plots were also generated to explore the mechanisms leading to decreased severe weather frequencies in the GoM region during Phase 6. Analysis of those plots found that atmospheric pressures were higher-than-normal across much of the region, mid-tropospheric temperatures were above-normal in a large portion of the area, and the subtropical jet stream was displaced southward, likely reducing the frequency of midlatitude perturbations and cyclones passing through the region that would aid in thunderstorm development. Jointly, these anomalous patterns suggest that

thunderstorms are less frequent in the GoM during Phase 6, therefore leading to reduced severe weather frequencies.

## 6.5 Future Research

Strong evidence is provided here that the MJO influences cool season cyclogenesis rates, daily precipitation through all seasons, and cool season severe weather frequencies in the GoM region. Opportunities for future research related to GoM cool season cyclones include a look into whether sea surface temperature (SST) variability exerts an influence on cyclogenesis rates. The high heat capacity of the ocean means that SST changes are much slower to occur relative to the atmospheric variability discussed here, and therefore the ocean may have a limited impact on subseasonal variability. Nonetheless, additional research and modeling would be needed to quantify or eliminate oceanic heat content as a modulator of cool season cyclogenesis frequency in the GoM. An additional opportunity for future research is an investigation of the impact that climate change may have on cool season GoM cyclogenesis variability. Because substantial research suggests that polar and mid-latitude areas will continue to warm to a greater extent than the tropics (a phenomenon known as Arctic Amplification (e.g., Serreze and Barry 2011), is it possible that as the planet warms the thermal contrast that aids in the development of baroclinic low pressure systems will diminish?

The relationship between the MJO and daily precipitation could be examined in a slightly different manner than what was done here. Would the use of gridded precipitation data instead of single station data show more

distinct precipitation patterns in the GoM for specific phases of the MJO? Additionally, while this study categorized all precipitation types (i.e., liquid and frozen) together, it would be interesting to investigate whether ice and/or snow is more or less frequent in the region during particular phases of the MJO. The limited frequency of frozen precipitation in the region may present some sample size issues but restricting an analysis of this sort to the northern GoM Coast may help overcome those limitations.

Finally, the associations between the MJO and severe weather frequencies present some opportunities for future research. The analysis done here largely focused on synoptic-scale pressure and moisture patterns as mechanisms responsible for modifications of severe weather frequencies. Additional research could focus on measures of atmospheric instability such as convective available potential energy (CAPE) which indicate how much sensible and latent energy (i.e., enthalpy) is available for thunderstorm development, with increasing values known to lead to increased chances of severe weather. Analysis of vertical wind shear might also provide some insight into how specific phases of the MJO affect severe weather frequencies in the GoM region. Regardless of the specific form it takes, future weather prediction in the southeastern U.S. is likely to benefit from more sound, scientific research on the impacts of the MJO. Increasing predictability provided by numerical modeling and a more thorough understanding of the MJO may lead to improved subseasonal forecasts of cyclogenesis potential, daily precipitation variability, and daily severe weather frequency variability.

## 6.6 References


Crawford, A.D., and M.C. Serreze, 2016: Does the summer Arctic frontal zone influence Arctic Ocean cyclone activity? Journal of Climate 29(13), 4977–4993.

Kalnay, E., M. Kanamitsu, R. Kistler, W. Collins, D. Deaven, L. Gandin, M. Iredell, S. Saha, G. White, J. Woollen, Y. Zhu, M. Chelliah, W. Ebisuzaki, W. Higgins, J. Janowiak, K. C. Mo, C. Ropelewski, J. Wang, A. Leetmaa, R. Reynolds, R. Jenne, and D. Joseph, 1996: The NCEP/NCAR 40-year reanalysis project. Bulletin of the American Meteorological Society, 77(3), 437–471.

Klotzbach, P.J., E.C. Oliver, R.D. Leeper, and C.J. Schreck III, 2016: The Relationship between the Madden–Julian Oscillation (MJO) and southeastern New England snowfall. Monthly Weather Review, 144(4), 1355–1362.

Maloney, E.D., and D.L. Hartmann, 2000: Modulation of hurricane activity in the Gulf of Mexico by the Madden-Julian oscillation. Science, 287(5460), 2002–2004.

National Centers for Environmental Information, 2018: Storm Events Database (https://www.ncdc.noaa.gov/stormevents/ftp.jsp, last accessed 5/23/2018.

Oliver, E.C., and K.R. Thompson, 2011: A reconstruction of Madden–Julian oscillation variability from 1905 to 2008. Journal of Climate, 25(6), 1996–2019.

SC ACIS, 2018: State Climatologists Applied Climate Information System. Available online at: http://scacis.rcc-acis.org/. Last accessed: 05/15/2018.

Serreze, M.C., and R.G. Barry, 2011: Processes and impacts of Arctic amplification: A research synthesis. Global and Planetary Change, 77(1–2), 85–96.

Wheeler, M.C., and H.H. Hendon, 2004: An all-season real-time multivariate MJO index: Development of an index for monitoring and prediction. Monthly Weather Review, 132(8), 1917–1932.

Wheeler, M.C., H.H. Hendon, S. Cleland, H. Meinke, and A. Donald, 2009: Impacts of the Madden–Julian oscillation on Australian rainfall and circulation. Journal of Climate, 22(6), 1482–1498.

# VITA

Stephen Caparotta was born in New Orleans, Louisiana, and grew up in the suburb of Metairie. He earned a Bachelor of Science degree in geography/meteorology from the University of South Alabama in May of 1998. Stephen began his career as a broadcast meteorologist at KPLC-TV in Lake Charles, Louisiana, in 1999. After spending two years in Lake Charles, he accepted a similar position with WIS-TV in Columbia, South Carolina, in 2001. Stephen spent a little more than two years in Columbia before returning to his home state and accepting a job with WAFB-TV in Baton Rouge. He began his graduate studies at Louisiana State University in August of 2004 while working at WAFB and earned a Master of Science degree in geography in 2008. He is still an on-camera meteorologist at WAFB and plans to graduate with a Ph.D. in geography during the August 2018 commencement at LSU.